The Application of Passive and Active Acoustic Techniques in Process Monitoring

Manuel Tramontana

A Thesis submitted in fulfilment of the requirement for the degree of Doctor of Philosophy

Centre for Ultrasonic Engineering, University of Strathclyde, Royal College Building, 204 George Street, Glasgow, G1 1XW
e-mail: manuel.tramontana@gmail.com

19th April 2011

Copyright protection

Ai miei nonni (To my grandparents)

Abstract

Acoustic techniques are of particular interest in process monitoring as they can be employed non-invasively, in situ, in real time and are relatively inexpensive compared to optical techniques. This Thesis presents a detailed investigation to quantify the size and concentration of particles in heterogeneous mixtures using either passive or active acoustic monitoring techniques.

A Finite Element (FE) modelling approach was utilised to analyse acoustic emissions (AE) generated through the impact of particulates with a reactor vessel wall. A 4-layer model was developed comprising a liquid load medium and a glass-oil-glass combination corresponding to the jacketed vessel reactor. The FE simulations predict: an increase in energy with an increase in either particle size or concentration; the intensity of the AE signals at lower frequencies increases with increasing particle size; and the reactor vessel has a low pass filtering effect on AE signals. From these FE simulation results, two customised transducer configurations were manufactured; a narrow-band resonant device and an off-resonance piezocomposite transducer. Importantly, these devices operate in a complementary manner in which the sensitivity of the resonant transducer provides enhanced discrimination of particle concentration and the broader bandwidth of the off-resonance device gives information on changes in the mean particle size.

Investigations into the application of both linear and non-linear active acoustic monitoring techniques to a system comprising chemical particulates suspended in water were also undertaken. A customised experimental test

cell was manufactured which could incorporate a range of commercial ultrasonic transducers and utilised polyvinylidene fluoride (PVDF) hydrophone receiving elements. Measurements of velocity and attenuation verified the performances of the test cell in the linear regime of cellulose particles in water. Second harmonic signals arising from the non-linear interaction of ultrasonic contrast agent in water with ultrasound were detected.

It is considered that the work described in this Thesis will provide a platform for new, improved passive and active acoustic monitoring techniques, which can be applied in the control of particulate based processes.

Acknowledgements

This is perhaps the easiest and hardest part of the Thesis that I have to write. It will be simple to name all the people that helped to get this done, but it will be tough to thank them enough. I will nonetheless try.

I seize the opportunity to record my deep sense of gratitude and thanks to my supervisors, Prof. Anthony Gachagan, Prof. Alison Nordon, Prof. David Littlejohn and Prof. Gordon Hayward. Their inspiring guidance, suggestions, friendly attitude with motivation and persistent efforts to instil interest in this field of research has made all the good throughout the course of my investigation. I wish to thank also all of my workmates in CUE and in the Chemistry Department and my friends in Glasgow for their kind help and presence.

Special thanks to Gillian Carson and Tony Mulholland for developing the mathematical model of the impact functions used for the FE reactor vessel. Richard O'Leary is gratefully thanked for his help on the FE code and modelling.

I have been supported financially by The Centre for Process Analytics and Control Technology (CPACT), Sira (UK) and Engineering and Physical Sciences Research Council (EPSRC). For this assistance I am very grateful.

I am highly thankful to my 'mamma', my brother and my sister, Enzo e Francesca in Italy for their constant encouragement and their phone calls. At last but not the least Vesna, my life companion for for her endless love and patient throughout this entire journey.

Contents

List of Tables

List of Figures

The following is a **list of symbols** referred to throughout the Thesis. All units comply with International System of Unit (SI).

Table 1: List of symbols

Parameter	**Symbol**	**Unit**
β	Compressibility	m^2/N
Φ	Volume Fraction	
α	Attenuation Coefficient	dB Hz / m
D	Distance	m
t	Time	s
A	Amplitude	V
F	Force	N
m	Mass	Kg
η	Viscosity	Kg / s m
Fs	Scattering Intensity	dB
K	Complex Propagation Constant	$Np\ m$
ω	Angular Frequency	rad/s
v	Velocity	m / s
ω_0	Stirrer Velocity	1 / s
m_e	Mass of the Particle	Kg
rd	Radial Distance	m
l	Spatial Discretisation	m
ts	Time Step	s
N	Number of Particles	
a_T	Thermal Expansion Coefficient	1 / K
c_P	Specific Heat Capacity	kJ / kg K

Table 2: List of symbols

Parameter	**Symbol**	**Unit**
d	Thickness	m
A_i	Scattering Coefficients	
α_I	Intrinsic Absorption	dB / m
α_S	Scattering losses	dB / m
α_{VI}	Visco-Intertial Absorption	dB / m
α_T	Thermal Absorption	dB / m
r	Radius of the Particle	m
T_h	Particle Impact Time	m
λ	Wavelength	m
f_R	Resonant Frequency of the Micro-bubble	Hz
R_o	Radius of the Micro-bubble	m
γ	Ideal Gas Constant	J / (K mol)
β_{NL}	Coefficient of nonlinearity	
$\frac{B}{A}$	Ratio of coefficients in a Taylor series	
S_{shell}	Stiffness of the Micro-bubble	Pa
P	Pressure	Pa
f	Frequency	Hz
θ	Angle	rad
Rf	Reflection Coefficient	
μ	Average	
SD	Standard Deviation	
EX_{total}	Signal Area over the Total Bandwidth	
$EX_{f_1-f_2}$	Signal Area between f_1 and f_2	
EX	Percentage of Area	
DL	Detection Limit	
Sl	Sensitivity of AE Response	V / Hz

Table 3: List of symbols related to piezoelectricity. All symbols comply with the ANSI-IEEE 176 (1987) Standard on Piezoelectricity.

Parameter	**Symbol**	**Unit**
ν	Poisson Ratio	
Y	Young Modulus	N/m^2
S	Strain	
T	Stress	Pa
E	Electric Field	N/C
D	Electric Displacement	C/m^2
C_T	Courie Temperature	$^{\circ}C$
ρ	Density	kg/m^3
v_l	Bulk Longitudinal Velocity	m/s
v_s	Shear Velocity	m/s
Z **or** Z_A	Acoustic Impedance	$MRayls$
e_{ij}	Piezoelectric Stress Constant	C / m
g_{ij}	Piezoelectric Voltage Constant	V m / N
d_{ij}	Piezoelectric Charge Constant	C/N
k_{ij}	Piezoelectric Coupling Factor	
c_{ij}	Piezoelectric Elastic Stiffness	Pa
k_t	Thickness Mode Coupling Factor	
N_f	Near Field Region	m
Dm	Transducer Diameter	m
ϵ_r	Relative Permittivity	F/m
ϵ_0	Permittivity in the free space	F/m
Rf	Reflection Coefficient	
BW	Transducer Bandwidth	Hz
$H(f)$	Sensitivity Response	V
$M_T(f)$	Hydrophone Curve of Response	V
Q	Quality Factor	
AR	Aspect Ratio	
$Damp_l$	Longitudinal Damping Coefficient	dB/m
$Damp_s$	Shear Damping Coefficient	dB/m

Table 4: List of symbols related to electrical operation

Parameter	**Symbol**	**Unit**
i	Current	A
V_{OS}	Offset Voltage	V
I_B	Bias Current	A
I_{OS}	Offset Current	A
Ib	Noise Spectral Current Density	V / $\sqrt{Hz}$
en	Noise Spectral Voltage Density	V / $\sqrt{Hz}$
V	Voltage	V
C	Capacitance	F
L	Inductance	H
R	Electrical Impedance	Ω
k_0	Boltzmann Constant	$m^2kg/(s^2K)$
T	Temperature	$^\circ C$
Res	Electrical Impedance (Real Part)	Ω
ees^2	Noise Spectral Density	V / $\sqrt{Hz}$
G	Gain	
f_L - f_H	Low - High cut-off frequency	Hz
$en1t^2$	Total RMS Noise Spectral Density	V / $\sqrt{Hz}$
$en1tRt^2$	Total RMS Noise Spectral Density (Rt included)	V / $\sqrt{Hz}$
$Etot_{RMS}$	Output RMS Noise	V
$E_{Rt}tot_{RMS}$	Output RMS Noise (Rt included)	V
A_{RMS}	Amplitude RMS	V
Eq_n	Equivalent Noise Spectral Density	V / $\sqrt{Hz}$
e_{out}	Output Noise Spectral Density	V / $\sqrt{Hz}$
$S(f)$	Signal Spectrum	Hz

Chapter 1

Introduction

"The important thing is not to stop questioning.

Curiosity has its own reason for existing"

Albert Einstein.

In chemical, pharmaceutical and food industries the need to determine the concentration and the size distribution of particles with ease, accuracy and speed is well recognised [3]. Continuous in-line measurement of substance concentration in liquid mixtures is valuable in improving industrial processes in terms of material properties, energy efficiency and process safety [4]. The ability to monitor and control industrial processes will result in reducing the product waste and time of manufacturing. Moreover, the manufacturing processes will be safer and more consistent [3]. It is estimated that such improvement could lead to an increase of profit up to 20% for manufacture of high value products such as pharmaceutical companies [5]. For instance, the ability to produce an excipient component, which is necessary to fabricate a tablet, to a specified particle size distribution with less variability, would decrease the number of batch failures owing to poor blend uniformity [6]. The estimated cost of a failed pharmaceutical batch is $0.25 million [5].

The methods to monitor particle size and particle concentration have been developed in response to the technology available at the time. Laser diffraction is currently the most widely used technique for evaluating particle size in dry powders, suspensions and emulsions in the range between 0.1 μm to a few millimeters [7]. Optical techniques such as infrared spectrometry and photon correlation spectroscopy are employed successfully because of the reproducibility, simplicity and speed of the measurement procedure. However, since they require the transmission of light through the sample and assume single particle scattering, the methods are limited to making measurements on dilute and transparent samples [8]. Acoustic waves interact with the particles in a similar way to light but have the advantage that they can travel through concentrated suspensions and emulsions and opaque materials [9].

Acoustic monitoring techniques have considerable advantages over optical technologies because they can be applied to systems that are optically opaque without the need for any sample preparation [10]. The ability of acoustic waves to penetrate optically opaque media enables ultrasonic techniques to be, in principle, applied directly to relatively large concentration of particles. Acoustic monitoring systems can be non-invasive; therefore no probes or windows are required in the process line. Information may be obtained from a dynamic system *in situ* and in real-time; this makes acoustical techniques attractive for process control [11]. Hence, the development of improved acoustic techniques, which are relatively low cost in comparison to many optical techniques, is desirable for more effective process investigation, monitoring and control.

Despite the fact that active acoustic spectrometry has found comprehensive uses in the laboratory for the characterisation of particle size [7], there

are few reported examples of applications in a process environment [12]. In comparison, the feasibility of using acoustic techniques as a monitoring tool has been applied in several industries such as pharmaceutical e.g. for monitoring high shear granulation [13], crystallization [4], granulation [14] and flow of powders [3]; or food manufacturing for monitoring of emulsions [15], slurries [16] and reaction monitoring [17].

Acoustic techniques can be active (where the ultrasound energy is passed into a material of interest [15]) or passive (a process is the source of acoustic energy [18]), and yield information on the physical properties of the sample.

Non-invasive acoustic methods are useful for process analysis as, in principle, an acoustic sensor can simply be attached to the outside of a process vessel or pipe. The sensor is not in direct contact with the sample and so does not cause any contamination [13]. However, the vessel and additional instrumentation can also contribute to the received ultrasonic signal. This effect can mask the weak interactions between the ultrasound and the reaction of interest. The information that can be obtained from acoustic emissions (AEs) signals is also dependent on the frequency range of the transducer and the way in which the signal is acquired and stored [19]. Generic broadband transducers are often employed without knowing exactly the real frequency range of interest of the process under investigation.

Different commercial ultrasonic systems employing active acoustic techniques are available for monitoring off-line processes. They are based on analysis of the linear response employing "pitch and catch" technology that requires transmission of the acoustic wave through the sample [15]. However, in many applications the physical nature of the material involved prevents acoustic transmission measurements and more useful process information can

be achieved through the study of wide-band ultrasonic backscatter [20].

In the first part of the Thesis, a novel approach to investigate the generation of acoustic emission (AE) signals through chemical particles striking against the inner wall of a vessel reactor and the design of a prototype passive acoustic system will be presented.

In the second part of this research, preliminary investigations will be performed into the ultrasonic-particle interactions in water, employing a range of active acoustic techniques, to evaluate the generation of linear and non-linear responses from stable particles suspended in a fluid medium.

The approaches of employing the passive and active acoustic techniques presented in this Thesis demonstrate how changes in both particle size and concentration could be derived from the broadband acoustic emission signals and offer a potential for in-situ process monitoring.

1.1 Thesis content

The study of the process monitoring system begins in Chapter 2, with a comparison of the advantages and disadvantages of the most popular optical techniques. A literature review follows describing the background and history of the most important passive and active acoustic monitoring techniques. A number of important studies and theories of ultrasonic propagation in heterogeneous mixtures, that will be compared and referenced throughout this Thesis, are outlined here.

Chapter 3 explains the starting point of the research on a passive acoustic heterogeneous system employing a commercial transducer and a vessel reactor. The filtering effects of the reactor and the commercial sensor transfer

function are identified and demonstrated as main contributors on the acoustic spectra. Importantly, the objectives for the development of a prototype passive acoustic monitoring system are also detailed in this Chapter.

A novel approach to analyse the complicated interactions of chemical particles and the vessel reactor using the Finite Element (FE) modelling method is the subject of Chapter 4. The mathematical modelling of the excitation function, and the FE two dimensional model of the reactor vessel, is presented. The validation of the models is also illustrated and discussed. The overall model is then employed to predict the various particle responses in different situations on the acoustic emission spectra.

The research output from Chapters 3 and 4 is used in the development of the new passive acoustic system and it is presented in Chapter 5. Initially, a background of piezoelectric ceramic composite transducer technology is given to the reader to explain the advantages of the technology. The prototyping and development of complementary off-resonance and resonant piezocomposite sensors, to match the desired specifications for the passive acoustic system, follows in this Chapter. The design of a low noise pre-amplifier and its analysis completes the development of the prototype passive system. The experimental validation of the performance of these two transducer designs completes the passive acoustic monitoring aspects of this Thesis.

The broadband active acoustic approach is described in Chapter 6. Here the acoustic energy is propagated through the system for the evaluation of the generation of both linear and non-linear ultrasonic responses from chemical particles suspended in fluids. The experimental arrangement, and the digital signal processing approach for the characterization of cellulose par-

ticles suspended in distilled water are described at first. Experimental work follows with linear measurements of velocity and attenuation employing the through-transmission technique. A non-linear ultrasonic approach is evaluated using the second harmonic backscattered data from contrast agent micropheres and cellulose particles. Interestingly, the Avicel particles used in this work exhibited a wetting phenomenon which is discussed in the Chapter. This work illustrates the potential advantages of using a active acoustic approach for the monitoring of particulate suspensions.

Chapter 7 summarises the approaches discussed and states the overall conclusions from the points raised in each Chapter. Proposals for future work are also given to conclude the Thesis.

1.2 Contributions to the knowledge of the acoustic monitoring techniques

The following lists the major achievements of this Thesis and their contribution to the field of ultrasound.

- Finite element modelling has been utilised to investigate the acoustic emission signals generated by particulate suspensions within a jacketed reactor vessel. This approach was used to analyse the complex interactions between chemical particles and the vessel wall. The FE model has been used to predict the effects of particle impact positions, particle concentration and particle size on the generated AE spectra. Importantly, this approach has provided predictions of the frequency range

of interest which has been used in the design of customised ultrasonic transducers.

- The manufacture of a wide-band off-resonance transducer gave the opportunity to confirm the FE modelling results in which a energy shift towards lower AE frequencies corresponds to an increase in particle size. This could be an important index for in situ particle size characterisation using a non-invasive passive acoustic monitoring system.

- Two prototypes consisting of a non-resonant and a resonant transducer have been developed for enhanced sensitivity over commercially available devices. These have resulted in an improved detection limit value which is considerably lower than that reported in a former study [17](0.1 $\frac{g}{dm^3}$ for unsieved itaconic acid particles).

- A number of custom software tools, developed in Matlab © environment, have been specifically implemented to analyse the data collected from the active experimental cell. These enable the acquisition and analysis of linear and non-linear signal components using cross correlation and pulse compression techniques. The experimental work demonstrates the feasibility of performing velocity and attenuation measurements of cellulose particles in water and extracting the potential harmonic signals from the backscattered data of ultrasonic contrast agent (UCA) in water.

1.3 Dissemination of the research results

Journal proceedings

- *Estimating Particle Concentration Using Passive Ultrasonic Measurement of Impact Vibrations* G. Carson, A.J. Mulholland, A. Nordon, M. Tramontana, A. Gachagan and G. Hayward, IEEE transations on Ultrasonics Ferroelectrics and Frequncy Control. Volume: 56 Issue: 2 Pages: 345-352 Published: 2009

- *Particle sizing using passive ultrasonic measurement of particle-wall impact vibrations.* G. Carson, A. J. Mulholland, A. Nordon, M. Tramontana, A. Gachagan and G. Hayward, Journal of Sound and Vibration. Volume: 317 Issue: 1-2 Pages: 142-157 Published: 2008

Conference proceedings

- *Ultrasonic Monitoring of Heterogeneous Chemical Reactions.* M. Tramontana, A. Gachagan, G. Hayward, A. Nordon, and D. Littlejohn. IEEE International Ultrasonics Symposium p. 910-913, Vancouver 2006, Canada.

- *Particle Sizing in the Process Industry using Hertz-Zener Impact Theory and Acoustic Emission Spectra*, G. Carson, A. J. Mulholland, A. Nordon, M. Tramontana, A. Gachagan and G. Hayward, IEEE Ultrasonics Symposium, p. 1051-0117, Vancouver 2006, Canada.

- *Passive acoustic monitoring in the pharmaceutical industry* M. Tramontana, A. Gachagan, G. Hayward, A. Nordon, and D. Littlejohn,

APACT06 Advances in process analytic and control technology, Oxford 2006, U.K.

- *Development of a Passive Acoustic Monitoring System* M. Tramontana, A. Nordon, A. Gachagan, D. Littlejohn and G. Hayward., APACT06 Advances in process analytic and control technology, Oxford 2006. (First Prize Poster Award)

- *Passive Acoustic Monitoring in the Pharmaceutical Industry* M. Tramontana, A. Nordon, A. Gachagan, G. Hayward and D. Littlejohn Ultrasound06, Ultrasound in the Processing of Industrial Soft Materials, Leeds 2006, U.K.

- *Advanced modelling of particle interactions associated with passive acoustic measurements* M. Tramontana, A. Nordon, A. Gachagan, D. Littlejohn, G. Hayward. APACT05 Advances in process analytic and control technology, Bath 2005, UK.

- *Investigation into the non-linear response from active ultrasonic monitoring systems for application in the pharmaceutical industry.* A. Gachagan, M. Tramontana, A. Alsada, N. Ramadas, G. Hayward, A. Nordon and D. Littlejohn, IEEE Ultrasonics Symposium, 2004, Montreal, Canada.

Chapter 2

Techniques for monitoring heterogeneous mixtures

In chemical, pharmaceutical and food industries, the need to determine the concentration and the size distribution of particles with ease, accuracy and speed is well recognised [3]. Indeed, a continuous on-line process for monitoring particle characteristics would be of great interest for such fields.

A brief overview of the optical monitoring techniques is explained in the next Section. The background and history of the most popular passive and active acoustic methods will follow. Important studies regarding the propagation of ultrasonic waves in heterogeneous mixtures, subsequently referred to throughout this Thesis, are outlined here.

2.1 Optical monitoring techniques

2.1.1 Low Angle Laser Light Scattering (LALLS)

This technique passes a laser beam through a sample containing particles, and collects light intensity data at different scattering angles (low) away from the axis where the beam was originated. Intensity data is collected at many different angles (most instruments use 64 angles). The light intensities at the observed angles are related to the distribution of particle sizes. Complex light scattering calculations are applied to determine this relationship. LALLS is applied to samples containing relatively low concentration of particles, to ensure multiple scattering (where light scattered from one particle is scattered by a second particle before reaching the detectors) is minimal, since multiple scattering makes it difficult to generate an accurate size distribution based on scattering angles [21].

Advantages

- Very fast data collection.
- Very broad dynamic range (commonly claimed from <0.1 μm up to mm sizes).
- Relatively simple to use.
- Can measure both powders (with suitable powder sampling equipment) and fluid suspensions.
- Testing is non-destructive, so samples can be recovered if necessary.

- The method is widely used; so many people are familiar with the method and have confidence in the results.

Disadvantages

- High-resolution measurements are not possible to achieve.
- Accuracy depends on the accuracy of the optical parameters (refractive index, light absorption) available for the particles, as well as the accuracy of information about particle shape, as these are used to calculate the scattering properties of the particles.
- Light absorption characteristics are often unknown and must be "estimated".
- Mixtures of particles with different optical properties cannot normally be measured.
- Materials that absorb light strongly can present problems, because the back-scattering signal is very weak.
- The calculations used to generate the distribution are complex and often proprietary, so it is very difficult to verify instrument performance except in the simplest of cases.
- Relatively low resolving power [21].

2.1.2 Photon Correlation Spectroscopy (PCS)

This method is only applicable to relatively small particles suspended in a liquid, which are in a state of random movement. The motion of the suspended particles is inversely proportional to the particle size (the smaller the

particles are, the faster they move, or diffuse) [22]. When light hits small particles, the Rayleigh scattering occurs (the light scatters in all directions) so long as the particles are small compared to the wavelength (below 250 nm). If the light source is monochromatic and coherent (such as a laser beam), then a time-dependent fluctuation in the scattering intensity can be observed due to Brownian motion. This scattered light then undergoes either constructive or destructive interference by the surrounding particles and within this intensity fluctuation, information is contained about the time scale of movement of the scatterers. The movement can be discerned by analysing the time dependency of the light intensity fluctuations. As the near-order of fine particles dissolves faster than the near-order of coarse particles, the particle size can be deducted. The average size of the particles (between few nm to 3 μm) can be accurately determined and some information about the size distribution can be calculated [23].

Advantages

- A minimum amount of information about the sample is needed to perform an analysis. Even mixtures of different materials can be accurately measured; only the viscosity of the medium must be known accurately.
- It is possible to measure very small particle size.
- The analysis is relatively fast and simple.
- Testing is non-destructive, so samples can be recovered if needed.

Disadvantages

- Extremely low resolution

- Only small particles (with significant Brownian motion) can be measured, all larger particles are beyond the instrument's range [22].

- Any contribution of multiple scattered light leads to erroneous PCS results and misinterpretations. As a consequence, PCS requires highly diluted suspensions in order to avoid multiple scattering.

2.1.3 Back-scattering Spectroscopy

A powerful light beam (laser) is directed into a mixture of particles, and the angular intensity distribution of light scattered backward, at high angles, is measured. This technique is complementary to LALLS, where the scattered light is at "low angles", close to the original beam direction. Again, elaborate light scattering calculations are applied to the scattering data to generate a particle size distribution. Back scattering is often used with samples containing a high concentration of particles that cannot be diluted without changing the size distribution [24].

Advantages

- Can measure samples that are highly concentrated when compared to most other sizing methods, including on-line measurements of particles (if there is an optical window available).

- Relatively simple operation. No sample preparation needed. Non-invasive/non-destructive test method.

Disadvantages

- The particle size distributions are low resolution, even compared to LALLS. Multiple scattering from high concentration samples affects potential resolution.
- The optical properties (refractive index/absorption) and shape of the particles must be known to generate accurate results.
- It is not a very sensitive technique. Concentrations below 0.1% are not detected.
- Strongly absorbing particles can present problems because they may not produce a usable scattering signal.

2.1.4 Infrared spectrometry

Infrared (IR) spectroscopy deals with the IR region of the electromagnetic spectrum [25] with wavelengths ranging from 0.8 to 1000 μm. It covers different techniques and can be used to identify a compound and the composition of a sample. IR spectroscopy measures the wavelength and intensity of absorption of IR light by a sample. When light at a specific wavelength is directed towards a sample, some of that light will be reflected, some will be absorbed by specific molecules and some will be transmitted through the sample. The proportion of light falling into each of these categories will depend largely on the wavelength chosen and on the nature of the sample [26]. An IR spectrophotometer can measure the particle size of nano-particles in high-solids content dispersions. It compares the light reflected or transmitted by samples at specific points in the IR spectrum. Typical applications include particle-size measurements during granulation and blending processes.

This is achieved by integrating measurement strategies in relation to their wavelength in the visible spectrum, fundamental light propagation models and multivariate statistical modelling techniques.

The IR portion of the electromagnetic spectrum is divided into three regions; the near-, mid- and far- infrared, named for their relation to the visible spectrum.

- The higher energy near-IR (NIR), can excite overtone or combinations of fundamental absorptions. The wavelength range of the NIR is approximately 0.8 - 2.5 μm. NIR spectroscopy involves the absorption of near-infrared light by a sample. The infrared absorption spectrum of a substance is sometimes called its molecular fingerprint. Although frequently used to identify materials, infrared spectroscopy also may be used to quantify the number of absorbing molecules [27].

- The mid-infrared (MIR) may be used to study the fundamental vibrations and associated rotational-vibrational structure. The wavelength range of the MIR is approximately 2.5 50 μm. This is the region of most interest for chemical analysis which corresponds to changes in vibrational energies within molecules.

- The far-infrared (FIR), with the wavelength range of 50 1000 μm, lying adjacent to the microwave region, is useful for molecules containing heavy atoms such as inorganic compounds but requires rather specialised experimental techniques. Hence this regime will not be discussed further in this Thesis.

NIR advantages

- Sample preparation is simple.
- Analysis is rapid in that each sample spectrum is derived within a few seconds and several different constituents can be estimated from the same spectral measurements.
- Generally good signal to noise ratio (SNR).
- Testing is non-destructive.
- Offers advantages of low-cost and low-power consumption.

NIR Disadvantages

- As NIR absorptions are weak, a long sample (of order of mm) path-length is required if concentrations are low.
- Liquid phase spectra are dependent upon temperature.
- A high water concentration can obscure other species in the spectrum.
- Multivariate techniques needed.

MIR advantages

- Sample preparation is simple.
- Features are fundamental and distinct.
- Good SNR.
- Testing is non-destructive, so samples can be recovered if necessary.

MIR Disadvantages

- Requires tailored and expensive optical elements [25].
- Liquid phase spectra are dependent upon temperature.

2.2 Passive acoustic monitoring techniques

Passive ultrasonics is also known as active acoustic emission (AE) [28] where the source of acoustic energy is the process itself. Generally AE relates to the noise generated by natural process arising from changes in its physical, chemical or environmental parameters. Collisions of particles among themselves and with the walls of a vessel, cavitations, boiling, and other chemical reactions are some of the main sources of acoustic energy in a process [18]. In the context of passive acoustic monitoring, the sources of sound monitored during the process are mainly collisions of particles with the wall of the vessel and stirrer; other sources of AE exist but may not be detectable [29][30]. Most processes emit sound that is not audible to the human ear (above 20 kHz); hence a broadband acoustic sensor with high sensitivity is used to discern this acoustic fingerprint, which can often be related to the properties of the process under investigation [31].

Leach, Rubin and William [32] first described an innovative method for measuring the size and size distribution of rigid spheres. Their acoustic measurements were performed using a commercial microphone positioned close to a rotating vessel containing glass and steel spheres of known size distribution. The collision and vibration of particles striking upon each other cause acoustic emission (AE) events. Different modes of vibration are possible and the frequency of each mode is related to the shape and the size of the par-

ticles and their acoustic properties. In particular, when two rigid spheres of different sizes collide against each other they emit AE signals at frequencies related to the acoustic mean of their fundamental frequencies. The reciprocal of the mean frequency of the beat patterns increased linearly with the average diameter of the rigid spheres and hence average particle size could be estimated [32][33].

Acoustic emission has been employed successfully in a process environment for monitoring of crystallisation [19] [34]. Bourchard and Szyszko [19] used a piezoelectric transducer mounted on a probe of a reactor vessel to monitor a batch crystallisation process. AE was generated by glass ballotini of known sizes colliding against a simulated temperature probe (steel rod). Important parameters like the pulse count rate and total acoustic noise were monitored in the acoustical signal. It was initially demonstrated that the pulse count rates increased with increasing particle size and increasing mass. Moreover the state of the crystallisation process was estimated using neural network modelling. This provided a reasonable agreement with the experimental results. It was emphasised that for industrial applications, the network would have to be trained using data from the system where it is to be installed [31].

Methods of measuring the state of granulation processes were also investigated [13] [14] [35]. In particular, Whittaker and Baker [13] reported on-line determination of particle size, flow properties and compressional properties of a high shear granulation process. Monitoring particle size changes during granulation is important as flow and compressional properties are influenced by particle size. The acoustic data were collected using three piezoelectric AE sensors (Physical Acoustics UK) covering frequencies from 20 to 350 kHz,

with main resonances at 30, 70 and 150 kHz. These transducers were attached to the outer wall of the high shear mixer bowl. For each batch and each piezoelectric sensor, the spectral data recorded from the previous 20 s of the granulation process were averaged out before comparison with the physical properties, using partial least squares (PLS) multivariate analysis. A linear trend was obtained between the frequency spectrum of the acoustic data and the physical property of the granule before dry screening, although, after dry screening of the granule, the quality of the relationship degraded. It was, therefore, possible to relate AE from the granulation process to the final flow properties of the powder.

Friesen and Brusewitz [36] proposed the passive acoustic measurement as a method of measuring the moisture content in grains (wheat, corn, soybeans) flowing from the bottom of a silo onto a pile of grain. The sound pressure level was found to increase as the moisture content of the grain decreased. The variation between sound pressure level and moisture content was also dependent on the type of grain under investigation.

A few application studies of particle suspensions have assessed the source of the AE [12]. However, several simulation and theoretical studies have successfully modelled AE from particle impacts [29][33][37].

For example, in studies where the source of AE was the impact of a rigid object with a large surface, the emission frequency was inversely proportional to the size of the impacting object [38][39].

Papers of note include work by Thorne [40][41][42] where it was observed that the AE frequency decreased as particle size increased for particle-particle collisions of spheres. The amplitude of the acoustic emission from collisions between glass spheres of known diameter increased as the number of spheres

increased [41]. However, the frequency information of the ultrasonic spectra collected was independent of the number of impacting objects [29][41].

Tily, Porada, Scruby and Lidington simulated mixing of two solids in an orbital mixer [35]. The root mean square (RMS) of the acoustic voltage signal was followed over time for several mixtures and it was found that the mixing end point could readily be recognised when the AE signal became constant. Furthermore, the amplitude of the emissions increased with increasing size and mass of the particles involved. When the AE signal is converted to RMS values, the frequency information is lost but it is still possible to obtain information relating to e.g. particle size, particle concentration and flow rate signals using multivariate regression techniques [30]. Nevertheless, the separation of particle size and particle concentration from the RMS signals has proven difficult as the effect of a change in either factor is the same; e.g. an increase in particle size or concentration causes an increase in signal amplitude [4][17].

Despite these experimental and theoretical studies, AE has not been used to estimate both particle size and particle concentration for industrial processes [43].

2.3 Active acoustic measurements techniques

2.3.1 Velocity and attenuation techniques

It is possible to employ ultrasonic spectroscopy to obtain information about the concentration and size of particulates suspended in a liquid.

Monitoring of particle size using ultrasonic spectroscopy involves two steps: firstly, it is necessary to measure the attenuation coefficient and the

ultrasonic velocity over a wide range of acoustic frequencies, typically between 0.1 and 200 MHz, which enables the analysis of particles with a radius between about 10 nm and 1000 μm [44]. Secondly, these measurements are converted into a particle size distribution using a suitable mathematical model [45].

The attenuation and velocity are ruled by interactions between the acoustic wave and the particulate suspension e.g. reflections, transmission, absorption and scattering [8].

It is possible to define the ultrasonic velocity v and the attenuation coefficient α as follows:

- The ultrasonic velocity is the distance that the ultrasonic wave propagates through the sample per unit time [46]. The ultrasonic velocity can be determined by measuring the time, t, taken for a pulse of ultrasound to propagate a known distance, D:

$$v = \frac{D}{t} \tag{2.1}$$

  or measuring the wavelength of an ultrasonic wave, λ, at a known frequency, f:

$$v = \lambda f \tag{2.2}$$

- The attenuation coefficient is determined by measuring the decrease in amplitude of an ultrasonic wave through a known distance D in a specific material

$$\alpha = -\frac{1}{D} \ln \frac{A_D}{A_o} \tag{2.3}$$

  where A_o is the initial amplitude of the ultrasonic wave, and A_D is the

amplitude after it has travelled a distance D.

The experimental methods employed to determine the frequency dependency of the ultrasonic properties of particles in fluids can be divided into three categories: *pulse-echo, through transmission and interferometric*. The major differences between these techniques is the nature of the ultrasonic input signal applied to the sample (*sinusoidal wave, tone-burst pulse, broadband pulse*), and the experimental approach used to assess the measurements as shown in Figure 2.1 and Figure 2.2, respectively [47].

Through-transmission techniques

The sample to be analysed is poured into the measurement cell so that it is placed between two ultrasonic sensors, one which acts as a generator (G) and the other as a receiver (R) (as shown in Figure 2.2a). The generating transducer produces a pulse of ultrasound that travels across the sample and is detected by the receiving transducer. The ultrasonic velocity and attenuation coefficient of the mixture are calculated by measuring the time-of-flight t and amplitude A of the ultrasonic pulse that travels across the sample [47].

Two input signals are available for this technique: the *broadband pulse* or the *tone burst* (See Figure 2.1).

When a *broadband pulse* (single pulse which contains a wide range of different frequencies) is employed as an excitation signal, a Fourier transform algorithm can be used to determine the value of t and A as a function of frequency [46]. To cover a wide frequency range three or four ultrasonic transducers with different resonant frequencies are typically used.

In the second approach, an ultrasonic *tone-burst* is used. The *tone burst* is

a single pulse which contains a number of cycles of ultrasound at a particular frequency. The ultrasonic transmitter is tuned to a particular frequency, and velocity and attenuation measurements are performed. The sensor is then tuned to another frequency and the process is reiterated. This approach is more time consuming than one that uses broadband ultrasonic pulses.

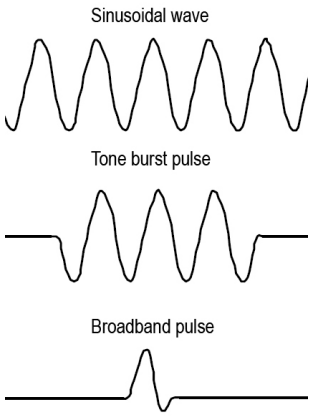

Figure 2.1: Different types of ultrasonic input signals.

Pulse echo-techniques

The frequency-dependent ultrasonic properties of the sample are measured in almost exactly the same way using this technique as the *through-transmission* method, except that a single transducer is used to both generate and receive the ultrasonic pulses [15]. The ultrasonic sensor fires a pulse of ultrasound which travels across the sample, is reflected from the back wall of the measurement cell, travels back through the sample and is then detected by the same transducer [37]. Velocity and attenuation coefficients are computed in exactly the same way as described for the *through-transmission* technique, except that the input pulse has now (obviously) propagated a distance $2D$ rather than D [47].

Interferometric techniques

Again the signal generator produces a sinusoidal signal of tailored amplitude and frequency that is applied to the ultrasonic transducer to be converted into an ultrasonic wave. This wave propagates into the sample and is reflected back and forth between the transducer and reflector plate, which results in the formation of a standing wave in the heterogeneous mixture. When the distance between the transducer and reflector plate is varied the amplitude of the signal received by the transducer goes through a series of maxima and minima owing to constructive and destructive interference, respectively. The distance between successive maxima (ΔD) is equal to half the ultrasonic wavelength of the sample ($\lambda/2$), and so it is possible to deduce the velocity: $v = f\lambda = 2f\Delta D$. The amplitude of the maxima decreases as the distance between the reflector plate and sensor is increased because of attenuation by the mixture. The attenuation coefficient is calculated by measuring the amplitude of the maxima as a function of the separation between the reflector plate and the transducer for both the sample and the calibration material [48].

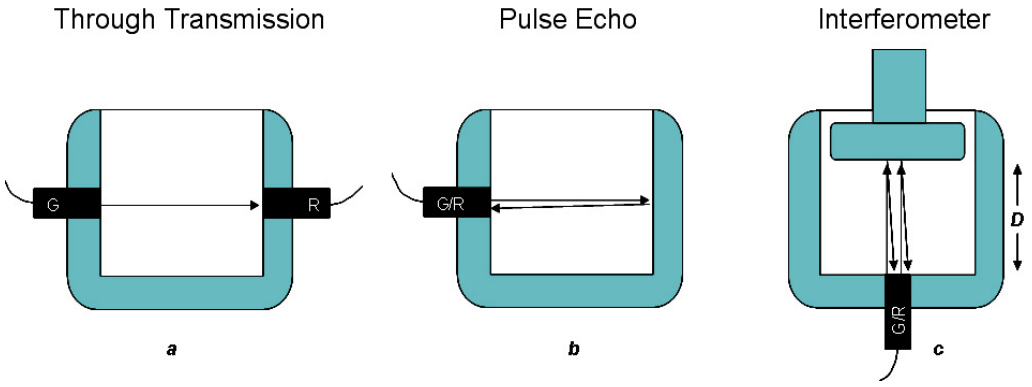

Figure 2.2: Measurements cells for determining the ultrasonic properties of heterogeneous mixtures as a function of frequency.

2.3.2 Commercial instrumentation

Available instrumentation employing passive acoustic techniques include instrumentation for process monitoring such as the GranuMet XP [49], the SITRANS AS 100 [50] or the Senaco AS100 [51] for bulk solids flow detection. For example, with the GranuMet XP [49] is possible to detect the high-shear granulation at the end of the process. This it is based on the fact that variations in particle size obtained during granulation will influence powder flow and compression properties. As particle size will affect the AE, this monitoring technique is likely to prove useful in assessing changes in the relevant physical properties of the particles.

Certain systems such as the HR-US by Ultrasonic Scientific [52] or DT-100T by Dispersion Technology [53] or Ultrasizer by Malvern Instruments [54] utilise velocity and attenuation techniques for measuring both the disperse phase volume fraction and particle size distribution of suspensions in a few minutes [15].

The high-resolution HR-US family of ultrasonic spectrometers is an example of the commercially available instrumentation for particle characterisation using active acoustic techniques.

The HR-US 101 device is equipped with 10 mL ultrasonic cells which allows stirring of the sample and can also accommodate aggressive liquids. With the HR-US 101 it is possible to determine concentrations of components, transition temperatures and temperature intervals, sizes of particles in suspensions kinetics of chemical and physical processes in materials, and other parameters of their samples [55].

The high resolution spectrometer performs analyses by measuring ultrasonic attenuation and velocity of the sample with resolution down to 1-5%.

This can be achieved under controlled temperature conditions (down to 0.01 $^{\circ}C$) and frequency range of 0.1-200 MHz. Its high resolution makes it possible to perform measurements in solutions of small concentration, typically about 1 mg/mL scale.

In general ultrasonic spectroscopy instruments are sensitive to particles with radius between 10 nm and 1000 μm and particle concentrations between about 5 and 40 wt% depending on the nature of the system. On the other hand, the technique is unsuitable for analysing dilute suspensions, i.e. particle concentrations below about 1 wt%. The other major limitations of the spectrometers are that the physical properties of the component phases are needed to interpret ultrasonic spectra and micro-bubbles of air can interfere with the measurements [37]. Importantly, the vast majority of instruments for particle size characterisation are for off-line laboratory use [56]. Hence, there is an industrial need for in-line non-invasive ultrasonic monitoring techniques for the characterisation of particulate suspensions.

2.4 Theories of ultrasonic propagation in heterogeneous mixtures

When an ultrasonic wave is propagating through a medium (including an ensemble of particles), a range of physicochemical processes occur [57]. These mechanisms assume different forms, comprising *absorption* of the ultrasonic energy due to viscous flow and *thermal conduction*; *scattering* of the wave into various directions, and *interference* between the waves that travel directly through the surrounding liquid medium (called the component phase). A knowledge of the interactions between the ultrasonic waves and the par-

ticles immersed in the fluid is necessary to understand how ultrasound can be employed to determine the size and concentration of particles [45]. This Section attempts to review the most important theories of wave propagation in order to understand the active acoustic experimental results obtained for different mixtures of chemical particles suspended in water presented in Chapter 6.

2.4.1 Urick's equation

When an ultrasonic wave propagates into a liquid medium containing solid particles, the variations of solids and/or gas bubble concentration inside the liquid will change the density as well as the compressibility of the medium and consequently the speed and the attenuation of the acoustic signal. In principle, accurate measurements of the variations in velocity and attenuation of the acoustic wave will indicate the nature of the mixture.

In 1947, Urick [1] used an ultrasonic interferometer for measuring the adiabatic compressibility of suspended particles in a liquid. He assumed an effective density and an effective compressibility of the sample by taking a weighted volume average of the densities and compressibilities of the two phases (solid and liquid parts of the medium) with the sound velocity found from the Wood's Equation [58]

$$v = \frac{1}{(\rho_{eff}\beta_{eff})^{1/2}} \tag{2.4}$$

where ρ_{eff} and β_{eff} are the effective density and compressibility respectively, of the mixture. The Equation uses averaged values of density and compressibility:

$$\rho_{eff} = \rho_S \phi + \rho_L (1 - \phi) \tag{2.5}$$

$$\beta_{eff} = \beta_S \phi + \beta_L (1 - \phi) \tag{2.6}$$

where ϕ is the volume fraction of the solid phase and the subscripts *'S'* and *'L'* correspond to the solid and liquid phase respectively. Urick demonstrated the validity of the these formulae by conducting measurements of a suspension of kaolin particles (1 to 10 μm) in water at a driving frequency of 1 MHz.

Urick found a parabolic relationship between the ratio of the sound speed in the mixture with respect to that of the volume fraction of the continuous phase (in Figure 2.3). Unfortunately, Urick's theory is limited when the effects of scattering, thermal and viscous losses are dominant (e.g. at high dispersed phase concentration). However, Urick's experimental work with kaolin were in agreement with theory for concentrations up to 10% for any given frequency up to 15 MHz [59].

2.4.2 Ultrasonic scattering

Another important effect to consider about the propagation of ultrasonic waves through heterogeneous mixtures is scattering. Mathematical analysis of one particle scattering is well understood and there is excellent agreement between theory and experiments [60][61]. One of the first models and most rigorous mathematical formulation to explain the scattering of an ultrasonic wave in dilute systems was developed by Allegra and Hawley [57]. The model described a single isolated particle immersed in an infinite continuous medium, and considered lossless scattering, as well as thermal and viscoinertial

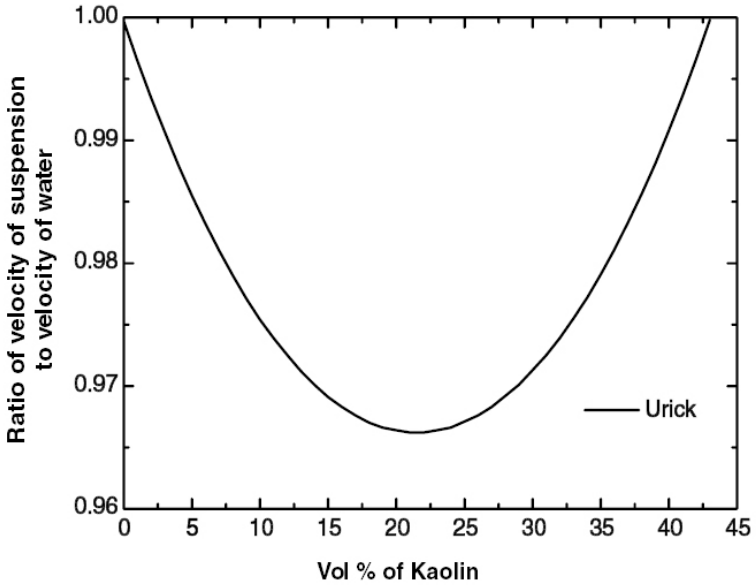

Figure 2.3: Velocity of sound in a suspension of kaolin plotted versus dispersed phase volume fraction, following Uricks method [1].

losses. As there was no effect from neighbouring particles in the analysis, a relatively simple stress-strain relation was employed, which allowed for an analytical solution of the problem.

Waterman and Truell [62] extended this theory for a set of scatterers (particles) distributed in a fluid by developing a theory of multiple scattering to predict the complex wave number of the effective medium.

A comprehensive overview of the theory of scattering of ultrasound is given by Challis et al [20]. This Section reviews the most important theories in this area.

The ultrasonic properties of multiple scatterers are described in terms of a complex propagation constant (K);

$$K = \frac{\omega}{v} + i\alpha \tag{2.7}$$

where α is the attenuation coefficient of the scattering material, ω is the angular frequency ($\omega = 2\pi f$) and v is the classical acoustic velocity [57]. In 1961, Waterman and Truell provided one of the most used scattering theories [62] derived from Allegra's findings:

$$(\frac{K}{k_1})^2 = 1 + \frac{4\pi N f(0)}{k_1^2} + \frac{4\pi^2 N^2}{k_1^4}[f^2(0) - f^2(\pi)] \tag{2.8}$$

where

$$f(0) = \frac{1}{ik_1}\sum_{n=0}^{\infty}(2n+1)A_n \tag{2.9}$$

$$f(\pi) = \frac{1}{ik_1}\sum_{n=0}^{\infty}(-1)^n(2n+1)A_n \tag{2.10}$$

f(0) and $f(\pi)$ represent the far-field scattering intensities of the waves scattered from individual spherical particles, N is the number of particles per unit volume and k_1 is the complex propagation constant of the continuous phase. The scattering coefficients of different types of waves scattered from the individual particles are include in the A_n terms, e.g. monopole *(A_o)* or dipole *(A_1)*, quadrupole (A_2) etc. Approaches for calculating the scattering coefficients are available in the literature [9][57]. The relative thermophysical properties of the component phase together with the ultrasonic frequency used and the size of the emulsion particles influence the relative values of the scattering coefficients.

The terms containing N in Equation 2.8 account for the direct scattering effects, whilst those containing N^2 account for multiple scattering effects. Multiple scattering becomes dominant as the concentration of particles in the mixture increases but it becomes more difficult to describe mathematically. Further work is needed in this area before ultrasound can be used to provide

quantitative information about the nature of particle-particle interactions in media with high concentration of particles, or before these interactions can be adequately accounted for in the existing multiple scattering theories [44][47].

2.4.3 Simplified mathematical models

As mentioned previously, the interactions between an ultrasonic wave propagating in mixtures containing chemical particles are complex, involving various forms of scattering, diffraction, absorption, reflection, and resonant behaviour [63]. This accounts for the complexity of the mathematical theory.

However, under certain physical situations reported by McClement [59], the number of physical and chemical interactions involved in the study are reduced and the mathematical description of the propagation of an ultrasonic wave can be simplified significantly. In practice, it is convenient to divide the wave propagation in mixtures into three categories depending on the relationship between the radius (r) of the particle versus the ultrasonic wavelength.

- The long wavelength regime (LWR): $r \ll \lambda$
- The intermediate wavelength regime (IWR): $r \sim \lambda$
- The short wavelength regime (SWR): $r \gg \lambda$

Ultrasound can be employed to characterise the size of large particles ($>$ 1 mm) in the SWR, but ultrasonic imaging, rather that ultrasonic spectrometry, is preferred in this regime [47]. For this reason, only ultrasonic analysis of mixtures in the LWR and IWR will be considered in the active acoustic work.

2.4.4 Long wavelength regime

In the LWR there are different interactions between ultrasonic waves and particles. The most important are:

Intrinsic absorption

The intrinsic ultrasonic absorption of a composite mixture is the volume average of the absorption contribution from each of the individual component phases. The propagating compression wave travels through the suspended particle and the liquid phase, and will be influenced by diffraction effects at particle borders and the impedance mismatch at the boundary between the particle and the continuous phase. Intrinsic absorption is independent of particle size.

Compressibility and density contrast (visco-inertial losses)

The propagation of ultrasonic waves through a liquid causes coherent oscillations of local pressure which determine local expansion and compression of the liquid phase as the wave energy is stored elastically and subsequently released in a kinetic form. The suspended particle is also subjected to the same pressure oscillations, hence it compresses and expands accordingly. Figure 2.5 shows the effect of ultrasound on a particle that is more compressible than the surrounding liquid; the particle contracts or expands by a greater or smaller volume than the continuous phase in the same region. Consequently, this cyclic flow causes a loss of wave energy through friction.

Each particle behaves as a local radiator of sound tuned to the same frequency as the incident wave. When a spherical particle is small compared to the sound wavelength then, as represented in Figure 2.6, the local field

around the particle will be analogous to that of a simple monopole source. This process known as *monopole scattering* refers to the ultrasonic energy being scattered in different directions.

Moreover, the presence of the ultrasonic wave also causes oscillations of the particle backwards and forwards, this is due to the different densities between the particle and that of the surrounding fluid. Oscillations of this type lead to the generation of a scattered wave which radiates in the same plane as that of the original wave: this process is referred to as *dipole scattering*, again represented in Figure 2.6. The viscosity of the surrounding liquid damps this oscillation, causing some of the ultrasonic energy to be converted to heat, and therefore leads to a reduction in the intensity of the ultrasonic wave. Obviously, the magnitude of these visco-inertial losses increases as the density difference between the particle and the continuous phase liquid increases [64].

Importantly, Equations 2.8 to 2.10 can be simplified because the effects of compressibility and density of heterogeneous mixtures in the presence of an ultrasonic field are contained in the *scattering coefficients* A_0 and A_1 respectively. All higher order scattering coefficients are negligible in the LWR.

$$(\frac{k}{k_1})^2 = 1 - \frac{i4\pi N(A_0 + 3A_1))}{k_1^3} - \frac{48\pi^2 N^2 A_0 A_1}{k_1^6} \tag{2.11}$$

In addition, an explicit analytical expression for the A_0 and A_1 terms can be employed in the LWR, rather than having to solve the full set of complex linear simultaneous equations needed in the general solution [59].

Thermal dissipation losses

Propagation of ultrasound through a heterogeneous mixture of particles in a fluid, also affects temperature. In fact, the temperature of the particle periodically decreases and increases relative to that of the surrounding liquid because of differences between the thermal conductivities and thermal expansion coefficients of the material that constitute the two phases [46].

Figure 2.7 represents energy losses through thermal dissipation. The propagation of the ultrasonic wave produces local heating and cooling of the material in the wave path. The result is that heat will flow between the particle and the fluid. Moreover, as mentioned previously, the oscillating wave pressure causes differential expansion and contraction between the two phases causing acoustic re-radiation in the form of a monopole field. In addition, heat flows away from the particle resulting in loss of energy from the acoustic wave. Thermal dissipation losses could depend on the size of the particle [61].

In conclusion, to a first approximation, these interactions decrease the amplitude of the propagating wave within the mixture and the overall attenuation can be considered to be the sum of these various contributions (although in reality some of these mechanisms are coupled to each other). In particular, attenuation can be suitably divided into four contributions: intrinsic absorption (α_I), scattering losses (α_S), visco-inertial absorption (α_{VI}) and thermal absorption (α_T)

$$\alpha_{total} = \alpha_I + \alpha_S + \alpha_V + \alpha_T \tag{2.12}$$

Mathematical expressions for the different terms can be found in the litera-

ture [59].

Importantly, at relatively low frequencies, the visco-inertial and thermal loss mechanism are usually predominant, while at higher frequencies intrinsic absorption and scattering losses become dominant and are considered the main form of attenuation when approaching the IWR [47].

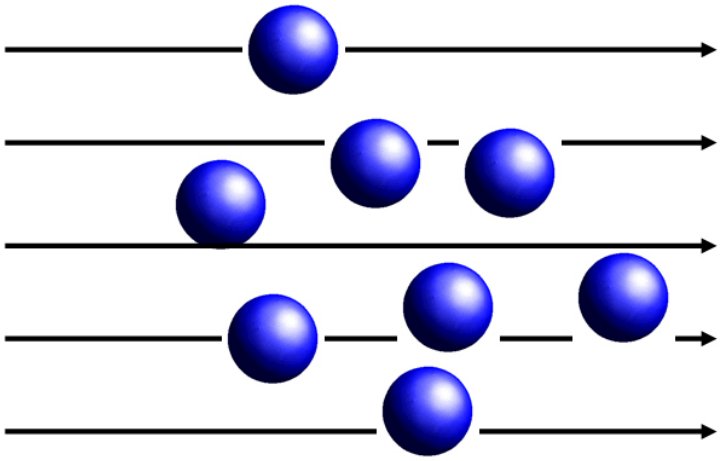

Figure 2.4: Intrinsic absorption represented by some parts of the wave propagating through particulate material as well as through the continuous phase

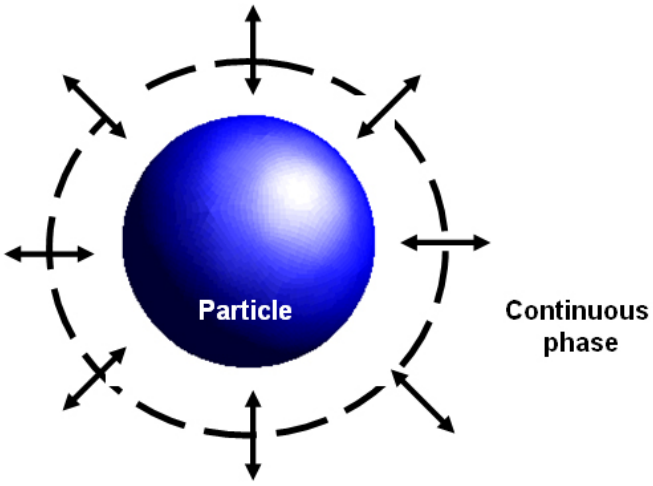

Figure 2.5: The expansion and contraction of the particle with respect to the continuous phase as result of cyclic local pressure variation in the wave.

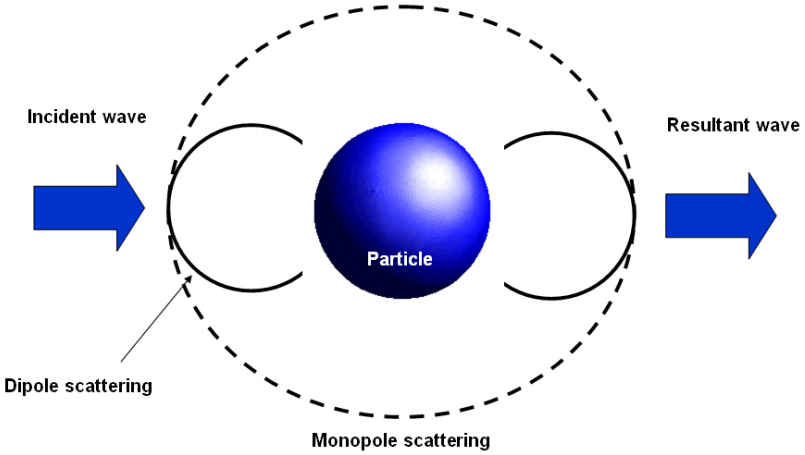

Figure 2.6: Oscillations and pulsations effects: pulsations of the particle in a surrounding medium leads to the generation of a monopole wave, whilst oscillation leads to the generation of the dipole wave.

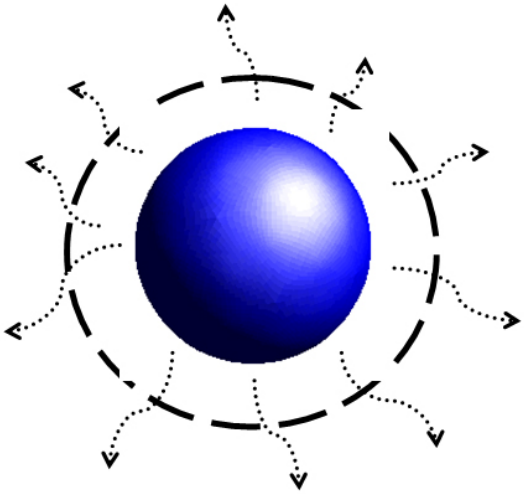

Figure 2.7: The heat flows away from the particle, again with monopole field geometry, resulting in energy loss from the acoustic wave

2.4.5 Intermediate wavelength regime

In the IWR, the interactions between ultrasonic waves and solid particles are more complicated, and many different types of scattered waves are generated. Consequently, it is necessary to include many more scattering coefficients (A_n) in the calculation of the ultrasonic properties of the heterogeneous mixture, than the two (A_0 and A_1) required in the LWR (Equation 2.8) [20].

Approaches for calculating the scattering coefficients of both fluid and solid particles are available in the literature [57][62][9].

The most rigorous approach calculates the A_n terms by solving a series of 6x6 complex linear simultaneous equations at each value of n [57][62][9]. In the IWR the A_n number of terms can reach 60 and the determination of the A_n can be very complicated. In order to calculate the scattering coefficients, the values for a number of thermophysical constants are required for each phase, and these are given for the constituents of the model system. In fact, the number of A_n terms required for computing the ultrasonic properties of a mixture depend on the thermophysical properties of the component phases, the ultrasonic frequency employed and the size of the emulsion droplets.

McClements [59] simplified these calculations and he found that the number of A_n terms required at each frequency can be found by incrementally increasing the value of n until the complex propagation constant k does not change any more [20]. The theory states that as the particle size increases relative to the ultrasonic wavelength, the attenuation coefficient increases until it reaches a maximum when $r \sim \lambda$. Above this value the attenuation coefficient decreases, and at a high ratio of r to λ it becomes negligible. Also the ultrasonic velocity decreases dramatically when $r \sim \lambda$ until it reaches a constant value (equal to the velocity in the pure continuous phase) at a high

ratio of r to λ. Consequently, the ultrasonic properties of heterogeneous mixtures are particularly sensitive to particle size in the region of $0.1 < r/\lambda < 50$ in the IWR [65].

2.5 Practical and theoretical limitations of the acoustic methods

Having mentioned the advantages of employing acoustic measurement techniques, it is essential to consider some of the disadvantages of these monitoring methods. The first is the common limitation to any single frequency instrument. A single frequency instrument cannot differentiate between a change in particle size distribution and concentration. Another factor that has limited the widespread use of active acoustic spectrometry for characterising heterogeneous mixtures is the need to know the acoustic properties of the medium being analysed. This information includes: density, ultrasonic velocities, viscosity, specific heat capacity, thermal expansivity and attenuation coefficient [8].

Moreover, air bubbles can interfere with ultrasonic measurement techniques. Gas bubbles are very strong scatters of ultrasound and so if present (even at low concentrations) the ultrasonic signal can be severely attenuated [66]. Changes in the ultrasonic signal on addition of $< 0.5wt\%$ particles to a liquid is of the same order of magnitude as the experimental measurement error (below the detection limit) [59]. On the other hand, ultrasound techniques also have limited application to very concentrated systems ($> 40wt\%$). Clearly, ultrasonic waves can propagate through these concentrated solutions, but the theories which describe the ultrasonic properties of the particle size

distribution are limited due to the complexity of the mathematical models [47].

In general, ultrasonic spectrometry is more useful for characterising concentrated or optically opaque materials, whereas light scattering measurements are preferable for dilute mixtures and emulsions ($\phi < 0.5wt\%$) [20]. At the present time many optical and acoustic methods are available for the characterisation of particulate suspended in fluids [65]. All of the techniques reviewed in the previous paragraphs, however, are affected by limitations that render the methods ineffective in some applications or for certain particles.

Different approaches employing passive and active acoustic monitoring techniques are needed to overcome some of the limitations mentioned above. In particular, techniques for deriving the changes in both particle size and concentration from the broadband acoustic emission signals have not been deeply investigated. Ideally, these methods should also be not-invasive. Non-invasive acoustic methods are valuable for process analysis as, in principle, an acoustic sensor can simply be attached to the external wall of process vessel under investigation. The transducer is not in direct contact with the sample and, hence no contamination occurs [13]. Moreover, the extracted AE signals are also dependent on the frequency range of the transducer and the data acquisition approach adopted [19]. Generic broadband transducers are often employed without knowing exactly the real frequency range of interest of the process under investigation. Ideally, the sensor should be customised for each process.

In the first part of this work, a novel method to study the generation

of acoustic emission (AE) signals through chemical particles striking against the inner wall of a vessel reactor will be presented. The approach will lead to the prediction of vital information for the design of a non invasive passive acoustic system employing a customised sensor. Estimations of both particle size and concentration information will also be conducted.

In the second part of this research the active acoustic method will be investigated. Active acoustic spectrometry is widespread in the laboratory for the discrimination of particle size [7]; this has been developed over the last twenty years mainly for laboratory applications, unfortunately there are few reported examples of applications in a process environment [12]. The reason why the USS has been not transfer from the laboratory to the process more quickly is due limitations of electronics and digital signal processing. Only, recent developments in electronic systems and DSP techniques have increased the capabilities of the USS method to enable it to be viable on a wider range of applications which makes it a more suitable process sensor. Moreover, process sensors for viscous liquids, high concentration and soft colloids are difficult to implement using traditional analytical techniques as the complex nature of the materials renders it difficult to handle, dilute or measure the sample. In the majority of cases the sample must be measured off line using manual methods with significant sample handling and preparation in the laboratory.

Any received ultrasonic signal from an acoustic process is influenced by the container and additional instrumentation. This effect can mask the weak interactions between the ultrasound and the reaction of interest. A system capable of extracting only the physical information of the particulate sus-

pension the vessel without the acoustic signature of the container is very challenging to achieve but potentially more information could be extracted from the process under investigation.

Naturally the active acoustic methods can be less practical than the passive techniques, where the sensor is installed on the outside of the vessel wall and it does not require access into the vessel. The active method can be intrusive because it may requires the probe presence (for sampling or measurement) inside the vessel tank. However, the active acoustic techniques are still attractive for process investigation, monitoring and control [11] because the process information may be figured out from a dynamic system *in situ* and in real-time;

Preliminary investigations will be performed into the ultrasonic-particle interactions in water, employing a range of active acoustic techniques. The aim is to evaluate the generation of linear and non-linear responses from stable particles suspended in a fluid medium. Harmonic signals from the backscattered data of a heterogeneous mixture is the first step for discerning the information between the container and the reaction under analysis. In theory, only the particles inside the container will resonate at these harmonic frequencies. These frequencies are different compared to the natural resonance frequencies of the container. In the non-linear regime, the concept of using the second harmonic response, which may be attributable directly to the particles themselves, opens a new way of implementing an ultrasonic techniques for process monitoring. The approaches of employing the passive and active acoustic techniques presented in this Thesis will propose new ideas for in-situ process monitoring.

Chapter 3

Passive acoustic monitoring of a heterogeneous system

The investigations to quantify the size and concentration of particles in heterogeneous mixtures begin with the passive ultrasonic monitoring approach.

This Chapter will illustrate the previous research study at Strathclyde University from a model heterogeneous system and its limitations. From these, the motivations of the research programme will be disclosed. These will be tackled in the subsequent Chapters with a novel approach to develop a complete passive acoustic system.

3.1 Experimental setup of the passive acoustic system

Work conducted through a collaboration between the Chemistry and Electronic Engineering Departments at Strathclyde University investigated the effects of a number of experimental factors on the broadband AE spectra

obtained from a typical heterogeneous system [17]. The research study elucidated the information content of broadband acoustic measurement and related these to particle size and concentration quantities. Hence, the potential usefulness of this type of measurement for process monitoring and control was evaluated. In this Chapter, the most pertinent results from this work will be presented and used to explain the impetus for the passive acoustic research undertaken for this Thesis.

Figure 3.1 illustrates the experimental apparatus for measuring acoustic emissions (AE) from a heterogeneous system in a reactor vessel. It is a 1 L glass reactor (VWR International, Dorset, UK) incorporating a heating jacket, mechanical stirrer and additional instrumentation, which can be inserted through the ports in the top of the vessel. A Haake heater/chiller was used to maintain the desired temperature of the oil jacket, set to 25^{o}C during the experiments.

Particles of itaconic acid were stirred in toluene to investigate the effects of particle size and concentration on broadband AE signals. The itaconic acid was sieved into three fractions as described in Table 3.1.

Table 3.1: Itaconic acid particle properties

Mnemonic	Particle size distribution [μm]
A	$0 < x \leqslant 251$
B	$251 < x \leqslant 500$
C	$500 < x \leqslant 853$

Each size range was added stepwise, up to 200 g, and stirred into 500 mL of toluene at 250 rpm. The mechanical vibrations from the reaction were converted to voltages by a ceramic piezoelectric transducer bonded onto the reactor vessel. The commercial transducer (Nano30, Physical Acoustics Li-

mited, Cambridge, UK) had a diameter of 7.8 mm, and was specified to operate in the frequency range 150-750 kHz. The transducer was attached to the reactor using silicon-based vacuum grease and heavy-duty adhesive tape. The output of the sensor was amplified through a 2/4/6 pre-amplifier (Physical Acoustics Limited) without any internal filter. The gain of the pre-amplifier was set to 60 dB. An Agilent 54624A oscilloscope (Agilent Technologies, UK) was employed to acquire the AE data and linked to the computer via a general purpose interface bus (GPIB) to a universal serial bus (USB) interface.

The data were acquired, sampled at 2 MHz and saved in binary format; and, all the acoustic signals were imported into Matlab © version 6.5 [67] for analysis. The power spectrum of each signal was calculated and, to improve the signal to noise ratio (SNR), spectra were summed up to give a composite spectrum. Signal area was also computed by added the intensities of the power spectra over the desired frequency range. The effects of particle size and concentration on spectral characteristics were assessed.

3.2 Preliminary experiments results

An example of acoustic emission spectra of different concentrations of itaconic acid in toluene is illustrated in Figure 3.2. The plots show that only signals with frequencies below 380 kHz were detected and, at certain frequency regions (e.g. 30, 100 and 250 kHz) the sensitivity of the response was higher than at other frequencies. The energy for different frequency ranges was computed by calculating the area of the spectrum over the desired frequency range. It was demonstrated that as the concentration of itaconic acid

Figure 3.1: Reactor vessel. 1: Stirrer 2: Transducer 3: Oil Jacket

was increased, the signal increased in all the spectral regions. In particular, the signal area increased linearly with concentration, indicating the presence of a greater number of particle-wall collisions. This effect was in agreement with previous experimental and theoretical studies [29][30].

A typical example of acoustic emission spectra of different *particle sizes* A, B and C at a fixed concentration of 40 $\frac{g}{dm^3}$ of itaconic acid in of toluene is shown in Figure 3.3. When the itaconic acid particles were not present inside the vessel reactor, AE was negligible because the acoustic signals produced by the heater/chiller of the oil, the stirrer and any environmental noise were insignificant. On inspection of the AE spectra, differences in the relative intensities of the spectral features are apparent in the Figure. An increase in particle size causes an increase in emission amplitude, the relative intensities of the signals in the lower frequency regions increase as particle size is increased. This experiment will be replicated and further investigated in the next two Chapters.

The effects of temperature, stir rate and the position of the transducer were also quantified in the research study. Nordon et al [17][56] provide full details of this work.

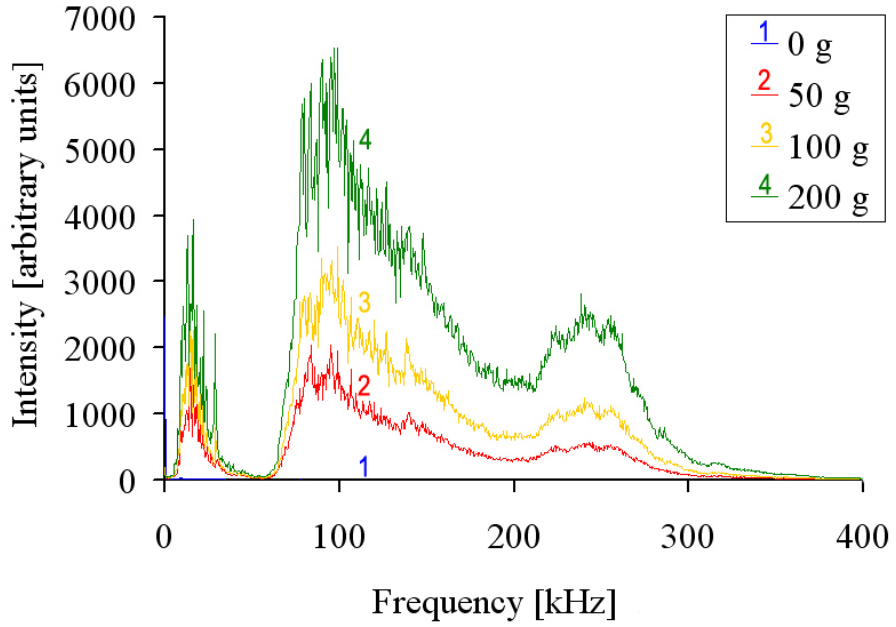

Figure 3.2: Acoustic emission spectra of different concentrations (0, 100, 200 and 400 $\frac{g}{dm^3}$) of unsieved itaconic acid particles

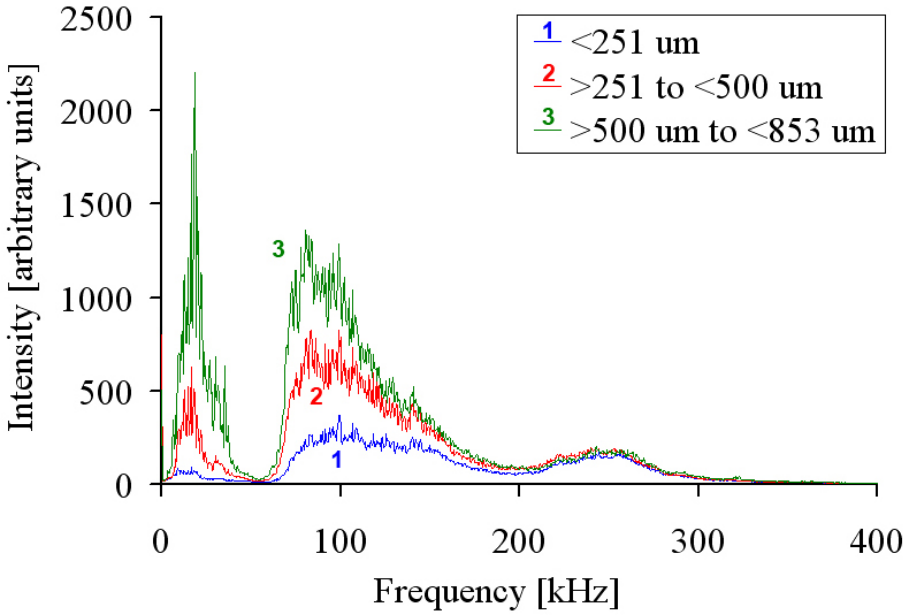

Figure 3.3: Acoustic emission spectra of 40 $\frac{g}{dm^3}$ itaconic acid with A, B and C particle sizes.

3.3 Stimulus for the research programme

The first analysis of the experimental AE spectra showed a number of common features: all the spectra have similar shape and bandwidth, irrespective of the experiment performed. To fully understand this observation, a complete characterisation of the acoustic system was undertaken. In order to characterise the experimental equipment, the inner face of the vessel was excited in front of the acoustic sensor using a simulated AE source through the 'pencil lead break' technique (Hsu-Nielsen source [68][69]).

The author's role on this work was to improve and fully understand the factors which contribute to the AE spectra recorded on a previous research work ([56]). This has been accomplished by characterising the vessel reactor using the Hsu-Nielsen technique, model the container using the FE, validating experimentally the FE model and to develop a new passive acoustic system. The research program was supervised by Prof. Anthony Gachagan, Prof. Gordon Hayward, Prof. Nordon and Prof. David Littlejohn.

The pencil lead break experiment is an aid to simulate an AE emission event using the fracture of a brittle graphite lead in a suitable fitting. The Hsu-Nielsen test consists of breaking a 0.5 mm diameter pencil lead approximately 3 mm (+/- 0.5 mm) from its tip by pressing it against the surface of the piece. This generates an intense acoustic signal, that the sensors detect as a strong burst of energy [69].

Figure 3.4 shows the measured frequency impulse response of the total system when subjected to this evaluation test on the inner wall of the reactor vessel. On comparing the experimental AE spectra of different concentrations and sizes of itaconic acid particles in toluene (Figure 3.2 and 3.3) with this

measured impulse response, the similarity of same profile and common peaks at 110 kHz, 260 kHz and valley at 50 kHz are clearly evident.

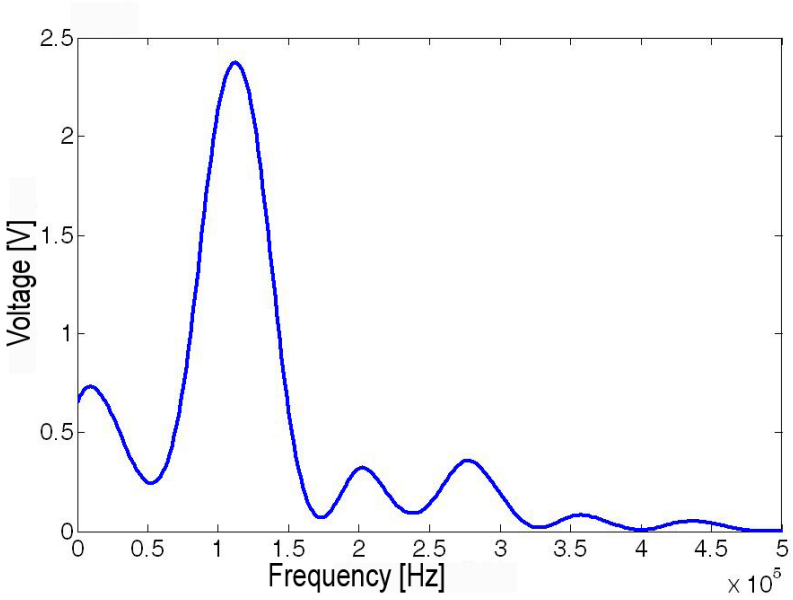

Figure 3.4: Vessel-transducer-amplifier response obtained with the pencil lead test

The impulse response of the commercial Nano30 PZT transducer was also characterised by breaking the pencil lead on the surface of the sensor. Figure 3.5 illustrates the results of this test. The two peaks at 75 kHz and 275 kHz indicate two resonance modes, possibly due to the lateral and thickness mode of the piezo-device. At these frequencies the sensitivity of the transducer is greater than at other frequencies, hence the two peaks contribute to the overall profile of the AE signals of the passive acoustic experiments. Therefore, the AE signals observed have been modified by the frequency transfer function of the transducer, and by the filtering effects of the reactor vessel material and electronic devices.

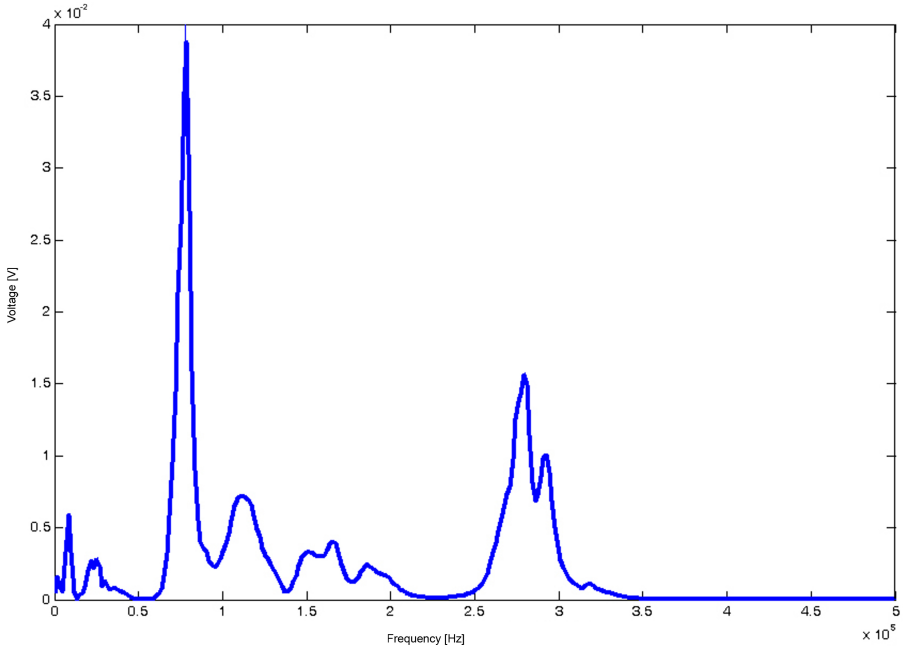

Figure 3.5: PZT-transducer Nano30 response obtained with the Hsu-Nielson source test.

3.4 Aim of the work programme

Once the contributions of the frequency response of the commercial sensor and the filtering effects of the reactor and electronic amplifier were assessed, a step back was necessary to understand, and improve, the passive monitoring system approach.

Firstly, it is vital to comprehend the origin of the broadband emissions and to investigate the effects of the signal input variations on the signal output. Mathematical modelling can be used to simulate the source of the acoustic signals (particle impacts input functions) to describe the impact of particles with a vessel wall.

Secondly, the influence of the reactor vessel on the AE spectra has to be assessed. The materials of the vessel and its dimensions have their own specific frequency, mode, shape, and each contributes to the overall behavior

of the structure. In particular, the vibrational modes of the reactor vessel itself and the analysis on its nature are substantial factors to consider.

Last but not the least, to use the knowledge programme gained from the modelling to design an ultrasonic sensor that is sensitive across the required frequency range; the design of a customised transducer for the acoustic system that will improve the heterogeneous acoustic system is a paramount objective for this research study.

Taking advantage of the power computation of a modern PC, it will be possible to model a system of liquid load medium and the glass-oil-glass combination corresponding to the vessel reactor using the finite element (FE) modelling software package PZFlex [70]. Thus, it will be possible:

- To investigate the factors that affect the broadband acoustic emission signals. Understanding those agents that contribute to broadband emission signals should allow identification of the emission frequencies that are relevant.

- To model particle interactions with the reactor vessel wall in order to investigate their overall behaviour on the acoustic data received by the ultrasonic transducer.

- To model the reactor vessel structure and its mechanical low pass filtering effects.

- To employing the outcomes from the modelling results of the reactor vessel in order to design an ultrasonic transducer which would be sensitive in the frequency range associated with the AE events.

- To scrutinise the most efficient transducer design for different monitoring systems and to develop customised passive acoustic monitoring

systems for in situ process analysis.

- To analyse and resolve changes in particle size and particle concentration using the passive monitoring approach.

3.5 Conclusions

Previous work at Strathclyde University [17][56] investigated the spectral characteristics from a model heterogeneous system and related these to particle size and concentration quantities. It was concluded that the acoustic signals observed were highly dependent on the transfer function of the ultrasonic receiver and on the filtering effects by the vessel reactor itself.

The aims and objectives of the research study have been disclosed and listed. These will be tackled in the subsequent Chapters.

Importantly, it has been proposed that understanding the factors that contribute to broadband emission signals should allow identification of emission frequencies that are important for the monitoring of heterogeneous systems, i.e. include information of interest for various processes. Therefore, measurement systems could be designed that are tailored to a particular process, for extraction of optimal information.

Chapter 4

Modelling of the passive acoustic system

Process simulations are increasingly being used in decision-making and problem solving. Process simulation is a model-based representation of chemical, physical, and other technical processes in software. Basic prerequisites are a thorough knowledge of chemical and physical properties of mixtures, of reactions, and of mathematical models which, in combination, allow the calculation of a process in computers. The model development for a better representation of real processes is the core of the further development of the simulation software [71].

The modelling of any process can be represented by the graph in Figure 4.1. The *problem entity* is the system, situation or idea to be modelled. The *conceptual model* is the mathematical and logical representation of the problem entity developed for a particular study. The *computerised model* is the *conceptual model* implemented on a PC. The *conceptual model* is developed through an *analysis and modelling phase*, whilst the *computerised model*

is developed through a *computer programming* and *implementation phase*. Information about the problem entity is obtained by conducting computer experiments on the *computerised model* in the *experimentation phase*. In addition; *validation* of the *computerised model* is necessary to ascertain the model's accuracy [72, 73].

In this work, the *problem entity* to model is the heterogeneous mixture of particles suspended in a fluid and stirred inside a vessel reactor. The mathematical model of the particles striking against the inner wall of the vessel and the vessel structure itself is represented (in Figure 4.1) as the *conceptual model*. The approach undertaken to analyse such complex interactions uses the FE modelling technique. The FEM model of the reactor vessel is clearly represented in Figure 4.1 as the *computerised model*. Importantly, all these aspects of the modelling process are required to predict the effects of particle size and concentration on the acoustic emission spectra. This Chapter will describe the development, validation and implementation of a FE model to investigate the AE from a heterogeneous reaction. A number of important results will be presented which will be employed to influence the transducer design process described in Chapter 5.

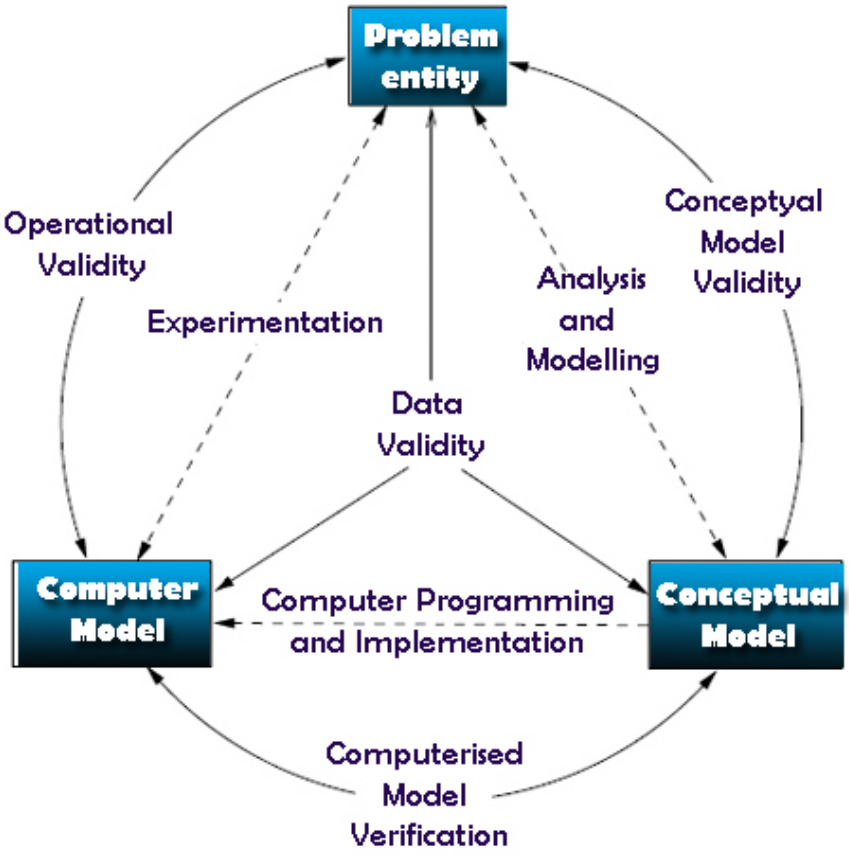

Figure 4.1: Simplified version of the modelling process

4.1 Broadband acoustic emission analysis

When solid particles make an impact with a planar surface, their kinetic energy is redistributed into a combination of kinetic energy in the rebounding particles and acoustic elastic waves propagating away from the surface wall. The fraction of energy dissipated as elastic waves will propagate through the medium (in this work by the constituent materials in the reactor vessel structure) according to its elastic properties and can be detected by a suitable

acoustic sensor. In this work, it is supposed that particle breakage does not occur during the impacts.

The resulting signal observed at the sensor will therefore be dependent not only upon the particle's physical properties and the dynamics of the impact itself, but also upon the propagation of sound in the target medium and the functional response of the acoustic sensor. This can be represented as follows:

$$y(t) = a(t) * g(t) * d(t) \tag{4.1}$$

where "$*$" denotes the convolution operation, y(t) represents the observed AE signal and *a(t)*, *g(t)* and *d(t)* are the acoustic source, propagation and detection functions respectively, all of which will be functions of time, t.

All the information concerning the particles will be contained in the source function. The problem of broadband acoustic emission analysis can be divided into three sub-problems: modelling the excitation function corresponding to the particle impact on the inner wall of the vessel, modelling the wave propagation through the reactor vessel and modelling the ultrasonic transducer in reception mode. The first two models are described in this Chapter. It was not possible to model the Nano30 commercial transducer [74] with FE due to its unknown internal characteristics. Instead, the complete modelling and design of two ultrasonic acoustic transducers is reported in Chapter 5.

4.2 Particle impact input function

During the experimental work carried out in the laboratories at Strathclyde University and described in Section 3.1, the continuously stirred reactor vessel contains a particle-laden fluid. To this end, a model of a particle being

transported in a stirred vessel and its subsequent collision with the vessel wall is considered.

The following mathematical model of the impact function used to generate the excitation functions which are used in the subsequent FE modelling work has been developed by Gillian Carson and Anthony J. Mulholland of the Department of Mathematics University of Strathclyde [75]. The author has contributed to this work by providing experimental validation to support the developed theory in which the particle impact equations are crucial to the research described in this Thesis. Details of this research work are described in Reference [75]. Here, the most relevant aspects of the impact model are reported.

From Newton' second law:

$$F = m\frac{\delta^2 x}{\delta t^2} \tag{4.2}$$

where F, the net force, is equated to the product of the mass, m, and the acceleration ($\frac{\delta^2 x}{\delta t^2}$). The particle in the vessel is subjected to centrifugal and drag forces:

$$m_e\frac{\delta^2 x}{\delta t^2} = m_e\omega^2 x - 6\pi r\eta\frac{\delta x}{\delta t} \tag{4.3}$$

where ω is the stirrer rotation rate, η is the viscosity of the fluid, r the spherical radius of the particles, m_e is an effective mass of the particles defined by

$$m_e = \frac{4\pi}{3}r^3(\rho_s - \rho_f) \tag{4.4}$$

where ρ_s and ρ_f are the density of the particle and fluid, respectively.

Each single particle impact creates an impulsive force at the surface of

the wall with a duration equal to the impact time, and a spatial force depending on the nature of the impact. Assuming an elastic normal impact, each particle colliding against the wall of the vessel generates a force normal to the surface. Determination of the impact source function with respect to time will yield the impact time and the magnitude of the force, both of which depend upon the particle size and velocity associated with the collision.

The adopted model of the source input function is based on Hertz theory developed at the end of 19^{th} century [76]. This theory has been corroborated by a number of experiments, especially when used for non-plastic collisions, for example the collision of two glass balls [28, 76, 77]. The expression for the contact force developed during the elastic impact of a spherical particle of radius r with the rigid surface of a semi-infinite solid is represented as a point force with a squared half-period sine-wave time history [78],

$$F(r,t) = \sin^2 \frac{w_0 t}{2\pi r} \quad 0 < t < \pi/w_0 \tag{4.5}$$

where $w_o = \frac{\pi}{T_h}$. The impact time, T_h, is derived from a known theoretical formulation for elastic normal impact predicted by Hertz for infinitely rigid surfaces. In addition, T_h depends on the size, velocity and material properties of the particle [78, 79]. The impact time T_h for a spherical particle striking an elastically deforming plane is given by Hutchings [80]

$$T_h = 2.94(\frac{5\pi}{4})^{\frac{2}{5}} {\rho_s}^{\frac{2}{5}} (\frac{r}{v^{\frac{1}{5}}})(f(E))^{\frac{2}{5}} \tag{4.6}$$

where v is the velocity of the impact, *f(E)* is a function of the elastic constant

of the particle and target material (in this case, glass) and it is given by:

$$f(E) = (1 - {\nu_1}^2)/Y_1 + (1 - {\nu_2}^2)/Y_2 \tag{4.7}$$

where ν_1 and ν_2 and Y_1 and Y_2 are Poisson's ratio and Young's modulus respectively for the target (denoted 1) and the particle material (denoted 2).

For the stirring of itaconic acid particles in toluene, the following information is required: the stirrer velocity ω_o equals 250 rpm; the particle material is itaconic acid with density $\rho_s = 1573$ kg m^{-3}; the density of toluene is $\rho_f = 860$ kg m^{-3} and viscosity of toluene is $\eta = 6.8\text{x}10^{-3}$ kg $m^{-1}s^{-1}$.

Particle size selected as representative of each gaussian particle distribution are detailed in Table 4.1. These were selected in order to map the simulations onto the experimental work. With this information it is possible to derive properties (such as T_h and F) for a particle of itaconic acid striking normally and elastically against a rigid glass surface [6].

The details and laws of the impact function predicted by Hertz for spheres colliding against infinite surfaces are published by Buttle [28] and Besenyei [6] and Carson [43, 75]. Table 4.2 shows the calculated values for the contact time and impact force of different particle sizes to be utilised in the FE models.

Figure 4.2 and Figure 4.3 illustrate examples of time and frequency responses, respectively corresponding to the impact of particles of size A, B and C (see Table 4.2). Importantly these functions were used as the input stimulus for all the FE simulations mentioned in this Chapter.

It is important to highlight that as the particle size increases, the impact force amplitude increases and the duration of the contact is longer. Corres-

pondingly small particles have wider bandwidth than larger particles.

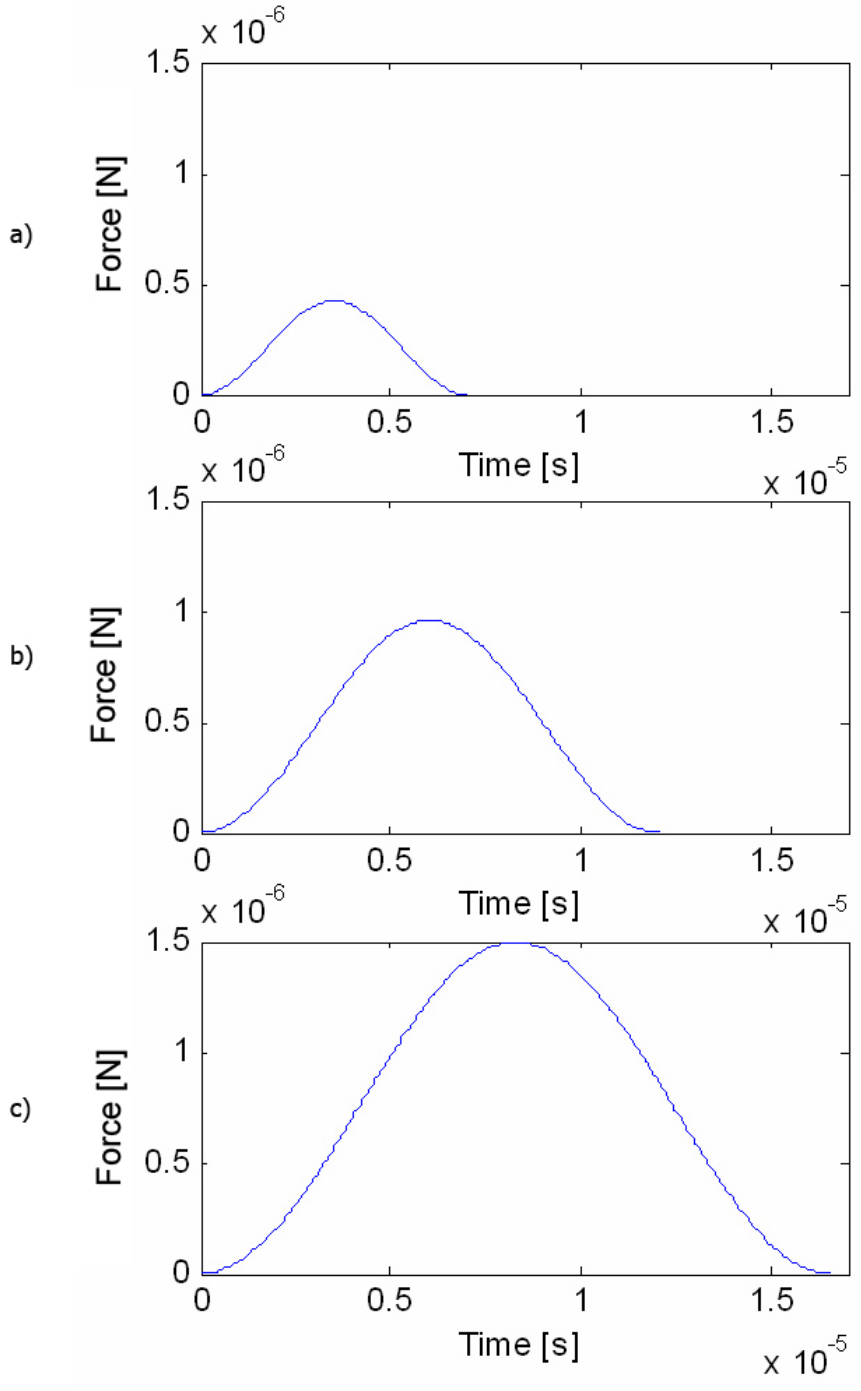

Figure 4.2: Predicted particle impact function in time domain for particles of sizes a) 200 b) 400 c) 600 μm, respectively

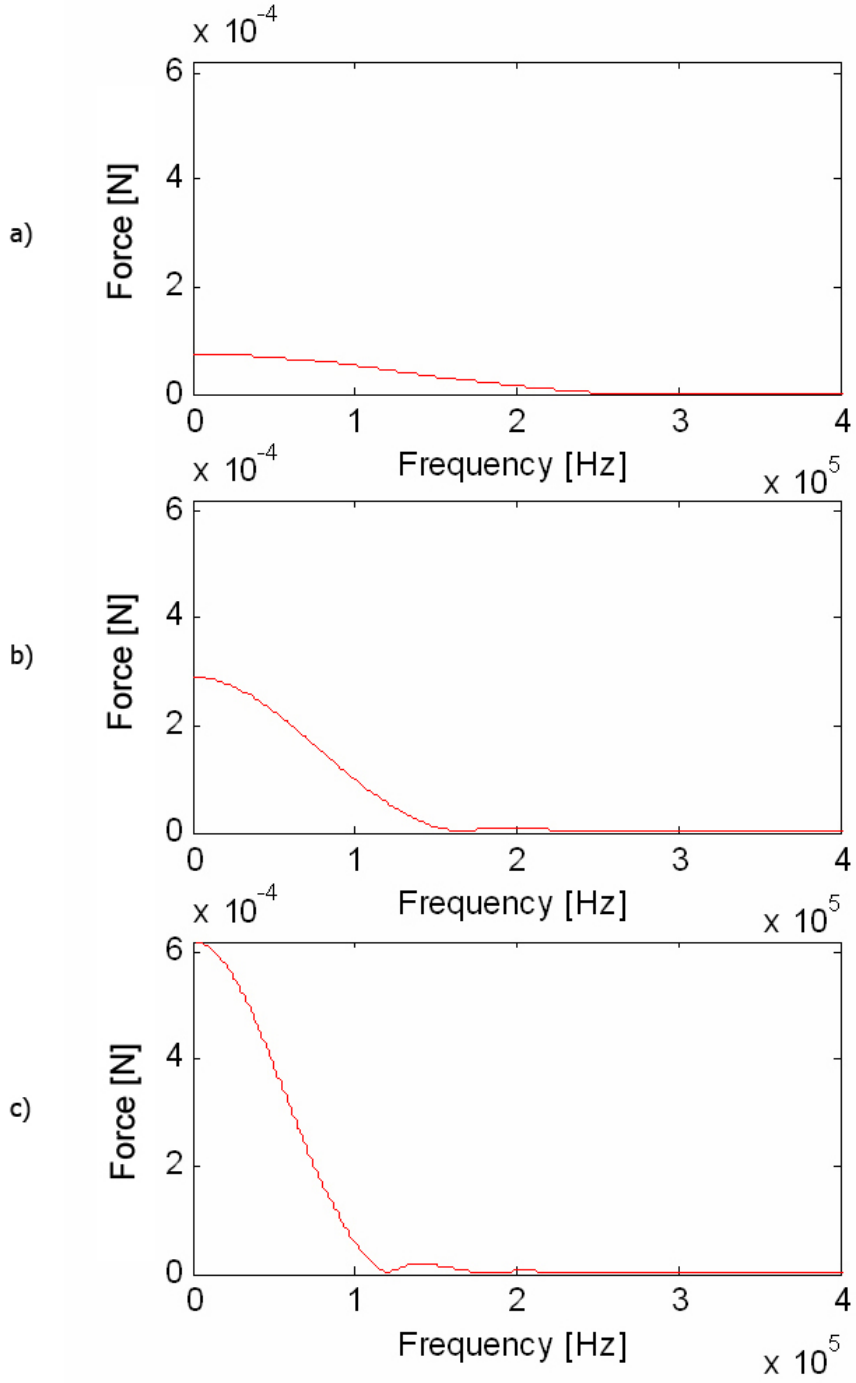

Figure 4.3: Predicted particle impact function in frequency domain for particles of sizes a) 200 b) 400 c) 600 μm, respectively

Table 4.1: Itaconic acid particles employed in the simulations.

Mnemonic	Particles size distribution [μm]	Simulated [μm]
A	$0 < x \leqslant 251$	200
B	$251 < x \leqslant 500$	400
C	$500 < x \leqslant 853$	600

Table 4.2: Contact time and force of impact calculated for different particle sizes

Particle size (r) [μm]	**Contact time** (T_h) [s]	**Force (F)** [N]
200	7.08 x 10^{-6}	4.25 x 10^{-7}
400	1.20 x 10^{-5}	9.60 x 10^{-7}
600	1.65 x 10^{-5}	1.50 x 10^{-6}

4.3 Modelling of the reactor vessel

For studying the interactions of mechanical bodies, a numerical method like the finite element modelling (FEM) is preferred, owing to the complexity of the physical system. The finite element (FE) method is a numerical procedure used for solving differential equations encountered in a variety of engineering applications. The finite element package used in this work is PZFlex developed by Weidlinger Associates [81]. PZFlex is a specialised software tool for piezoelectric, ultrasonic, and bioengineering wave propagation problems. The code has been applied to a wide range of problems including geotechnical, seismic wave propagation and ballistic structure interaction [82, 83, 84]. Recent work has also shown that FE modelling can be used to effectively simulate wave propagation in plates [78, 83, 85]. The main disadvantage of the FE technique is that it is computationally demanding. However FE modelling does have advantages over finite difference and finite

volume techniques in that complex designs can be accommodated, including piezoelectric behaviour [86].

A complete description of finite element modelling is given in many works [84, 86, 87], hence, only a description of the most important features used in this work will be given here to assist the reader.

Figure 4.4 (a) shows a representation in three-dimensions (3D) of a 4-layer model, developed using PZFlex comprising a liquid load medium and the glass-oil-glass combination corresponding to the reactor vessel described previously. The actual dimensions of the reactor vessel were used in the model and are presented in Figure 4.6 . The vessel was modelled as a cylinder with a radius of 50 mm and a height of 100 mm. Due to the computational demand of the FE analysis, a 2D longitudinal section of the cylindrical model, illustrated in Figure 4.4 (b), was utilised throughout this work.

The purpose of the FE model is to provide information about the effects of varying: the position of the particle-impact on the inner surface of the vessel (the resonance analysis of the ultrasonic wave propagating through the material layers), the influence of different thickness of layers and the particle size and concentration effects.

Samples of glass and oil from the reactor were collected and their acoustic and physical properties were characterised in the CUE Laboratories [88]. These values were obtained by measuring the time of flight in a glass sample of thickness 10 mm and a sample of 50 mL of oil at 500 kHz. Table 4.3 reports the measured acoustic material properties (density, longitudinal velocity, shear velocity and acoustic attenuation) subsequently utilised in the FE modelling programme.

Excitation of the model corresponds to a pressure loading at the inner

Table 4.3: Material properties (at 1 MHz and 25^o C)

Material	Density	Long. vel.	Shear vel.	Long. attenuation
	$[kg/m^3]$	$[m/s]$	$[m/s]$	[dB/cm]
Toluene	860	1225	0	0.3
Oil	929	962	0	0.5
Glass	2484	6192	3143	1.0

glass wall using signals derived from the mathematical model related to the impact of particles of different sizes as discussed in Section 4.2. The model output was selected as the out-of-plane displacement on the outer glass wall at the centre of the wall, located at the position where the piezoelectric transducer would be positioned. The FFT (Fast Fourier Transform) of the signal output in the time domain (transient analysis) was then used to compute the power spectrum.

In order to avoid interference from the acoustic wave reflection from the edges of the model, the time of simulation was chosen so that any such edge reflection would arrive at the output position after a suitable time delay. This will depend on the position of the excitation function but was typically twice the time necessary for a wave to propagate within the model. This is effectively windowing the time domain response to ensure that any subsequent frequency domain analysis does not include contributions from reflected waveforms which can mask the particle information and the frequency response of the system. Absorbing boundaries were also incorporated into the model, as shown in Figure 4.5, for simulating an infinite medium and hence, and this avoids further wave reflections from the top and bottom of the vessel interfering with the output signal of the model.

When simulating interactions between bodies using FEM, the modelling itself, as well as the consideration of the resulting wave propagation are

the critical issues. Attention has to be paid to the choice of simulation parameters, such as spatial discretisation (l) and time step sizes (ts). To get an accurate representation of the wave propagation with FEM, the smallest wavelength λ_{min} should be discretised by at least 20 nodes and the period of the wave at the highest frequency f_{max} should be discretised by at least 20 time steps [86] [89].

$$l_{max} = \frac{\lambda_{min}}{20} = \frac{v_{min}}{20 f_{max}} \tag{4.8}$$

$$ts_{max} = \frac{1}{20 f_{max}} \tag{4.9}$$

where f_{max} is the highest frequency under consideration and v_{min} the lowest wave speed of any of the constituent materials.

From measurements using the Nano30 commercial transducer (see Section 3.2), it is known, that frequencies up to 500 kHz are dominant. Considering that the lowest wave speed of 929 m/s occurs within the oil layer, therefore the required maximal element length becomes 92.9 μm and the maximal time step is equal to 10^{-7} s. These values were used to discretise the entire model.

Moreover, assuming that for elastic particle impacts no deformation occurs and the contact region of the particle-wall is smaller than the particle diameter, the excitation function was applied to only one element. This approach also takes into account that the particle is small compared with its distance from the transducer, so that it can be modeled as a point source [28]. The 2D model developed had approximately 128400 elements. The simulation of the particles striking against the inner wall of the vessel on a computer with a 2 GHz double processor and 4 Gb of RAM took about 1.5 hours computation time. Due to this high computation time only a 2D model was utilised for this research study.

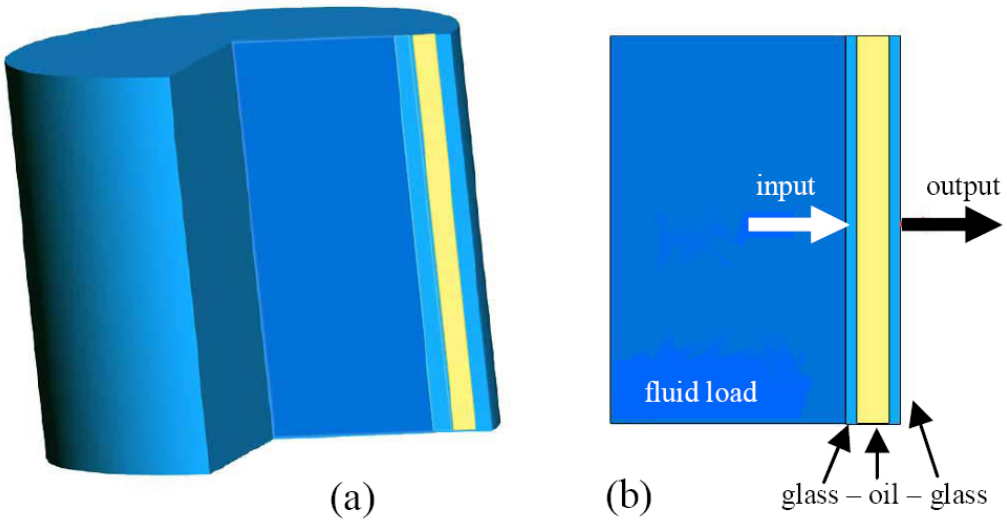

Figure 4.4: a) Three and b) two dimensional representations of the reactor vessel

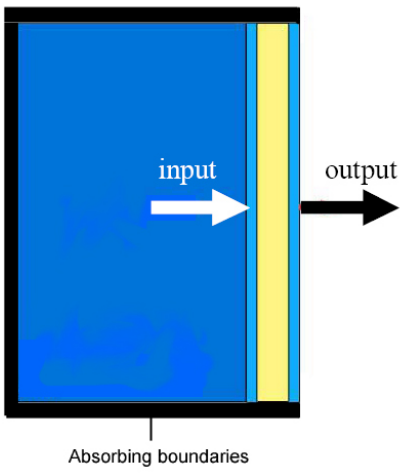

Figure 4.5: Absorbing boundaries

4.3.1 Resonance analysis

Attention has to be paid during the simulations and results analysis phase due to the resonance effects of the reactor vessel itself. A resonant object, whether mechanical, acoustic, or electrical, will generally have more than one resonant frequency. These frequencies are determined by the geometry and acoustic velocities (both longitudinal and shear, if present) associated with each material.

Considering a vertical infinite plate of glass with thickness d, the resonance frequency occurs due to its finite thickness and its wavelength and it is equal to twice the thickness of the plate. The frequency of this mode (called the thickness mode) is dependent upon the plate thickness and the velocity of sound in the thickness direction v_T. For a given d, the frequency of the thickness mode f_n can be shown to be:

$$f_n = \frac{nv_T}{2d} \quad for \quad every \quad n = 1, 3, 5... \tag{4.10}$$

where v_T is the wave velocity in the thickness direction and f_1 is the fundamental frequency of the thickness mode (for n=1). If a layered structure is considered, the resonant frequencies will be dependent on the total thickness of the plates considered and the local acoustic velocities of each material in the thickness direction. Hence, the resonant frequency of the glass layer f_1, the resonant frequency of the oil layer f_2 and their combinations f_3 and f_4 can be calculated:

$$f_1 = \frac{1}{2t_1} \quad where \quad t_1 = \frac{d_{glass}}{v_{glass}} \tag{4.11}$$

$$f_2 = \frac{1}{2t_2} \quad where \quad t_2 = \frac{d_{oil}}{v_{oil}} \tag{4.12}$$

$$f_3 = \frac{1}{2(t_1 + t_2)} \tag{4.13}$$

$$f_4 = \frac{1}{2(2t_1 + t_2)} \tag{4.14}$$

The resonant longitudinal modes of the glass-oil-glass layer combination are shown in Figure 4.6. 1 MHz is the highest resonant frequency and it is generated by the 3 mm layer of glass, while the 5.4 mm layer of oil causes the 90 kHz mode. The combinations of the plate of glass with the layer of oil leads to lower frequencies of 82 kHz and 75 kHz, respectively. It is expected that these resonant frequencies will have lower amplitude compared to the resonances caused by the single layers because their energy will be reduced by trasmission and reflections of the interface layers causing acoustic mismatch. It should be noted that the resonant frequencies below 500 kHz could interfere with the AE signals associated with the particle impacts, therefore their effect has to be taken into account during the analysis phase.

A plane wave propagating with longitudinal mode was considered for identifying the theoretical resonance frequencies. However, sound waves can also propagate depending on the elastic and inertial properties of the load medium as other ultrasonic modes, such as *shear waves, Rayleigh waves*, and importantly in thin materials as *plate* or *Lamb waves*. These propagating modes can generate other resonance effects within the structure.

In *longitudinal waves*, the oscillations occur in the direction of wave pro-

pagation or longitudinal direction. Since compressional and dilational forces are active in these waves, they are also called pressure or compressional waves. Compression waves can propagate in the water layer as well as in the glass layer because the energy travels through the atomic structure by a series of compression and expansion (rarefaction) movements. The essential characteristic of the longitudinal wave which distinguishes it from other types of waves is that the molecules of the medium move in a direction parallel to the direction of energy propagation [90].

The *shear or transverse wave* propagates in the glass layers because they require an acoustically solid material for effective propagation, and therefore, are not supported in the water or oil phases. Shear waves are relatively weak when compared to longitudinal waves and are usually generated in materials from longitudinal waves using refraction due to Snell's Law (See 7.2.2). The shear waves have no normal component, and they travel at a different velocity compared to the longitudinal wave.

Rayleigh (or surface) waves travel the surface of a relatively thick solid material, such as glass, penetrating to a depth of one wavelength. The particles in the glass, through which a Rayleigh surface wave passes, move in elliptical paths, because both a longitudinal and transverse motion combine the surface waves. Surface waves also travel along the interface of each layer and their velocity is approximately 90% of the shear wave velocity of the glass [58].

Lamb waves are similar to longitudinal waves, with compression and rarefaction, but they are bounded by the sheet or plate surface causing a waveguide effect and they can only be generated in materials a few wavelengths

thick. Lamb waves are complex vibrational waves that propagate parallel to the test surface throughout the thickness of the material. Propagation of Lamb waves depends on the density and the elastic material properties of a component. A number of modes of particle vibration are possible with Lamb waves, however the two most common are asymmetrical and symmetrical. In the asymmetrical Lamb wave mode, a large portion of the motion moves in a normal direction to the plate, and a little motion occurs in the direction parallel to the plate. In this mode, the body of the plate bends as the two surfaces move in the same direction. Symmetrical Lamb waves move by "stretching and compressing" the plate in the wave motion direction. Wave motion in the symmetrical mode is most efficiently produced when the exciting force is parallel to the plate [90][58].

Importantly, the analysis of all these propagating modes requires complex mathematical modelling and equations. For this reason, FEM was utilised in this work.

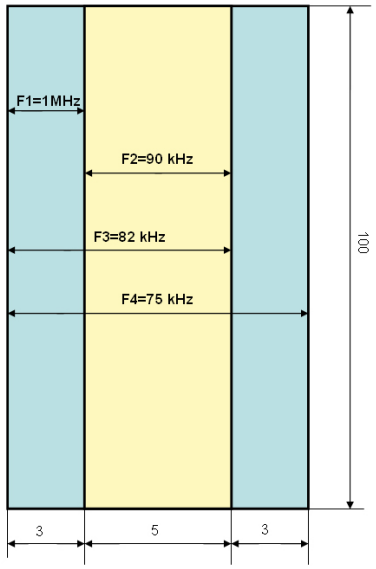

Figure 4.6: Resonant modes of the reactor vessel. The dimensions are in millimeters.

4.4 Validation of the model

Once the development of the FE model was complete, it was necessary to ascertain its validity. *Conceptual model validity* is defined as determining that the theories and the assumptions underlying the model are correct and that the model representation of the problem entity is 'reasonable' for the intended purpose of the model [73]. This Section describes the *computerised model verification approach* to ensure that the computer simulation and the implementation of the conceptual model are reasonably accurate.

Model validation and verification are critical in the development of a simulated model. Unfortunately, there is not a set of specific criteria that can be easily applied to determine the 'correctness' of the model. The mathematical model of the impact of the particle striking a surface has been validated in the literature [28], hence only the validation of the reactor vessel model was performed for this work. The validation consisted in reproducing an identical input for the experimental and modelled cases, and then comparing the functional output of the two approaches.

4.4.1 Experimental arrangement for the validation

A customised tank was built taking into account the 2D nature of the computerised model as shown in Figure 4.7. The tank frame of dimensions 300x450x300 mm^3 was manufactured using Plexiglass material. Only the front wall was composed of two parallel sheets of glass (3 mm of thick) with a 5 mm cavity in between the glass sheets, into which 450 mL of oil collected from the heater/chiller reactor used in the experimental heterogeneous reaction work was placed. During the validation experiments, a wide-band

immersion transducer (Alba Ultrasound Ltd Glasgow [91]) was positioned at 10 mm from one side of the square tank and in the middle of the container as shown in Figure 4.7. The transducer, employed as ultrasonic transmitter had the center frequency fundamental mode of resonance at approximately 250 kHz.

A 90 mm diameter (with active area of 25 mm diameter) membrane type Polyvinylidene Fluoride (PVDF) hydrophone was immersed in the middle of the tank and at 250 mm from the transmitter. A PVDF strip (size 30 x 80 mm) attached on the outer wall of the container acted as broadband receivers in both cases. An aluminium case was also used to shield the PVDF strip from the environmental noise in the laboratory. The receivers were directly connected via a coaxial cable to an Agilent Infiniium 54642 oscilloscope for acquiring data from the experiments.

The validation of the reactor vessel (as represented in Figure 4.8 (a)) was conducted in two different stages.

In the first stage, a tone burst (10 Vpp, 250 kHz center frequency, 20 cycles) fired by the ultrasonic transducer was collected by the hydrophone and the PVDF strip receivers. The first arrival waveform on the hydrophone was selected manually and stored into a file. Careful alignment was necessary to achieve the optimum transmission from the Alba transducer to the PVDF receivers. In the second stage of the validation, the signal output acquired by the hydrophone was employed as the signal input for the computerised model as illustrated in Figure 4.8 (b). This is a simple way to simulate the ultrasonic transducer response without knowing its internal characteristics, as the measured signal is dependent upon the frequency response of the acoustic transmitter. Thus, the predicted output pressure variation was collected at

the centre of outer glass layer, where the PVDF sensor strip was situated in the experimental work, and compared with the experimentally measured waveform.

An ultrasonic transducer will exhibit a characteristic pressure distribution due to the relationship between the transducer lateral dimension and the wavelength of the sound energy in the load medium [92]. In fact, in the majority of cases, the pressure field can be considered as comprising two regions: the near field and far field. Within the near field region (Fresnel zone) constructive and destructive interference between the plane wave emitted from the front face of the transducer and the edge wave from the outer edge of the device. This region can be problematic for ultrasonic applications due to the close proximity of pressure maxima and minima. Therefore, it is desirable to operate in the far field (Fraunhofer zone) of the transducer as this region is characterized as a plane wave with an angle of divergence relative to the centre plane of the transducer itself. In this region the ultrasonic propagation is easily understood and positioning of a receiving transducer, for example, is not critical. The formula presented in Equation 4.15 can be used to determine the near/far field boundary :

$$N_f = \frac{Dm^2}{4\lambda} \tag{4.15}$$

where Dm is the diameter of the transducer, λ is the wavelength of the transmitted signal. For the Alba 250 kHz transducer (Dm = 3 inch = 76 mm), N_f corresponds to 240 mm; importantly, the hydrophone was positioned at 250 mm (Fraunhofer zone) distance from the ultrasonic transducer for this validation phase.

Note that, the aim of this set of experiments is to validate the FE model of the reactor vessel. The same approach could not be used for characterising the Nano30 transducer because it is designed as a receiver and it is not waterproof.

It is interesting to consider how the measured plane wave signal was incorporated into the FE model. A series of 100 nodes in the model corresponding to the position and width of the hydrophone were utilised as point sources, with a pressure excitation function applied to each node. This pressure function was the measured plane wave signal and hence, an accurate representation of the operation of the 250 kHz transducer was able to be simulated. This approach is based on Huygens Principle [92].

It is also important to state the limitations of the validation approach. Firstly, the model does not take into account the 3D nature of the vessel. Secondly, the model validation employs plane wave propagation spreading into the water, where these waves will be converted into shear waves and Lamb waves in the glass walls at the water/glass interface. It is considered that it is not necessary to individually simulate the excitation of all possible ultrasonic modes and in fact, such an undertaking would overly complicate the validation process. Finally, the fact that the excitation process utilises point source excitation is important as the particle impacting on the vessel wall will utilise a similar excitation technique.

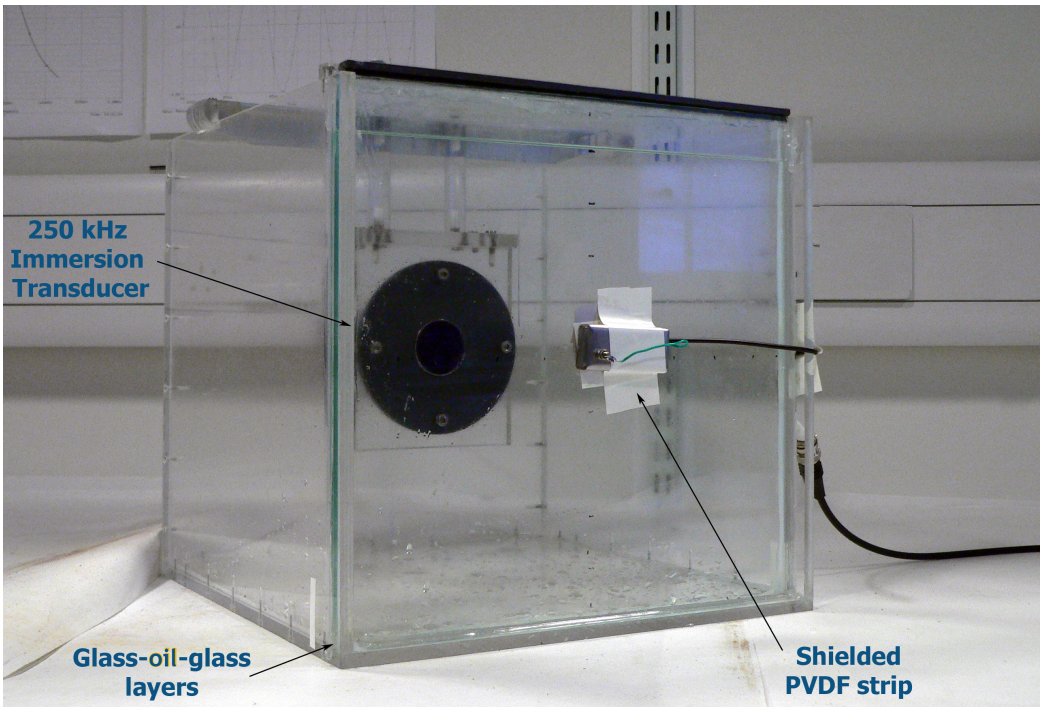

Figure 4.7: Square tank for validation

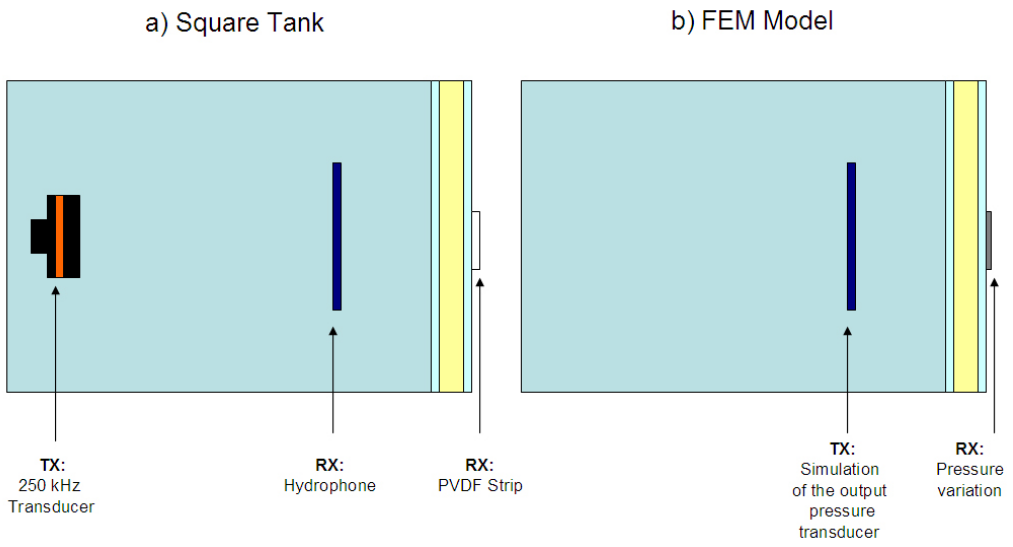

Figure 4.8: Top view of the experimental apparatus employed the model validation

4.4.2 Validation results

The experimentally measured and FEM predicted frequency spectra are compared in Figure 4.9 to assess if the model's output behaviour has sufficient accuracy for its intended purpose. The plots show an approximately 90 kHz standing wave pattern established by the oil layer structure. These standing wave modes arise from interference in which the reflected waves add constructively with the incident waves propagating inside the oil layer. The maximum of the wave is located at 265.5 kHz and this corresponds to the thickness mode of the ultrasonic transmitter used during the validation process. In general, the model shows excellent correlation with the experimental response; the error in the predicted maxima positions is less than 9% for the main four peaks (these are situated within the maximum frequency of interest of the FEM model). This good agreement is in part due to the careful characterization of all of the relevant material properties utilised in the model and the right alignment from the Alba immersion transducer to both the PVDF receivers.

4.5 Simulation results

Once the FEM model was validated, a number of parameters were selected to provide an insight into the AE associated with the particle impact on the inner wall of a vessel. One objective of the modelling work was to ascertain if the conceptual model prediction of the system output would be consistent with the experimental feasibility study and the published theory in the literature regarding particle concentration and particle size effects.

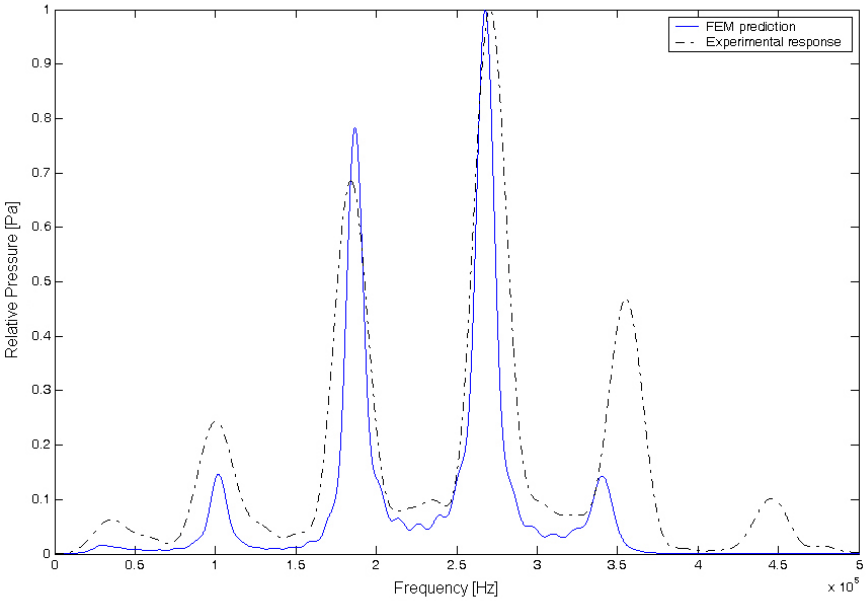

Figure 4.9: Comparison of the experimentally measured and FEM predicted frequency spectrum

4.5.1 Finite element prediction of ultrasonic wave propagation

Transient analysis investigations to simulate the propagation of ultrasonic waves through the material layers of the FE model were carried out.

The FE model was excited at the center of the inner wall by a 200 μm particle impact and its effect was observed. The top-down view of the ultrasonic wave through the reactor vessel is presented as a series of frameshots from a movie generated using PZFlex. These images are shown in Figures 4.10 a), 4.10 b) 4.11 c) 4.11 d).

Sound energy that is transmitted from one layer to another refracts in accordance with Snell's Law (See 7.2.2). Hence, as the angle of an incident longitudinal wave with respect to a surface increases, an increasing portion of the sound energy is converted to a shear wave in the second material, and

if the angle is high enough, all of the energy in the second material will be in the form of shear waves.

However, if there is a large difference in the acoustic impedance of the two materials, as in the case of glass-oil materials, then due to that acoustic impedance mismatch there will be a significant reflection from the boundary. The amount of energy reflected, or reflection coefficient, is related to the relative acoustic impedance of the two materials. For any two materials, the reflection coefficient as a percentage of incident energy pressure can be calculated through the formula

$$Rf_{1-2} = (\frac{Z_2 - Z_1}{Z_2 + Z_1})^2 \tag{4.16}$$

where Rf_{1-2} is the reflection coefficient (percentage of energy reflected), Z_1 is acoustic impedance of the first material and Z_2 corresponds to the acoustic impedance of the second material [93].

Knowing the impedance of each material it is possible to calculate the percentage of the overall energy transmitted as:

$$Tr = 1 - (Rf_{1-2}Rf_{2-3}(Rf_{3-4}) \tag{4.17}$$

where Rf_{1-2} is the reflection coefficient between the toluene-glass interface, Rf_{2-3} is the coefficient at the glass-oil interface and Rf_{3-4} is the reflection coefficient between the oil-glass interface.

The acoustic impedance of each layer can be computed as

$$Z = \rho v) \tag{4.18}$$

where ρ is the density of the medium and v is the longitudinal wave speed according to the Table 7.1. For simplicity, the influence of the coupling of each layer with the the layer beside was not taken into account for the impedance calculation.

This is a highly attenuating system; only 1.1% (Tr) of the initial mechanical energy of the particle impact is able to reach the sensor positioned outside the container.

The images presented in Figures 4.10 and 4.11 show also the effects of different ultrasound propagation modes and mode conversions. The input spherical wave propagates across the first glass layer as combination of longitudinal and shear waves. At the boundary of the glass layers, Rayleigh waves with an elliptical particle motion travel across the surface of the material, penetrating to a depth of approximately one wavelength. Also Lamb waves with complex mode of vibration travel across the cross-section of the glass medium.

The snapshots shows a few microseconds after the moment of impact. The spherical pressure wave spreads through the glass layer and part of its energy bounces back to the water. The pressure source is incident on the glass wall and its energy radiates in all directions from the starting point into the glass plate. The simulation shows that most of the acoustic energy (98.9%) becomes trapped in the layers of the reactor vessel and these guide the sound within their boundaries in waveforms propagating normally to the desired energy flow from inner to outer surfaces.

At the boundary of each layer constructive and destructive interference create complex acoustic waves. The medium of each layer supports the sound propagation mainly in the vertical direction (through the layers) guiding the

sound waves such as an acoustic waveguide i.e., a spatially inhomogeneous structure which counteracts the beam expansion that would normally be caused by diffraction.

Finally, the acoustic energy is transferred from the internal surface to the external surface where measurements can be conducted.

The example demonstrates also the powerful capabilities of FEM as a design aid. It is also possible to use FEM to predict the effects of: particle striking position, particle concentration and particle size. These simulations follow.

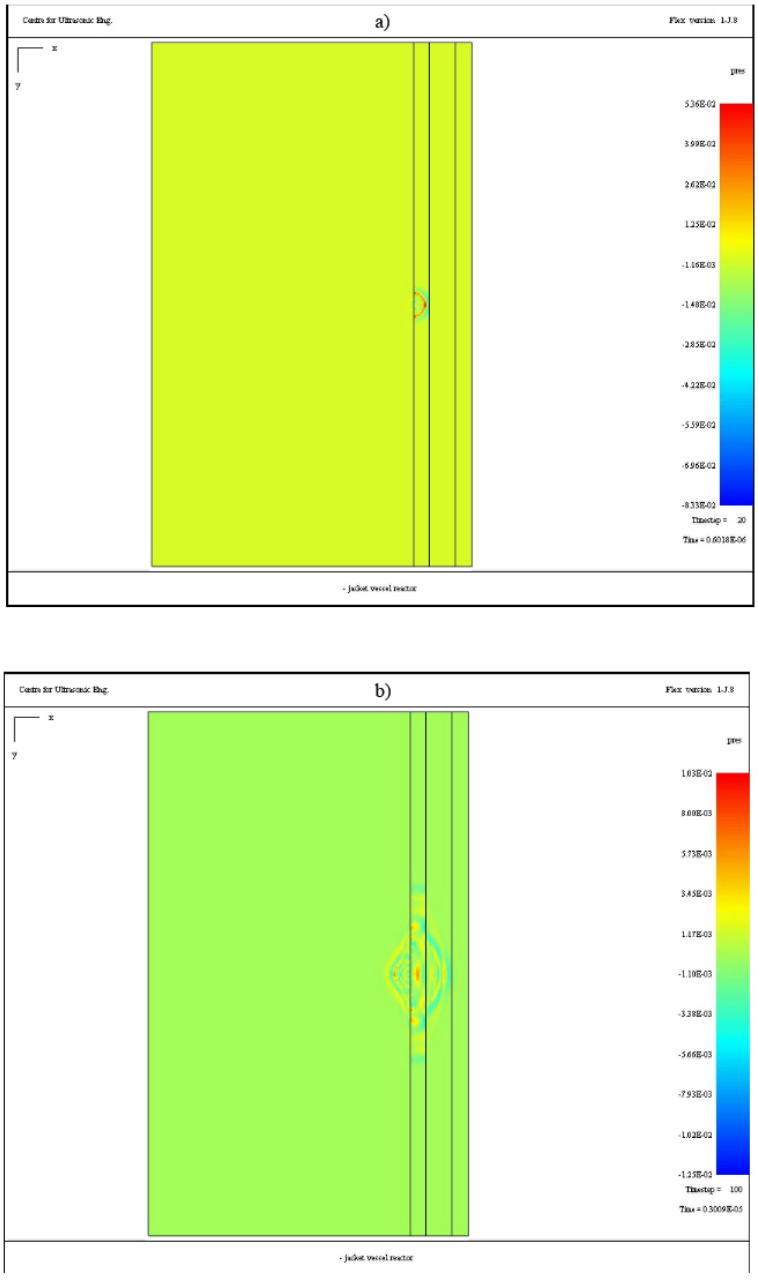

Figure 4.10: Propagation of the ultrasonic wave, lateral view. Time steps: a) 0.6 ns, b) 3 μs.

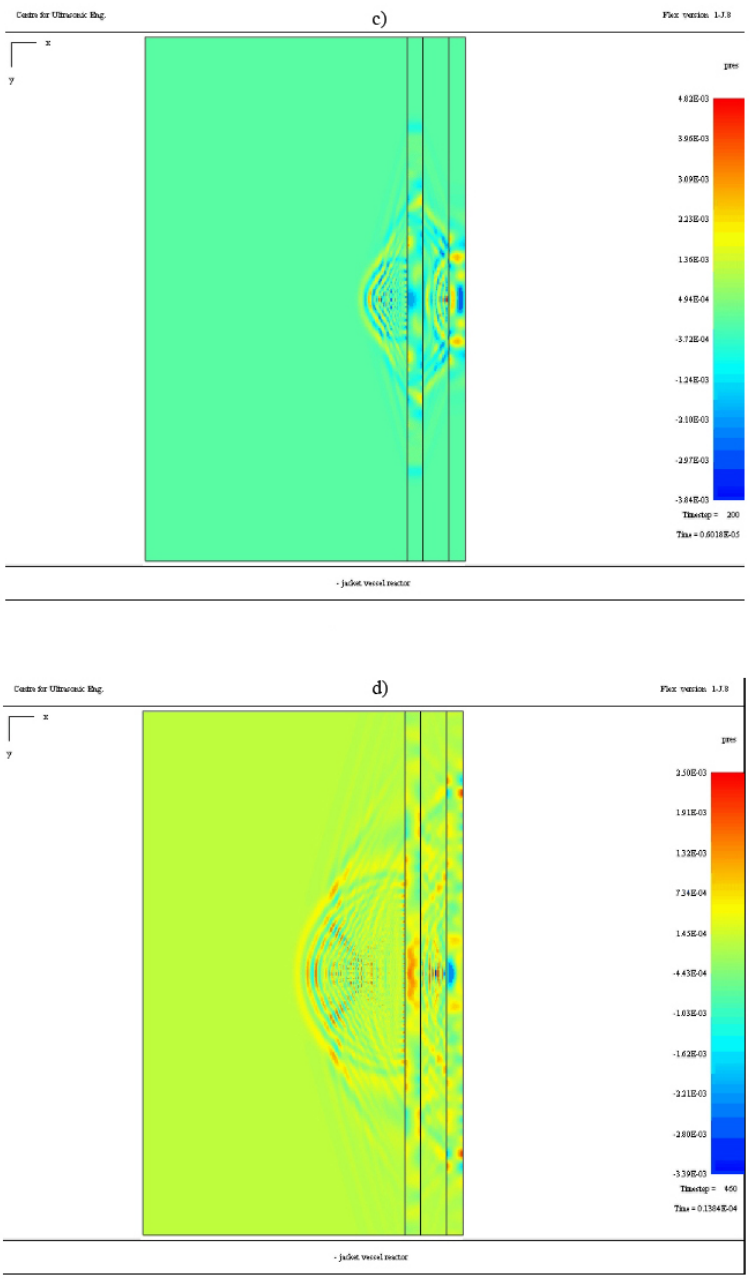

Figure 4.11: Propagation of the ultrasonic wave, lateral view. Time steps: c) 6 μs, d) 13 μs.

4.5.2 Position effects

Simulations were conducted by exciting the inner part (on the left) of the FE model with an impulse in the time domain. The inner surface of the vessel was excited at different positions via application of impulse pressure loadings at different nodes of the internal vessel surface (1 to 6 - Figure 4.12). An impulse was chosen as input stimulus to assess the maximum frequency of the signal output and to evaluate any resonant feature across the whole frequency spectrum. Again, the model output was the out of plane displacement at the centre of the outer surface of the glass wall as in previous experiments and simulations. Figure 4.13 shows the resultant normalised output signal spectra.

As expected, the spectra obtained vary with input position and in accordance with the horizontal symmetry of the model, the spectra obtained at positions 1 - 6, 2 - 5 and 3 - 4 produced identical results. Overall, their bandwidth is independent of the position of the input collisions and the predicted AE is restricted to the frequencies below 180 kHz (not clearly visible in the Figure due to the normalization). In this work the term 'bandwidth' is defined as the frequency range in which the signal's Fourier transform is non-zero. Usually bandwidth is defined as the range of frequencies where the FFT signal has a power above a certain amplitude (usually half the maximum value, or -3 dB); in this work -30 dB was considered negligible, hence it was assumed as 'zero' signal amplitude.

Moreover, some of the features can be attributed to the resonant modes of the vessel layers. Peaks arising from the oil layer, glass-oil, glass-oil-glass combinations at 90 kHz, 84.5 and 76.7 kHz, respectively are evident in all spectra.

In a previous study [56], the acoustic waves were found to propagate through and around the circumference of the oil jacketed glass vessel; the output energy was not strictly dependent on the vertical position of the particle impacts. Hence, the measured signals do not arise just from the particle-wall collisions in the proximity of the transducer.

This outcome is in agreement with the computerised simulation results.

The average area of the plots μ_{Area} is 50.29 with a standard deviation SD of 6.61. This means that the particles impacting at different positions have similar energy.

Each layer of material acts as a duct for propagating the sound waves. This 'transmission line' carries the acoustic energy of the particle collisions through the material layer in a vertical direction, and due to the impedance mismatch, the ultrasonic waves travel back and forth many times until they are fully damped, as shown in the previous Section. The ultrasonic energy of the particle impact reaches the outer side of the model and is not strictly dependent on the position of the input signals. This is because the energy of the collisions is largely reduced by the acoustic impedance mismatch of the layers (horizontal direction) rather than the acoustic attenuation within each material (vertical direction). From the FE simulations of the previous Section, this phenomenon was attributed to the presence of guided waves.

Observations during the experimental work [17][18][60] highlighted that the position of the attachment of the sensor is not critical when the attenuation in the horizonal plane is considerably larger than the attenuation in the vertical plane. These observations are significant when the position of the attachment of the piezoelectric transducer has to be considered.

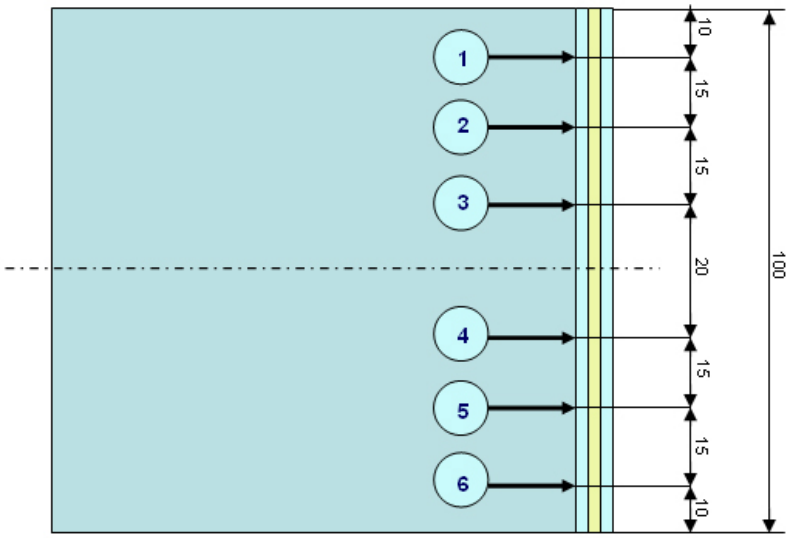

Figure 4.12: Different input positions on inner surface of the vessel wall (dimensions in mm)

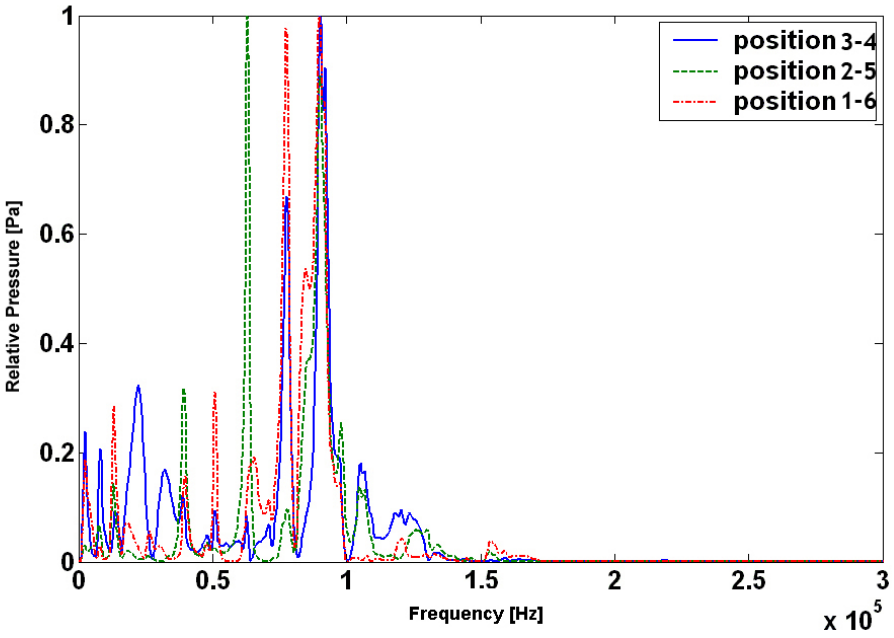

Figure 4.13: Normalised spectra obtained using different input positions.

4.5.3 Concentration effects

Investigation of the effects of particle concentration was simulated by varying the number of particles hitting the inner wall of the reactor vessel. An example of the predicted AE spectra from the impact of 1, 3 and 7 particles of a fixed diameter of 200 μm, at the same node in the middle of the inner wall of the vessel is shown in Figure 4.14.

The pressure variation of the external wall was considered as the output of the system; hence, the shape of the predicted frequency spectra was not influenced by the transfer function of the transducer, as was the case for the experimental results obtained during the feasibility study. Here, only the filtering effects of the reactor structure itself moderates the simulated data. In particular, the reactor vessel behaves as a mechanical low pass filter, with the generated AE restricted to frequencies below 180 kHz. Interestingly, the original experimental work demonstrates frequency components up to 380 kHz, see Figure 3.2. These higher frequency components correlate directly with resonant modes in the transducer itself (Figure 3.5).

From Figure 4.14, the FE model predicted a resonant mode at 89 kHz corresponding to the resonance associated with the oil, which was calculated to be 90 kHz. In all the spectra, 85% of the acoustic energy is concentrated between 0-60 kHz and 70-110 kHz.

The changes in signal area between 0 to 180 kHz for the three different particle size ranges, as a function of number of particles N, is illustrated in Figure 4.15. An increase in the number of impacting particles corresponds to an increase in particle concentration and resulted in an overall increase of AE spectral energy. The feasibility study of the heterogeneous reaction (Section 3.2) produced a similar relationship. These effects are consistent

with published theoretical and experimental studies of rigid spheres described by Leach et al [32][94] and other investigations of the mixing of solid systems [29][35][42].

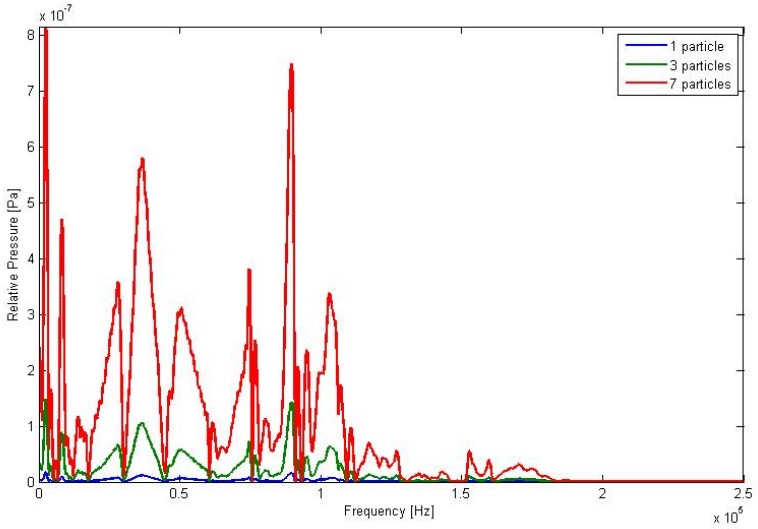

Figure 4.14: Predicted AE spectra for different numbers of particle impacts. (Particle size = 200 μm)

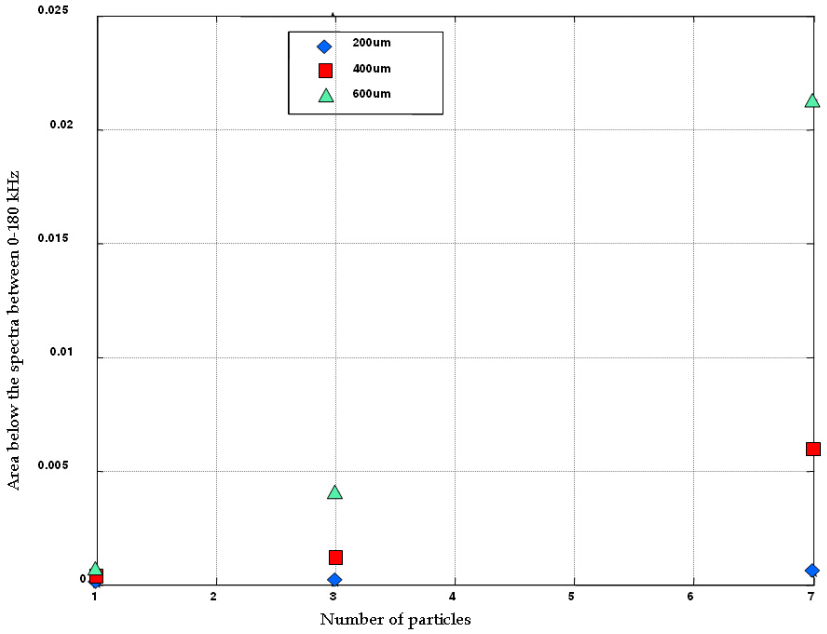

Figure 4.15: Effects of both particle concentration and size on the AE signal area between 0 and 180 kHz.

4.5.4 Particle size effects

To evaluate the effects of particle size, the excitation functions (illustrated in Figures 4.3 and 4.2) corresponding to one particle of each size (A, B, C) were applied in the middle of the inner wall as the input to the FE model. The resultant normalized signal profiles are plotted in Figure 4.16 and extend between 0-180 kHz. Figure 4.16 is distorted by the normalisation computed to highlight the spectra features. Note that below 20 kHz the spectra result overlapped, but above 20 kHz the bandwidth of each spectrum depends on the particle size considered. The spectra extend to 180 kHz, 130 kHz and 110 kHz for particle size of 200, 400 and 600 μm respectively. Importantly, an increase of particle size causes an increase of energy in the lower region (below the resonance frequency caused by the oil layer at 90 kHz) and a decrease of energy in the upper region.

Moreover, one thousand particles of fixed size impinging against the first glass layer of the vessel were also simulated to evaluate the effect of multiple particle impacts. The position across surface of the FE model and the time of the impacts were randomised. Each particle could strike randomly any position of the inner wall and with random time between 0 and 1 ms. The output AE signals in the time domain were collected from the FE model and their spectra were computed. Figure 4.17 illustrates the predicted output (normalized) when the system is subjected to multiple particle collisions. These plots show the effects of a highly complex field containing nodal and antinodal regions, which produce pressure fluctuations at the walls of the container. All the AE spectra profiles are strongly dependent on the particle sizes considered. Interpretation of the power spectra is complicated by the fact that the AE originating in the system is distorted by several factors, in-

cluding transmission, reflection and frequency transfer characteristics. From the Figures 4.16 and 4.17 another important feature is evident: as the particle size increases, the energy of the spectra shifts toward lower frequencies (frequency shifting). The phenomenon follows the spectral trend of particle striking against a rigid wall as modeled in Section 4.2. A large particle will cause an impact of smaller collision time compared to the collision of a small particle as shown in Figures 4.2 and 4.3. Thus, the signal pressure generated by the collision of a particle size A (200 μm) will have a larger bandwidth compared to the signal pressure originated by a larger particle (400 or 600 μm).

These effects are again consistent with the experimental work discussed in Section 3.2 and with the previously reported studies [29][41] [42]. Changes in AE frequency with particle size could be an important index for particle size characterisation. Further details and demonstration of this peculiar characteristic will be reported in the experimental results of Chapter 5.

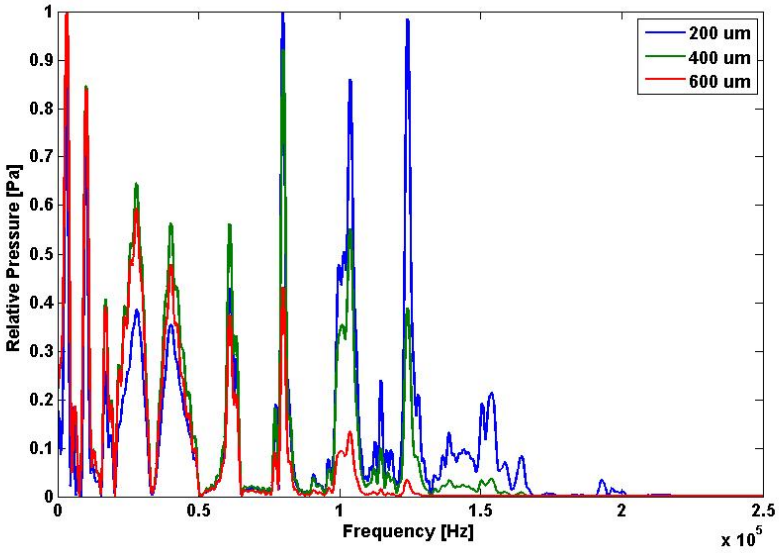

Figure 4.16: Predicted AE spectra (normalised) from the impact of one particle of different sizes.

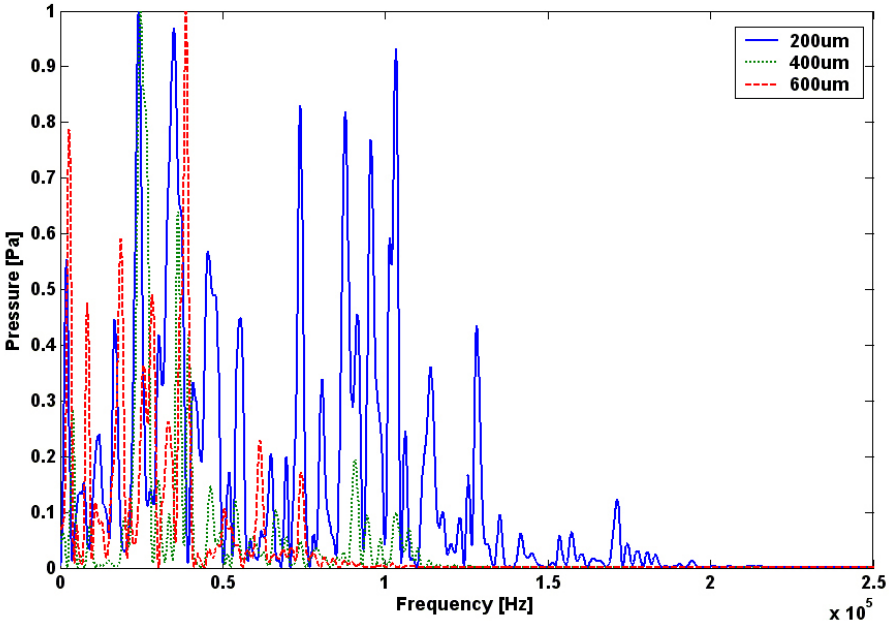

Figure 4.17: Predicted AE spectra (normalised) from the impact of 1000 random particles of different sizes.

4.5.5 Energy distribution

Figure 4.18 presents the predicted AE spectra shown in Figure 4.17 without magnitude normalisation and amplitude distortions in order to emphasise the changes in magnitude of the spectra versus particle size. Now, it is possible to note that the energy of the spectra increases when the particle size increases. A large particle will cause an impact of larger magnitude compared to the collision of a small particles according to the mathematical model described in Section 4.2.

The energy distribution was calculated for each particle size. The percentage of energy of six portions of each spectrum (30 kHz wide) was computed against the total energy of each spectrum (between 0-180 kHz). Table 4.4 presents the results and Figure 4.19 shows what proportion of energy falls into each range of frequencies. Between 0-60 kHz the distribution is 51%, 79.7% and 90% for the particle size A, B and C, respectively. The energy distribution of each spectrum is particle size dependant, and it extends between the DC component until 180 kHz with the main contribution at lower frequencies.

Table 4.4: Energy distribution

P. size	0-30	30-60	60-90	90-120	120-150	150-180kHz	Total
200 μm	19.9%	31.1%	17.9%	23.2%	5.5%	2.2%	99.8%
400 μm	49.4%	30.3%	8.9%	11.0%	0.2%	0.0%	99.8%
600 μm	53.5%	35.4%	10.4%	0.5%	0.0%	0.0%	99.9%

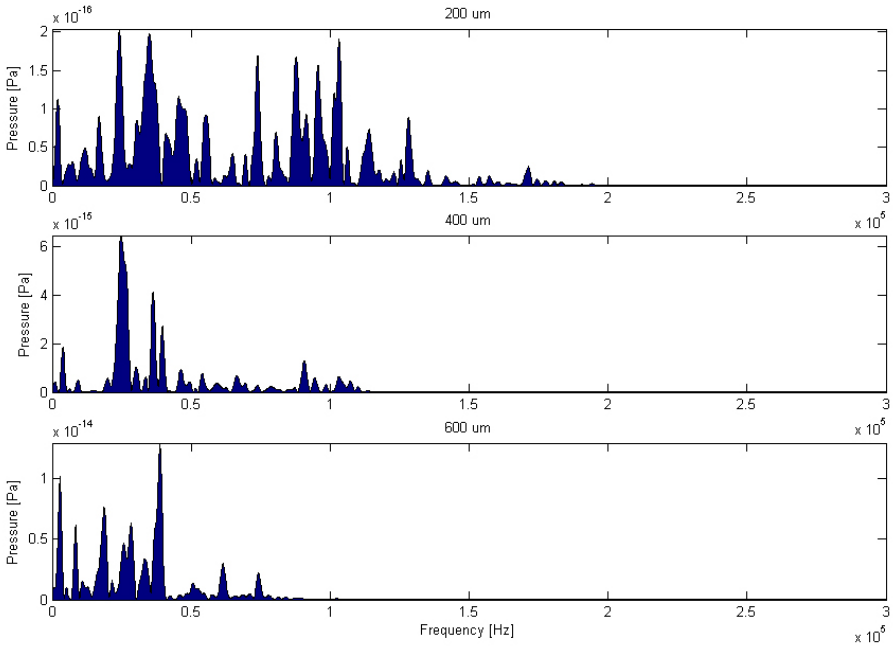

Figure 4.18: Energy distribution due to impact of random particles of different size and concentrations.

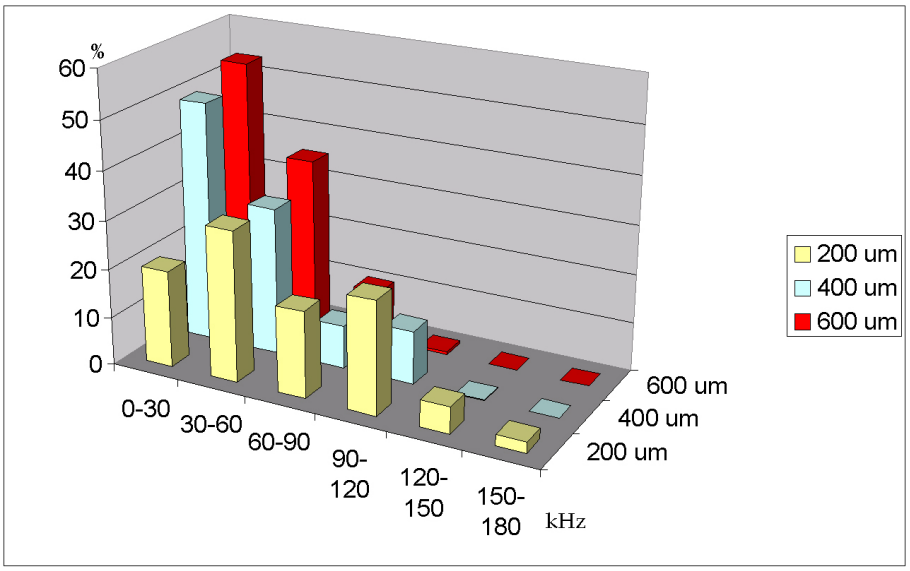

Figure 4.19: Histogram of the acoustic energy distribution.

4.5.6 Discussion

This Chapter is very important for the design of the passive acoustic system. Before designing any system it is necessary to assess all its requirements. In this work, mathematical and FE modelling techniques have been used for a better understanding and underlying dynamics of the complex system of the heterogeneous mixture in a reactor vessel. The input function of the particle impact has been mathematically modelled and the jacketed reactor vessel has been simulated using the FE method. The excitation functions representing the chemical particles impacting the inner wall of the vessel and the FE vessel itself represent the passive acoustic system under analysis. The FE model has been experimentally validated and excellent correlation has been obtained between experimental and FEM predictions.

The major contributions of this Chapter to the design of the passive system are listed below.

- The presence of resonant longitudinal modes of the glass-oil-glass combination have been assessed mathematically and confirmed with the FE model. The oil layer will produce standing waves at 90 kHz that are dominant on the acoustic signature of the vessel. The effect of the resonant modes has to be taken into account for distinguishing between the energy contribution of the particle impacts and the acoustic signature of the vessel.

- The reactor vessel is a highly attenuating system; only 1.1% of the energy in the horizontal plane is transferred through the system to the receiver, therefore attention has to be paid to the sensitivity of the ultrasonic transducer.

- Each layer of material behaves as a duct for propagating the sound waves and the acoustic energy of the particle collisions is mainly propagated in the vertical direction. This means that the energy of the particle collision, able to reach the outer side of the model, is not strongly affected by the position of the input signals. The particle impact at the furthest collision point is only 3% weaker than the closest point. These observations are important when the position of the transducer attachment or the position of the stirrer has to be considered during the experimental work.

- An increase in energy with an increase in either particle size or concentration. This results in an overall increase in the ultrasonic energy.

- All the AE spectra profiles are strongly dependent on the particle sizes considered. A lowering in frequency of the principal frequency components is predicted with increasing particle size.

- A significant outcome is that the overall energy distribution extends to 180 kHz, with main contributions between 0 and 60 kHz and a peak around 40 kHz.

The results presented so far aim to offer a new approach to the design of a passive acoustic monitoring system, in which FEA can be used to model almost any vessel reactor. Predicting the frequency range of interest from the AE spectra associated with particle collisions is fundamental for the designing of suitable sensors for monitoring these heterogeneous systems. This was not possible to achieve with the commercial resonant transducer because the AE signals observed were altered by its frequency transfer function.

The AE observed at the transducer will therefore be dependent not only upon the particle's physical properties and the dynamics of the impact itself, but also upon the propagation of sound in the target medium and the functional response of the acoustic sensor.

If the transfer function of the Nano30 transducer is known, then it is feasible to perform deterministic deconvolution [95]. However, if the fingerprint of the Nano30 transducer are unknown in advance, then its estimate is needed. As already mentioned, it was not possible to estimate or to model the Nano30 commercial transducer [74] due to its unknown internal characteristics. Instead, this was accomplished by using the 'pencil lead break' technique (Hsu-Nielsen source [68][69]).

It is important to underline that, even though each plot of the frequency response of the Nano30 was repeatable (See Section 3.3), the pencil lead test tends to give the overall characteristic of the resonance modes of an acoustic sensor, and due to its inconsistency, it is not an absolute technique for evaluating the frequency response of an acoustic sensor [69]. Hence, its estimate will be incorrect for the deconvolution. In turn, the estimate of particles impacts will also be incorrect. The lower the estimate of the frequency response of the acoustic sensor, the worse our estimate of the deconvolved signal will be. That is the reason why usually inverse filtering the signal is not a good solution.

By modelling the predicted system response to changes in particle size and particle concentration it will be possible to produce a methodology to determine the size and concentration of particles in optically opaque heterogeneous mixtures without the need for physical sampling of the suspension. This approach could be extended to any chemical process and it is an inno-

vative idea for applications in process analysis.

4.6 Conclusions

This Chapter has presented the modelling of a heterogeneous mixture of itaconic acid particles suspended in fluid in a reactor vessel. A simulation approach to analyse the complex interactions between the chemical particles and the vessel wall using finite element (FE) modelling has been undertaken.

The excitation function was derived from the Hertz's theory and used as the model stimulus corresponding to particles striking the inner glass wall. A 4-layer 2D model has been developed comprising a liquid-load medium and a glass-oil-glass combination corresponding to the jacketed reactor vessel. Excellent correlation has been obtained between experimental and FEM prediction during the model's validation procedure.

Modelling has then been used to predict the effects of particle impact position, particle concentration and particle size on AE. All the predictions have shown consistency with other published theoretical and experimental studies as discussed throughout the Chapter.

Chapter 5

Development of a new passive acoustic system

The modelling of particle-wall interactions with the glass wall of the reactor vessel led to a better understanding of the frequency range required for passive acoustic monitoring of heterogeneous systems. The study has provided the basis of transducer design specifications for the development of passive acoustic monitoring systems.

The main transducer design characteristic is the frequency range of the AE signals produced by the particle wall interactions. The modelling in Chapter 4 predicted that this range extended between 0-180 kHz. It was considered extremely difficult to produce an efficient transducer which would cover this wide frequency range. Consequently, the work described in this Chapter will consider two transducer design approaches, with complementary characteristics. In order to capture and analyse the full frequency bandwidth associated with the particle AE, an off-resonance transducer design will be investigated. Unfortunately, due to the nature of this design this device will

provide low sensitivity and a second resonant device will also be developed. It is important to note that each transducer design will enable different aspects of the particle suspension to be evaluated: frequency effects using the wide-band off-resonance device; and measurement of low concentrations using the highly sensitive resonant transducer approach. Moreover, the design of a low noise pre-amplifier and its analysis will complete the development of this new passive system approach. Importantly, the information provided in this Chapter can be used as the basis for the development of a more sophisticated and complete commercial acoustic system

5.1 System requirements

In the previous Chapter, the energy transfer between the internal and external wall of the reactor vessel was shown to be 1.1%, owing to the acoustic impedance mismatch between the layers of the vessel. One way of maximising this energy transfer is to match the acoustic impedance of the sensor to the acoustic impedance of the glass wall, which is 15.3 MRayls. This can be achieved by the combination of a piezoelectric ceramic with a polymer phase, to form a piezoelectric ceramic composite [87], which can offer performance advantages over conventional piezoceramic transducers especially for operation into low acoustic impedance media. The transducer composite configuration offers advantages in terms of being able to tailor the acoustic impedance of the device, to enhanced electromechanical coupling efficiency and a reduction of parasitic lateral modes [96] compared to conventional piezoceramic based devices. A considerable amount of work has been directed toward the development of these devices since the microstructure geo-

metry and material parameters can have a large effect on their operation [87][96][97][98][99][100][101][102]. Although there are many ultrasonic transducers on the market, none is able to satisfy all of the system requirements detailed in Chapter 4.

Consequently, piezoelectric ceramic composite transducers were designed using two distinct transducer specifications:

Off-resonance tranducer	**Resonant transducer**
Wide frequency: 0-180 kHz	Operating frequency : 40 kHz
Flat frequency response	High sensitivity at operating frequency
Conformable	Small transducer footprint
Good acoustic match to glass	Good acoustic match to glass

In addition, to improve the signal to noise ratio (SNR), a low noise preamplifier, was also designed and fabricated. The design was developed to enable the amplifier to be incorporated into the transducer housing and hence, become an integral part of the passive monitoring system.

The author's role on this research fully covered the whole aspects of the design of the ultrasonic system, starting from the FE model of both transducers, the amplifier design, and their characterisation and experimental work and analysis of the passive monitoring system.

5.2 Piezoelectric transducer materials

Todays transducer technology demands the use of advanced piezoelectric materials. The piezoelectric effect was first discovered by the Curies in 1880, in naturally occurring quartz [71]. A wide range of materials now exist that are piezoelectrically active, including piezoelectric ceramic, piezoelec-

tric polymers, piezoelectric single crystal materials and piezoelectric ceramic composite materials.

5.2.1 Piezoelectric ceramic materials

The piezoelectric ceramic family is the most commonly available piezoelectric material used for transducer applications today. These materials have a number of characteristics which make them suitable for a wide range of sensors actuators applications, and offer more advanced properties than the quartz material discovered by the Curies. Piezoceramics give improved transducer efficiency properties because of their high electromechanical coupling coefficient *(k_t)*, typically around 0.5. Piezoceramics also have high specific acoustic impedance (typically 30 to 35 MRayls), which has a direct influence upon the transmission and reflection of energy at the material boundaries with the external load media [97]. Thus, they couple well into metals such as steel and copper (Z of 45 and 42 MRayls, respectively), but unfortunately, poorly into low impedance media such as water (Z of 1.5 MRayls). Their high permittivity (ϵ_r), ranging from 1000 to 3500, allows good electrical matching because it reduces the transducer input electrical impedance [97]. Furthermore, these materials can be used at elevated temperatures between 190 $^{\circ}C$ and 600 $^{\circ}C$ depending on the Curie temperature of the individual piezoceramic material. It is important to mention that there is not an ideal ceramic material for use in all transducer applications; a designer must choose the ceramic carefully for each individual circumstance. The lead zirconate titanate (PZT) family has found widespread use because of its good piezoelectric properties, allowing construction of extremely efficient devices. An example of a piezoceramic utilised in the manufacture of the transducers employed

in this work is PZ26 (also called PZ4D Navy I). This material is commonly employed for the design of PZT transducers and its manufacturing process has been well established. PZ26 is a hard PZT material with a good coupling factor ($k_t = 0.57$), high Curie temperature (320 $°C$), low dielectrical loss and very good stability over time [99].

5.2.2 Piezoelectric polymers

Another type of piezoelectric material is the piezopolymer group, such as polyvinylidene fluoride (PVDF). This material is fabricated in thin flexible sheets (25 to 110 μm) with a very low specific acoustic impedance (4 MRayls), allowing higher transmission and reception sensitivities in materials such as water or air [103]. Unfortunately its low electromechanical coupling factor coefficient ($k_t = 0.15$) and its relatively low permittivity ($\epsilon_r \simeq 9.7$), make it a poor transmitter of ultrasound [87]. Examples of experimental applications can be found in the literature [104][103], and importantly, in this Thesis in Section 4.4.1 and in Chapter 6. Polyvinylidene fluoride was employed for the manufacturing of a broadband sensor, employed for the validation of the FE vessel model, and a broadband hydrophone for the active acoustic work.

5.2.3 Piezoelectric single crystal materials

The new ranges of perovskite single crystal piezoelectric materials such as pmn-pt and pzn-pt offer extremely exciting possibilities for ultrasonic transducer design in a number of applications, including biomedicine, non destructive evaluation and sonar. Such materials can demonstrate extremely high electromechanical coupling in the thickness direction ($k_t > 0.9$), leading not only to improved efficiency but also to much wider bandwidths (approa-

ching two octaves) than those realised by more conventional piezoelectric ceramic designs, provided that the device is subject to appropriate fabrication procedures. This may be achieved by combining piezoelectric composite transducer configurations with the single crystal material as the active component. However, the range of materials available to date is costly, suffers from inhomogeneity and fragility, and renders the required manufacturing processes difficult and not particularly cost effective.

5.2.4 Piezoelectric ceramic composite transducers

Piezocomposite transducers incorporate active piezoceramic elements within a passive polymer phase, to yield enhanced piezoelectric properties with respect to the parent ceramic. These devices are expressed in terms of the connectivity of each phase (the representation corresponds to connectivity in the ceramic phase, followed by the polymer phase), where this refers to the number of orthogonal directions in which each particular phase is continuous [89]. There are a number of possible connectivity patterns, but for the purposes of this Thesis only the 1-3 connectivity [96] and the 3-1 connectivity [89] devices will be discussed. In particular, the general concept of piezoelectric ceramic composite transducer behaviour will be described in this Section using the 1-3 connectivity configuration, while a more detailed discussion of the 3-1 composite configuration will be given in Section 5.4.

With reference to Figure 5.1, 1-3 composites offer considerable advantages for operation into low acoustic impedance media when compared to standard piezoceramic materials. Mechanical stiffness may be adjusted by an appropriate choice of filler material and ceramic volume fraction [105]. Moreover, further design optimisation is possible by varying ceramic rod shape and dis-

tribution, an aspect which is critical at the low volume fractions required for application in reception [106]. As a result of the inherent structural complexity and large number of constructional and operational variables, design understanding and possible optimisation of 1-3 connectivity composites is not a straightforward matter. The design process benefits greatly from the availability of accurate computer simulation models [105][107].

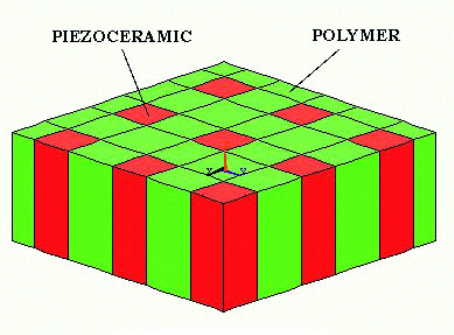

Figure 5.1: Ceramic/polymer composite transducer

For many applications the theoretical behaviour for 1-3 connectivity composites is well documented. Provided that the ceramic pillars are sufficiently tall, with narrow inter-pillar spacing, composite transducer behaviour may be predicted well via one-dimensional (1-D) theories [105][107]. However this approach can be difficult to justify at the extremes of ceramic-polymer volume fraction where inter pillar (or internal modes within the ceramic) resonances can corrupt the desired thickness mode. Furthermore, manufacturing constraints do not always permit the proper geometry for 1-D operation and more computationally intensive methods are required for prediction of composite performance [106].

The introduction of a modelling strategy for 1-3 connectivity transducers, by Smith et al [105], enabled the generation of computer models for the prediction of composite transducer behaviour. This modelling approach requires

the simultaneous solution to the piezoelectric-elastic equations for both active and passive phases in the composite transducer, resulting in a single set of equivalent thickness mode parameters. For a given ceramic/polymer composite configuration, the specific acoustic impedance $\overline{Z_A}$, the thickness mode electromechanical coupling factor $\overline{k_t}$ and the bulk wave velocity in the thickness direction $\overline{v_l}$ of a composite transducer can be expressed in terms of Smith's equivalent parameters $\overline{c_{33}^E}$, $\overline{e_{33}}$ and $\overline{\epsilon_{33}^S}$ as described in Equations 5.1 and 5.2.

$$\overline{k_t} = \overline{h_{33}}/\sqrt{(\overline{c_{33}^D}/\overline{\epsilon_{33}^S})}; \quad \overline{Z_A} = \sqrt{\overline{c_{33}^D}; \overline{\rho}}; \quad \overline{v_l} = \sqrt{\overline{c_{33}^D}/\overline{\rho}}; \tag{5.1}$$

$$\overline{c_{33}^D} = \overline{c_{33}^E} + (\overline{e_{33}})^2/\overline{\epsilon_{33}^S}; \quad \overline{h_{33}} = \overline{e_{33}}/\overline{\epsilon_{33}^S} \tag{5.2}$$

The overline bar symbol denotes a composite parameter, the superscripts E, D, and S indicate a constant electric field, a constant electric displacement and a constant strain, respectively. Hence, $\overline{c_{33}^D}$ is the elastic stiffness under a constant electric displacement D or $\overline{c_{33}^E}$ under costant electric field E. $\overline{\epsilon_{33}^S}$ is the permittivity under constant strain S and $\overline{e_{33}}$ represents the reciprocal of the piezoelectric voltage constant. Here, the density of the composite $\overline{\rho}$ is derived from the equilibrium densities of the ceramic ρ^c and filler materials ρ^f as in Equation 5.3.

$$\overline{\rho} = \Phi\rho^c + (1 - \Phi)\rho^f \tag{5.3}$$

where Φ represents the volume fraction. Note that all the piezoelectric symbols have their usual meaning as defined in [108] and in Table 7.3.

This one dimensional modelling approach requires the piezoceramic pillars to have a low width-to-height ratio (aspect ratio AR) and sufficiently fine

lateral pillar spacing in order to promote homogeneous behaviour from the composite. Through implementation of the above Equations, it is possible to obtain characteristic responses for 1-3 composite transducers, assuming the above geometrical constraints, over the entire ceramic volume fraction range.

For the purposes of reviewing the behaviour of 1-3 composites, a PZT5A piezoceramic and CIBA-GEIGY CY1301/HY1300 epoxy combination, operating at 500 kHz, has been analysed. The frequency range of operation was indicative and it was selected because of the availability of the all material properties at that frequency range on the acoustic Tables.

From this evaluation, the electromechanical coupling coefficient, $\overline{k_t}$ and specific acoustic impedance $\overline{Z_A}$, are of particular relevance to this work and are presented in Figures 5.2 and 5.3, respectively.

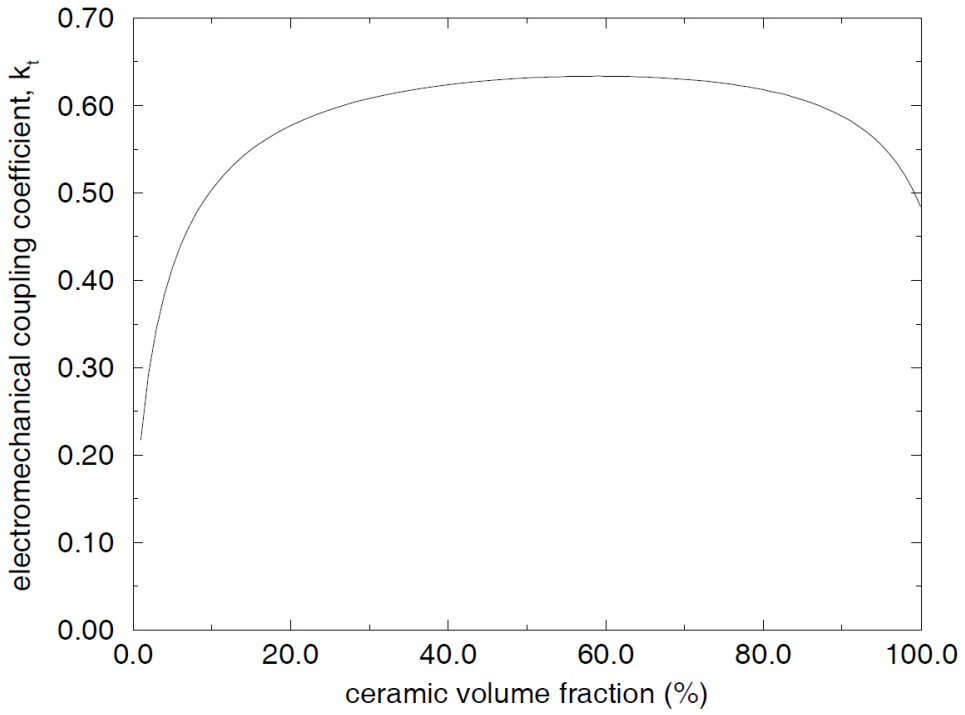

Figure 5.2: Variation in electromechanical coupling co-efficient predicted by Smith's model

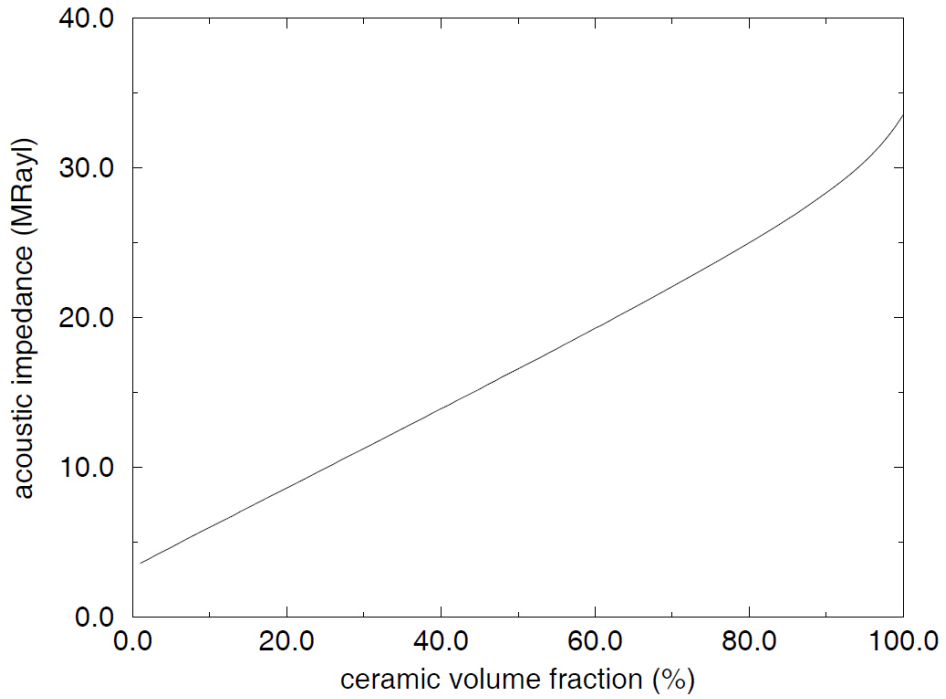

Figure 5.3: Specific acoustic impedance as a function of ceramic volume fraction, as predicted by Smith's model

From Figure 5.2, it can be observed that the electromechanical efficiency of the composite transducer approaches the value of k_{33} equal to 0.7 for the ceramic and is relatively constant over the volume fraction range 30% - 80%. At the extremities, the values for $\overline{k_t}$ have fallen due to either lateral clamping by the polymer, at high volume fractions, or through the elastic loading of the surrounding polymer, in the lower volume fraction range.

The estimated specific acoustic impedance $\overline{Z_A}$, shown in Figure 5.3, confirms the ability of these composite transducers to realise a better match to low acoustic impedance loads, when compared to conventional piezoceramics. For the PZT5A/hard set composite, an essentially linear acoustic impedance range between 5 - 28 MRayl has been predicted, although this could be re-

duced further through application of a lower acoustic impedance polymer filler. It is also interesting to note that the relative permittivity ϵ_r can be reduced from that of pure ceramic allowing greater versatility when matched to electronic circuits [89][99].

5.2.5 Summary of piezoelectric materials

In conclusion, there are four types of piezoelectric materials generally employed for ultrasonic transducers: piezoelectric ceramics which are very efficient for energy conversion but have a large acoustic mis-match with low impedance media; piezoelectric polymers which are significantly less efficient but have a close acoustic match to water; piezoelectric single crystal materials which offer great potential but are still in the early research stage for many applications; and piezoelectric composites comprising both ceramic and passive polymer phases which have been developed to provide efficient transduction into low acoustic impedance media.

Piezoelectric ceramic/polymer composites have superior properties when compared to single phase ceramic materials for this application because they combine high coupling, have few spurious resonance modes, intermediate dielectric constant and ability to tailor acoustic impedance. A detailed account of two transducer designs employing piezocomposite materials will be provided in the following Sections.

Bandwidth and sensitivity of ceramic piezocomposite transducers are usually complementary characteristics [109]. Hence, the requirements of a very sensitive device operating over a wide frequency range (0-180 kHz) is very challenging to achieve. This led to the decision to adopt two transducer design approaches. The first approach is a 1-3 connectivity piezocomposite

transducer which is designed to work below its thickness mode and this is termed the off-resonance transducer for the remainder of this Thesis. The design goal is to produce a flat frequency response covering the predicted AE spectral characteristics as discussed in Chapter 4. Whereas, the second approach utilized a resonant stacked piezocomposite structure which operates in the thickness mode regime. In particular, the resonant stacked transducer was designed to be very sensitive for discriminating the weak interactions of smaller particles and low particle concentrations, but with limited bandwidth, whilst the off-resonance composite sensor would benefit from a flat frequency response across the desired operating frequency range, although with a reduced sensitivity.

5.3 Design process and development of a broadband off-resonance transducer

The monitoring of chemical particles for process analysis has provided the motivation for the development of a transducer with low frequency performance and high bandwidth.

As mentioned, the system requirements are represented in the following Table 5.1, the most important target parameter starts from the top of the table:

Table 5.1: Target parameters of the off-resonant sensor

Wide frequency: 0-180 kHzd
Flat frequency response
Electrical Impedance: matched to 15 MRayls (glass)
Maximised Electromechanical coupling factor
Maximised Capacitance

The design of the piezo-transducer process involves:

- Piezocomposite structure selection
- Material selection
- Parameter choice such as: AR, VF, k_t, Z.
- Matching layer design
- Backing layer design (if needed)

To accommodate such a specifications, a 1-3 connectivity piezoelectric ceramic composite transducer was designed to operate below its fundamental resonant mode, in order to produce a flat frequency response, thus maximising its bandwidth. Figure 5.1 illustrates the general 1-3 ceramic/polymer composite transducer configuration, which comprises piezoelectric ceramic pillars embedded in a polymer matrix.

Two piezoelectric materials were selected for the design. PZT-5H provided a very high permittivity, coupling coefficient, and piezoelectric constant; whereas PZT-4D was selected for its good piezoelectric voltage constant, an important factor for assessing a material's suitability for acting as a receiver, and its low mechanical and dielectric losses. Soft setting epoxy CIBA/GEIGY CY208/HY956 [88] was also incorporated into the design due to its high damping characteristics which would minimise unwanted lateral resonances (The Appendix in Chapter 7.2.2 details the material properties)).

After selecting the most suitable sensor configuration and its material's choice, the Smith's Equations 5.1 and 5.2 were used to target the design requirements. To achieve high electromechanical properties and an acoustic impedance close to the glass acoustic impedance (15.3 MRayls), the VF of

the ceramic in the composite was selected to be equal to 35% [99]. This would guaranteed high performance for the sensor as a receiver.

The thickness mode matrix manipulation based on linear systems modelling (LSM) [110], an uni-dimensional, in house software developed for the design of piezoelectric transducers was employed for the design of the sensors. Uni-dimensional modelling techniques have been well documented for prediction of piezoelectric response. The model utilised for this work [107][111] has the facility to investigate the influence of electrical loading in reception to predict impedance, reception for piezoceramic, piezocomposite transducer performance as a function of the operating environment.

Four 1-3 connectivity devices were designed and manufactured to operate below their fundamental resonant modes of 1.2 MHz, 800 kHz, 400 kHz and 190 kHz. The sensors had the same lateral dimensions of 18 x 18 mm^2 but different thicknesses of 1.5 mm, 1.8 mm 3.7 mm and 7.8 mm respectively. It is important to note that a trade-off exists between the sensitivity of the off-resonance transducer and its unimodal behavior: increasing the transducer thickness results in decreasing its mechanical frequency mode, and hence, the sensitivity of the device for operation as an off-resonance receiver in the frequency range below 180 kHz is improved because of its first resonant mode gets closer to this operating frequency range. However, a transducer with the thickness dimension closer to its lateral dimension cannot be completely unimodal. The main concern was to achieve a 1-3 composite transducer which exhibits a low cross-talk between longitudinal and lateral modes.

Due to the limitation of the LSM software to one-dimension, this concern was further investigated through Pz-Flex FE software.

First, different sets of composite characteristics were modelled to minimise

the lateral mode in terms of amplitude and to ensure that good frequency separation between the lateral and fundamental thickness mode was achieved.

Unfortunately, after several empirical tests and experiments, only the device with the lowest fundamental resonant thickness mode had sufficient sensitivity to work off-resonance for this application and with moderate cross-talk between the lateral and longitudinal mode. This corresponded to the sensor with the thickness resonance mode at 190 kHz, and hence only this device, is reported herein. Hossack and Hayward [106] were among the first to apply the FE analysis for the modelling of such composite transducers. They studied the vibrational and electromechanical characteristics of a wide range of composite transducers with 1-3 connectivity. In their work, it was demonstrated that a small pillar aspect ratio AR and relatively high volume fraction VF maximised the uniformity in thickness dilatation and the electromechanical efficiency. It was also demonstrated that using higher aspect ratio pillars in low ceramic volume fraction piezocomposites, resulted in a strong lateral resonant activity within the polymer at the frequencies near the thickness resonance.

In order to minimize the contribution of lateral modes in the off-resonance transducer, the passive polymer phase was selected to exhibit a high shear damping characteristic. CIBA/GEIGY CY208/HY956 has a measured shear damping coefficient of 6063 dB/m and offers a solution to minimize the parasitic lateral modes in the piezocomposite structure. It should be noted that this material also exhibits a high longitudinal damping coefficient, 825 dB/m, which will limit the device sensitivity. This was considered to be acceptable as the overriding design objective was to produce a wide operational frequency range for this transducer.

The final composite microstructure had a saw pitch and saw width of 2 and 0.8 mm, respectively. The AR was 0.138 and the dimensions of the device were 18 x 18 x 7.8 mm^3.

Figure 5.4 shows the magnitude and phase of the simulated impedance using FEA. A thickness of 7.8 mm was designated to achieve a fundamental

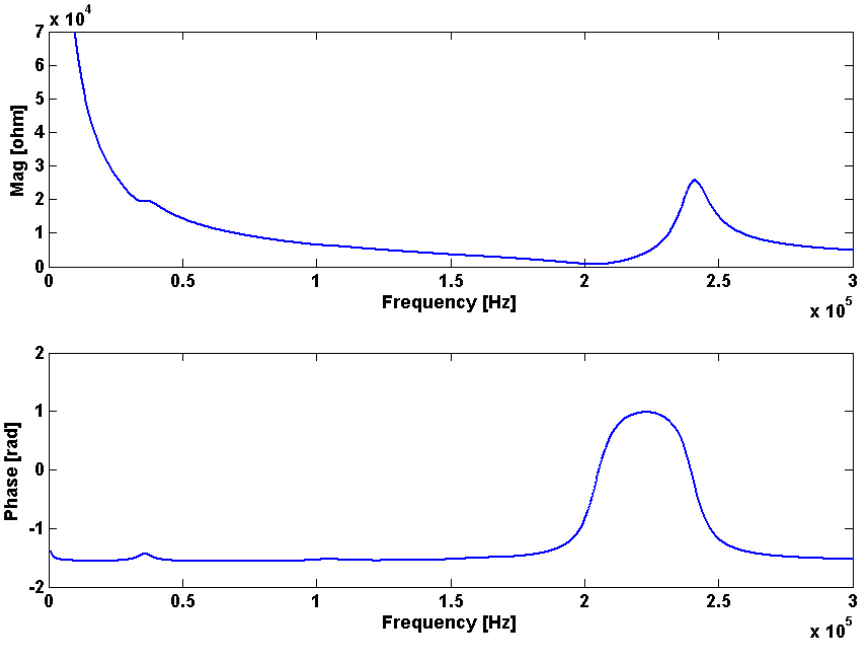

Figure 5.4: Predicted impedance magnitude and phase of the off-resonance transducer

thickness resonance mode required at 190 kHz. FE shows the presence of a weak mode at 35 kHz. This lateral mode is damped down by the soft polymer and there are no other unwanted significant resonance modes within the operational frequency range. This matched the system requirement and achieved the total acoustic impedance close to the vessel wall acoustic impedance. The acoustic impedance of the composite transducer and the glass vessel was $Z_1 = 13.18$ MRayls and $Z_2 = 15.3$ MRayls, respectively. Due to the mismatch in acoustic impedance between these materials, there will be

reflection and transmission of sound at the interface. Although, this will not be significant due to fact that the piezocomposite has been designed with an acoustic impedance close to glass. Nevertheless, it is important to ensure that the transducer has good coupling to the curvature associated with the reactor vessel. It was originally considered that another reason for using a soft setting polymer filler material was to introduce a degree of conformability into the piezocomposite device. Unfortunately, due to the use of the lowest frequency design, the thick nature of this device restricted the materials flexibility. Thus a mechanical shoe was required to ensure good coupling between the vessel and the transducer. The general formulae to predict the acoustic impedance of an intermediate layer (generally considered as a matching layer to promote the transfer of energy between two media) is the geometric mean between the acoustic impedances of the two outer layers and given by Equation 5.4.

$$Z_{ML} = \sqrt{Z_1 Z_2} = 14.53 MRayls \tag{5.4}$$

where Z_1 is the acoustic impedance of the first medium (vessel glass wall) and Z_2 is the acoustic impedance of the second medium (composite transducer). Sourcing a suitable material with this acoustic impedance proved difficult and for ease of manufacture, it was decided to use Aluminium as a mechanical shoe, which has an acoustic impedance of 17.6 MRayls. This material closely matches the design requirements, is readily available, easily machinable and it resists corrosion.

At frequencies between 0-180 kHz the conventional quarter-wavelength rule would not guarantee a broadband behaviour of the sensor because a fixed matching layer thickness would not cover the whole frequency range.

Instead, a 1 mm thin interface layer was tailored to provide a curved 'shoe' interface between the transducer and the vessel. As the 'shoe' employed was thin, the attenuation of ultrasonic waves from the face of the element could be neglected and any unwanted features would occur outside the frequency range of interest. This would ensure wide-band performance of the receiving sensor. Driving the piezo-electric element off-resonance resulted in smaller received amplitudes compared to conventional resonant devices. This was the main disadvantage of the transducer design. In order to maximise the response in the operating frequency range, elements were air backed, so that the maximum energy was received into the active elements.

5.3.1 Construction of the device

The 1-3 transducers were manufactured using the "Dice and Fill" construction technique [112]. Initially the ceramic block was diced using a mechanical 0.8 mm saw and cut at regularly spaced intervals to a specific depth (7.9 mm). The block was then rotated 90 degrees and the procedure repeated until the block consisted of a matrix of ceramic pillars surrounded by air [112]. The gaps were then filled by the soft setting epoxy CIBA/GEIGY CY208/HY956. The composite block was then cut to a thickness of 7.80 mm to produce the desired frequency of operation for the transducer. An evaporated gold electrode was applied to both faces and electrical connection between the transducer faces and the pre-amplifier (See Section 5.5) used 0.5 mm diameter wire.

Once the electrical impedance and surface displacement profile (SDP) measurements had been taken (using an HP-212 electrical impedance analyser and a PSV-400 Scanning Vibrometer, respectively), each transducer was

placed in a holder case incorporating the interface layer and connected to a coaxial cable (1 m long) to provide the electrical connection.

5.3.2 Analysis of off-resonance transducer

The impedance profile of the composite device was measured experimentally and compared with simulations performed at the design stage using FEA (finite element analysis). The results are shown in Figure 5.5 and detail the magnitude and phase of the acoustic impedance. FEA predicted the electrical resonance of the thickness mode with an error of 10%. However, the mechanical mode is not predicted accurately by FEA. This is attributed to the damping model utilized in the FEA . The damping coefficients used in the model were obtained in an empirical manner, by an iterative process of varying the damping to match the electrical impedance of the modelled and experimental data as Reynolds suggested during his work when incurred in the same limitations of the material properties [99]. It is evident from Figure 5.5 that there is a mismatch between the experimental and the predicted data at frequencies above 180 kHz. However, no strong or intra-pillar modes exist in the vicinity and below the main thickness mode resonance, with only a discontinuity at 35 kHz. In the measured impedance profile, this lateral mode is even more damped down respect to the predicted one. The main feature of the transducer design is that in the operating frequency range of 0-180 kHz, the overall impedance profile is uniform in both the experimental and FE plots (including the mode at 35 kHz). In general, the high velocity of sound in ceramic, coupled with the low aspect ratio employed in the device ensure that any inter-pillar modes are at a higher frequency (833 kHz), and consequently have little impact on device performance [96]. The surface

displacement profile (SDP) was obtained at the main resonance indicated by the impedance profile, while operating in air. In each case, electrical excitation was applied by a signal generator delivering a 10 cycle sinusoid and the displacement was assessed using a laser vibrometer system with a sensitivity of 2.5 $\mathring{A}$ which scanned the front surface of the transducer in a raster fashion [99]. The SDP at the thickness resonance is displayed in Figure 5.6 in both magnitude and phase. Figure 5.7 shows each ceramic pillar displacing by a slightly greater quantity than the surrounding polymer, with overall pillar displacement magnitude increasing in the centre of the device due to the lack of support at the transducer edges. Even though the transducer was designed to operate in the reception mode, its behavior when acting as a transmitter was tested to ensure that the sensor displacement was uniform and unimodal at the thickness mode. Importantly, this uniform ultrasonic displacement observed on the surface of the composite is a clear indication of the efficient coupling of the mechanical energy from PZT to the epoxy.

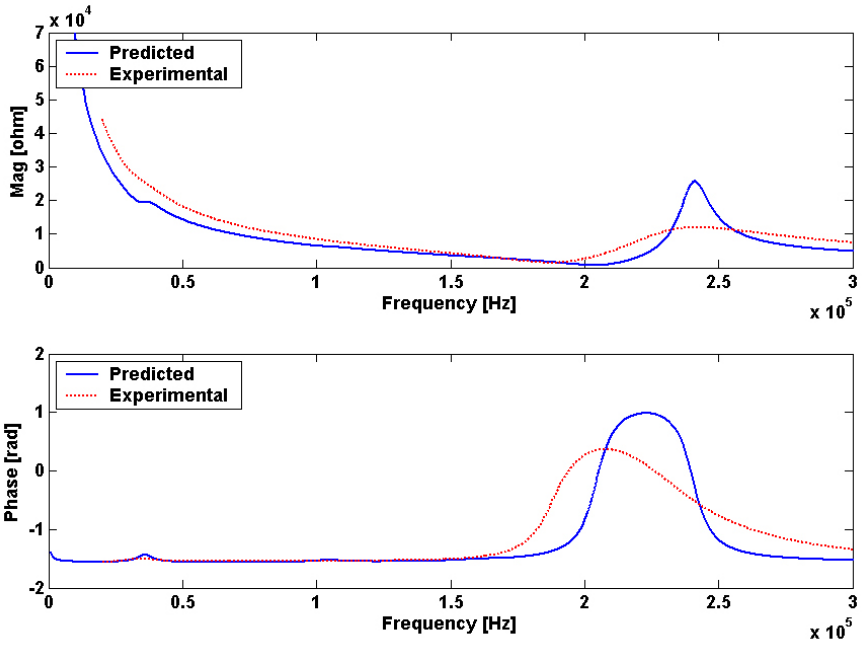

Figure 5.5: Impedance profile of the off-resonance transducer

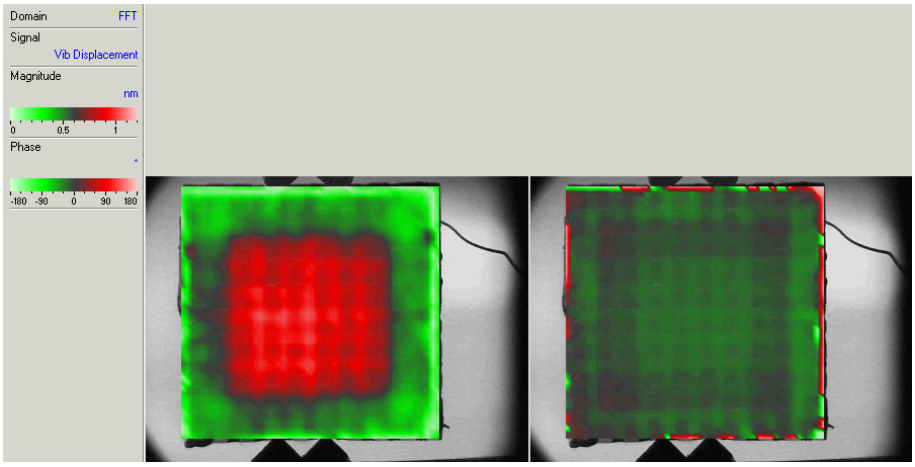

Figure 5.6: Experimental SDP of the off-resonance transducer, magnitude (left) and phase (right) at 190 kHz

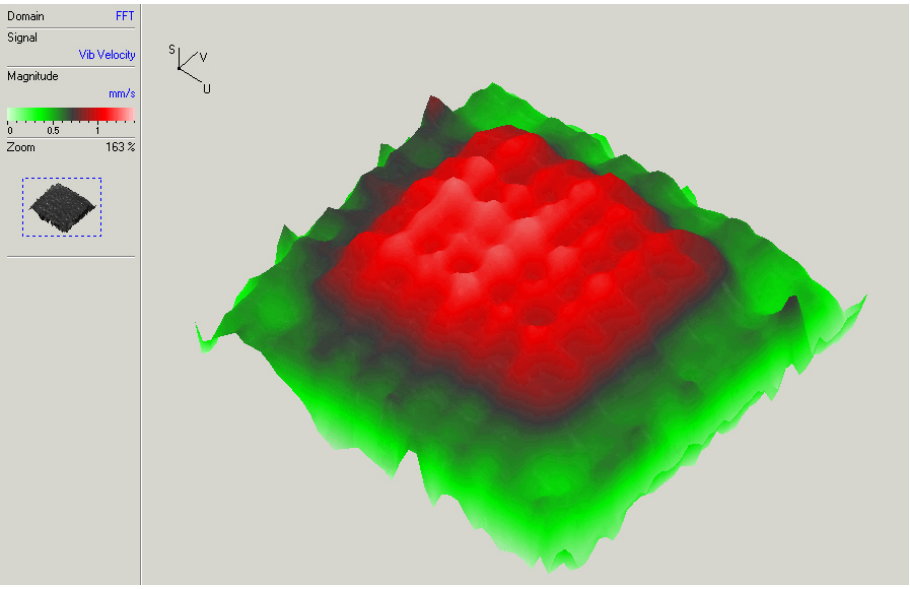

Figure 5.7: Experimental three dimensional SDP of the off-resonance transducer at 190 kHz

5.4 Design and development of a low frequency resonant stacked transducer

The analysis of particle interactions from the model, in combination with the experimental results using the commercial transducer, showed that a large contribution of energy produced by the interacting chemical particles is concentrated at low frequencies between 0-60 kHz (see Section 4.5.5).

Hence, the desirable target parameters are summarised in Table 5.2, starting from the most important:

Table 5.2: Target parameters of the stacked sensor

Operating frequency : 40 kHz
Maximised the sensitivity at the operating frequency
Electrical Impedance: matched to 15 MRayls (glass)
Maximised Electromechanical coupling factor
Maximised Capacitance
Small transducer footprint

In order to achieve such a low frequency mode of operation, a stacked type of piezoelectric transducer is an appropriate solution [113]. A stacked conventional piezoceramic transducer is made by connecting individual layers mechanically in series and electrically in parallel (see Figure 5.9) to reduce the fundamental thickness mode resonance. This can be achieved by bonding layers of materials with the polarity of neighboring layers reversed and alternating electrodes connected together [100]. There have been a number of reports concerning stacked transducers made from piezoceramics, piezocomposites and piezopolymers [100][101][114][113].

Multilayered piezoelectric composite devices with 1-3 connectivity prove difficult to manufacture because each layer must be produced individually and then bonded together. This introduces the complication of attaining alignment of the microstructure in the thickness dimension and at the same time, achieving thin bond lines [101]. Therefore, a piezocomposite design with an alternative connectivity (using the R. O'Leary multilayer piezocomposite design approach [101]) was chosen to work in the thickness mode regime. The stacked composite transducer comprised five layers of PZ26 (known also as PZ4D [115]) ceramic with a single slot in each vertical side incorporating a soft polymer CIBA/GEIGY CY208/HY956 [101] for reducing the lateral resonances and reducing the acoustic impedance. The ceramic rods were connected continuously in three directions, while the polymer was connected continuously in one direction. This configuration is described as possessing 3-1 connectivity as the active phase is uniform across three dimensions and the polymer phase is only uniform across one dimension (thickness).

The transducer was designed to operate as a receiver at its mechanical

resonance frequency, where the peak reception voltage occurs [113]. Figure 5.9 illustrates the structure of the stacked transducer configuration as described above. Furthermore, the bonded layers were cut longitudinally and filled with soft setting epoxy for damping the unwanted lateral modes and reducing the ceramic volume fraction.

The device had lateral dimensions of 9x9 mm^2 and saw cuts width of 0.9 mm and overall thickness of 37 mm. This resulted in a ceramic volume fraction close to 87% and acoustic impedance Z of 29.8 MRayls. The transducer case had an inner diameter of 45 mm and it was also used for casting the filler polymer; the soft polymer CIBA/GEIGY CY208/HY956 surrounded the active phase of the PZT stacked transducer as shown in Figure 5.8.

A thickness of approximately 7.4 mm was chosen for the individual layers of the prototype stack, with a predicted fundamental electrical resonance of 40 kHz with 50% 3dB bandwidth without the presence of a backing or matching layer as shown in Figure 5.9.

The matching layer was not included in the design because the piezocomposite stacked transducer was 20 times more sensitive (in transmission mode) than the off-resonance device (see the SDP analysis of Figures 5.6 and 5.11). Moreover, the contact surface between the transducer active element and the reactor vessel was considered satisfactory due to the relative small dimensions of sensor the front face (81 mm^2).

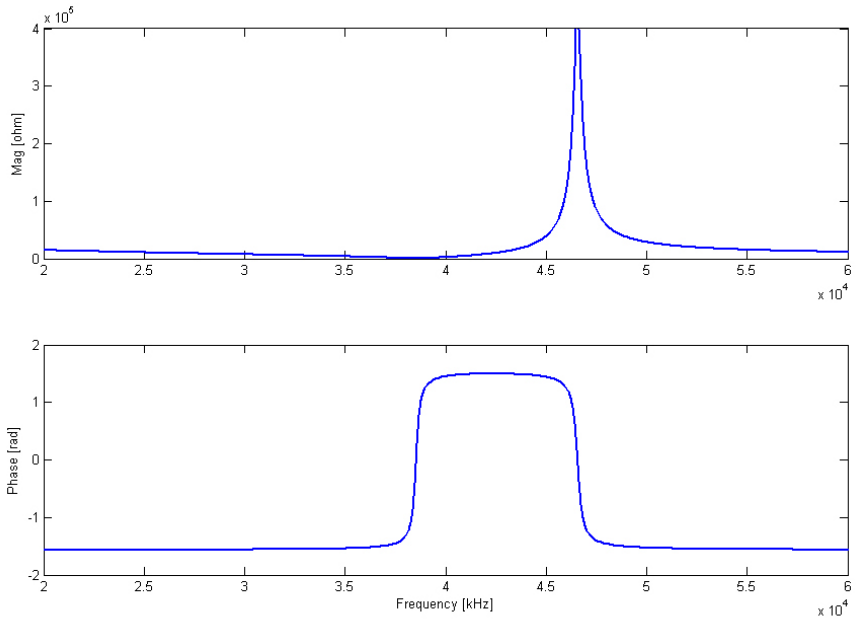

Figure 5.8: Predicted impedance magnitude and phase of the stacked transducer

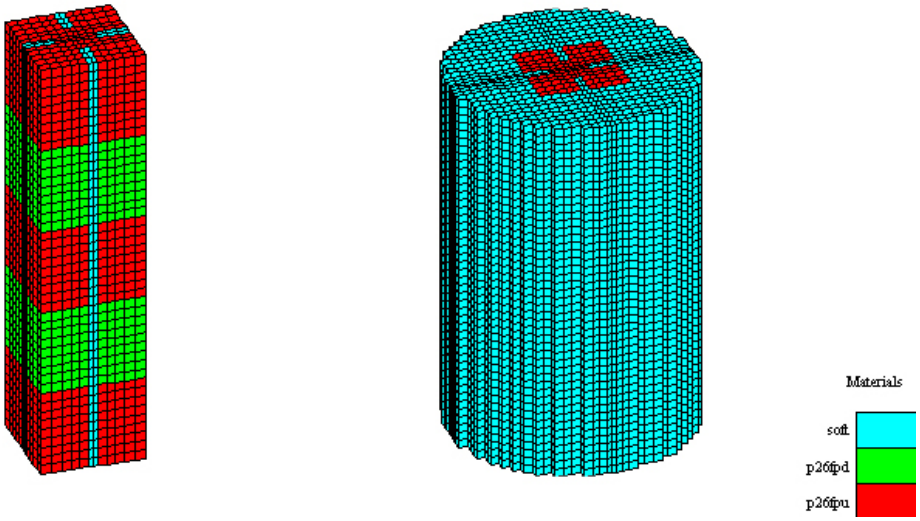

Figure 5.9: Diagram of the active phase unit consisting of a 3-1 connectivity composite (on the left) and the stacked composite block surrounded by polymer (on the right)

5.4.1 Construction of the device

Five individual sintered piezoelectric PZ4D blocks were cut and lapped to size (7.4 mm) resulting in each face possessing an average surface roughness of 9 μm. The layers were then bonded together using an epoxy adhesive and cut longitudinally. The bristle blocks were then turned over to repeat the dicing process from the rear to produce the structure illustrated on the left side of Figure 5.9. A Loadpoint Microace [116] dicing saw was used for the cutting process of the slots. The saw cuts were measured using a microscope at 0.9 mm. Importantly, the piezoceramic transducer was made by connecting individual layers mechanically in series and electrically in parallel. This was achieved by bonding layers of ceramic with the polarity of neighboring layers reversed and alternating electrodes connected together. Care was taken, not only to ensure that the saw cuts that from the opposing faces of the device were in line, but also to ensure electrical continuity was retained across both faces. A 0.5 mm diameter wire was used for connecting the electrodes to the pre-amplifier. The stacked transducer was fully potted into the 45 mm cylindrical case for casting. The soft polymer CIBA/GEIGY CY208/HY956 backfilled the mold and fully surrounded the active phase of the PZT.

5.4.2 Analysis of multilayered stacked transducer

After bonding the five layers into a stack, the electrical impedance of the complete stack transducer was measured using the electrical impedance analyser. The electrical impedance magnitude and phase are shown in Figure 5.10 along with the equivalent FE predicted characteristics. Clearly there is a good correspondence with the overall impedance magnitude and phase of the experimental measurement. The fundamental electrical resonance was

predicted at 40 kHz and measured at 39 kHz.

The absence of any sign of activity due to lateral layers or any unwanted resonant modes indicates excellent interlayer adhesion. Importantly, the transducer will be most efficient as a receiver at the fundamental mechanical resonance corresponding to 48 kHz.

The surface displacement profile (SDP) was measured when the active phase was operating in air. Again, electrical excitation was applied by exciting the transducer at the resonant frequency and the displacement was measured by scanning the front surface of the stacked device in a raster fashion.

The experimental displacement magnitude and phase results at 40 kHz are shown in Figure 5.11. What is of practical importance is that the piezoelectric device output shows good uniformity and piston-like behaviour as also shown by the three dimensional displacement of Figure 5.12. There is no evidence of displacement due to any parasitic vibrational modes in the vicinity of the thickness mode as also indicated by the electrical impedance characteristics.

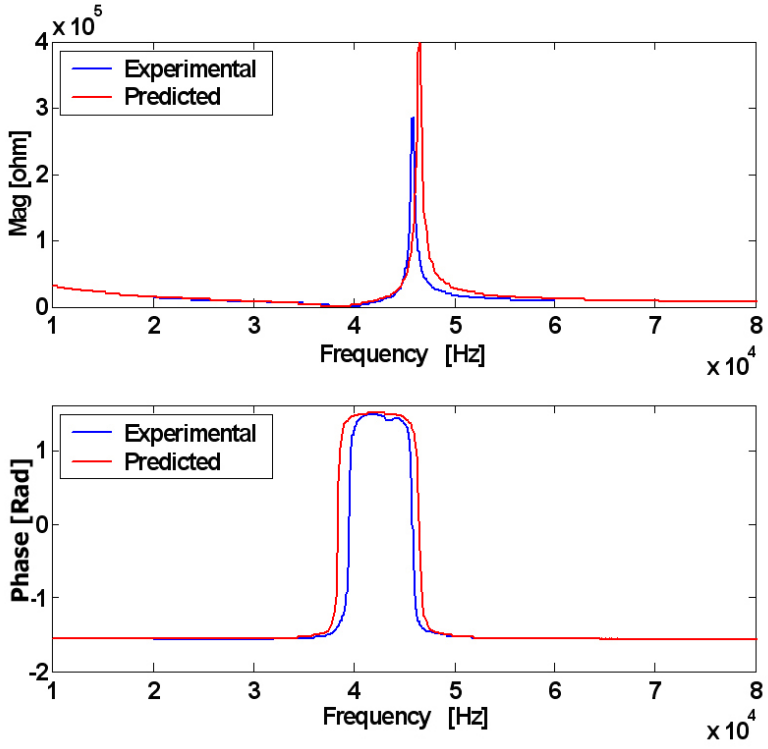

Figure 5.10: Simulated and predicted impedance of the stacked piezocomposite device.

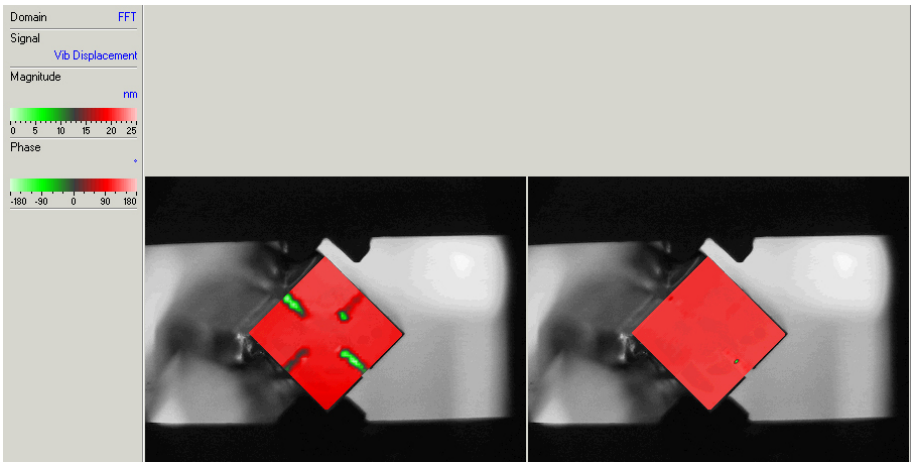

Figure 5.11: Experimental SDP magnitude (on the left) and phase (on the right) of the stacked transducer at 40 kHz.

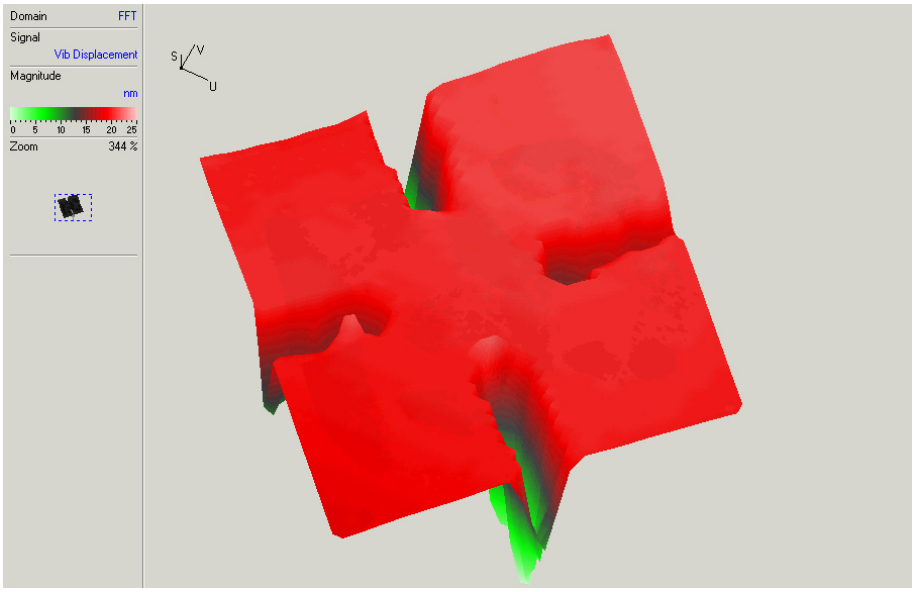

Figure 5.12: Experimental three dimensional magnitude SDP of the stacked transducer at 40 kHz.

5.5 Design of a pre-amplifier for ultrasonic transducer

Preliminary tests were performed for evaluating the amplitude of received signals from the newly fabricated transducers. The same experimental setup reported in Section 3.1 was utilised. Itaconic acid particles (100 g, size A) were added to 500 mL of toluene stirred at 250 rpm. The transducers output was directly connected to an Agilent 54624A oscilloscope (Agilent Technologies, UK) for data acquisition. The amplitude of the signal output from the off-resonance transducer was less than 10 μV. It is apparent that some form of amplification was necessary to produce discernible signals.

Both the piezo-composite transducers have very high electrical impedance values at their mechanical resonant frequency ($> 5k\Omega$) and hence, low signal power can be obtained if the electronic receiver is not designed properly. The pre-amplifier design needs careful consideration to achieve a reasonable signal to noise ratio (SNR). In these Sections, the design of a low noise and high gain schematic circuit suitable for both sensors is proposed.

Different approaches for designing the architectural front end (AFE) electronics could be taken into account [117]. In this work, the architecture based on a two stages ultra-low noise monolithic operational amplifier (OA) was chosen. The schematic circuit of the two stages amplifier is reported in Figure 5.13. A low gain pre-amplification and a buffer between the sensor and the electronics is provided by the first stage and a non-inverting OA configuration is selected because its high input impedance. The high-gain second stage OA utilises the same OA for improving the overall gain of the system. As the bandwidth increases, the noise increases, hence, the bandwidth of the

amplifier was limited to the frequency of operation of the acoustic monitoring system (plus a 40% margin to avoid distortions) [117]. A band-pass filter corresponding to the transducer bandwidth will enable rejection of contributions to noise outside the frequencies of interest. *C3* and *R3* reduce the DC gain and flicker noise by providing a high pass operation with a low cut-frequency f_L. The *R3* resistor also compensates the second stage OA bias current i_B and biased the OA non-inverting input. The upper limit of the bandwidth f_H was $f_H = \frac{1}{2\pi C5R7}$, and is controlled by the C5 capacitor and the R7 resistor. Noise performance of this circuit was studied and compared using the output noise power spectral density model of several components. Their optimum choice is presented.

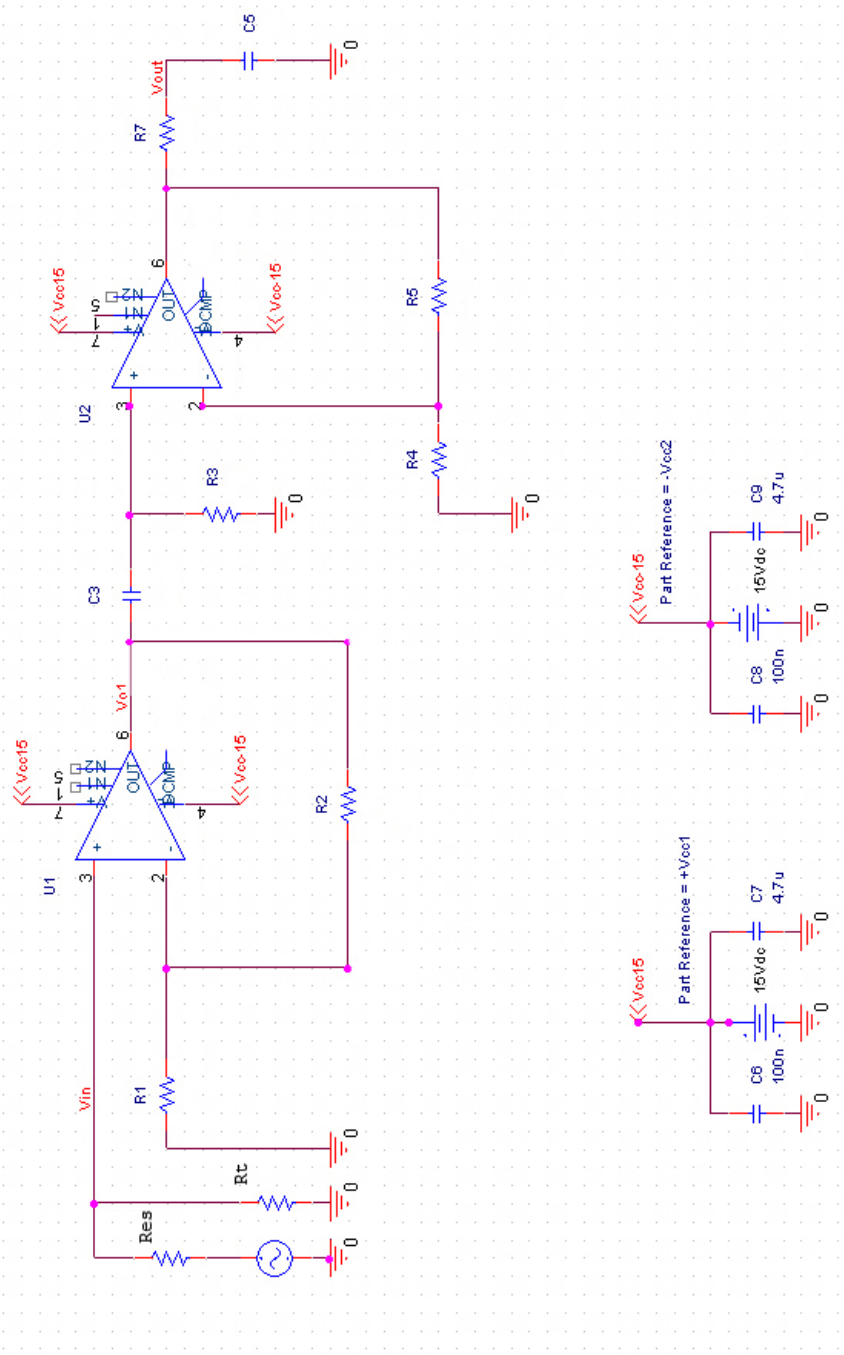

Figure 5.13: Initial concept of the schematic of the pre-amplifier

5.5.1 Noise model

The noise model can be developed either into analytical form or be modelled using some circuit oriented software like PSPICE [118]. Although the PSPICE modelling could have provided the easiest approach, in this work an analytical model was developed to enable noise contributions to be better understood and analysed separately. The approach in noise error calculation is to identify the noise sources, compute their root mean square RMS value and then combine them by root-sum-squares to get the RMS total noise [117].

The pre-amplifier equivalent electrical circuit (5.13) to be modelled is reported in Figure 5.14. Operational amplifiers noise performance can be described by two uncorrelated current noise generators of spectral densities $Ib+$ and $Ib-$ and one noise voltage source en connected to the OA inputs. These densities take the form of a mixture of flicker and white noises and can be characterised by the noise floor, and the corner frequency fie which determine the borderline between frequency ranges where either one type or the other type is predominant [117]. In this case, only the white noise is a concern because far above the corner frequency noise ($fie > 60$ Hz for all the devices selected in Table 5.3) the noise is basically white.

The current noise sources can be thought of as time varying input bias current components and the voltage sources as input offset voltage components. They are randomly related to each other in time and there is no systematic phase relationship between them [117].

The noise spectra density of each resistor R is

$$er^2 = 4k_0TR \tag{5.5}$$

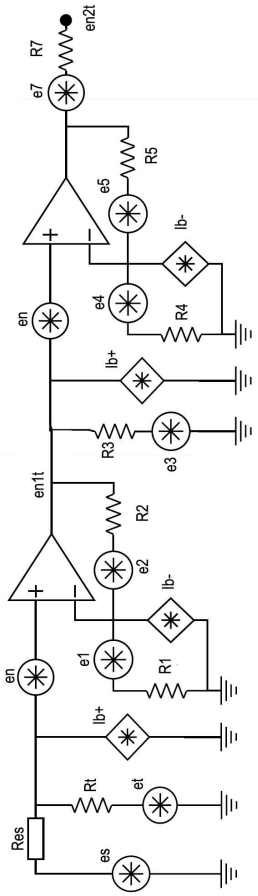

Figure 5.14: Equivalent noise model of the pre-amplifier

where $k_0 = 1.380610^{-23} \frac{m^2 kg}{s^2 K}$ is the Boltzmann constant, T is the absolute temperature at ambient temperature $T = 298$ K (equal to $25^o C$). It is important to underline that, the transducer impedance profile has the largest influence on the noise performance of the ultrasonic receivers. The transducer noise is directly related to the real part of the transducer electrical impedance ($Res = Re(Z_{transd})$) and it is frequency dependant. The transducer noise spectral density is equal to:

$$ees^2 = 4kTRes \tag{5.6}$$

The analysis of the circuit in Figure 5.13 results in the equivalent noise model of the pre-amplifier, as shown in Figure 5.14, where all the voltage noise sources can be independently analysed using a nodal analysis and superposition. Equation 5.7 combines all the noise sources for the first stage amplifier referred to its output.

$$en1tRt^2 = ees^2(\frac{Rt}{Rt+Res})^2G1^2 + en^2G1^2 + et^2(\frac{Rt}{Rt+Res})^2G1^2 + \\ +Ib^2(\frac{RtRes}{Rt+Res})^2G1^2 + e1^2(1+\frac{R2}{R1})^2 + e2^2 - R2^2Ib^2. \quad (5.7)$$

Where the gain *G1* of the first stage pre-amplifier is

$$G1 = 1 + \frac{R2}{R1} \quad (5.8)$$

e1 - *e7*, *et* are the noise voltage spectral densities from R1 to R7 and Rt, respectively. The current noise generators $Ib+$ and $Ib-$ are generally equal, therefore $Ib = Ib+ = Ib-$. Equation 5.9 reports the total output RMS noise spectral density:

$$en2tRt^2 = en1tRt^2G2^2 + Ib^2R3^2G2^2 + en^2G2^2 + e3^2G2^2 - \\ -Ib^2R5^2 + e4^3\frac{R5^2}{R4^2} + e5^2 + e7^2 \quad (5.9)$$

Again, *G2* is the gain of the second stage amplifier considering the feedback resistors *R5* and *R4*. It is of interest to know the expression of output noise power spectral density when Rt tends toward infinity. The output noise power spectral density of the first stage amplifier, when *Rt* is omitted,

results:

$$en1t^2 = ess^2G1^2 + en^2G1^2 + Ib^2Res^2G1^2 - Ib^2R2^2 + e1^2(\frac{R2^2}{R1^2}) + e2^2 \quad (5.10)$$

in consequence, $en2t^2$ results:

$$en2t^2 = en1t^2G2^2 + Ib^2R3^2G2^2 + en^2G2^2 + e3^2G2^2 - Ib^2R5^2 + e4^3\frac{R5^2}{R4^2} + e5^2 + e7^2 \quad (5.11)$$

The output noise can be calculated by integrating $en2tRt^2$ and $en2t^2$ over the frequency range according to Equations 5.12 and 5.13. The pre-amplifier behaves as a pass-band system with corner frequencies f_L and f_H and a roll-off equal to -20 dB/decade [117]. The lower and upper limits of the bandwidth f_L and f_H correspond to 72 Hz and 310 kHz ($f_L = \frac{1}{2\pi C3R3}$ and $f_H = \frac{1}{2\pi C5R7}$), respectively.

$$E_{Rt}tot_{RMS} = \int_{f_L}^{f_H} en2tRt^2 df \quad (5.12)$$

$$Etot_{RMS} = \int_{f_L}^{f_H} en2t^2 df \quad (5.13)$$

These Equations are expressed in Volts, however the magnitude of the spectrum is usually given in decibel milliVolt dBmV, a typical unit of measurement. Hence, $Etot_{RMS}$ in dBmV is equal to $20log_{10}(Etot_{RMS}/1mV)$.

For low noise performance, the equivalent resistance of the feedback network should be as low as possible. In order to neglect the *R1*, *R2, R4* and *R5* noise, their voltage spectral density has to be at least two orders of magnitude lower than the total noise [119]. In consequence low value resistors were selected: *R1* and *R2* were chosen equal to 1 kΩ and 2 kΩ respectively

Table 5.3: OA parameters

Manufacturer	Model	I_B $[nA]$	I_{OS} $[nA]$	V_{OS} $[\mu V]$	en $\frac{nV}{[\sqrt{Hz}]}$	Ib $\frac{fA}{[\sqrt{Hz}]}$
Analog	AD797	0.25	80	10	0.9	2000
National	LMH6624	13	50	250	0.95	2300
Maxim	MAX4016	5.4	100	450	0.75	2500
TI	OPA847	19	100	100	0.85	2500

and they provided a gain of 3. The values of the resistors $R5 = 35$ kΩ and $R6 = 1$ kΩ were chosen to obtain a gain of 36, leading to a total gain of $3x36 = 108 = 40.66$ dB. The Rt resistor biases the operational amplifier non-inverting input. To avoid excessive losses at the non-inverting operational amplifier input voltage, the requirement is given by Equation 5.14. Rt was imposed to be 2.8 MΩ since the maximum impedance magnitude of the stacked transducer is equal to $Res = 270$ kΩ).

$$Rt > 10Res \tag{5.14}$$

An operational amplifier with good noise performance has to be designed in order to maximise the signal to noise ratio SNR. Major manufacturers of integrated circuits have very low noise versions of the OA which are suitable for ultrasonic receivers because their high gain-bandwidth product GBWP. Four OAs were chosen as representatives of achievable limits. Their parameters are presented in Table 5.3.

The AD797 OA [120] was attending its high performance in terms of all parameters: I_B=*input bias current*, I_{OS} = input offset current, V_{OS} = input offset voltage, en = noise voltage and Ib = noise current. The AD797 was designed as a low noise, low distortion OA, ideal for use as a pre-amplifier.

Moreover, the low noise voltage en, the low noise current Ib, excellent slew rate of 20 $\frac{V}{\mu s}$ and 110 MHz gain bandwidth product make the AD797 highly suitable for low noise, low frequency ultrasound applications [120].

$E_{Rt}tot_{RMS}$ *and* $Etot_{RMS}$ were calculated using Equations 5.12 and 5.13 and using the measured electrical impedance magnitude Res of Figures 5.10 and 5.5 for the stacked and the off-resonance transducer, respectively. In this way it is possible to estimate the RMS output noise behaviour versus the input resistance Rt. The results are presented in Tables 5.55.4, for each OA chosen. As expected, the lowest noise performance are achieved by employing the Analog Device OA.

Table 5.4: Total RMS noise of the pre-amplifier when the off-resonance transducer is employed

Model Ic	$EnTotal_{Rt}$ $[mV]$	EnTotal $[mV]$
AD797	43.82	1.68
LMH6624	43.83	1.88
MAX4106	43.83	1.88
OPA847	43.83	2.09

Table 5.5: Total RMS noise of the pre-amplifier when the stacked transducer is employed

Model Ic	$EnTotal_{Rt}$ $[mV]$	EnTotal $[mV]$
AD797	21.97	0.56
LMH6624	21.97	0.60
MAX4106	21.97	0.62
OPA847	21.97	0.63

It is evident that $E_{Rt}tot_{RMS}$ is larger than $Etot_{RMS}$ for all the operational amplifiers since the biasing resistor Rt increases the overall total noise. Rt was rejected from the schematic and the output of the sensor was brought directly to the high-input impedance of the OA. This solution was suitable for

both the piezo-devices. With this configuration, even high electrical impedance transducers such as the stacked transducer (270 kΩ at the mechanical resonance frequency), are not loaded and the first stage OA can easily drive the next voltage amplifier stage.

The $en2t^2$ spectral density noises of the off-resonance and stacked transducers are plotted in Figures 5.15 and 5.16, respectively. From each Figure, it can be confirmed that the noise generated is frequency dependent and the noise peak depends on the real part of the impedance profile of the sensor [121][117].

The overall noise density of the off-resonance transducer is higher than the noise density of the stacked sensor within the f_L-f_H designed bandwidth. Hence, the $Etot_{RMS}$ corresponds to 1.68 mV and 0.56 mV for the off-resonance and the stacked transducer, respectively.

Taking full advantage of the very high bandwidth of the AD797 required some precautions: in particular, power supply bypassing was recommended for any precision application. A 1.0 μF ceramic bypass capacitor is sufficient in most applications but for the best results, a 4.7 μF *C7* capacitor was put in parallel with a 100 nF *C6* ceramic capacitor [119]. A capacitor *C2*, of 10 pF was connected between pin 8 and the OA output for external compensation. Optimum flatness and stability at noise gains greater than 1 required a small capacitor *C1* connected across the feedback resistor *R2*. The recommended value of *C1* by Analogue Device was 10 pF [120]. In this configuration, *C1* and *R2* also acted as a low pass filter with cut off frequency equal to 160 MHz. Therefore, this configuration did not affect the bandwidth of interest.

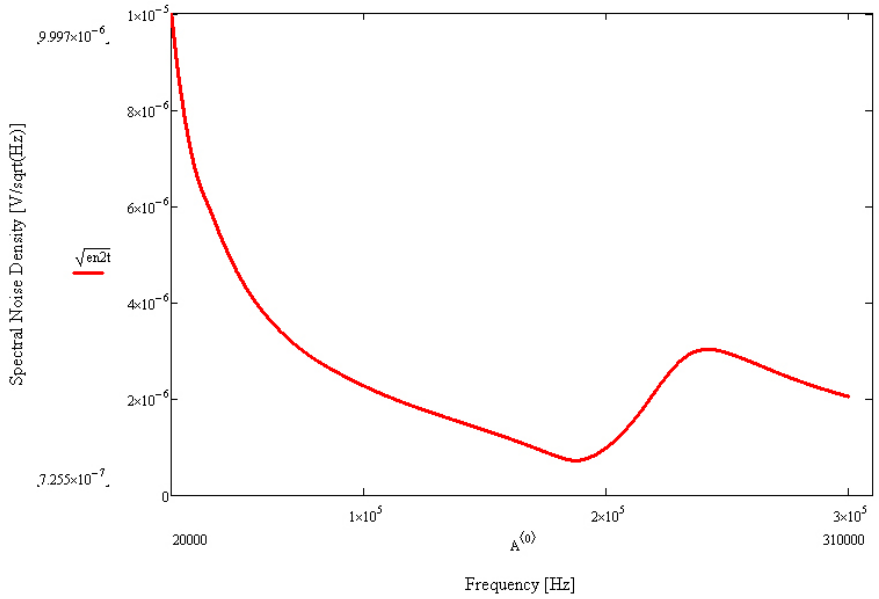

Figure 5.15: Spectral density noise of the off-resonance transducer and pre-amplifier

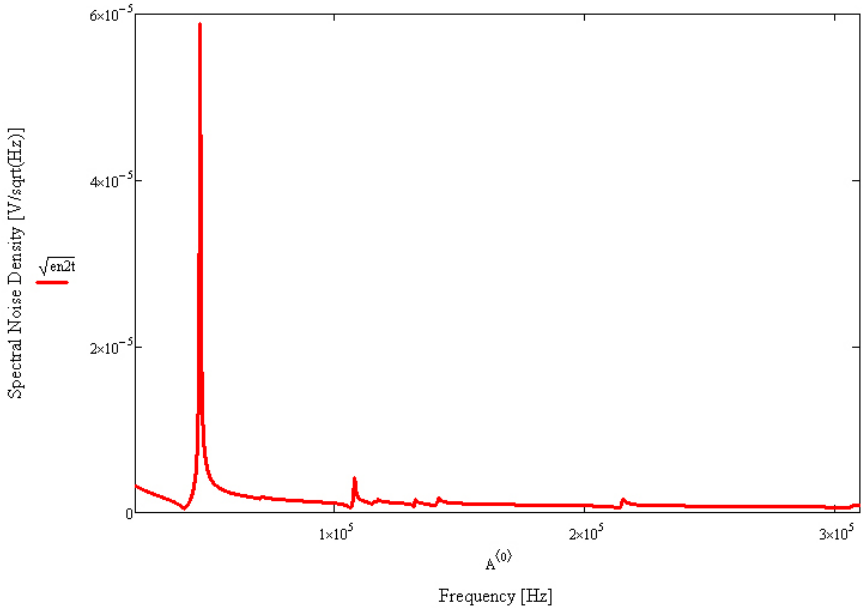

Figure 5.16: Spectral density noise of the stacked transducer and pre-amplifier

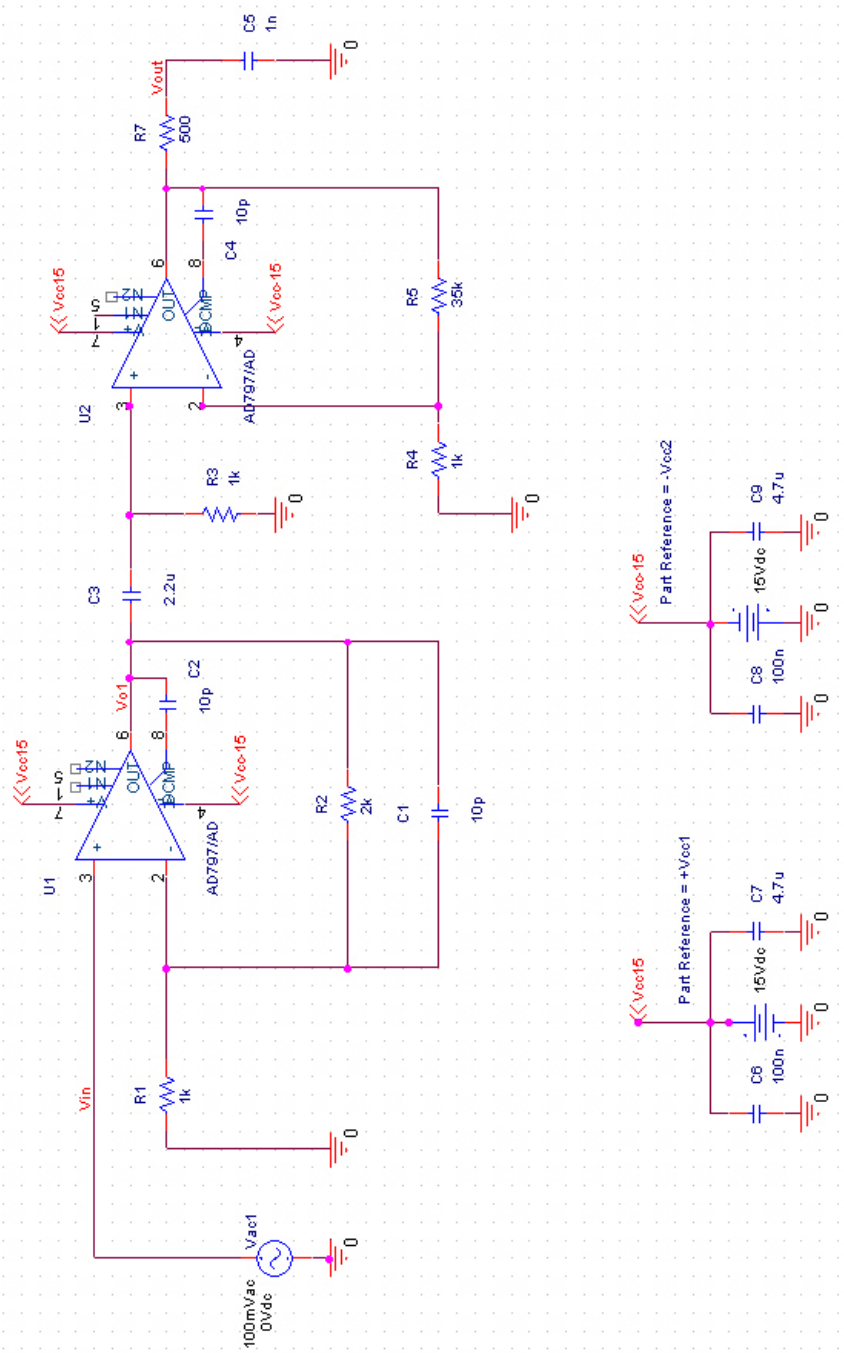

Figure 5.17: Final schematic of the pre-amplifier suitable for both the ultrasonic transducers

5.5.2 Analysis of the low noise pre-amplifier

The schematic circuit was developed using *Orcad*® Schematics version 10.0 [122], a circuit-oriented software package, and a two layered printed circuit board (PCB) was also designed with Orcad Layout Plus and then fabricated. Careful attention to PCB layout is required in order to achieve an optimum noise performance, hence board layout rules provided by manufacturers are of great help in the design. Surface mounted components were employed to achieve minimal PCB dimensions (1x1.5 $inch^2$). The PCB Orcad Layout traces and components are shown in Figure 5.18 (A) and (B), while 5.18 (C) and (D) represent the top view of the board with surface mounted components and a dimensions reference.

Two identical PCBs were manufactured and tested. Once all tests were completed, one board was housed inside each transducer case and its ground was electrically connected to the case. In this way, the connections from the ultrasonic transducer to the pre-amplifier were minimised and the electronics were shielded from the environmental noise. A diagram of the internal transducer arrangement is provided in Figure 5.19.

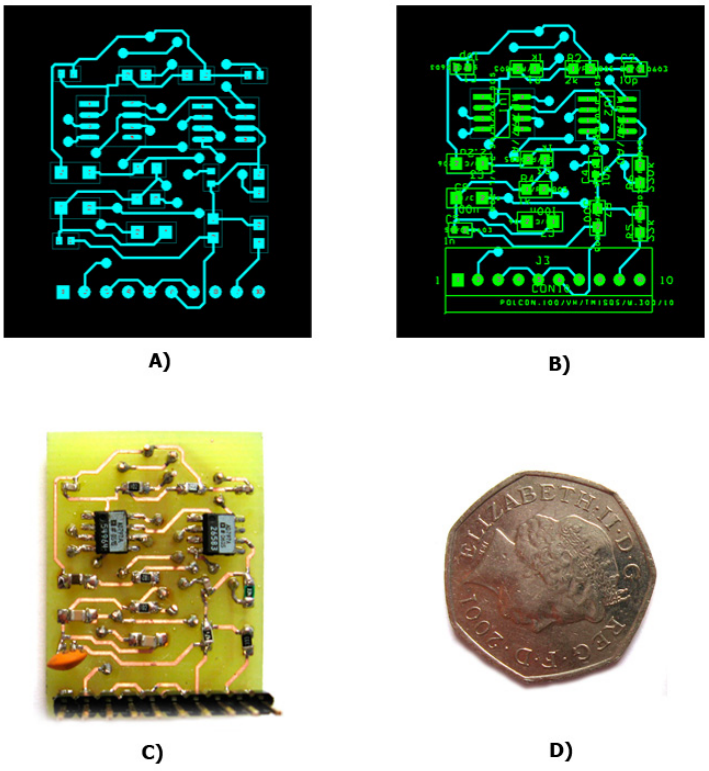

Figure 5.18: PCB design of the pre-amplifier. (A) PCB bottom layer, (B) PCB top layer, (C) Assembly with surface mounted components, (D) Reference for size comparison.

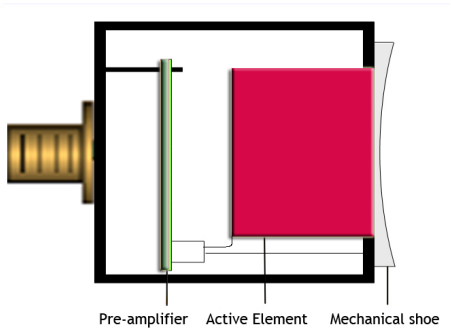

Figure 5.19: Internal arrangement of the transducer housing. The mechanical shoe was employed only for the off-resonance device.

5.6 Experimental analysis of the ultrasonic reception system

It has been demonstrated that the non-inverting configuration with no compensation of input bias current is a suitable topology for the amplifier when minimal output noise has to be achieved. Before any analysis of the system noise could be undertaken, it was imperative to fully characterise the amplifier arrangement.

Frequency response of the amplifier configuration

As with all amplifier arrangements, there is only a certain range of frequencies over which the amplifier is designed to operate, which is usually defined by the device bandwidth in ultrasonic applications. With most low noise reception systems, the bandwidth of the system is minimised, encompassing only the signal frequencies of operation, because as the bandwidth increases, the noise bandwidth is also increased. Experimental characterisation of the frequency response for each amplifier was undertaken to allow a full appraisal of the receive system response. The measured frequency response was then directly compared with the frequency profile predicted using the Orcad analysis tool.

The pre-amplifier was tested before inserting it into the transducer case. An external ±15V DC power supply was connected to the board and an electrical excitation was applied using a Hewlett Packard Signal Generator producing a fixed 50 mVpp sinusoid wave over a range of frequencies. There was no need to employ any attenuator as there was no risk of saturating the system. The pre-amplifier was tested in a open-circuit condition, as the signal output was measured using an oscilloscope Agilent 54642A with 1 $M\Omega$

of internal impedance.

The experimental and predicted frequency responses were determined as shown in Figure 5.20.

It can be seen that the simulated model approximates closely to the measured performance.

Although the PSPICE modelling was not strictly necessary for the preamplifier design, it added our confidence that the amplifier behaved as expected.

The measured gain is equal to 108.8 = 40.73 dB with f_L and f_H equivalent to 73 and 315 kHz respectively. All these values are very close to the analytically calculated values *(G=40.66 dB, f_L=72 Hz and f_H= 310 kHz)* In this case the PSPICE modelling was not strictly necessary, but the modelling approach provided further confidence that the calculated frequency response was as expected.

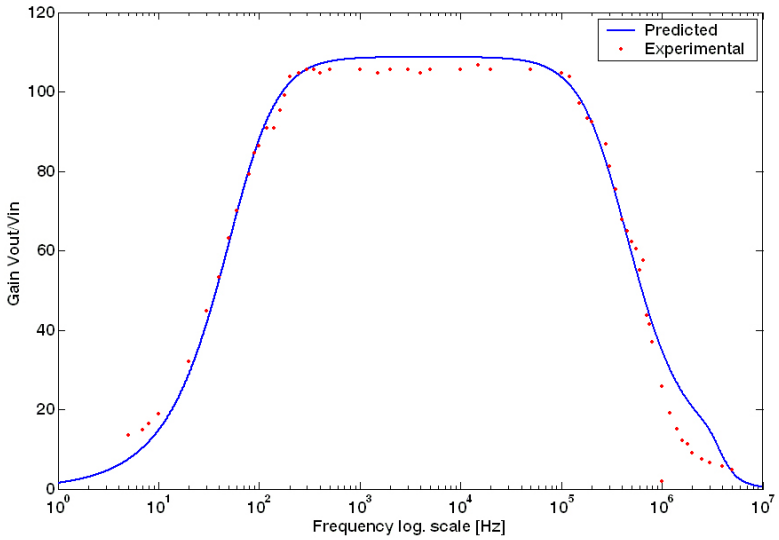

Figure 5.20: Experimental and predicted frequency responses of the preamplifier

Determination of the equivalent noise voltage

The next part of the investigation was to determine experimentally the equivalent noise voltage of the low noise pre-amplifier configuration in order to compare it with the commercial pre-amplifier.

Whilst noise generated by an amplifier is generated within the system, the degree of noise is evaluated by referring it to the amplifier input. This noise is considered as the equivalent noise at the input (as though it were being generated at that point). The equivalent noise voltage spectral density Eq_n was calculated by dividing the noise measured at the amplifier output e_{out} by the total gain of the amplifier [117].

Ideally these measurements should be performed within a Faraday Cage to shield the system from background noise external to the amplifier system, however for these tests the amplifier housing provided a degree of electrical shielding reducing the environmental noise.

A HP8590L Spectrum Analyser (SA) was connected to the output of the amplifier arrangement and the inputs of the amplifier were short-circuited to the electrical ground. This was done in order to refer the intrinsic noise of the amplifier to the output. The equivalent noise voltage produced by the pre-amplifier was measured to be in the region of 113 $nV/\sqrt{Hz}$ RMS in comparison to 180 $nV/\sqrt{Hz}$ RMS of the commercial pre-amplifier from Physical Acoustics. These values include the gain of the developed and the commercial pre-amplifier equal to 40 dB and 60 dB, respectively. Note that equivalent noise voltage of the pre-amplifier does not include the thermal noise from the piezo-transducer (ees^2), which it the largest contributor of noise to the model, since OA first stage inputs are shorted to ground.

In conclusion, the design of the pre-amplifier with surface mounted low

noise components improved the noise performance over that of the commercial pre-amplifier employed in the previous experimental work programme. Hence, the newly designed pre-amplifier will be employed with the new acoustic transducers.

5.6.1 Impulse response of the ultrasonic system

Once the characteristics of the ultrasonic transducers and the low noise pre-amplifier were fully detailed, the overall frequency response of the total system was required to characterise its behaviour. From Chapter 3, it emerged that the reactor vessel, the commercial piezoelectric transducer and the commercial pre-amplifier transfer functions had a significant influence on the AE spectrum detected. Hence, the same experimental arrangement, as was used in the preliminary passive acoustic experiments (Section 3.2), was employed to evaluate the performances of the newly fabricated transducers. The impulse response of the fabricated transducers and the impulse response of the overall system (comprising the reactor vessel, the transducer and electronic pre-amplifier) were measured using the Hus-Nielson pencil lead test [68] as an effective AE stimulus. The two measurements were then compared with the AE spectra acquired of 100 g of itaconic acid of particle size A in 500 mL of toluene at the stir rate of 250 rpm using the off-resonance and stacked devices.

Direct comparison of the power spectrum of AE itaconic acid particles along with the frequency response of the off-resonance transducer and the curve of response of the total system are shown in Figure 5.21. Even if the Hus-Nielson pencil lead test is not considered as a precise way for estimating the frequency response of a piezo-sensor, there are no unwanted major

resonant modes [68] that significantly influence the received data and the transducer can be considered broadband. The frequency response of the total system shows a main resonance mode at 90 kHz that can be attributed to the oil-glass layer as confirmed by the analytical and simulated results of the oil-glass layer combination effect reported in Section 4.3.1. Moreover, other resonance modes at 25, 100, 180 and 270 kHz are evident, owing to a standing wave travelling across the structure layers. This is in agreement with the FEM prediction and the experimental work to validate the model. Other modes at 55 and 215 kHz are considered to be caused by the 3D nature of the reactor vessel and the mechanical stirrer.

The same experiments were repeated using the stacked device. A comparison of the results obtained is reported in Figure 5.22. It is important to underline that, even though each plot of the frequency response was repeatable, the pencil lead test tends to give the overall characteristic of the resonance modes and it is not an absolute technique for evaluating the frequency response of an ultrasonic system. However, during this experimental work, good approximation of the resonance modes was achieved. As expected, the sensitivity of the sensor was greatest at about 40 kHz, which corresponds to the thickness mode of the sensor. The overall shape of the AE spectrum is mainly dominated by the sensitivity profile of the stacked transducer.

In conclusion, during the tests with the off-resonance device, the itaconic acid spectrum was mainly influenced by resonance modes of the reactor vessel as the characteristic profiles of the off-resonance transducer and the pre-amplifier have shown uniform behaviour during the experimental work. While, the AE spectrum from the itaconic acid particles was mainly domina-

ted by the sensitivity profile of the narrow-band stacked device. These tests have ascertained the overall contribution of each component of the system to the AE signal spectra. This information contributes to the understanding of information content of the signals obtained using these ultrasonic devices, and described in the following Section.

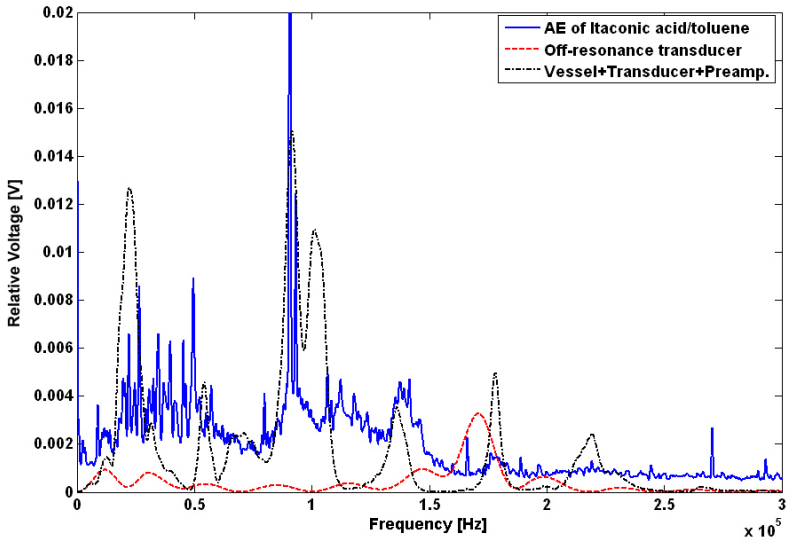

Figure 5.21: Power spectra AE of itaconic acid particles, frequency response of the off-resonance transducer and the curve of response of the total system

5.7 Passive acoustic monitoring experimental results

Investigation of the effects of particle size was also carried out by employing the same experimental apparatus for measuring AE from a heterogeneous system in a reactor vessel reported in Chapter 3. Masses of different fractions (A, B and C of Table 3.1) of particles of itaconic acid were added stepwise, up to 100 g, and stirred at 250 rpm into 500 mL of toluene to

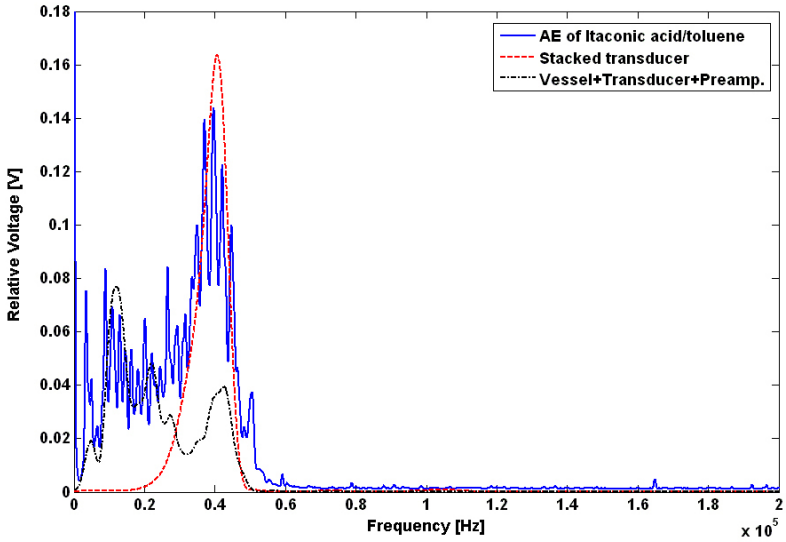

Figure 5.22: Power spectra AE of itaconic acid particles, frequency response of the resonant transducer (stacked) and the curve of response of the total system

investigate the effects of particle size and concentration on broadband AE signals. The temperature of the mixture was maintained constant throughout the experiments at 25 $^{\circ}C$.

Both the off-resonance and the resonant stacked transducers were employed simultaneously for all the passive acoustic experiments. These were attached on the stirrer plane of the reactor vessel using ultrasonic couplant and heavy-duty adhesive tape. The output of each transducer was amplified through the new integrated 40 dB low noise pre-amplifier embedded inside the case of each sensor. A two channel Agilent 54624A oscilloscope was employed to acquire and sample at 1 MHz the AE data. Again, all the data was saved in binary format and imported into Matlab for the post-processing analysis.

The effects of particle size and particle concentration on spectral characteristics were assessed as follows.

5.7.1 Particle size effects

Figure 5.23 illustrates the spectra for particles of different sizes at a fixed concentration of 100 g of itaconic acid in 500 mL toluene collected using the off-resonance transducer.

The broadband features of each spectrum arises from the wide frequency range characteristic of the sound radiated by impacts as shown during the modelling work in Section 4.2. The signal bandwidth of the AE is circa 180 kHz. Again, in this work the bandwidth was defined as the frequency range in which the signal's Fourier transform is nonzero. Because this range of non-zero amplitude may be very broad, this definition is often relaxed so that the bandwidth is defined as the range of frequencies where the signal's Fourier transform has a power above a certain amplitude threshold, commonly half the maximum value, or -3 dB, in this work -30 dB was assumed as negligible signal amplitude.

The piezo-composite sensor provides a wide-band behaviour and the shape of the spectra are not significantly influenced by the transducer's profile. The only feature that can be attributed to the ultrasonic sensor is the peak at 175 kHz. This is due to the mechanical resonance frequency of the off-resonance composite device. Note also again that the prominent peak at 90 kHz corresponds to the resonance of the glass-oil combination.

The sensitivity of the spectra depends on the size range of the itaconic particles examined. Differences in the relative magnitude of the spectral features of Figure 5.23 were apparent at different frequencies.

For instance, across the entire concentration range, the magnitudes of the signals in the range 0-60 kHz were more sensitive to changes in particle size that those in the 60-170 kHz range and the position of the resonances of the

reactor vessel remained unaltered.

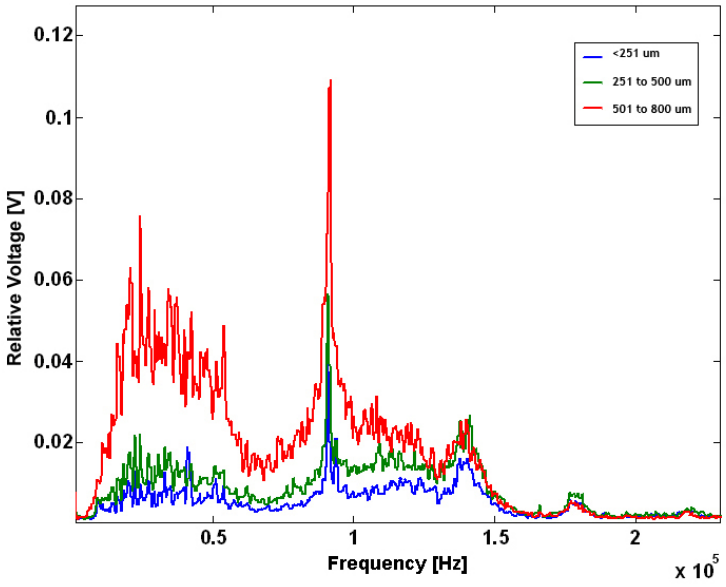

Figure 5.23: Power spectra of different particle sizes (A, B and C) of itaconic acid particles in toluene acquired employing the off-resonance piezocomposite transducer

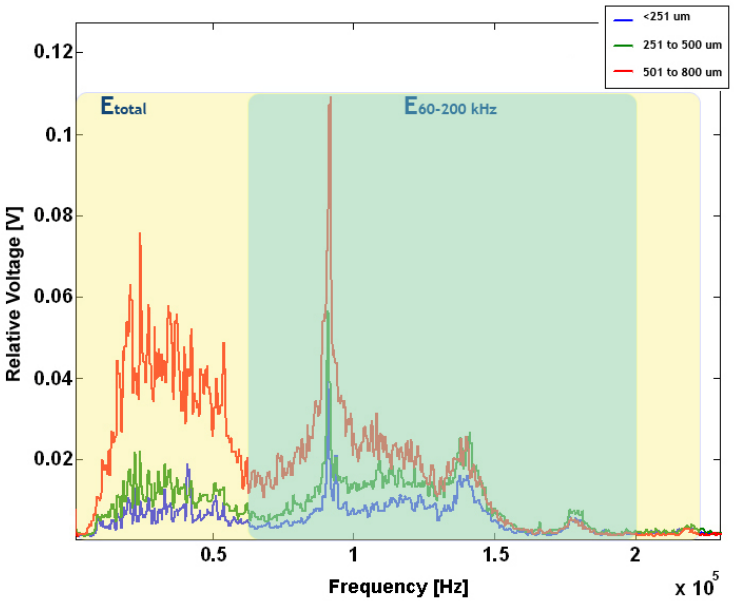

Figure 5.24: Spectra windowed for calculating the particle size effects.

Apparently it was not possible to notice any shifting of the spectra energy across the frequency axis as the modelling work in Chapter 4 predicted. However, a deeper investigation of changes in the frequency content of the spectra was carried out. Figure 5.25 shows the approach for investigating the frequency shifting of the spectra by comparing relative areas within the frequencies of interest.

Firstly, the area of the AE signal over the total bandwidth EX_{total} was calculated for each spectrum. Then, the area below a portion of a specific frequency range of each spectrum was computed *(*$EX_{f_1-f_2}$*)*, and the ratio between the two areas was calculated according to Equation 5.15; X represents the spectrum number.

$$EX = \frac{EX_{f_1-f_2}}{EX_{total}} \tag{5.15}$$

If the concentration of the heterogeneous solution increases and the size of the particulate is fixed, no frequency shifting of the spectra occurs. As Figure 5.25a) depicts, the percentage of area *E1* below the first spectrum and the percentage *E2* are equal. Thus, when the concentration is fixed and the particle size increases, the energy of second spectrum should move toward lower frequencies. *E2* is less than *E1* because the area $E2_{f2-f1}$ in Figure b) is lower than the area $E2_{f2-f1}$ in Figure a).

In the real experiments, the spectra were dissected into a number of frequency ranges (chosen empirically) to examine their potential to discriminate between different particle sizes. The best results were achieved choosing the frequencies *f1* = 60 kHz and *f2* = 200 kHz. The area below each spectrum in the range 60-200 kHz (EX_{60-200}) was computed as a percentage of area over

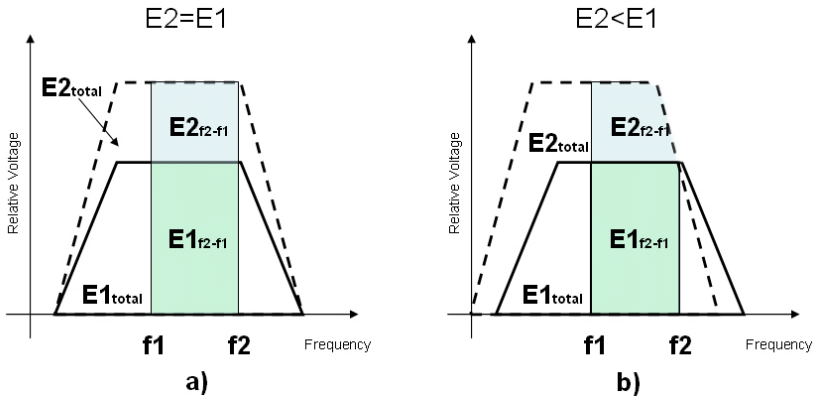

Figure 5.25: a) Increasing concentration, constant particle size. b) Constant concentration, increasing particle size

the total bandwidth of each spectrum (EX_{total}) as shown in Figure 5.24.

Figure 5.26 illustrates the percentages of area for all experiments performed. From the Figure, it was not possible to differentiate the contribution of both particle size and concentration when the mass was equal to 1 g. Nevertheless, for masses above 10 g, the percentage of area was invariant with concentration, but decreased when the particle size range increased. This means that when the particle size increases, the magnitude of the signal increases at lower frequencies and frequency shifting of the spectra occurs.

This was one of the most important outcomes for distinguishing between the energy contribution of particle size and concentration.

In different passive systems [94][13], it is not possible to discern the contribution due to an increase in particle size or an increase in mass of the solution because often AE signals are converted to a DC level, hence the energy increases in both cases. With the energy shifting method, it could be feasible to identify the mean size and concentration of any spectrum.

The increase in the relative magnitude of the signals in the lower frequency regions as particle size increased is in agreement with previous re-

ported studies [40][42][56] and with the modelling work discussed in Chapter 4. An increase in particle size causes an increase in AE magnitude and a decrease in AE frequency owing to a dependence on the particle surface area and impact time, respectively [41].

The power spectra plots of the same experiment using the stacked sensor are reported in Figure 5.27. Comparisons between the spectra acquired using the off-resonance and the resonant transducers (Figure 5.23 and Figure 5.27, respectively) were made. The magnitude of each spectrum (between 0-30 kHz) acquired using the stacked device is almost five times larger that the magnitude of the relative spectrum acquired using the off-resonance transducer. However, the bandwidth of the spectra is limited to 60 kHz by the profile of the resonant device. Importantly, the AE signals for estimating the frequency shifting above 60 kHz are not detected.

Importantly, both transducers are needed at the same time for differentiate between the size and concentration effects in the AE experiments. From a single measure the off-resonance transducer will be discerning the size of the particles using the shifting in frequency characteristic of the spectra (e.g. in Figure 5.26), while the stacked resonant sensor will be used for discriminate their concentration information. The shift of energy towards lower frequencies, corresponding to an increase in particle size, could be an important index for in situ particle size characterisation also due to its relatively low computation time. Both information of the shifting and energy increase of the spectra can be extracted simultaneously using both sensors and they could be utilised for real time, non-invasive monitoring systems.

This approach illustrates the benefits of employing both transducers for

estimating the mean size and concentration of particulate in a liquid. Although information relating to the mean particle size was successfully achieved by analysing the energy spectrum of the AE signals, the distribution of particle size could not be directly deduced from the experiments. This information could be extracted using attenuation and velocity measurements employing active acoustic techniques as shown in Section 6.9.2. However, the vast majority of instruments available such as the High Resolution Ultrasonic Spectrometer HR-US 101 [52], for this purpose are for off-line (laboratory) use. Moreover, in many high throughput investigations (e.g. polymers, multi-components formulations) the physical nature of the particle material involved prevents acoustic transmission [31]. Hence, further work is needed for develop theoretical or empirical models that would achieve the extraction of both particle size distribution and particle concentration information.

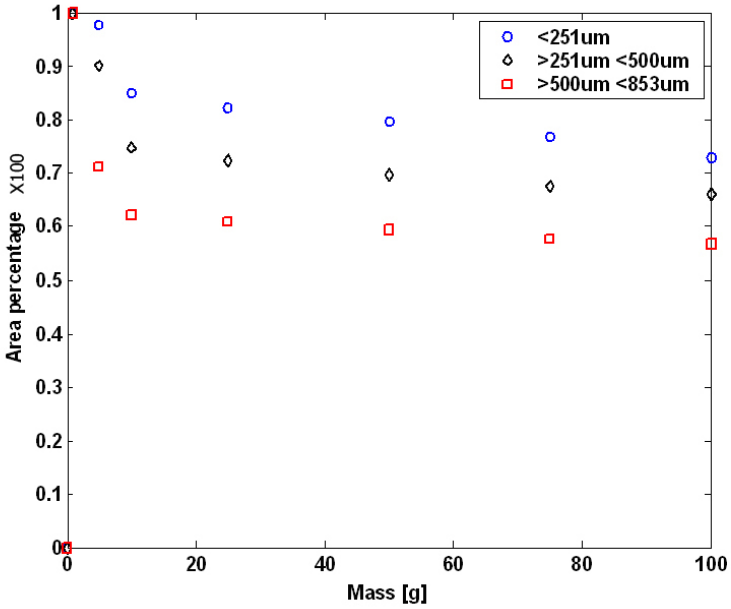

Figure 5.26: Particle size information derived from the power spectra generated by the off-resonance transducer.

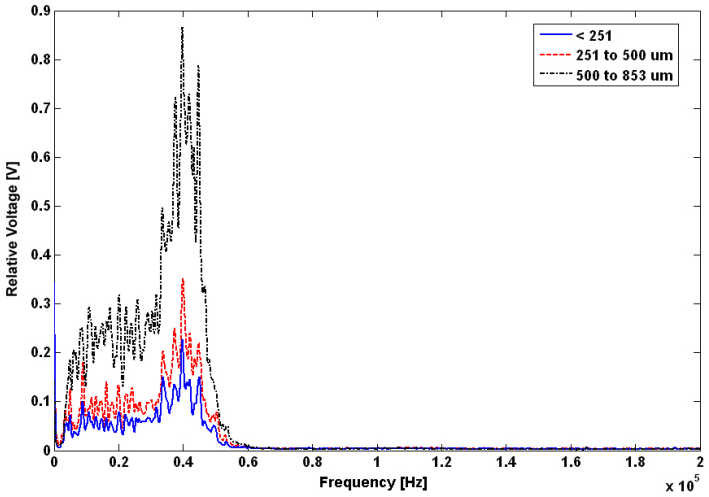

Figure 5.27: Power spectra of different particle sizes (A, B and C) of itaconic acid particles in toluene acquired employing the stacked piezocomposite transducer

5.7.2 Concentration effects

Experiments on varying the concentrations of fixed size particles were also carried out using the transducers simultaneously.

Figure 5.28 shows the power spectra recorded using the off-resonant device corresponding to different concentrations of itaconic acid of fixed particle size A. Also in these experiments the peaks corresponding to the resonance glass-oil combination of the reactor vessel and the mechanical resonance of the off-resonance device are evident at 90 and 170 kHz, respectively.

The same AE signals employing the stacked sensor are presented in Figure 5.29. The spectrum obtained for 0 g (called blank in analytical chemistry) was insignificant in comparison to that obtained when itaconic acid particles were present inside the vessel. Again, the response characteristics of the composite stacked transducer limited the bandwidth of the signal spectra to 65 kHz and the resonant transducer governs the overall profile of the AE spectra (see Figure 5.22).

All the spectra show that the bandwidth and sensitivity of the two manufactured devices are complementary. The stacked transducer was designed to be very sensitive but with limited bandwidth, whilst the off-resonance composite would benefit from a broad response across the desired operating frequency range, although with a reduced sensitivity.

The magnitude of all the spectra acquired using both transducers increases when the mass of the acid particles increases. In particular, the change in signal energy for the particle size ranges of Table 3.1, as a function of concentration, employing the stacked transducer is illustrated in Figure 5.30.

All the spectra showed a linear increase in signal energy with concentration up to 10 g/dm^3, which is in agreement with the simulations results and previous theoretical and experimental studies [30][29]. Above this concentration the sensitivity changes due to the onset of the saturation of particles in toluene or the presence of other sources of AE (particle-impeller collisions, particle-particle collisions) [17].

From Figure 5.30 alone there is no improvement on the information that is achieved using RMS signals because it would not be possible to recover, for example, the signal energy of a high concentration of small particles from a low concentration of large particles. For this distinction, information about the variation of the spectral content is needed, as demonstrated in the feasibility study discussed in Section 5.7.1.

Based on the AE spectra acquired, the detection limit was determined. In analytical chemistry, the detection limit (DL), the lower limit of detection, is the lowest quantity of a substance that can be distinguished from the absence of that substance (called blank value) within a stated confidence limit (generally 1%); in this work, the detection limit is 'the minimum concentration that can be determined, with 99% confidence, that the true concentration is greater than zero [71].

The DL was calculated according to Equation 5.16.

$$DL = \frac{3SD}{Sl} \tag{5.16}$$

where SD is the standard deviation of the signal areas determined across the toluene spectrum (i.e. background noise, no particles present) divided by the sensitivity Sl of the AE response for itaconic acid. The Sl was calculated as

the slope of the graph of the signal area of Figure 5.30 against concentration [56].

Table 5.6 shows the calculated *DLs* for particles of size A, B, C for both transducers. As expected the lowest *DL* is achieved when the stacked piezo-sensor is employed because its SNR and its sensitivity are much greater than the off-resonance transducer SNR and sensitivity. This means that the stacked device can detect smaller concentrations of particles (two order of magnitude) in fluid compared to the off-resonance device. Theoretically, it would be possible to determine 4.72 mg and 280 mg of itaconic acid particles C size in 500 mL of toluene with the stacked and the off-resonance devices, respectively.

In both sensors, the *DL* decreases as the particle size increases because the ratio between SD and Sl decreases when the mean particle size increases; the slope of the signal area is steeper for larger particle sizes.

While the off-resonance transducer offers the benefit of discriminating particle size information, the stacked transducer resulted in the ability to determine smaller particle concentration information. In fact, the DL values obtained with the resonant stacked transducer are considerably lower (at least one order of magnitude) than that reported in a previous study [56] (0.1 $\frac{g}{dm^3}$ for unsieved itaconic acid particles).

In conclusion, the new piezoelectric stacked device together with the improved noise performance of the electronic pre-amplifier has demonstrated improved discrimination in concentration information.

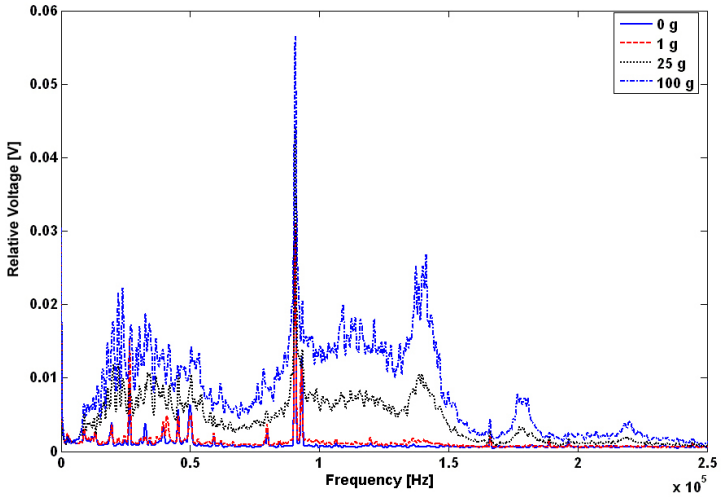

Figure 5.28: Power spectra of different concentrations of itaconic acid particles size in toluene employing the off-resonance piezocomposite transducer

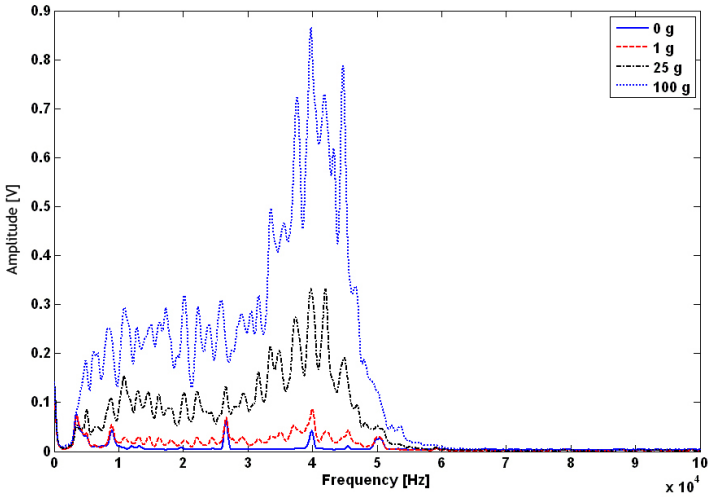

Figure 5.29: Power spectra of different concentrations of itaconic acid particles size in toluene employing the stacked piezocomposite transducer

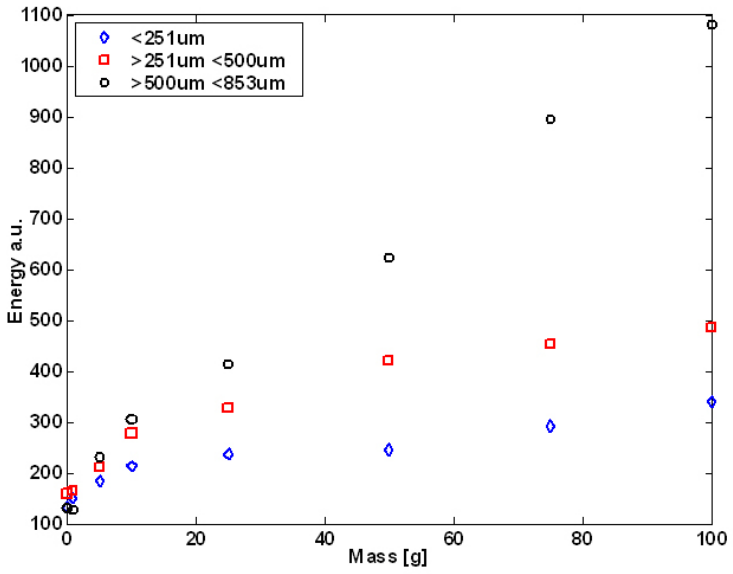

Figure 5.30: Effects of both concentration and particle size employing the stacked sensor.

Table 5.6: Detection limits using the off-resonance and the resonant transducers

Particle size	**Off-resonance T.** g/dm^3	**Stacked Resonant T.** g/dm^3
A	2.03	$5.08\ 10^{-2}$
B	1.27	$2.73\ 10^{-2}$
C	$5.61\ 10^{-1}$	$9.44\ 10^{-3}$

5.8 Conclusions

The results from the model-based approach, used in Chapter 4, have been used to design transducers utilised to investigate particles immersed in fluids and stirred inside a chemical vessel. Importantly, the frequency range of interest was below 180 kHz with the major components between 0-60 kHz.

An off-resonance piezocomposite transducer has been designed and manufactured to fulfill the requirements for a wide-band passive monitoring system approach with operating frequency range between 0-180 kHz and acoustic matching to glass load. Another piezocomposite resonant device, designed to work in the region of major spectral activity associated with the AE (0-60 kHz), has been also manufactured.

The passive acoustic system has been completed by the design of a low noise pre-amplifier with improved noise performance characteristics compared to the commercial pre-amplifier employed during the preliminary experimental work.

The wide-band off-resonance transducer has given the opportunity to confirm the modelling results described in Chapter 4: the energy trend of the AE signals at lower frequencies increases as the particle dimension increases. With this approach it has been possible to discriminate the mean size and concentration of each AE spectrum.

The enhanced sensitivity of the new stacked piezoelectric device, together with the improved noise performance of the electronic pre-amplifier has decreased the detection limit for determination of itaconic acid in toluene when compared to previous experiments employing a commercial system.

Ideally, with the new approach proposed in this work, any chemical system can be simulated using FEM and designing customised sensors according

to the outcomes from the simulations. Generic broadband transducers are often utilised without knowing exactly the real frequency range of interest of the process under investigation.

The new passive acoustic system is also non-invasive. Non-invasive acoustic system are valuable for process analysis as, in principle, the ultrasonic transducer can be attached to the vessel under investigation without being in direct contact with the sample and, hence no contamination occurs [13].

The ultrasonic system is relatively low cost in comparison to many optical techniques [24][27][123]. More effective process investigation, monitoring and control can be achieved by employing more sensors. In chemical or pharmaceutical industries, being able to control the industrial processes will result in reducing time of manufacturing and the product waste. The contribution to process analysis field has been shown in this work: importantly, the mean size and the concentration of the particles could be discerned by analysing the magnitude and frequency content of the AEs spectra. The peculiar characteristic of magnitude changes towards lower frequencies, corresponding to an increase in particle size, could be exploited for in situ and in-line particle size characterisation for process analysis such as high shear granulation [13], granulation [14] and flow of powders [3]; or food manufacturing, and reaction monitoring [17]. By measuring the size of the particles and their concentration, this will also improve the industrial processes in terms of energy efficiency, material properties, and process safety [4].

The design of a passive acoustic monitoring system using two complementary transducer designs is also considered part of the novelty of this work. The work described in this Chapter has clearly illustrated the benefits of using wide-band and narrow-band approaches in the monitoring of particu-

late suspensions. Hence, it is obvious that a monitoring system combining both of these approaches would enhance the characterisation information available to Chemical Process Engineers. This forms the basis for the development of a new acoustic monitoring approach and further considerations will be expended in the "Future Work" Section of Chapter 7.

Chapter 6

A broadband active acoustic monitoring approach

Ultrasonic monitoring systems are an attractive measurement technique as they can be non-invasive and are relatively inexpensive [18]. The advantages of employing acoustic techniques in process control include a reduction in time and cost of production, and improvements in the safety, consistency and quality of the product. This will reduce the "time to market", and result in companies gaining economic benefits. Hence, the development of improved acoustic techniques, which are relatively low cost in comparison to many optical techniques, is desirable for more effective process investigation, monitoring and control [5].

Most chemical reactions take place within complex containment structures, with the ultrasonic instrumentation being placed externally, usually on the wall of the container. The type of transducer and the influence of the container on the transmitted and received ultrasonic data are critical [18]. For example, as shown in the previous Chapters when a passive acoustic sensor

was placed on the external wall of the container and 'listened' for the characteristic frequencies associated the process activity, with the reactor vessel acting as a waveguide, and before selectively filtering the modes propagating acoustic waves. Furthermore, it has been shown that the reactor vessel is a highly attenuating system; only 1.1% of the initial mechanical energy of the particle impact was able to reach the sensor positioned outside the container. Hence, the passive acoustic approach depends on the application considered.

In the second part of this research, it is thus proposed to perform preliminary investigations into the ultrasonic-particle interactions in water employing the active acoustic technique. A number of commercial ultrasonic systems are available for the monitoring of off-line processes and are used to determine parameters such as particle size and concentration [59][60]. These techniques are based on an analysis of the linear response employing "pitch and catch" technology that requires transmission of the acoustic wave through the sample [15]. However, in many applications the physical nature of the material involved prevents acoustic transmission measurements and more useful process information can be achieved through a study of wideband ultrasonic backscatter [20].

The experimental work presented in this Chapter will complete the range of acoustic techniques examined in the Thesis where exploratory investigations into *linear* and *non-linear* ultrasonic-particle interactions in water have been evaluated.

A customised test cell was constructed for the experimental measurements. The experimental setup of the active acoustic system, its characterisation, and the digital signal processing (DSP) approach employed in the Matlab environment will be discussed. Linear measurements of attenuation

and velocity will be performed for verifying and testing the novel active system described in Section 6.8. These experiments will provide the evidence of a wetting phenomenon; a physical effect of the contact between the water and the surface of the particles.

The newly developed test tank will be then be used for assessing the capabilities of discerning the 2^{nd} harmonic signal using a solution of contrast agent (microspheres) in water. Other experimental examples of the second harmonic response from Avicel cellulose particulate suspended in water will be presented at the end of the Chapter.

6.1 Research objectives

The main objectives of the active acoustics experimental programme is to appraise the generation of linear and non-linear responses from chemical particles suspended in a fluid and to develop a suitable digital signal processing technique for relating the signals obtained to the sample properties.

The velocity at which an ultrasonic wave propagates through a particulate suspension, and the amount by which it is attenuated, are governed by interactions between the ultrasonic wave and the particles, e. g. transmission, reflections, absorption and scattering. The results of these interactions are used to obtain information about the concentration of the particles. In particular, the linear response generated from the heterogeneous mixture of particles in water can be used to compute velocity and attenuation measurements [124]. However, generation of a non-linear response by the mixture may produce important information related to the process itself. The study of the non-linear response from particulates was inspired by ultrasonic ima-

ging in biomedicine which employs a contrast agent (micro-bubbles) to obtain quantitative imaging and measurement of tissues [125][126][127].

When micro-bubbles are insonated they resonate with a specific frequency depending on their diameter. However, the main resonance frequency is not the only resonance frequency of the bubble; frequencies at multiples of the fundamental are generated, just like in a musical instrument. These harmonic frequencies have decreasing intensity, but the second resonant frequency, known as the second harmonic, is still strong enough to be employed for detection purposes. In theory, only the contrast agent micro-bubbles resonate with harmonic frequencies, while adjacent tissues do not resonate, or else their harmonic resonation is insignificant by comparison [128].

In a similar way, the theoretical advantage of any potential harmonic response from a particulate suspension over the fundamental excitation frequency is that only the particles suspended in the medium would resonate with harmonic frequencies, while adjacent walls of the system do not contribute at these frequencies. Thus, for instance, by extracting the second harmonic from the ultrasonic backscatter data, it could be possible to show the effects caused by the particulate only, without any artefact from the surrounding structures and instrumentation [129].

However, it is important to distinguish that within microbubbles, the harmonic generation occurs as a result of non-linear oscillations from the shell (see Section 6.3.1), while for solid particles in fluid the non-linear effects are due to various contributions such as heat conduction, viscous drag and multiple scattering effects (see Section 2.4.2). Moreover, a micro-bubble suspended in a liquid medium and immersed in an ultrasonic field, is a stronger scatterer of sound compared to a solid particle because of the large difference

of density between the bubble and its surrounding.

A suite of processing software for data capture and analysis has been developed involving Fourier analysis, cross correlation and matched filtering techniques. These developments will contribute to the extraction of linear and non-linear responses from the medium under investigation. In this work, cellulose particles suspended in water have been used as the chemical system under investigation.

6.2 Linear and non-linear acoustics

Acoustic theory for heterogeneous system should yield a relationship between some measured macroscopic acoustic properties, such as sound speed, attenuation, acoustic impedance, and some microscopic characteristics of the heterogeneous system, such as its composition, structure, electric surface properties, particle size distribution, etc. This relationship, (abbreviated as ECAH, following the names of its creators: Epstein, Carhart, Allegra and Hawley [9][57]) should be valid for wide frequency range on a MHz scale and high volume fraction of the dispersed phase. Starting from the ECAH formulations, the sound velocity and attenuation coefficient of chemical particles in fluids have been widely investigated and the propagation of sound has been modelled as a linear process [15][16][20][65] [47].

Sound waves propagate linearly when both their amplitude and the times and distances over which they are observe are not too large. If either of these conditions are violate, one may have to take into account non-linear effects. Weak non-linear effects become important in long range propagation of a signal that locally satisfies the 'infinitesimal-amplitude' criterion for linear

acoustics; and if the amplitudes are small but larger than the infinitesimal amplitude of the wave, the important finite amplitude effects will simply occur over shorter times and distances [93].

For many applications of non-linear acoustic phenomena, the magnitude of non linearity in an acoustic medium can be quantified using a single value known as the parameter of non-linearity β_{NL}. The coefficient of non-linearity β_{NL} indicates the rate of distortion of a progressive plane wave of a finite amplitude propagating into a medium:

$$\frac{dx}{dt} = v_0 + v\beta_{NL} \tag{6.1}$$

where v_0 is the small signal sound speed with infinitesimal amplitude and v is the particle velocity. The Equation of the propagation speed of a acoustic wave shows that at each wavelet (point of the waveform) propagates at a speed determined by its value of particle velocity. This implies that the plane wave distorts during the propagation at a rate determined by

$$\beta_{NL} = 1 + B/2A \tag{6.2}$$

where B/A is a ratio of coefficients in a Taylor series expansion of the isentropic equation of state [130].

The quantity B/A is a fundamental aspect of the relation as it has a significant effect on sound speed:

$$\frac{B}{A} = 2\rho\ v_0(\frac{dv}{dp})_T + \frac{2a_T v_0 T_0}{c_P}(\frac{dv}{dT})_p \tag{6.3}$$

where

- v_0 = small signal velocity of sound
- v = local velocity of sound in the wave
- ρ = fluid density
- T_0 = absolute fluid temperature
- a_T = coefficient of thermal expansion
- c_P = specific heat capacity at constant pressure
- p = pressure
- T = temperature

In effect, the quantity B/A will vary depending on the temperature, hydrostatic pressure and density of the medium through which a finite amplitude sound wave is propagating. Examples of this quantity for two common load media are as follows; distilled water has a ratio B/A = 5 and air has B/A = 0.4, both calculated at a temperature of 25 $^{\circ}C$. The higher the ratio, the more likely a medium is to generate non-linear effects.

Since the B/A parameter reflects the stress dependence of the elastic parameters, it could provide the dynamic characteristics of the status of the particles, compared with the linear parameters.

Non-linear effects are due to diffusive mechanism such as viscosity, heat conduction and frequency dispersion (i.e. minute in pure air or water but large in micro-bubbles in liquids) and ultrasonic scattering [131]. In many common situations thermo-viscous effects are often dominated over the initial wave scales by dissipation and dispersion associated with relaxation process. In a multi-phase medium, such as a liquid containing solid particles, the

process of relaxation involve the transfer of macroscopic heat between phases [93]. Cumulative non-linearity effects also arise from variation in propagation speed over the waveform, causing distortion to develop with distance. These can be quantified using the finite amplitude method.

Finite amplitude method

The finite amplitude method has proved useful for measuring B/A values in various materials including biological tissue [132][133][134].

The finite amplitude method involves the measurement of the amplitudes of the first and second harmonics of a wave propagating through the medium to be characterised [135]. In this way it is possible to calculate the B/A coefficient.

Experimental determination of the non-linear parameter B/A with the finite amplitude methods could be complicated by the diffraction pattern resulting from the bounded nature of the ultrasonic source. The combined effects of diffraction, absorption, and non-linearity in directive sound beams can be modeled by the KZK (Khokhlov-Zabolotskaya-Kumetsov) non-linear parabolic wave equation [136].

For instance, a method for measuring the B/A coefficient was developed by Law et. al. [137] who worked in the extreme near field of a planar transducer and measured the value of B/A in several biological fluids using the through transmission technique. Working with small distances between the transmitting and receiving transducers permitted these authors to make a plane wave approximation to the beam, hence to simplify the problem by working in a limited region of the diffracting field, where a plane wave approximation to the beam is applicable.

They recorded the rate of change in the absolute values of pressure for the fundamental and second harmonic components as a function of distance, along the axis of the transmitted beam. In addition, by extrapolating their measurements back to zero separation distance between the transmitter and receiver, Law et. al. were able to compensate for any ultrasonic attenuation in the sample medium, without any assumption about the frequency dependence of the attenuation [137].

6.3 Non-linear response from ultrasonic contrast agent

Since the study of the non-linear response from particles floating in water was inspired by ultrasonic imaging which employs a contrast agent and the previous research on process control utilising a particulate suspension in water has been mainly focused on the linear response techniques, ultrasonic techniques exploiting the non-linear behaviour of UCA are presented in this work.

Over the past decade, with the introduction of contrast agent, significant improvements have been realised in the ultrasound imaging field. To extend the utility of ultrasound contrast imaging, research has been actively focused in developing efficacious ultrasound contrast agents and new contrast-specific imaging techniques. Ultrasound imaging uses short, relatively high power pulses, as they provide high axial resolution and high signal to noise ratio (SNR). Peak transmitted pressure and pulse energy are limited by regulatory agencies due to safety concerns. Peak transmitted pressure is also limited by the destruction of UCA microbubbles in UCA imaging methods.

With special coding techniques, one can increase pulse energy by transmitting longer pulses without increasing peak pressure and without decreasing pulse bandwidth. With proper decoding, axial resolution is not compromised. The most important code in this category is the linear frequency sweep or linear chirp as it is relatively robust to frequency shifts. A linear chirp is a long sinusoidal burst with an instantaneous frequency changing linearly in time. Chirp compression takes a matched-filter approach in which an autocorrelation filter with an impulse response that is the time inverse of the transmitted chirp is used. As the compression filter has the same bandwidth as the fundamental of the transmitted chirp, this is equivalent to extracting the fundamental from the echo signal and adjusting the phase of the frequency components.

6.3.1 Ultrasonic contrast agent

Ultrasound contrast agents (UCA) have been in clinical use for many years for applications such as imaging methods to increase the echoes reflected from blood stream [138], detecting and characterising liver [139], renal, breast and prostate tumors [128] and drug delivery [140].

Today almost all modern UCA for clinical use consist of a gas-filled kernel encapsulated by an albumin shell with a total bubble radius of 1-10 μm (micro-bubbles). In fact, bubbles larger than 10 μm may transiently obstruct the capillaries and act as gas emboli [141].

The compressibility of micro-bubbles is several orders of magnitude greater than water or tissue, and are smaller than the wavelength of the applied ultrasound field in the diagnostic frequency range. Therefore, they undergo volumetric oscillation [125]. When a gas bubble is hit by an ultrasound wave

it will expand in the negative half cycle of the wave and contract in the positive half cycle. The contraction and expansion of the gas bubble (vibration) depends on the amplitude of the ultrasonic waveform [125]. This vibration of a microbubble exposed to a ultrasound field produces a strong backscatter acoustic signal that can be detected by an acoustic receiver. The bubble behaviour can be classified into two regimes depending on the acoustic pressure amplitude of the ultrasonic incident wave. The bubble can oscillate in a symmetrical (linear) or in an asymmetrical way (non-linear). Consequently, when the bubble is insonified by acoustic energy, the bubble vibration will contain second and higher harmonics of the transmitted frequency (acoustic signature) [126]. If the acoustic pressure amplitude is increased, the backscatter level of the contrast agent increases abruptly for a short time. This has been associated with bubble explosion and release of gas. Figure 6.1 shows the regimes of reflection of micro-bubbles when excited by different levels of acoustic pressure amplitude.

The oscillations produced by the passing ultrasonic wave through the bubble cause a resonance effect. The resonance frequency f_R of a micro-bubble of radius R_o and mass m is:

$$f_R = \frac{1}{2\pi R_o}\sqrt{\frac{3\gamma P}{\rho} + \frac{S_{shell}R_o^2}{m}} \tag{6.4}$$

where γ is the ideal gas constant, S_{shell} is the stiffness of the shell of the bubble and P and ρ are the ambient pressure and the density of the surrounding liquid [129].

If the pressure of the ultrasonic wave at or near f_R is sufficiently high, non-linear oscillations of micro-bubbles occur. The reception of non-linear

signals from micro-bubbles is employed to detect their specific "footprint" and thus to better separate them from the tissue signal. In particular second harmonic response is evaluated for imaging and used within modern harmonic imaging techniques [141].

The ultrasound contrast agent used for the experimental work is a product of Bracco, which is called SonoVue. SonoVue contrast agent consists of hollow, gas-filled micro-spheres of diameter between 1 and 10 μm which are known to be very efficient scatterers of ultrasound [127]. The scattering effect is dependent on the excitation pressure incident on the micro-spheres and the frequency of excitation [129]. At low pressures the backscatter is linear, i.e. energy is scattered at the fundamental frequency, but increased pressure above a threshold, typically 100 to 120 kPa peak-to-peak, produces oscillations at the 2^{nd} harmonic which generates backscatter at this frequency [129]. The micro-spheres are susceptible to collapse due to localised osmotic pressures generated by the acoustic field allowing leakage of the fill gas, and further increase in pressure above the 2^{nd} harmonic oscillation threshold promotes rupture of the micro-spheres [142].

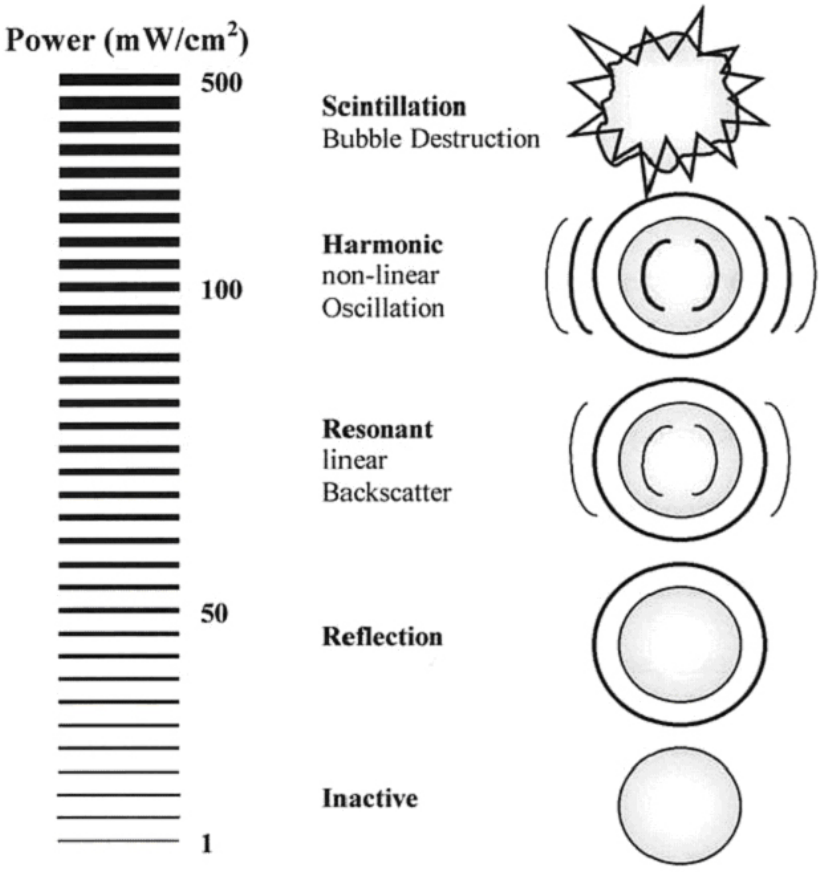

Figure 6.1: Regimes of reflection of microbubbles [2]

Previous work on UCA

Several scientists employed the use of microbubbles contrast agent for clinical use [128] [138] [139] [140] and investigations of its nonlinear effects [125][129][143][144].

Hamilton and Blackstock [133] have studied the non-linear propagation using simplified models. In this analysis, they describe the effect of bubbles in a medium on the index of non-linearity (B/A). They found that a moderate concentration of microbubbles can increase B/A from 5 to as high as 3000 for frequencies below the resonance frequency, but the increase in B/A is minimal for frequencies above the resonance frequencies.

Tang and R. J. Eckersley [143] employed both theoretical and experimental methods to explore the non-linear propagation of ultrasound transmission through microbubbles from an imaging perspective and to illustrate and quantify imaging errors caused by this non-linear propagation.

De Jong [144] has provided experimental results on the non-linear scattering behavior of AlbunexB (Molecular Biosystems Inc., San Diego, CA). He used the pulse-echo approach with a single broadband transducer centered at 3.5 MHz. The transmitted signal consisted of a burst of two acoustic periods at 2.2 MHz and the second harmonic component was extracted by digital signal processing. De Jong also showed that: 1) the second harmonic signal occurs only at frequencies that are in the vicinity of the resonance frequency of the insonified bubbles; and 2) due to the presence of a shell, the response of AlbunexB is smaller than that of ideal gas bubbles.

Interesting, Borsboom et. al. [145] used the harmonic chirp imaging method on simulated bubble echo signals and measured propagation harmonics. They simulated the echoes generated from 1.85 μm, 2.75 μm, and 4.50 μm

radius contrast agent bubbles with SonoVue parameters. At these sizes the resonance frequencies of the bubbles are 3.5 MHz, 2 MHz, and 1 MHz, respectively. Thus the bubbles are driven below, at and above their resonance frequencies for the given excitations. Their research consisted on measuring the reflections from a flat steel reflector that was positioned at 75 mm from a 3.5 MHz, 65% bandwidth unfocused, 12-mm diameter, single-element transducer in pulse-echo mode using the chirp waveforms at approximately 120 kPa peak pressure. The resulting echo was amplified and subsequently digitized and recorded with a digital oscilloscope. The measured echoes were compressed to extract the fundamental and the second harmonic.

The experimental results shown that the compression filter detected and extracted the fundamental and the second harmonic components using chirp excitations. Importantly, the second harmonic response was circa was 18 dB lower than the fundamental.

The problem of scattering from micro-bubbles differs from the weak scattering of particles for the following reasons. Firstly, the micro-bubble suspended in a liquid medium is a strong scatterer of sound, because of the large density difference between the bubble and the surrounding load medium. The greater sensitivity of ultrasound to bubbles suggest to its use for measuring bubbly systems, however to know the bubble size, bubble distribution and phase volume of gas are no so easy to measure; measurements in concentrated systems are likely to be of an empirical of semi-empirical nature [65].

Secondly, the micro-bubbles exhibit a resonant behavior in the presence of an ultrasonic field, this introduces further complexity in the single-particle scattering problem. Thirdly, the energy of the surface of a bubble plays a

fundamental role in the total energy of small bubbles and more than one mode of the oscillations of a bubble may be important [146]. The single scattering coefficients can no longer be determined by superposition of the single-frequency solutions [65]. This implies that the general solution of the scattering problem for a cloud of bubbles is much more complex than for multiple particles in a liquid medium.

6.4 Initial experimental arrangement

A prototype test tank designed for investigating the non-linearities generated by micro-bubbles was first employed in this study. Figure 6.2 depicts the schematic of the experimental arrangement. The model system under investigation was enclosed in a mixing chamber (volume of 450 mL) with two PVDF hydrophones (H_1 and H_2) and stirred by a magnetic stirrer.

Microcrystalline cellulose particles (Avicel PH-101, PH-102, PH-105, PH-112 and PH-200) suspended in water was the heterogeneous mixture used for the active acoustic experiments. Microcrystalline cellulose material is inert, harmless (unless inhaled), insoluble in water and easily stirred. The physical properties of different grades of Avicel are given in Table 6.1.

Wide-band, linear modulated chirp waveforms were downloaded to an arbitrary function generator (AFG) Agilent 33250A. These chirp sequences were used to drive a range of commercial ultrasonic transducers (see Table 6.2) to cover a wide range of resonant modes within the suspended particles and used to drive the transmitting transducer, via a power amplifier. The signals detected by the PVDF hydrophones were captured and saved on a digital oscilloscope (Agilent Infiniium 54642) and then transferred to a PC

Table 6.1: Physical properties for Avicel

Property	**PH-101**	**PH-102**	**PH-105**	**PH-200**
Average size (μm)	50	90	20	180
Size Range (μm)	19.6-139.7	29.6-258.7	7.3-50.9	unknown
Density (g/cm^3)	0.29	0.30	0.25	0.32
Shape	Granular	Granular	Granular	Granular

for subsequent processing and analysis.

The broadband nature of the PVDF material employed for the fabrication of the wide-band membrane hydrophones enabled the full bandwidth of forward and back-scattered ultrasonic responses to be acquired and analysed. The hydrophones were made using a thin PVDF film (110 μm) mounted across an aluminium support frame of 110 mm internal and 120 mm external diameter. In principle, it could be possible to acquire sub, second and higher order harmonics with little impact on the incident sound field as the specific acoustic impedance of PVDF is close to water.

The tank was also designed for future positioning of a second transducer, acting as a receiver on the opposite side of the mixing chamber for pitch and catch operations and to allow the detection of weaker signals with improved sensitivity compared to the wide-band hydrophones.

The preliminary results together with the limitations of the first prototype tank are reported in Section 6.7. These limitations have led to development of a second test cell. All components in the second test cell were fully characterised to assess for non-linear behavior. In addition, development of signal processing techniques was required. Development and characterisation of the test cell along with the development in signal processing are described in the next Section.

For these reasons a team, composed of four engineers and two chemists,

was conceived in order to solve these multi-disciplinary issues and improve the active acoustic system. Graham Benny (CUE [88]), addressed the design, the fabrication, the full characterisation of the proposed test cell and the experimental acquisition of the AE data. Dr. Alison Nordon was responsible for the experiment design. The author was part of this team and contributed at all stages of the system development. Moreover, he was in charge of the digital signal processing and data analysis. This involved the writing of the Matlab code and the post processing of the experimental data. The research program was supervised by Prof. Anthony Gachagan, Prof. Gordon Hayward, Prof. Nordon and Prof. David Littlejohn.

In principle, ultrasonic measurements are simple to carry out, but in practice there are a number of factors that must be considered if accurate and reliable measurements are to be obtained. The measurement cell must be carefully designed to minimise the reverberations of ultrasonic signals in cell walls and transducers, diffraction effects and phase cancellation due to non-parallel walls [15]. Following as close as possible these principles the new test cell was fabricated following the same overall arrangement of the tank employed for micro-bubbles studies given in Figure 6.2. However the *mixing chamber*, the *hydrophones* and the *ultrasonic transducers* were developed further with the aim to improve the mixing of the sample and its ultrasonic measurements.

6.5 Digital signal processing

Signals used in most popular forms of DSP are extracted from analogue signals which have been sampled at regular intervals and converted into a

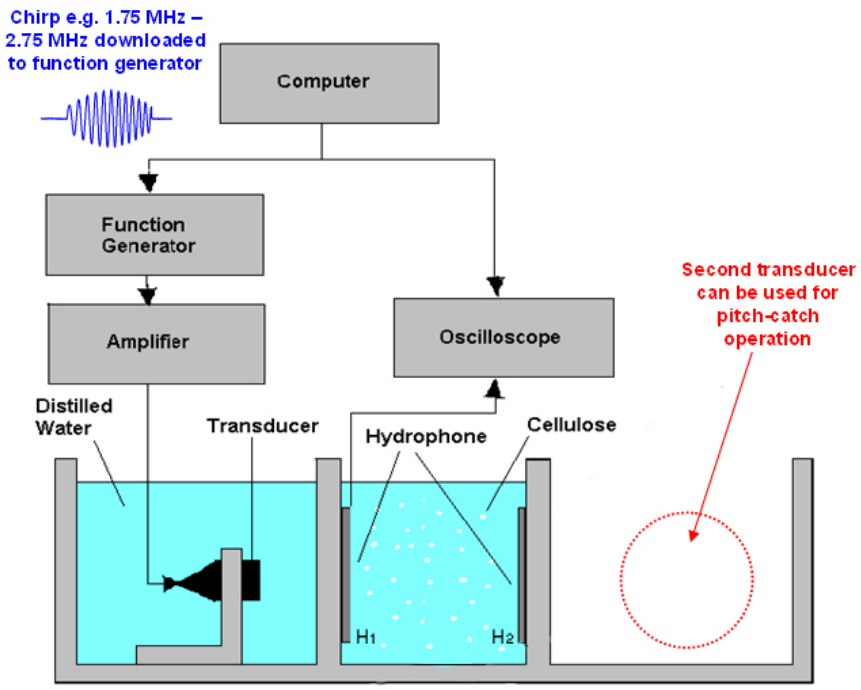

Figure 6.2: Experimental setup of the active monitoring system

digital form. In this work, the signals from the hydrophones were acquired, converted to a digital form and processed for different reasons. For example, to remove interference or noise from the acquired signal (e.g. by summing up the signals in the frequency domain, using pass band tailored filters etc.), to obtain the spectrum of the data or to transform the signal into a more suitable form and extract the second harmonic with a pulse compression technique [95].

The data measured from cellulose particulates were analysed using the following signal processing tools:

- Time response analysis.
- Fast Fourier Transform.

- Cross correlation.
- Pulse compression technique.

A suite of programmes, employing these techniques, provided a range of methods for extracting information from the captured signals. The majority of the analysis was performed in the frequency domain except for the attenuation and velocity analysis which was conducted in the time domain. Non-linear analysis was performed by extracting the second harmonic signal from the backscatter data, while for the linear measurements of attenuation and velocity, the pitch and catch acoustic technique was used.

It is assumed that the reader is already familiar with the first three basic DSP operations [95], hence only the advanced DSP pulse compression technique is described in this Thesis.

Computer as a controller

Through a standard PC (Dell Dimension 8400) it was possible to control the acquisition process and perform the data analysis. The software tools employed for these tasks were Matlab ver. 7.0 and the IEEE drivers, including those for the General Purpose Interface Board (GPIB).

Acquisition procedure

Two dedicated Matlab programs were developed for velocity/attenuation measurements and for the acquisition of any non-linear signals from particles. The same experimental arrangement was used for both experiment types and their acquisition procedure is summarised in Figure 6.3.

The acquisition procedure starts at the user interface layer. A graphical user interface (GUI) allows the user to specify the input waveform parame-

ters. The ultrasonic signal (e.g. broadband chirp) is then downloaded to the function generator.

After the input waveform selection, the user is prompted for the relevant acquisition parameters, i.e. sample rate, the time window to be captured and the number of insonifications to be achieved. As each signal is acquired, the captured data is displayed and it is saved to a text file.

In the software layer, a Matlab script controls the communication between the PC and a 80 MHz Agilent 33250A Function/Arbitrary Waveform Generator (AFG) via GPIB. The Matlab control program acts like a kind of "glue", linking all the elements of the apparatus together into a single coordinated unit. The software fully controls both the 54810A Infinium Oscilloscope for data visualisation and the 12 bit, 400 MS/s sampling CompuScope 12400 PCI acquisition card for the data acquisition.

In order to drive the transducer with a high voltage signal it is necessary to amplify the input signal using a power amplifier. The power amplifier used was a Kalmus 155LCR amplifier with 50 dB gain over a nominal bandwidth from 6 kHz to 12 MHz. Therefore, the transducer generates acoustic waves, which interact with the chemical particles and surroundings, generating linear and non-linear signals. The signals detected by the hydrophones (using the pulse-echo and through transmission techniques) are captured on the acquisition card and automatically transferred to the PC for subsequent processing and analysis.

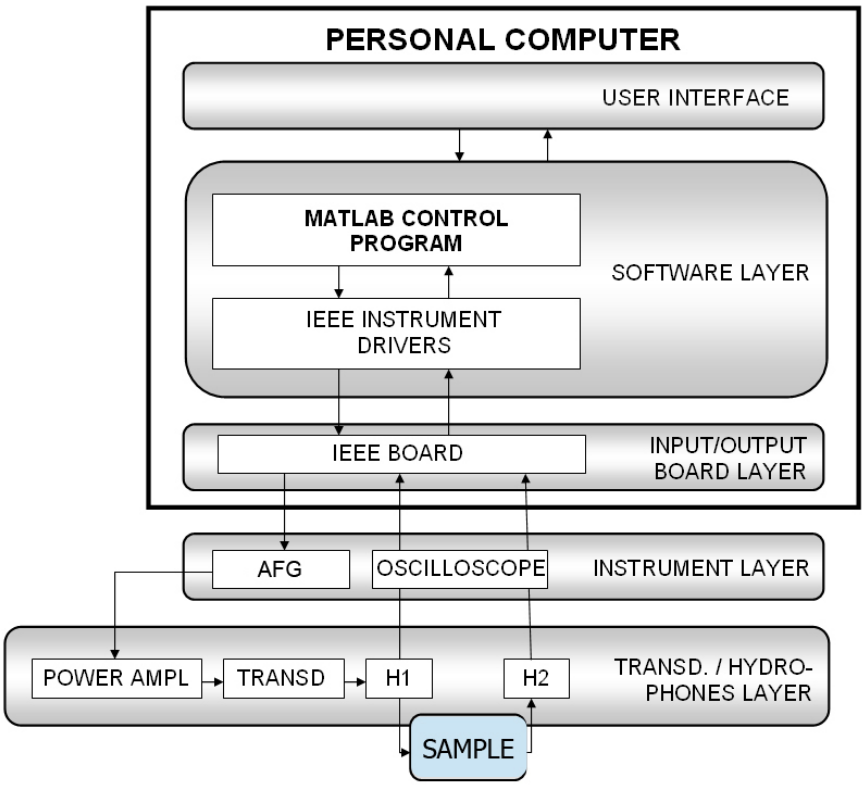

Figure 6.3: Schematic of the ultrasound control system for the ultrasound active monitoring

6.6 Second harmonic extraction using the pulse compression technique

The method of measuring the characteristics of heterogeneous media from acoustic backscatter data is based on extracting the frequency response of the non-linear effects from particles in fluid. Chirp signals with a centre frequency of 0.5, 1.0 and 2.25 MHz emitted from a transducer are directed towards the measurement volume. Particles in suspension will direct a portion of this signal back to the transducer. The strength of the backscattered signal allows calculation of particle concentration. The amplitude of the backscattered signal depends on the concentration, particle size, and acoustic frequency [47].

One of the main issues of using the pulse echo method for process monitoring is the presence of high coherent noise [60]. The noise could mask the weak attenuated echo signal completely. The easiest way of improving the SNR is by increasing the signal amplitude of the ultrasonic waveform transmitted into the system, but unfortunately this solution is limited to the peak power limitations of the transmitter and the non-linearities of the sytem.

Moreover, for achieving good resolution in the frequency domain, an ideal pulse should be employed to characterise the system. However, the duration of a pulse cannot be reduced indefinitely, because this would require an extremely wide-band ultrasonic transmitter and receiver [147].

To achieve high bandwidth without an enormous high peak power and to detect the incoming signal, from a known transmitted one, matched filtering is commonly used [95]. Matching filtering has been successfully used in a number of applications including radar applications [148], testing of solid

rocket motors [149] and food packaging [47]. This method is optimal when a known signal is to be detected among additive white Gaussian noise. Matched filtering is a generalisation of the pulse compression technique, which computes the correlation of the received signal with the transmitted signal. This involves correlating a signal with the required frequency component to be detected by convoluting the incoming signal with a conjugated and mirrored version of the transmitted signal. In other words, given a received signal *s(t)* and spectrum $S(f)$, the output of the matched filter is one which maximises the output signal to noise ratio. The success of the pulse compression technique heavily depends on the proper selection of the pulse. Broadband chirp signals are best suited for this purpose, because they can be easily synthesised by signal generators, and the frequency spectrum of chirp pulses can be adapted to the transfer function of the system, and consequently a maximum signal energy can be brought into the system [95][150].

The pulse compression technique is commonly used for improving the SNR of medical imaging techniques when employing contrast agents. The contrast agent is used to enhance the contrast of structures or fluids within the body in medical imaging and is a hollow shelled sphere. The micro-bubbles resonate with a specific frequency depending on their diameter and generate ultrasonic waves at multiple frequencies of the fundamental when they are subjected to a high intensity ultrasonic field. These harmonic frequencies have decreasing intensity, but the second frequency, known as the second harmonic, is still strong enough to be employed for imaging purposes [37].

In theory, only the contrast agent micro-bubbles resonate with harmonic frequencies, while adjacent tissues do not resonate, or else their harmonic

activity is low [127]. Thus, using a unit especially set to produce ultrasound at a given frequency f_o and receive an ultrasound signal at twice the frequency $2f_o$ as shown in Figure 6.4 [139], enables detection of the contrast agent only, without any artifacts from the surrounding anatomical structures, with a markedly improved SNR [150].

In a similar way in this work, chemical particles were employed instead of micro-bubble contrast agents. The idea behind this study is to exploit the known non-linearities to obtain particle size and concentration information using the second harmonic signal.

Hence, during the analysis of the active acoustic experiments, the resultant backscattered data (see Figure 6.6) was cross-correlated with a broadband chirp signal of double frequency to enhance the desired spectral characteristic at the second harmonic. This entailed centering the correlation function at the frequencies corresponding to the second harmonic response. The correlation function was designed to act as a matched filter, for extraction of the second harmonic components. In particular, the steps used to perform the matched filtering are shown in the flow chart in Figure 6.5.

First the backscattered data acquired were saved into a file for post processing analysis, then the algorithm automatically determined the sampling frequency and subtracted the DC component (a necessary operation to perform the cross correlation). At the same time, a chirp with double the frequency of the insonification frequency was artificially generated through Matlab. Then the two signals were cross-correlated and the absolute value of the FFT was computed to yield the magnitude spectrum.

The preliminary experimental work employing this technique for the second harmonic extraction follows.

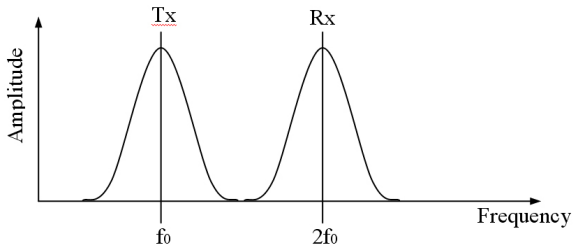

Figure 6.4: Principle of second-harmonic imaging

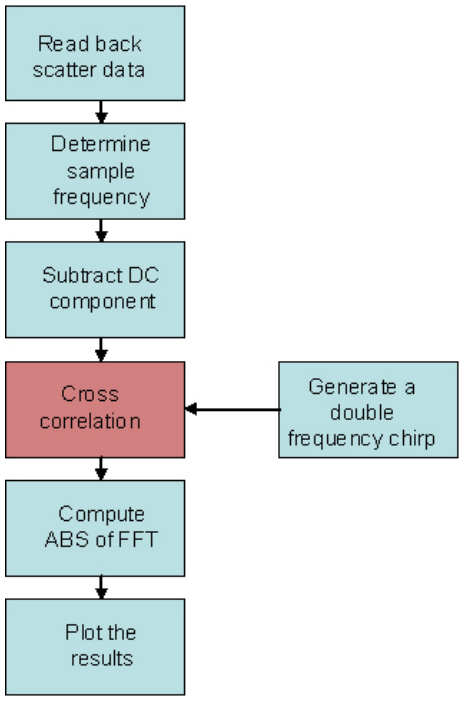

Figure 6.5: Flow chart of the procedure for extracting the second harmonic signal using the pulse compression technique

6.7 Preliminary experiments employing the first experimental arrangement

Introductory investigations employing the prototype tank designed for microbubbles studies (see Section 6.4) were carried out by adding various masses of microcrystalline cellulose particles (Avicel PH-101, PH-102, PH-105, PH-112 and PH-200) to 450 mL of distilled water. An example of the response of 50 g of Avicel (PH-102) with an average particle size of 90 μm is shown in Figure 6.6. The waveform was obtained by exciting the 2.25 MHz Panametrics transducer positioned inside the water tank with a 10 V_{pp} chirp waveform (start frequency = 1.75 MHz, end frequency = 2.75 MHz, time duration = 10 μs) and receiving the output signal at hydrophone H_1. The initial propagating pulse is evident at approximately 30 μs. This corresponds to the propagation path between the ultrasonic transducer and the hydrophone receiver H_1. The second large signal is the reflection from the second unconnected hydrophone H_2. Hence, the backscattered signals will be contained in the time window between these two signal components as highlighted in the Figure.

Backscattered signals were extracted automatically and the influence of particle concentration was examined. Here, the volume of the liquid inside the mixing chamber was constant in all experiments and the particle concentration was varied by altering the mass of the cellulose added between 0 g and 50 g. The 2.25 MHz transducer was used to insonify the sample and hence, the second harmonic response of the backscattered data was extracted between 3.5 and 5.5 MHz.

The spectral characteristics of the response obtained for each particle size

distribution are illustrated in Figures 6.7 and 6.8. Figure 6.7 presents the second harmonic response from the particles with an average size of 20 μm and 50 μm (PH-105, PH-101) and serves to illustrate both the positive and negative aspects of this experimental study. The 20 μm results are shown in the top plot of Figure 6.7 and it is possible to observe that the magnitude of the spectral characteristics increases with an increase in particle concentration for concentrations larger than 10 g. Unfortunately, in the results for particles with an average size of 50 μm, 90 μm and 180 μm (PH-101, PH-102, PH-200) no such trend is clearly identifiable. In fact, for particles with an average size of 90 μm, top plot in Figure 6.8, the peak response was in the middle of the concentration range.

To determine if the second harmonic data presented in Figures 6.7 and 6.8 showed any correlation with particle concentration, a plot of the total area under each curve was generated.

Figure 6.9 illustrates the four graphs, which show the amplitude of the non-linear response as a function of concentration for different particle sizes. There is an increase in signal magnitude at the second harmonic frequency with particle concentration at concentrations above 2.22% (corresponding to 10 g of particles). The response at a concentration of 2.22% for particles with an average size of 90 μm is clearly an error.

The preliminary experimental work is encouraging: a response in the second harmonic frequency range has been detected in all experiments with particles in water. Unfortunately, there is no clear distinguishable trend in the data, which is directly related to the particle size or concentration.

It is interesting to note that the best results were obtained for particles with an average size of 20 μm. Moreover, the number of particles present in

the 20 μm samples were circa 1000 times larger than those employed in the 180 μm samples. For this reason the plot at the top of Figure 6.7 is more pronounced in terms of spectra amplitude than the bottom plot of Figure 6.8.

However, the acoustic non-linearity in particle suspension is minimized when the particle diameter is comparable to the fundamental half wavelength, while the non-linearity is maximised when the particle diameter is comparable to the fundamental wavelength. The sound scattering by the particle governs the acoustic non-linear properties [131].

It is suspected that stirring was most efficient for the smallest particles and hence, less consistent data were obtained for larger particles.

The design of the new test tank with improved stirring to ensure uniform distribution of particles in the liquid and the characterisation of its components to ascertain that the non-linearities originated from the particulates only was undertaken.

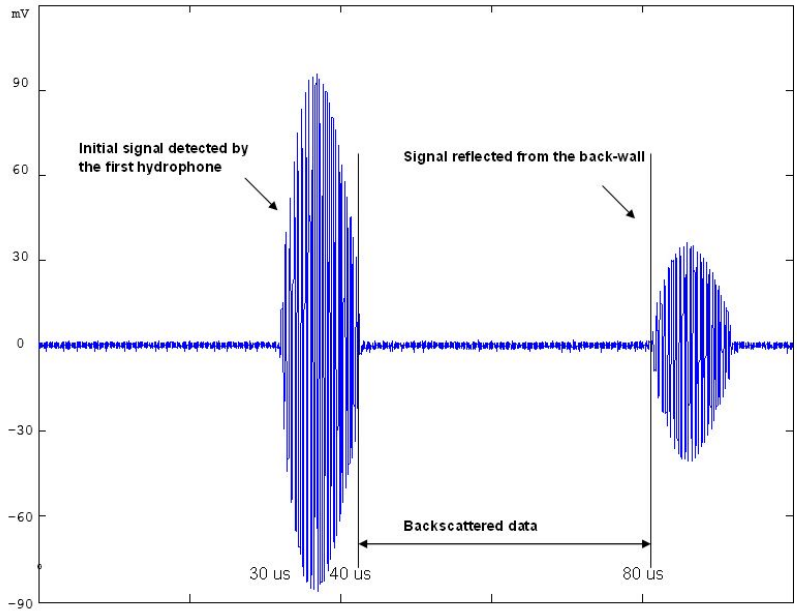

Figure 6.6: Measured temporal response at H_1 from cellulose particles in water

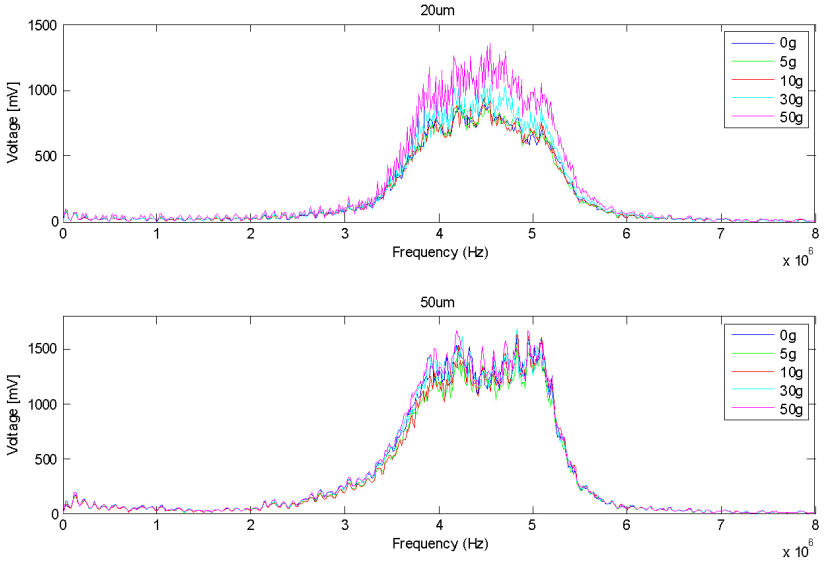

Figure 6.7: Second harmonic responses for particles with an average size of 20 μm (top) and 50 μm (bottom)

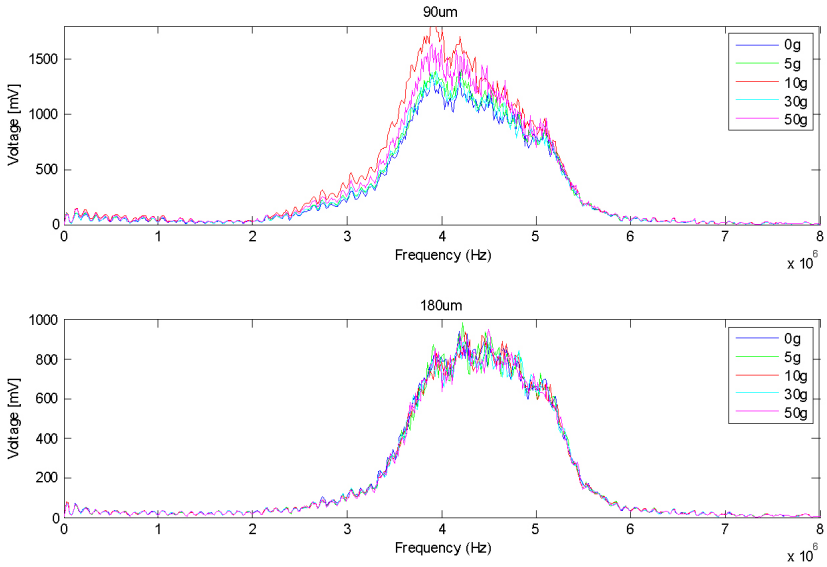

Figure 6.8: Second harmonic responses for particles with an average size of 90 μm (top) and 180 μm (bottom)

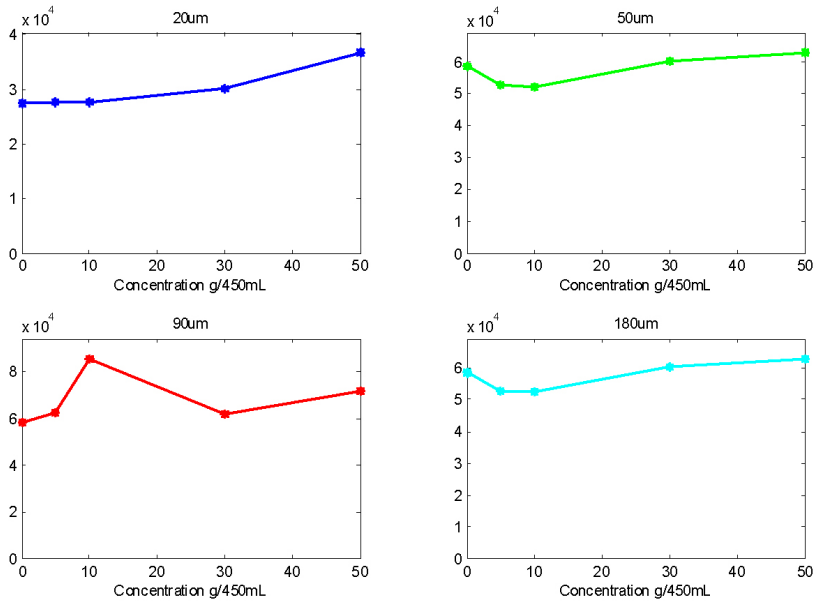

Figure 6.9: Concentration trends for each particle size: a) 20 μm, b) 50 μm, c) 90 μm, d) 180 μm

6.8 Second experimental arrangement: new test cell components and characterisation

6.8.1 New test cell and mixing chamber

The water tank was constructed from 10 mm thick perspex according to the dimensions given in Figure 6.10. The overall footprint of 800x150 mm^2 was necessary to allow the ultrasonic transducers to be used in their far field region. The area just beyond the near field is where the sound wave is well behaved and is at its maximum strength and where the ultrasonic beam is more uniform. According to Equation 4.15, the longest N_f of all the transducers available (see Table 6.2) corresponded to 24 cm (Alba 250 kHz).

The mixing chamber was machined from solid aluminium the dimensions detailed in Figure 6.11 with an inner volume of circa 1 L. Apertures were made to contain the hydrophones and to allow a free acoustic path. A mechanical stirrer was employed, instead of a magnetic stirrer which was used with the first cell in studies of micro-bubbles, to maintain a uniform distribution of particles in the mixture. A six blade stirrer propeller of 40 mm diameter provided the agitation and it was placed about 10 mm from the bottom of the mixing chamber. Transducers were mounted in collars which fit into the support brackets in Figure 6.10 (c) which were constructed using perspex. The complete test tank was then contained in a screened aluminium enclosure to provide sufficient immunity from environmental electromagnetic interference (EMI) to allow reasonable SNR to be achieved. The tank containing the ultrasonic transducers and the aluminium mixing chamber was filled with distilled water.

The influence of the stirrer on the acoustic beam passing through the mixing chamber was quantified experimentally. Moreover, the stirring efficiency was investigated by adding different concentrations of microcrystalline cellulose (Avicel) to water in the mixing chamber. To quantify any effect that the presence of the stirrer has on the acoustic beam, the experimental set up shown in Figure 6.12 was employed.

A 1 MHz tone burst was transmitted from the transducer T1 (Panametrics 1 MHz) through the mixing chamber and received at the hydrophone H_2. 50 g of microcrystalline cellulose (Avicel PH-102) was added to 850 mL of water in the chamber. The stirrer was positioned at 5 mm intervals across the mixing chamber from the maximum possible distance to one side (-X = -35 mm), through the acoustic centre (0) to the maximum distance at the other side (X = 35 mm).

Figure 6.14 illustrates the effects of the stirrer being passed across the acoustic beam for a range of stirrer rotational speeds and stirring positions on the received signal amplitudes. As would be expected, the stirrer interferes with the acoustic beam to the greatest extent around the acoustic centre line (at approximately -5 mm) and has minimal effect at either the side of the mixing chamber. The response is seen to be uniform, within experimental error, regardless of rotational speed of the stirrer. As the speed increases, attenuation increases owing to improved mixing and hence, suspension of particles. It is also evident that the attenuation reaches a constant value at 300 rpm. Plotting the average attenuation value across the chamber versus the stirrer rotational speed (Figure 6.15) confirms that the maximum attenuation is observed at 300 rpm above which it does not change. Importantly, the experimental work was performed using 250 rpm stirring speed and the

stirred was kept at a fixed position of 35 mm where not specified.

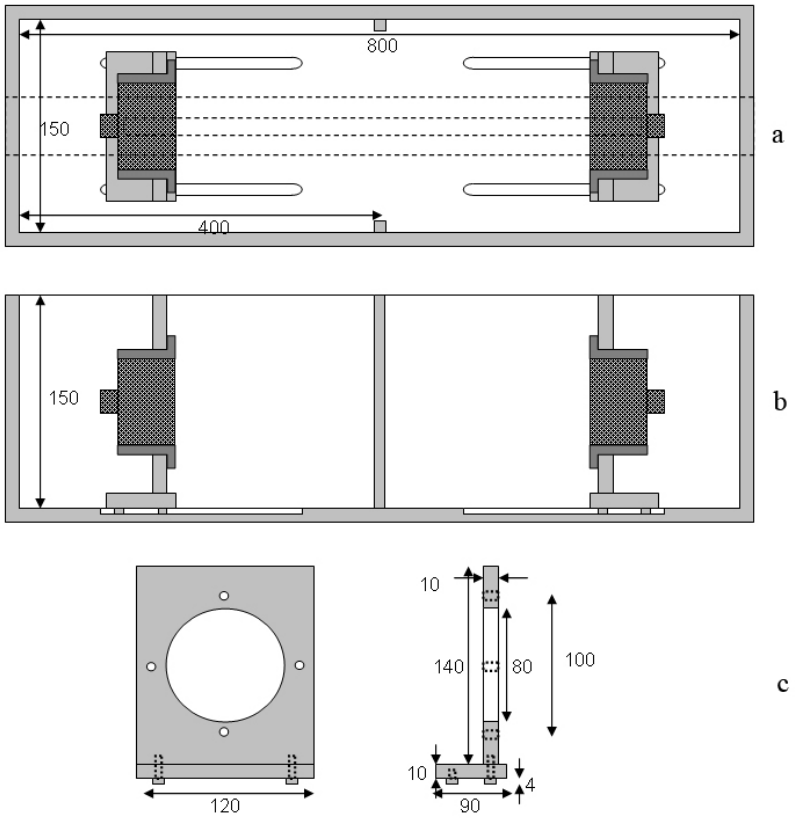

Figure 6.10: Mechanical drawings of the tank: a) view section at mid height showing transducers mounted in holders b) side view section on acoustic axis showing transducers in holders, c) transducer support bracket.

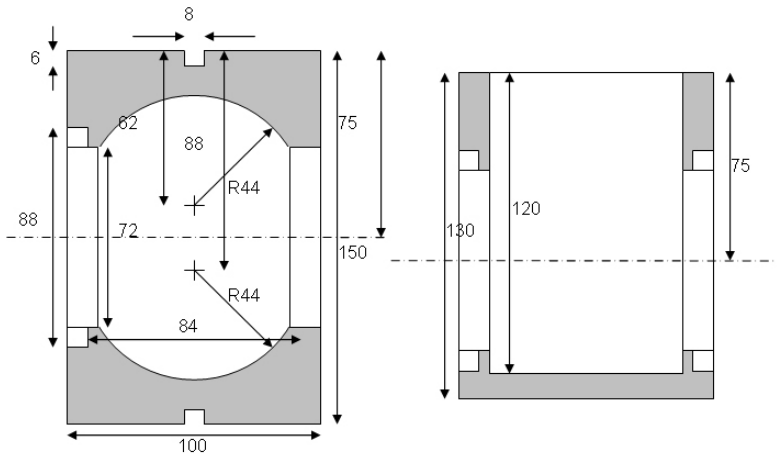

Figure 6.11: Mixing chamber top view (left) and side view section (right).

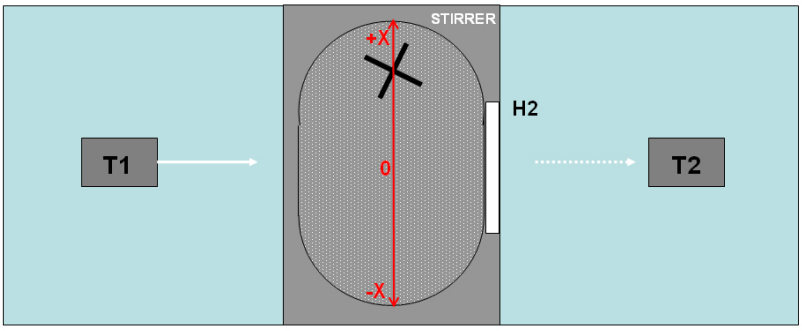

Figure 6.12: Top view of the design of the new tank

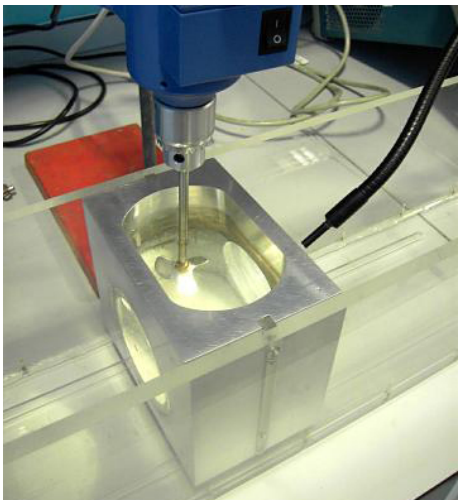

Figure 6.13: Mixing chamber and stirrer.

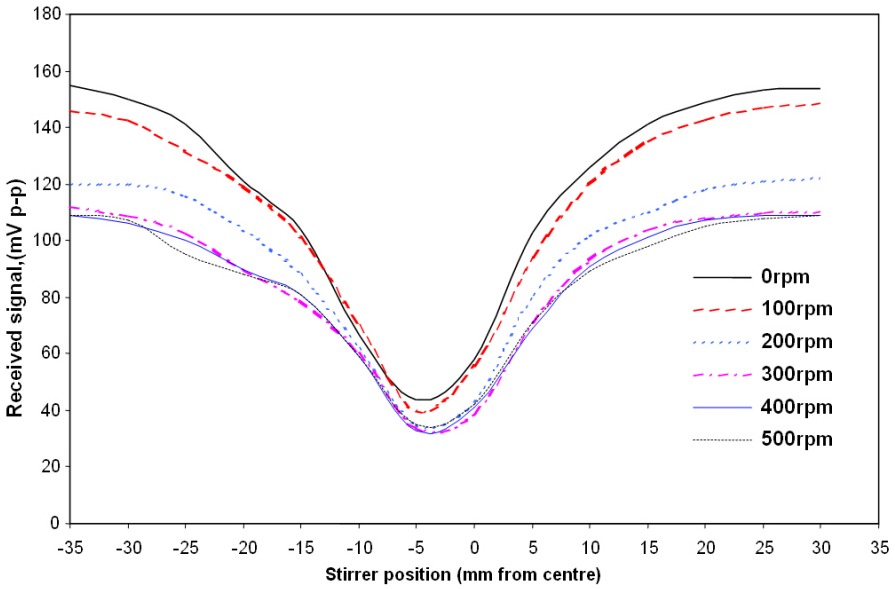

Figure 6.14: Received signal amplitudes for the range of stirrer positions and rotational speeds

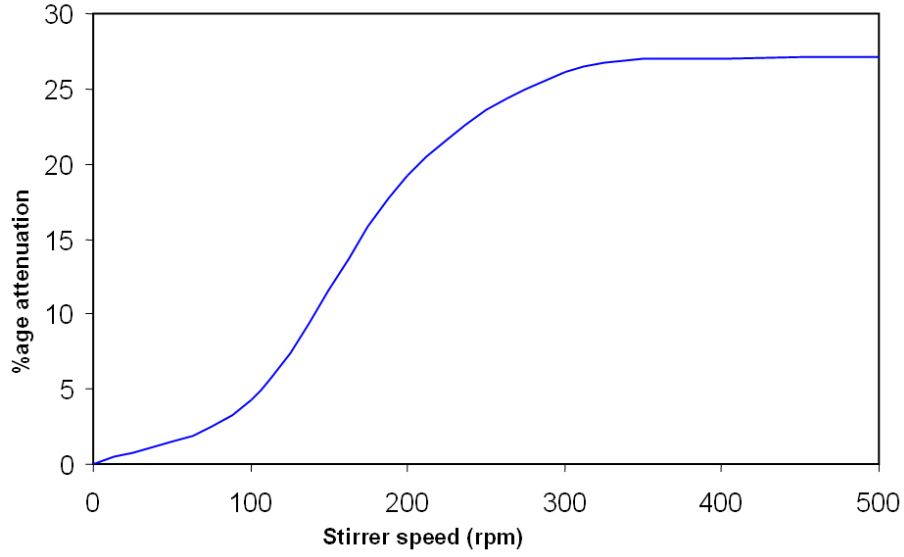

Figure 6.15: Average attenuation versus stirrer speed

6.8.2 Hydrophones

PVDF devices offer a significant improvement in performance characteristics compared with ceramic hydrophones [103]. The performance properties of membrane hydrophones are well understood and they can be used reliably for the detection of underwater signals or characterisation of transducer beams. Their temporal stability makes these hydrophones ideally suited as reference devices [104]. PVDF film hydrophones also exhibit low acoustic impedance and have a flat, broadband frequency response that can range from a few Hertz through to hundreds of Mega-Hertz. PVDF film has a linear response, is sensitive across a large dynamic range [103] and is resistant to a range of chemicals. These properties make it perfect for our aim of monitoring particles immersed in liquids.

The new membrane hydrophones, fabricated in the CUE laboratories, consisted of a thin PVDF film (110 μm) stretched across an annular frame of 90 mm internal diameter. The hydrophones were electroded by evaporation of aluminium onto the PVDF film to produce an active area of 25 mm diameter. The electroded membrane was glued between two un-electroded membranes to provide the electrodes with protection from any possible attack from chemicals in the mixing chamber. The composite films were glued to an aluminium support ring in a fixing jig then trimmed to size and finished with a protective end-cap. The connection regime between the hydrophone and a screened co-axial cable evolved into a robust arrangement. Figure 6.16 shows the mixing chamber arrangement comprising the prototype hydrophones.

The hydrophones were calibrated using the substitution method [151].

In calibration by substitution, a 'reference' hydrophone with known sensitivity versus frequency $M_R(f)$ and a 'test' hydrophone with unknown sen-

sitivity $M_T(f)$ are used. Firstly, the signal from the reference hydrophone, positioned at a known distance from the source transducer, is measured. Then, the reference hydrophone is replaced by the unknown hydrophone and its response is then measured. It is possible to calculate the curve of response of $M_T(f)$ from:

$$M_T(f) = M_R(f)\frac{H_T(f)}{H_R(f)} \tag{6.5}$$

where $H_T(f)$ and $H_R(f)$ are the measured voltage responses of the test and reference hydrophones, respectively. The reference hydrophone was a calibrated bilaminar membrane hydrophone, which was calibrated at the National Physical Laboratory, UK.

A number of ultrasonic transducers were used to cover the range between 200 kHz to 6 MHz. Hence, for each calibration the response of the 'unknown' hydrophone to each transmitter across a range of frequencies was compared to the response measured similarly on the standard hydrophone at the same distance in the field. In this way a complete spectral response of absolute sensitivity could be constructed by piecing together the measured responses from different transducers.

An example of the measured sensitivity response of the H_1 hydrophone is shown in Figure 6.17. It can be seen that this hydrophone exhibits a reasonably flat response across the operational frequency range of 0 - 5 MHz (the -3dB point measured was at 5.9 MHz). In the overall profile it is possible to notice the single measured response characteristic from each transducer. The broad characteristic means that any second harmonic response from chemical particles when subjected to insonification could be measured from the transducer range available.

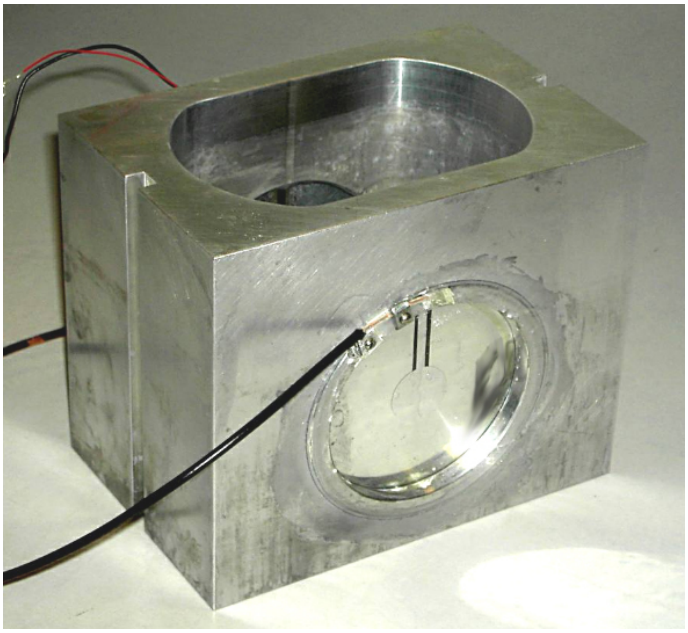

Figure 6.16: Mixing chamber with prototype hydrophones fitted.

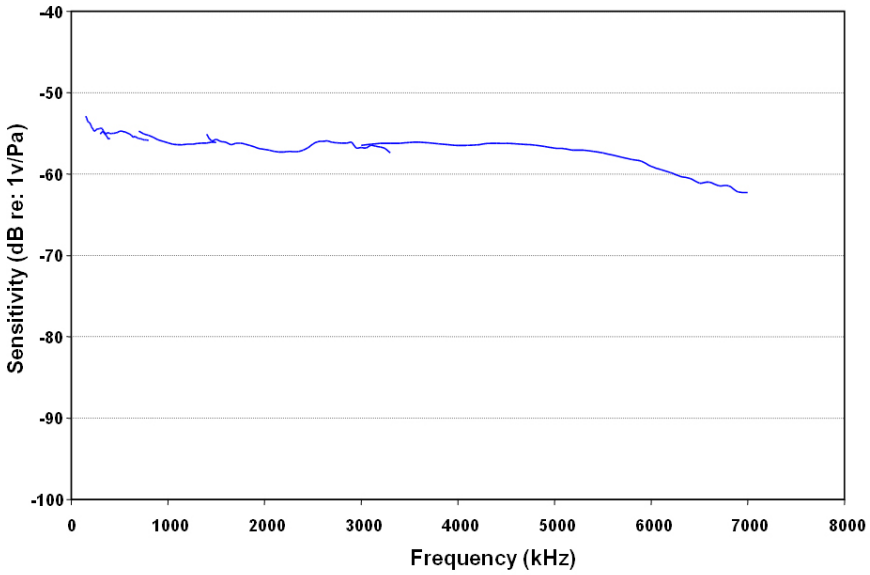

Figure 6.17: Hydrophone sensitivity response

6.8.3 Transducers

Immersion proof resonant transducers (Panametrics [152] and Alba [91]) were employed to cover a wide spectrum of frequencies. Each piezoelectric transducer was characterised by analyzing the impulse response derived from both pitch-catch and pulse-echo tests. The relevant data obtained are summarised in Table 6.2. *fc* corresponds to the central frequency of the device, and BW (at -3 dB) and Q the bandwidth and quality factor (Q=*fc*/BW) respectively.

Table 6.2: Characterisation of the resonant transducers

Transducer	fc (MHz)	Diameter (inch)	BW (MHz)	Q
Alba 250 kHz	0.271	3	0.043	6.30
Alba 500 kHz	0.525	2	0.137	3.83
Alba 2 MHz	2.2705	1	0.57	3.99
Panametrics 1 MHz	0.9522	1.5	0.31	3.08
Panametrics 2.25 MHz	2.1484	1	0.61	3.50

Transducer excitation

The three most common methods of exciting ultrasound transducers are *voltage spike, tone burst and frequency modulated (FM) chirp*. There is not a great difference between the three methods in terms of the overall efficiency of conversion of electrical to acoustic energy [47]. The *spike* method produces a broadband output, causing the transducer to vibrate at all possible frequencies and modes. The *spike* signal should be used in the case of highly damped transducers where a short pulse is required. The *tone burst and the FM chirp* techniques give much greater control over transducer excitation, since every aspect of the output of the equipment such as the signal generator, can be computer controlled. The *chirp frequency modulation* signal

employs sinusoidal waveforms whose instantaneous frequency increases or decreases linearly over time. The resonant frequency of the transducers can be matched by selecting the appropriate frequency of the *FM chirp*, hence an efficient conversion of electrical to acoustic energy can be achieved [47].

6.8.4 Analysis of non-linearities

Since the experimental programme involves evaluating the generation of non-linear responses from chemical particles suspended in a fluid, it was important to quantify any unwanted harmonic signals generated by the measurement system. Thus the equipment employed for the new prototype tank was examined and characterised.

It is known that pressure waves propagating in a fluid medium subject the medium to local changes in density due to the compressibility of the fluid (see Section 2.4.4). The density changes in turn produce local changes in acoustic velocity and introduce non-linear propagation [133][137]. This effect is more noticeable at the maxima and minima of the pressure wave and it is more prominent with an increase in peak-to-peak pressure [134]. It follows that small changes in velocity will be more significant at higher excitation levels.

System non-linearities

Sources of non-linearity were considered to be: the function generator providing the excitation waveforms; power amplifiers providing appropriate excitation levels; and non-linear propagation in the water load medium. The non-linear effects of the candidate equipment were quantified. Measurements were made using an HP 8590L spectrum analyser to establish the magnitude of the second and third harmonic content relative to the amplitude of the

fundamental signal at a range of frequencies from 200 kHz to 6 MHz.

For the arbitrary function generator at voltages of 100 mV_{pp}, 1 V_{pp} and 10 V_{pp}, the signal level of the 2^{nd} and 3^{rd} harmonics were at least 40 dB lower than the amplitude of the fundamental across the whole spectrum.

On connection of the power amplifier (Kalmus 155LCR), the level of harmonic content increased approximately by 15 dB and 13 dB for the 2^{nd} and 3^{rd} harmonics, respectively (over the range 100 kHz to several MHz).

It is often assumed that the propagation of ultrasound is a linear process i.e. that the travelling wave has constant velocity and so retains its shape as it travels through the load medium. This is valid under the assumption of the propagating signal harmonics have infinitesimal amplitudes. However, when input waveforms of higher amplitudes are used, is possible to generate sufficient pressure in a liquid medium to complicate linear models. When higher pressures are achieved, non-linear effects will become evident and the profile of the wave will be subject to distortions [133].

The compressional phase of the wave will cause an increase in the local density of the medium through which it travels, and given that the velocity of sound is dependent on the momentary value of density, points in the wave of greater amplitude will travel faster than those of lesser amplitude [134]. For example, time domain waveforms in Figure 6.18 (a) and (b), compare the received hydrophone signals for two excitation values at 2.25 MHz. Distortions of the waveform can be seen when the excitation voltage is increased from 20 V_{pp} to 200 V_{pp}. Thus, the positive cycle of an originally sinusoidal plane wave becomes increasingly 'steeper' over the course of its propagation.

Interesting, Fukukita used the distortion of the modulated waveforms due to their propagation in a liquid for obtaining depth distribution of the non-linearity parameter B/A and frequency dependent attenuation coefficient [134]. Due to this distortion of the wavefront in the time domain, the frequency spectrum of the wave will, as a consequence, also be altered as it can be seen from Figures 6.19 (a) and (b) that the 2^{nd} harmonic content relative to the fundamental increases from -65 dB to -30 dB by increasing the excitation voltage from 20 V_{pp} to 200 V_{pp} respectively.

The non-linear propagation effect was measured for frequencies from 250 kHz to 2.25 MHz and for excitation levels between 20 V_{pp} and 200 V_{pp}. Extracting the relevant values from the results in the frequency domain demonstrated the relationship between the relative amplitude of the 2^{nd} harmonic to the fundamental against excitation voltage at different frequencies as shown in Figure 6.20.

Spectral components, or harmonics, at integer multiples of the original frequency will become apparent in the Fourier transform of the temporal information. Finally, this steepening process leads to the formation of pressure discontinuities, known as shock fronts, which manifest themselves as vertical tangents in the waveform, i.e. the waveform transforms into a sawtooth profile, shown in Figure 6.18. It is clear that the 2^{nd} harmonic content increases with excitation voltage and with frequency.

Some materials may require excitation levels above a threshold value to generate backscatter [60] so non-linear propagation imposes serious restrictions on the experimental process; this may limit application to some materials. As can be seen from the analysis of sources of harmonic generation from the equipment and non-linear wave propagation, there will always be

some unwanted harmonic content intrinsic to the system and in the propagation of the wave across the medium load. However, as the harmonic content of the system has all been quantified, it can be subtracted from experimental measurements if necessary.

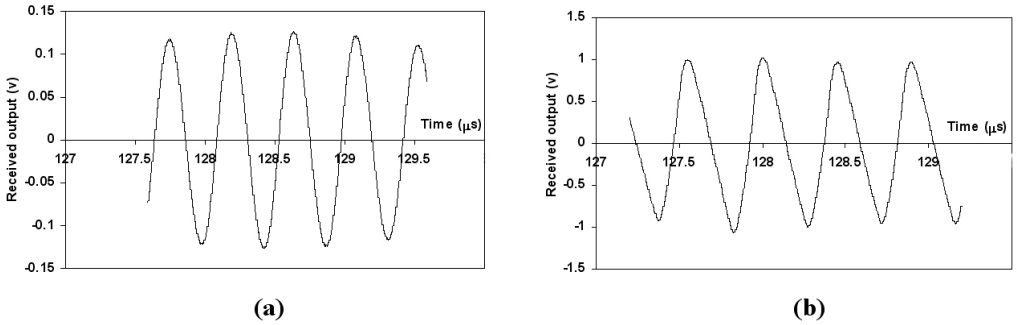

(a) **(b)**

Figure 6.18: Received time domain waveforms for 2.25 MHz excitation at (a) 20 V_{pp} and (b) 200 V_{pp} input.

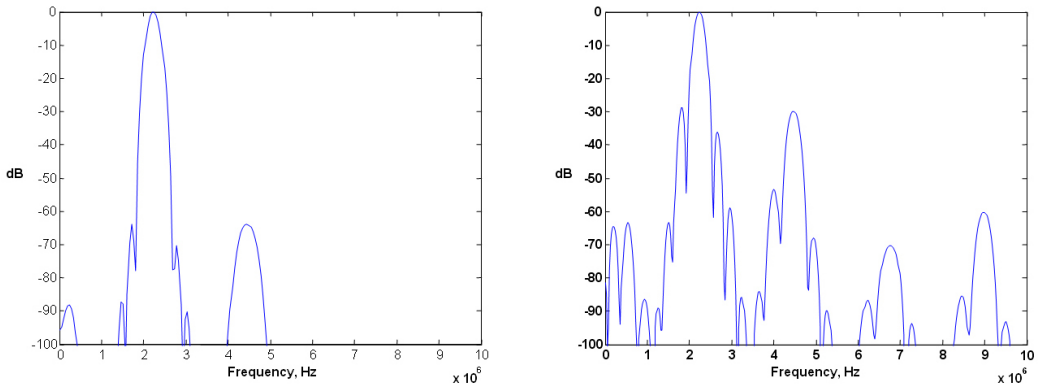

(a) **(b)**

Figure 6.19: Received frequency domain waveforms for 2.25 MHz excitation at (a) 20 V_{pp} and (b) 200 V_{pp} input.

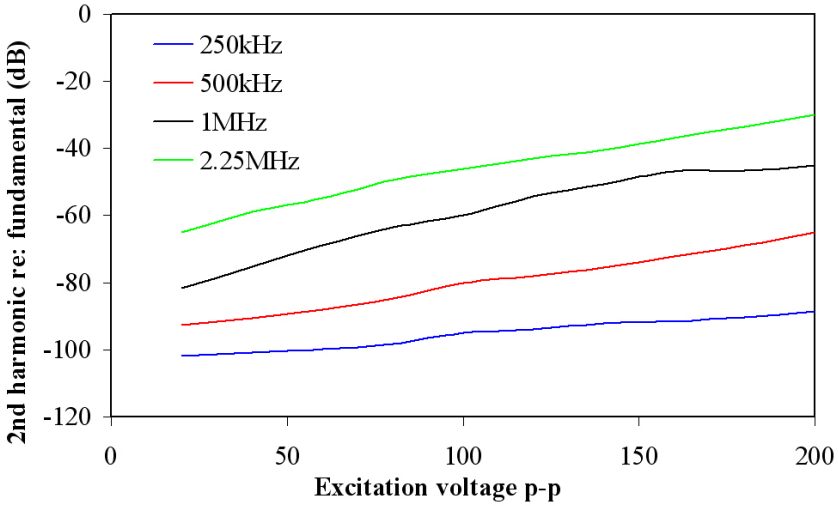

Figure 6.20: Relationship between 2^{nd} harmonic and fundamental for a range of excitation voltages and different frequencies.

6.9 Active acoustic experiments: linear response of particulate in water

6.9.1 Linear measurements of group velocity and attenuation technique

Measurements of velocity and attenuation for different concentrations of Avicel in water were undertaken using the new experimental arrangement described in Section 6.8

The sample to be analysed was a heterogeneous mixture made by adding different concentrations of cellulose particles to a fixed volume of distilled water. Acquisition of the signal on H_1 and H_2 enabled determination of velocity and attenuation information, as described in Section 2.3.1.

Measurements of the group velocity for each concentration were obtained by determining the time shifts associated with the maximum correlation of the time domain traces that correspond to precisely known differences in axial position.

The time values required for group velocity calculations were extracted using the cross-correlation technique, a typical DSP technique for estimating the time delay between two signals. The cross-correlation function provides a measure of the extent to which two signals correlate with each other as a function of the time displacement between them [95]. If the signals are identical, the cross correlation will be one, and if they are different, the cross correlation will be zero. Hence, cross-correlating the windowed signal waveform at H_1 with the signal detected at hydrophone H_2 enables determination of the time of flight between the two hydrophones for different mixtures. The

sample path-length D between the two hydrophones, corresponding to 87.3 mm $\pm$ 0.1 mm, was determined by measuring the time-of-flight through distilled water (v_{water} = 1496 m/s at 3 MHz and 25 $^{\circ}C$ [37]):

$$D = v_{water} t_{water} \tag{6.6}$$

The reasonable accuracy of 0.1 mm was calculated as a worst case analysis taking into account the possible sources of inaccuracies such as the temperature measurement, the zero crossing of the waveform and the transducer misalignment.

The attenuation coefficient α_2 was calculated by comparing the reduction in the amplitude of a signal that has traveled through a material whose attenuation coefficient was known, in this case distilled water, (α_{lit} = 0.193 Np/m at 3 MHz and 25 $^{\circ}C$) [153]:

$$\alpha_2 = \alpha_1 + \frac{1}{D} ln(\frac{A_R}{A_S}) \tag{6.7}$$

where the subscripts R and S refer to the signal amplitudes of the reference material and the sample, respectively [65]. Sixteen signals were averaged, hence accurate arrival time information and true amplitude values were obtained for the velocity and attenuation computations. Again Matlab scripts automated the acquisition of the measurements.

6.9.2 Linear measurements of group velocity and attenuation experiments

Quantities of PH-200 Avicel particles (average size of 180 μm diameter) were added to 850 mL of distilled water in the mixing chamber. All the measurements were performed at a measured temperature of 25 $^{\circ}C \pm 1\ ^{\circ}C$. Before conducting any experiments the mixture was stirred for 20 mins. Sixteen repeat measurements were averaged. The time and amplitude values required for calculation of velocity and attenuation were extracted using the cross-correlation technique. The relative standard deviation of these replicates was less than 0.2% indicating good reproducibility.

The experimental results are reported at the top of Figure 6.21. The plots clearly show that there is an increase in velocity with concentration. In particular, the velocity of the sample of water was equal to 1490 m/s and it is in agreement, with a modest discrepancy of 0.4%, with values in the literature (1496 m/s at 1 MHz and 25 $^{\circ}C$ [37][154]). In this case the Avicel particles were insonified by a 10 cycles of tone-burst at 3 MHz.

The effects of particle concentration on velocity were measured at a range of volume fraction ϕ from 0% to 6%. From the plots in Figure 6.21 (bottom), it emerges that the experimental results are in contrast with the Urick's theory. The data show an increase in acoustic velocity with increasing particle concentration (or volume fraction), while Urick's theory shows a decrease in acoustic velocity with increasing volume fraction up to 20% (see Figure 2.3).

This difference can be attributed to scattering effects. When the particle size is smaller than the wavelength of the signal (LWR), a simple phenomenological approach by Urick may be successfully applied [61]. However,

in this case, the ratio between the particle's radius (r = 90 μm) and the signal wavelength (λ = 500 μm) was 0.18. Consequently the plots are in the region of the intermediate wavelength regime IWR ($0.1 < r/\lambda < 50$) and another approach has to be considered. Improvements of Urick's theory have been proposed by Ament [155] and found to be useful in explaining the observed behavior of acoustic velocity by other investigators [16][156]. The improvements have been achieved by considering the effects of fluid viscosity and particle size in the effective density expression (Equation 2.4) and thus taking into account the heterogeneous nature of the medium.

The variation of velocity with particle concentration can be correlated using a modified form of Urick's equation as proposed by Pinfield et al [157]; their approach demonstrated accurate velocity measurements of the acoustic wave in the IWR regime [20].

Stolojanu and Prakash [16] also found that the acoustic speed increased with increasing concentration for water-glass beads slurries with a similar ratio to that used in the present study ($\frac{\lambda}{r} = 0.2$ insonified by a 3 MHz tone bursts).

Attenuation measurements were also estimated from the acquired data. The attenuation coefficient was computed according to Equation 6.7. Figure 6.21 presents attenuation coefficients obtained with increasing concentration of particles with an average size of 180 μm. The measured attenuation, for distilled water only, is $\alpha_{exp} = 0.175$ Np/m and it is close to the value reported in the literature ($\alpha_{lit} = 0.193$ Np/m at 3 MHz and 25 $^{\circ}C$) [153]. Importantly, it can be observed that attenuation increases with increasing concentration. The attenuation coefficient varies between 0.175 Np/m and 1.0 Np/m and is linearly dependent on the particle concentration. This behavior is attri-

butable to different loss mechanisms [8]. It has been reported that losses due to thermal conduction and viscous drag effects have a similar influence compared to multiple scattering effects when the particles are comparable to the signal wavelength as in this study [158].

Attenuation of ultrasonic signals in solid-liquid mixtures have been studied by many researchers [16][159][157][158]. Attenuation of an acoustic wave passing through a medium provides additional information about the composition of a mixture [44]. It was found that an increase in attenuation was almost monotonic up to a solid volume fraction of 20% and that attenuation is more prominent when the particle size becomes the same order of magnitude as the signal wavelength. In particular, the plot in Figure 6.21 agrees with the measurements of suspensions of glass-beads in water obtained by Stolojanu [16] and measurements of alumina powder in water measured by Guidarelli et al [158], where the overall attenuation coefficient was found to be proportional to the number of particles in the mixture.

In general, velocity and attenuation measurements provide a means of obtaining particle concentrations for a suspension of known particle size and could be employed to calculate the particle size distribution of a colloidal dispersion. The particle size distribution is then determined by finding the droplet size distribution that gives the best fit between the predictions of the ultrasonic scattering theory and the experimental ultrasonic spectra [60][46].

In the literature, there are two ways to solving this problem: model-independent inversion and model-dependent inversion. In the model-dependent inversion method it is assumed that the particle size distribution follows some common form which can simply be modeled mathematically, typically a log-normal distribution [59]

The droplet size distribution can then be characterised by only two parameters: the geometric mean and the standard deviation. The geometric mean and standard deviation which give the best agreement between the measured and predicted ultrasonic spectra are found by a least squares analysis [59]. Most commercial ultrasonic instruments assume that the particle size distribution follows either a monomodal or bimodal log-normal distribution [55]. In the model-independent analysis no a priori assumption is made about the form of the particle size distribution. Although this method is scientifically more satisfactory, because many suspensions do not have particle size distributions which can be described by simple mathematical expressions, it is extremely time-consuming to compute.

The experimental work using the through transmission technique reported here, is comparable to experimental findings in literature. However, the purpose of the work was to test and validate the second active acoustic system.

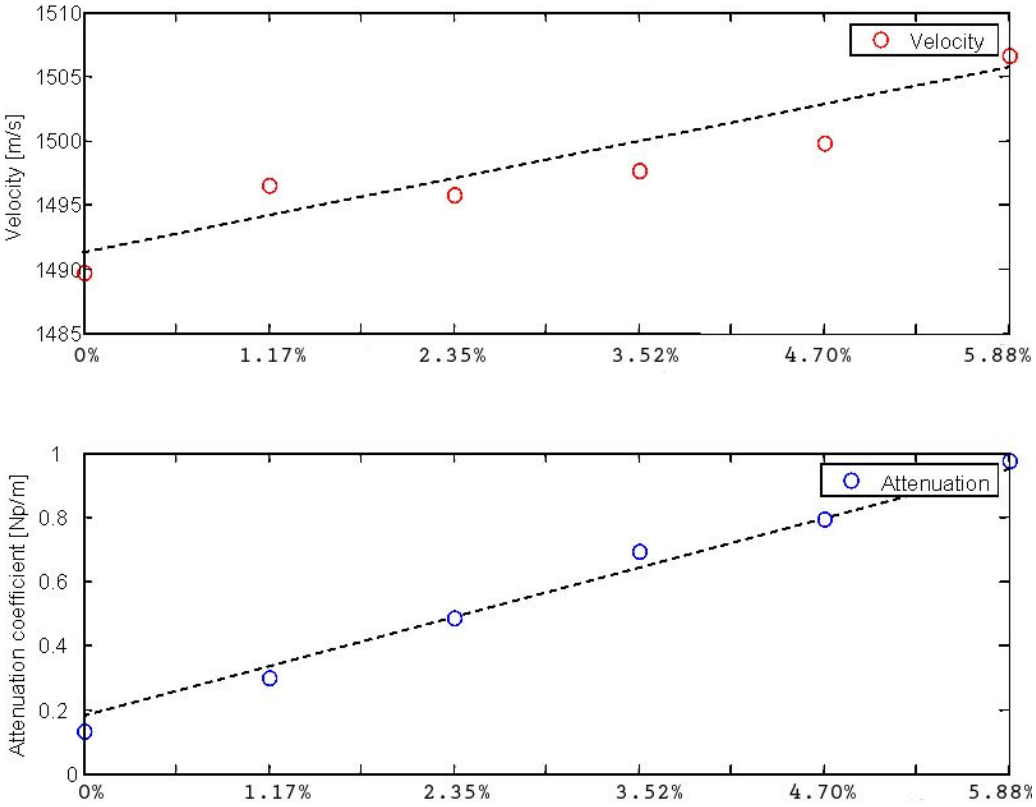

Figure 6.21: Velocity versus concentration and attenuation versus concentration measurements

6.10 Wetting phenomenon

When the cellulose particles were introduced inside the mixing chamber for analysis, severe attenuation of the through transmission signals was noticed. A series of experiments were performed to investigate this effect.

A fixed amount of 10 g of PH-102 Avicel particles was added sequentially to the same volume of distilled water (850 mL) every 15 mins. The amplitude of the through transmission signals (using a 10 cycles, 10 V_{pp} amplitude tone burst at 250 kHz) between the two hydrophones was measured at 30 s intervals. The signal acquired is shown in Figure 6.22.

The Avicel particles were added after 60 s, and hence the first two points on the plot record the stable state before addition. Immediately after the addition of the particles, the signal amplitude fell to a level less than 15 mV and was then seen to gradually increase with time. Importantly, the steady state was reached after about 15 mins for all the masses considered. Its final value was less than the start value; the final value represented the start value for the next addition, which provided a measure of the attenuation associated with wetting of the particles.

In fact, this phenomenon can be explained as wetting. Wetting is the ability of a liquid to maintain contact with a solid surface, resulting from intermolecular interactions when the two are brought together. The degree of wetting (wettability) is determined by a force balance between adhesive and cohesive forces. Adhesive forces between a liquid and solid cause a liquid drop to spread across the surface. Cohesive forces within the liquid cause the drop to ball up and avoid contact with the surface [71].

When the liquid has a high surface tension (strong cohesive internal

bonds), such as water (72.8 dyne/cm compared to 22.3 dyne/cm for ethyl alcohol [160]), it will not spread out over a great area of a solid surface such as the Avicel particles's surface.

Importantly, the wetting process was also hindered by the effects of air bubbles inside the mixture. When microcrystalline cellulose particles were initially mixed with water, air micro-bubbles were embedded in the surface structure of the particles. Air bubbles distributed in the pores of the cellulose particles, are the strongest scatterers in this system, due to the high impedance difference between air and the wetting liquid [65]. For this reason, air-bubbles have a profound impact on acoustic propagation since they cause severe attenuation of the through-transmission signals.

It should be possible to remove most of the the unwanted air bubbles by mechanical stirring or insonification using ultrasound. Povey [47] affirms that stirring the mixture removes the major part of air bubbles from the particle surface and minimises the interfacial energy between the cellulose particle surface and water. Stirring of the solution should be carried out until the particles are thoroughly wetted. A study [161], which demonstrated that high power ultrasound promotes penetration of liquids into porous materials, provides further corroboration of this. The research investigated the influence of high-power ultrasound at 40 kHz on wetting processes of paper. Wetting was monitored by measurement of the attenuation of ultrasound at 0.5-9 MHz which was transmitted through the immersed sample. It was possible to force an absorption process into the stationary state faster than by spontaneous wetting through use of high-power ultrasound.

The experiments on Avicel particles demonstrated that the mechanical stirring decreases the air-bubbles from the particles surface and enhances the

wetting process. This technique should be carried out until a stable state is reached [47].

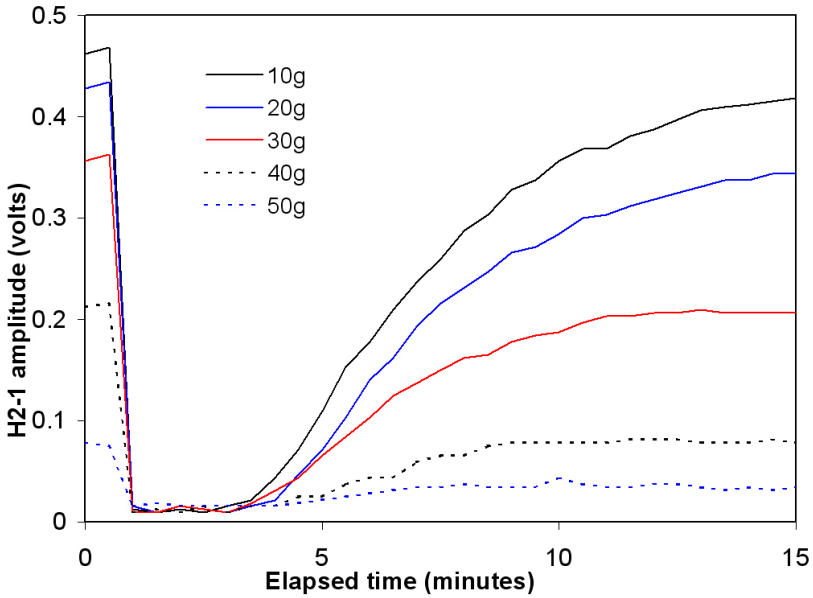

Figure 6.22: Wetting phenomenon: signal amplitude on H_2 versus elapsed time

6.11 Non-linear response from ultrasonic contrast agent in water

Once the design, manufacturing and the full characterisation of the new active tank was completed (Section 6.8), active acoustic measurements were performed using various concentrations of UCA in 850 mL of distilled water. These tests aimed to verify that the system is capable of extracting harmonic information from backscattered data.

The heterogeneous mixture was contained inside the mixing chamber of the new test cell, described in Section 6.8, and it was stirred at 250 rpm and at temperature of 25 $^{\circ}C$. The ultrasound contrast agent information employed for these experiments is reported in the previous Section 6.3.1.

Figure 6.23 shows a typical frequency response of SonoVue contrast agent detected on hydrophone H_1. These signals were acquired for a mixture of 25 mg of SonoVue (diameter 10 μm) in 850 mL of water. The micro-bubbles were excited by a Panametrics transducer using a 10 cycles tone-burst signal with an amplitude of 6 V_{pp} and a frequency of 2.4 MHz. The voltage versus frequency plot was determined by using the Fast Fourier Transform (FFT) Matlab script of the backscattered acoustic signal detected on H_1.

A noticeable response from 3.9 to 5.3 MHz with peak at 4.8 MHz can be discerned from the plots in Figure 6.23 when micro-spheres were added to the system. The Figure also show that some of the fundamental frequency components are attenuated and others are enhanced when the micro-bubbles are present in the mixture. The amplitude of the response of the 2^{nd} harmonic is circa 30 dB lower compared to the fundamental.

Similar outcomes using the chirps centered at 2 MHz and extracting the

fundamental and the second harmonic components using the pulse compression technique. In this study the second harmonic was circa lower 18 dB compared to the fundamental [145].

Other experiments were carried out using chirp waveforms (start frequency 1.75 MHz, end frequency 2.75 MHz, time duration 20 μs).

This time the pulse compression technique was applied to extract the relevant 2^{nd} harmonic signals from the backscattered data. This involve the cross-correlation of the backscattered signal on H_1 with each of the transmitted signal (chirp). Again a tailored Matlab scripts written by the author were used for the post-processing of the data.

The plot in Figure 6.24 shows the 2^{nd} harmonic response extracted from 25 mg of contrast agent at different excitation levels. It can be clearly seen that some of the 2^{nd} harmonic activity is present at low excitation levels but a dramatic increase occurs at 4 V_{pp} and this in turn is doubled at 6 V_{pp}. Hence, the 4 V_{pp} excitation level was sufficient to stimulate harmonic scattering but also low enough, when combined with a low number of repetitions, to avoid promoting the onset of rupture of the micro-spheres.

The results from micro-bubble suspensions indicate that multiple scattering effects may be observed if they are insonified with a sufficient excitation level. These outcomes demonstrates the capabilities of the active acoustic system to detect the 2^{nd} harmonic signal from gas filled contrast agent. Moreover, the pulse compression technique utilised herein shows the feasibility of extracting the 2^{nd} harmonic signals from the backscattered data of micro-bubbles.

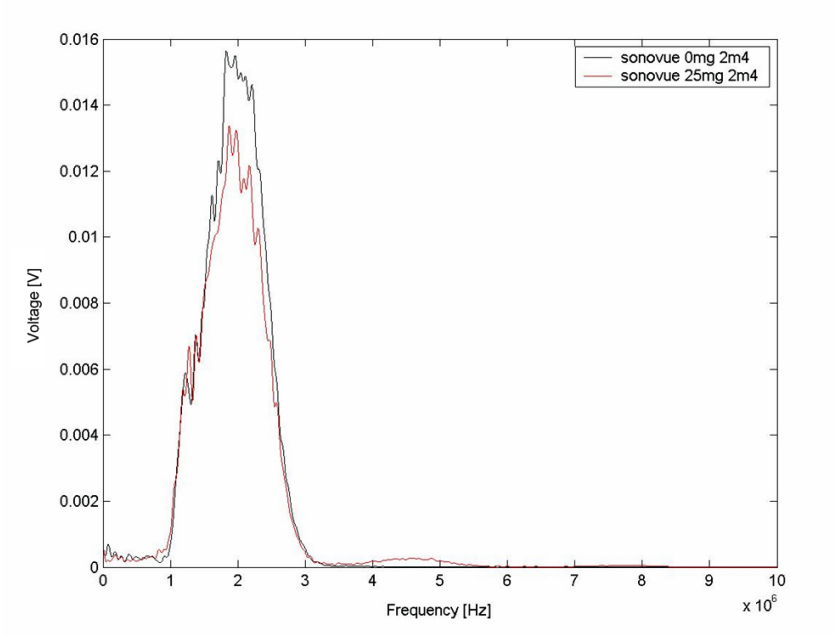

Figure 6.23: Comparison of the frequency responses from contrast agent in water and water alone.

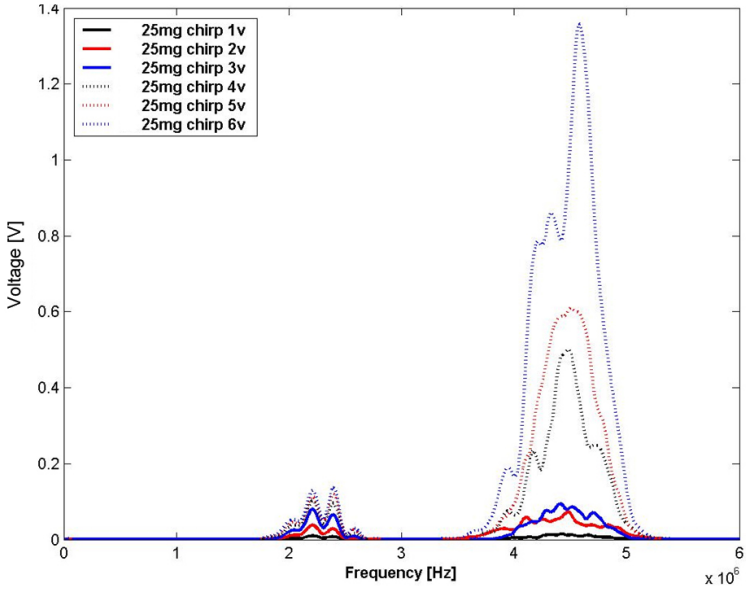

Figure 6.24: 2^{nd} harmonic response of contrast agent in water, extracted using pulse compression technique, for a range of excitation amplitudes.

6.12 Backscatter at the second harmonic from particulate in water

The preliminary active acoustic measurements of the non-linear response of Avicel particles in water were repeated with the new test cell arrangement. PH-200 particles with an average size of 180 μm were added to 850 mL of distilled water in the mixing chamber at ambient temperature. At each addition, the heterogeneous mixture was stirred for 15 minutes. Again, backscattered signals were automatically extracted from windowed portions of time domain data by Matlab algorithms during the acquisition process, while the matching filtering technique was applied to the signals to obtain the second harmonic component. Sixteen signals were captured for each concentration and excitation frequencies between 200 kHz and 3 MHz were employed via the range of the transducers available. Moreover, the extracted 2^{nd} harmonic data were summed up in the frequency domain to enhance the SNR. SavitzkyGolay smoothing filter [162] was also applied to the spectra. The main advantage of this approach is that it tends to preserve features of the distribution such as relative maxima, minima and width, which are usually 'flattened' by other adjacent averaging techniques (like moving averages, for example) [163].

Typical second harmonic spectra are shown in Figures 6.25 and 6.26. These were obtained for PH-200 particles with an average size of 180 μm and masses in the range 0-8 g and 0-50 g mixed in 850 mL of water. These were insonified by a 10 cycles tone-burst with an amplitude of 10 V_{pp} and a frequency of 200 kHz. The second harmonic signal is centered at 400 kHz and has 37% bandwidth. Although some differences in amplitude can be

observed there is no trend visible with concentration. Similar results were obtained at frequencies between 200 kHz and 3 MHz and utilising different particle sizes (PH-101 PH-102 PH-105 PH-200).

These results were disappointing. Obviously, the geometry and material composition differed greatly between the ultrasonic contrast agents (UCA) and Avicel particles. With the experimental procedure validated using the UCA approach, as described in Section 6.11, it may be deduced that the solid Avicel particles did not produce a sufficient non-linear response. The original optimism when the second harmonic signals were detected could be explained as the response from air bubbles trapped in the mixture. This is supported by the fact that the second harmonic content is present even at zero concentration levels. Even when the cellulose particles were mechanical stirred for 15 minutes to remove the air-bubbles from the particle 's surface, i.e. enhancing of the wetting process, it appears that these operations did not provide a satisfactory degassing of the samples under evaluation.

In this work the active system demonstrated the ability of extracting the 2^{nd} harmonic content from the backscatter data of contrast agent, it is known, however, that the effectiveness of micro-bubbles is due to the fact that they are strong backscatterers of ultrasound, much stronger than the Avicel particles. The drop in density on the interface between the gas in the bubble and the surrounding liquid strongly scatters and reflects the ultrasound back to the hydrophone. Hence, it is hypothesized that the second harmonic content is generated by the scattering signals from residual air bubbles distributed in the pores of the Avicel particles. Furthermore, these may have obscured the weak backscatter signal(s) produced by the Avicel particulates.

Moreover, another possible cause of the generation of the second harmonic

signals is non-linear propagation of sound through water. Therefore, as the wave propagates through the media, different parts of the wave experience different instantaneous speeds of sound due to the varying pressure, and consequently varying density, across the wave. The wave gets distorted, as the crest of the wave advances faster than the trough. Here, it can be seen that the ratio B/A is a measure of the non-linearity of the medium (See 6.2 and experimental characterisation of the system, where non-linearities were found in Section 6.8.4).

As mentioned before this pilot study was inspired by ultrasonic imaging in biomedicine which employs UCA. In the literature the non-linear response from the backscatter data was only extracted from microbubbles in liquid and (as far that the author is aware) there are not equivalent experiments using the backscatter data using the pulse-echo technique from particles to compare the results with.

Interesting, Ootaky et al, [131] employed the finite amplitude method to figure out the B/A parameter from particulates in silicone oil in terms of the relationship between particle diameter and ultrasonic wavelength using the through transmission mode. The particles employed for their study were Polymethyl methacrylate, Polystyrene and Ion-exchange resin. Samples were dispersed in silicone oil at 0.6 wt%. Busts at 1 MHz and 4 MHz signals were applied to the narrow band PZT transducer while the ultrasonic receiver was positioned at a fixed distance of 50 mm from the transmitter. The particle diameter ranged between 0.1 μm to 2130 μm.

The outcomes of this research are that: as expected, the acoustic non-linearity was enhanced when the particle diameter was comparable to half wavelength ($\frac{2r}{\lambda} = \frac{1}{2}$), while the non-linearity was reduced when the diameter

was comparable to the wavelength ($\frac{2r}{\lambda} = 1$). Since the sound waves are remarkably scattered when ($\frac{2r}{\lambda} = 1$), it is plausible that the decrease in the ultrasonic waves amplitude is due to the scattering of the waves. Ootaky et al suggest that the finite amplitude method could be employed successfully for the development of a new technique for particle characterisation [131].

It is evident that further work is needed for characterising the Avicel particulate. Hence, it is suggested to repeat the Ootaky's experimental work by employing the cell tank in through transmission mode. This is another way to assess a relationship between the concentration of Avicel particles and their second harmonic response. A proper degassing procedure is necessary prior to taking ultrasonic measurements. Degassing the sample and making measurements where the particles do not scatter significantly are strategies for overcoming the problems found on the backscattering experiments but effective methods to remove completely the air bubbles are still need to be developed [15].

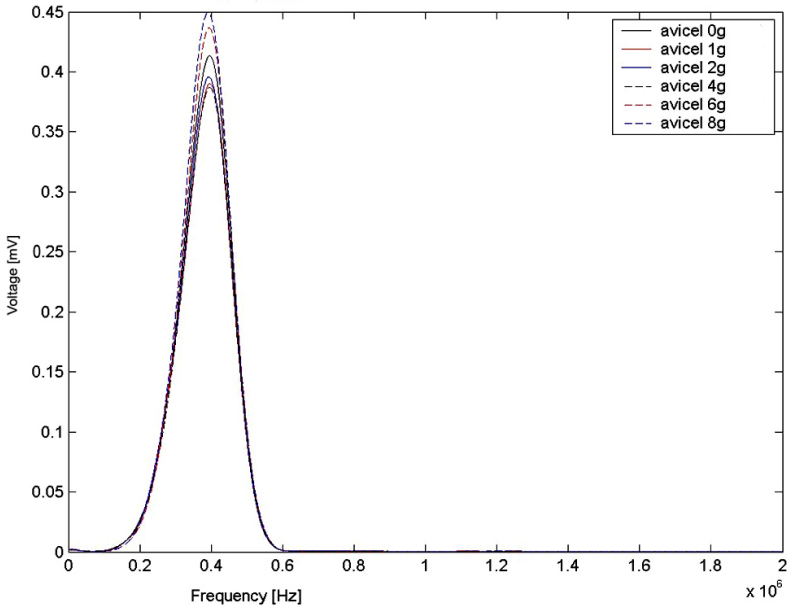

Figure 6.25: Second harmonic signal in the frequency domain of 0-8 g of Avicel in water (excitation frequency of 200 kHz)

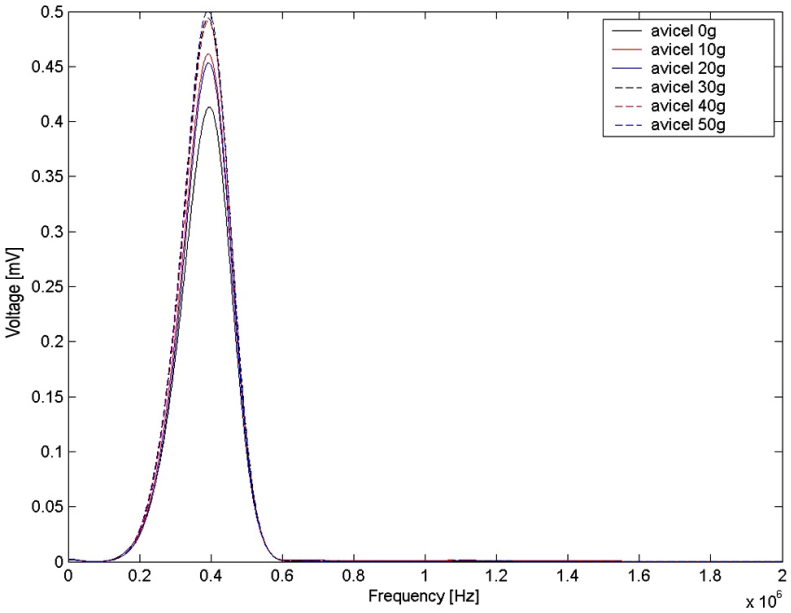

Figure 6.26: Second harmonic signal in the frequency domain of 0-50 g of Avicel in water (excitation frequency of 200 kHz)

6.13 Conclusions

This Chapter has presented exploratory investigations of linear and non-linear responses from chemical particles in water in an active ultrasonic system.

Linear measurements of velocity and attenuation for a range of concentrations have confirmed the operation of the new test cell in the linear regime and strengthened experimental findings of the literature regarding the effect of scattering in the IWR. Interestingly, the wetting phenomenon of Avicel particulates is also identified and used to define the experimental procedures utilised in this work.

The experimental work for investigating the non-linear response in backscattered data from the ultrasonic contrast agent is encouraging. The experiments demonstrate the capabilities of the active acoustic system devised to detect the 2^{nd} harmonic signal from micro-bubble suspensions. Moreover, the pulse compression technique utilised herein shows the feasibility of extracting the 2^{nd} harmonic signals from their backscattered data.

Further work is needed to extract the ultrasonic backscatter data from the Avicel particulates. The tests on the Avicel particles were unable to illustrate a clear correlation between the backscattered data and particle concentration where residual air bubbles trapped inside the the pores of the particles may have masked the weak backscatter signal(s) produced by the Avicel particulates.

The active acoustic experimental work has completed the full range of acoustic techniques examined in the Thesis. All results illustrated that the system is capable of detecting both linear and non-linear responses.

Chapter 7

Conclusions

In today's world, great expectations are placed upon the technology to deliver improved performance at a reduced cost and capable of being subjected more difficult operating conditions. No longer can any technology in the field of process monitoring be expected to last ten or twenty years unchanged, and any industry must remain at the leading edge of technology to remain competitive.

The ability to determine the size and concentration of particles in concentrated heterogeneous and optically opaque mixtures without the need of any form of sample preparation is extremely challenging and important in many applications. One of the areas where acoustic techniques are most likely to be employed is for the on-line characterisation of suspensions during processing [15]. Major improvements in the manufacture of many colloid-based materials such as petrochemicals, pharmaceuticals, food and cosmetics could be achieved using ultrasonic monitoring techniques.

This Thesis has presented both novel passive and active acoustic approaches to determine particle size or concentration information of chemical

particulate suspensions in fluids.

A simulation model of a reactor vessel has been developed using FEM and subsequently ultrasonic transducers have been manufactured to match the desired response characteristics from the outcomes of the FE simulations.

Finite element analysis can offer the opportunity to model almost any vessel reactor, in both time and frequency domains. By predicting the attenuation and the frequency range of the process under consideration it is feasible to design customised ultrasonic transducers able to monitor the desired physical changes.

This idea could be extended to any chemical process and it represents an innovative approach for applications in process analysis. Designing a robust acoustic sensor provides the basis for the development of instrumentation for on-line monitoring and control of particulate processes.

Exploratory investigations employing a range of active acoustic techniques have also been carried out. These have evaluated the generation of linear and non-linear responses from stable particulates suspended in water. A test cell has been fabricated for this purpose. Measurements of velocity and attenuation have confirmed the correct operation of the test cell in the linear regime. Second harmonic responses generated from the non-linear interaction of ultrasound with particulates have been detected. These have been related directly to the presence of the suspended particles. In conclusion, both the passive and the active acoustic approaches presented in this Thesis offer potential solutions for in situ and real-time process monitoring. The major contributions of this Thesis are listed below.

7.1 Main findings of this thesis

- A jacketed reactor vessel has been modelled using the FE method. The excitation functions representing the chemical particles impacting to the inner wall of the vessel have been derived from Hertz's theory.

- The model has been experimentally validated. Excellent correlation has been achieved between experimental and FEM predictions.

- The FE model supports the experimental results obtained by Nordon et al [56]. The FE simulations predicted: an increase in energy with an increase in either particle size or concentration; a decrease in the frequency of AE with increasing particle size. All the predictions have shown consistency with other published theoretical and experimental studies. Importantly, the FE modelling has led to a better understanding of the frequency range required for a passive acoustic system. The study has also provided the basis of design specifications for broadband and narrow-band passive monitoring transducer configurations.

- The ultrasonic transducer arrangement evaluated for use in a passive monitoring system comprised both broadband and narrow-band configurations. The concept is to use complementary properties to enhance the effectiveness of the passive monitoring approach. FEM has been used in the design of both devices, with 1-3 connectivity piezoelectric ceramic configurations adopted for both designs. The broadband transducer is designed to operate off-resonance and provide information on the frequency content across the frequency range of interest (0-180 kHz). Whereas, the narrow-band resonant device is designed to provide enhanced sensitivity at lower frequencies (0-60 kHz).

- A complete passive acoustic system comprising the chemical reactor, a low noise pre-amplifier and two customised ultrasonic sensors with complementary features have been developed and manufactured.

- A customised low noise pre-amplifier has been designed, simulated, manufactured and tested. The pre-amplifier, embedded into the case of the ultrasonic sensor, has resulted in improved SNR characteristics compared to the commercial pre-amplifier employed in the experimental work.

- Investigation of the effects of particle size have been presented. Benefits of employing a broadband off-resonance transducer for estimating the mean size of particles in a liquid have been shown. The mean size and the concentration of the particles have been discriminated by analysing the magnitude and frequency content of the AEs spectra. The peculiar characteristic of magnitude changes towards lower frequencies, corresponding to an increase in particle size, could be exploited for monitoring high shear granulation [13], crystallization [4], granulation [14] and flow of powders [3].

- The enhanced sensitivity of the stacked transducer together with the low noise performance of the pre-amplifier have improved the detection limit for determination of itaconic acid in toluene. The detection limit values are considerably lower ($9.44x10^{-}3\ \frac{g}{dm^3}$) than those reported in a previous study ($0.1\ \frac{g}{dm^3}$) using a commercially available transducer (Nano 30 - Physical Acoustic [74]).

- The passive acoustic experimental work has also given the opportunity to confirm the modelling outcomes and the findings from the literature.

- A tailored test cell system for active acoustic studies has been developed and characterised. This has been used to investigate the generation of both linear and non-linear responses from stable particulate suspended in water.

- Linear measurements of velocity and attenuation for a range of particle concentrations employing the through-transmission technique in the new test cell have been presented. The results obtained have confirmed the operation of the test cell in the linear regime and strengthened experimental findings.

- The wetting phenomenon of Avicel particulate has been identified as a cause of contamination of the response from AEs. It has been quantified and techniques for reducing it have been suggested.

- Software tools such as the acquisition and analysis of linear and non-linear response using the cross correlation and pulse compression techniques have been implemented. It has been demonstrated that the scripts are capable of performing velocity and attenuation measurements of Avicel particles in water and extracting the 2^{nd} harmonic signals from the backscattered data of ultrasonic contrast agent.

- Finally, while FEM has been shown to be a powerful tool in the modelling of chemical reactors and ultrasonic sensors, Although, further work will be required in the active acoustic work. The passive and active acoustic methods described could inspire a new way of monitoring particulate processes non-invasively.

7.2 Suggestions for future work

There are a number of topics (regarding the passive and active acoustic work) which require further study and hence suggestions for future work are detailed below.

7.2.1 Passive acoustic

Assessment of the limits of the passive acoustic monitoring system

The passive acoustic approach has clearly shown its potentials as an acoustic monitoring technique. Although further work is required to establish whether it has the capability to monitor the properties of any particles in fluids. In particular, changes in frequency distribution of AE could be a useful index for monitoring changes in particle sizes once the further experimental studies have been performed to fully understand the potentials of the approach, as well as any limitations. Further work on smaller sized and lower concentrations of particles would be useful to see if the relationship between size and spectral form are consistent with the measurements obtained here. It is recommended that a comprehensive series of chemical mixtures be developed for all suspensions likely to be used in any pharmaceutical or chemical process. The density, acoustic longitudinal and shear velocities, and damping at a range of frequencies should be obtained for each material and used in the FE model of the reactor vessel. This will allow the reliability of the FE model to be determined, and appropriate steps can be taken to ensure that the modelling is accurate for any mixture.

Increasing the complexity of the FE reactor vessel model

It is clear that a number of experimental factors such as temperature and stir rate can influence the acoustic signal. Therefore, good logging and control of these process parameters is important to interpret changes in AE signals. It is also apparent that AE is not caused purely by the collisions of particles on the inner wall of the reactor vessel [56]. More complex modelling could include the effects of the bell shape of the vessel, the temperature of the oil and the fluid dynamics caused by the stirring of the toluene.

In this study, the corresponding values of particle size (A, B and C) were selected as representative of each gaussian particle distribution (see Table 4.1). In future work, the particle size distribution could be taken into account for the simulation of the excitations corresponding to the particle impacts. It has been suggested that an understanding of the factors that contribute to broadband AE signals should allow identification of emission frequencies that are influential, i.e. include information of interest for various processes. Therefore, measurement systems could be devised that are customised to a process.

Development of theoretical and empirical model for both particle size and concentration extraction

Although information relating to the mean particle size was achieved by extracting the energy from the acquired AE signals, the distribution of particle size could not be deduced from the experiments. Hence, further work is needed to develop theoretical or empirical models that would achieve the extraction of both particle size and particle concentration information. This information could be extracted using attenuation and velocity measurements

employing active acoustic techniques as shown in Section 6.9.2. However, the vast majority of instruments available such as the High Resolution Ultrasonic Spectrometer HR-US 101 [52], for this purpose are for off-line (laboratory) use. Moreover, in many high throughput investigation (eg. polymers, multi-components formulations) the physical nature of the particle material involved prevents acoustic transmission [31]. The passive acoustic monitoring has a number of advantages over the existing techniques. In particular, it is non-invasive, inexpensive and has been shown to be sensitive. Experimental work performed has demonstrated that acoustic emissions can be used successfully to monitor these processes, allowing the changes in the average particle size to be identified. Such a technique has a wide applicability for the monitoring of particulate processes such as blending, milling and granulation.

A single electronic unit for real time commercial applications

If future work is to be conducted in order to ascertain the robustness of the technique, then by combining the piezocomposite transducers together with the low noise pre-amplifier and a DSP board in a single integrated unit, an optimum system for real time monitoring could be constructed. The work reported here used software written in Matlab for off-line data analysis. To obtain particle information in real time, an instrument incorporating the piezocomposite transducer together with the low noise pre-amplifier and a tailored real-time DSP hardware/software system for data acquisition and analysis could be designed for commercial applications. The commercial monitoring system would discriminate particle size and particle concentration from the spectral features of the acquired signals. The system would be based on a system on chip (SoC) approach employing field programmable

gate array (FPGA) and a DSP board embedded into the transducer case. A DSP system would eliminate analogue filters and could improve the SNR. Real time particle analysis would be possible without the need of an external oscilloscope for acquisition, with obvious benefits for the final cost of the commercial monitoring unit.

7.2.2 Active acoustics

Degassing of the sample

The preliminary active acoustic experimental work has highlighted some important areas and limitations in the study of backscattered data that should be investigated further.

The work has shown that the wetting phenomenon attenuates the propagation of the ultrasonic energy inside the sample. The heterogeneous mixture was mechanically stirred for 15 minutes to remove the air-bubbles from the surfaces of the Avicel particles and enhance the wetting process. However, it seems that this operation did not provide a satisfactory degassing of the mixture since a clear correlation between the backscattered data and the particle concentration was not found.

Alternative degassing methods such as vacuum ultrasonic bath and power ultrasound should be further investigated. For example, good degassing outcomes were achieved by Austin and Challis [164]. Two empirical methods for removing the trapped air bubbles from aqueous suspension of kaoline particles were used. The study compared the effects of vacuum ultrasonic bath and ultrasonic agitation by measuring the ultrasonic attenuation and phase velocity dispersion curves of the colloid. An ultrasonic cleaning bath (Model QX Walker Electronics Ltd.) 40 kHz ultrasound at 50 W was employed

for the first sample, while the second sample was exposed to 0.5 Torr for 5 min. It resulted that both methods are equally effective but the ultrasound method is less time consuming.

A degassing procedure is necessary prior to taking ultrasonic measurements in aqueous suspensions as well as many other liquid based colloids. Degassing the sample and making measurements where the particles do not scatter significantly are strategies for overcoming the problems found on the backscattering experiments but effective methods to remove completely the air bubbles are still need to be developed [15].

Backscatter response from cellulose or particles of other materials

Further investigations relative to the relationship between the concentration or size of cellulose particles and the backscatter voltage output are clearly needed, once the samples of Avicel particles in water are fully wetted and degassed. The experimental work should includes: voltage and frequency of the excitation signal versus Avicel particles concentration and size.

The relative large dimentions of the Avicel particles employed impacted the stirring in the medium fluid and their wetting process.

Other particle materials may be used such as wet silica of a known size distribution because most of the acoustic parameters are known. Silica (SiO_2) is a ceramic material that is being used in various industries. It is used as a performance additive, filler or processing aid in several product formulations, such as paints and coatings, plastics, adhesives, or insulation materials. Silica is available in a wide range of forms and is typically used in extremely fine particle size. Particles with high density or large diameter should be avoided due to their stirring problems. It is paramount to assess a uniform

distribution of the stirred particles in the fluid in the mixing chamber before carrying out any experiments. This could alter the relationship between the concentration levels and the backscattered signal.

Pitch and catch technique with a second transducer

The sensitivity for detection of the relative weak second harmonic signal could be improved.

The test cell was designed for future positioning of a second transducer, acting as a receiver on the opposite side of the mixing chamber for pitch and catch operations. This could allow the detection of weaker signals with improved sensitivity compared to the wide-band hydrophones. Hence, it is suggested to employ a couple of focused transducers designed to transmit at a central frequency of f_o and receive at a central frequency of $2f_o$.

It is suggested to use the first transducer to focus the transmitted signal (at f_o) on a generic focal point in the sample, and to employ the second transducer-receiver to get the weak backscattered data at the same point of the sample (at $2f_o$). This would achieve much higher sensitivity compared to the PVDF hydrophones and may improve discrimination of the concentration of particles.

Combination of optical and acoustic techniques

The principal advantages of acoustic techniques over optical techniques are that the equipment is relatively inexpensive. Hence the measurements can be multi-point, non-invasive, and without the need of a window. However, as shown in this work, the ultrasonic techniques, can provide details about the physical changes and not the chemical information about molecules [17].

Combined investigations using acoustic and optical (e.g. mid infrared, see Section 2.1) measurements could be beneficial in terms of providing a complete understanding of what is occurring during the evolution of the process.

Appendix

Convention

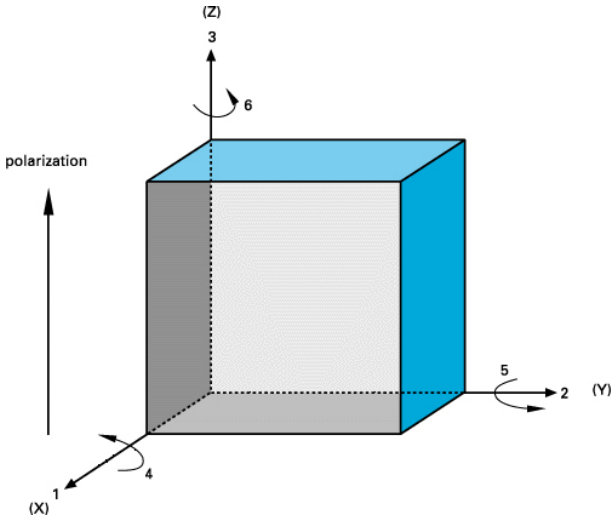

Figure 7.1: Direction of forces affecting the piezoelectric element

The piezoelectric ceramic is an anisotropic material and its physical constants relate to both the direction of the applied mechanical or electric force and the directions perpendicular to the applied force. Therefore, each constant generally has two subscripts that denote the directions of the two related quantities, such as stress and strain for elasticity. Direction X, Y, or Z is represented by the subscript 1, 2, or 3, respectively, and shear about one of these axes is represented by the subscript 4, 5, or 6, respectively. Importantly, the direction of positive polarization coincides with the Z-axis of a rectangular

system of X, Y, and Z axes according to Figure 7.1.

Snell's law

Snell's law is a formula used in optics and physics to describe the relationship between the angles of incidence and refraction, of waves (i.e. acoustic) passing through a boundary between two different isotropic media, such as water and glass.

Refraction is the change of the sound beam angle when it passes through a boundary between two materials of different acoustic velocities. A beam that is traveling normal to the interface will continue in a straight direction, but a beam that strikes a boundary at an angle will be refracted according to the formula:

$$\frac{sin(\theta_1)}{sin(\theta_2)} = \frac{v_1}{v_2} \tag{7.1}$$

where θ_1 is the incident angle in first material, θ_2 corresponds to refracted angle in second material, v_1 is sound velocity in first material and v_2 corresponds to the sound velocity in second material.

Material properties

Table 7.1: Material acoustic properties employed for the FE model (at 1 MHz and 25^o C)

Material	Density	Long. vel.	Shear vel.	Long. attenuation
	$[kg/m^3]$	$[m/s]$	$[m/s]$	[dB/cm]
Toluene	860	1225	0	0.3
Oil	929	962	0	0.5
Glass	2484	6192	3143	1.0

Table 7.2: Epoxy material acoustic properties.

Parameter	**Symbol**	**Unit**	**CY208/HY956**
Density	ρ	kg/m^3	6.932
Longitudinal Velocity	v_l	m/s	716
Shear Velocity	v_s	m/s	344
Long. Damping Coeff.	$Damp_l$	dB/m	825
Shear Damping Coeff.	$Damp_s$	dB/m	6036

Table 7.3: Ceramic material acoustic properties.

Parameter	**Unit**	**PZ4D**	**PZT5H**	**PZT5A**	**PVDF**
ρ	kg/m^3	7.6 (f)	7.5 (f)	7.7 (d)	1.7 (o)
k_t		0.51 (f)	0.50 (n)	0.48 (d)	0.15 (o)
k_{33}		0.700 (f)	0.752 (n)	0.705 (d)	0.08 (o)
ϵ_r	$10^{-11}F/m$	2500 (f)	3010 (k)	1800 (n)	9.7 (o)
d_{33}	$10^{-12}C/N$	290 (f)	583 (f)	350 (n)	15 (o)
g_{33}	$10^{-3}Vm/N$	24.6 (f)	19.1 (f)	23 (n)	14 (o)
C_T	$^\circ C$	320 (o)	190 (k)	365 (o)	100 (o)
Z	MRayls	35.5 (f)	32.6 (k)	34.5 (o)	4.0 (o)

Note: Pz26 is a traditional ceramic material from Ferroperm Piezoceramics. It corresponds to PZT4D, Sonox P4, EC64 or C5400. These data were compiled by the author from various sources of literature: (k) from [165], (o) from [166], (f) from [115], (n) from [167], (d) from [154].

Bibliography

[1] R. J. Urick. A sound velocity method for determining the compressibility of finely divided substances. *J. Appl. Phys.*, 18:983–987, 1947.

[2] C. Findlay. Ultrasonic drug delivery - microbubble detection using second harmonic imaging. Technical report, University of Strathcyde, 2002.

[3] E. Serris, L. Perier-Camby, G. Thomas, M. Desfontaines, and G. Fantozzi. Acoustic emission of pharmaceutical powders during compaction. *Powder Technology*, 128:296–299, 2002.

[4] J. G. Bouchard, M. J. Beesley, and J.A. Salkeld. Acoustic diagnostics in process plant: Crystallisation monitoring. *Powder Technol*, 4:261–277, 1993.

[5] P.L. Lee, R.B. Newell, and I.T. Cameron. *Process Control and Management*. Blackie Academic Professional, London, 1998.

[6] A. Besenyei, L. Gershouni, I. Plans, and A. J. Mulholland. Monitoring of a heterogeneous process using broadband acoustic emissions measurements. Technical report, University of Strathclyde Glasgow, 2004.

[7] F. Alba, G.M Crawley, J. Fatkin, D.M.J. Higgs, and P.G. Kippax. Acoustic spectroscopy as a technique for the particle sizing of high concentration colloids, emulsions and suspensions. *Colloids and Surfaces*, 153(1):495–502(8), 2004.

[8] P. Mougin, D. Wilkinson, K. J. Roberts, R. Jack, and P. Kippax. Sensitivity of particle sizing by ultrasonic attenuation spectroscopy to material properties. *Powder Technology*, 3(30):243–248, 2003.

[9] P. S. Eipsein and R. R. Carhart. The absorption of sound in sospension and emulsions. *J. Acoustic. Soc. Am.*, 23:533–565, 1953.

[10] M.S. Greenwood and J.A. Bamberger. Measuring fluid and slurry density and solids concentration non-invasively. *Ultrasonics*, 39(9):623–630(8), 2002.

[11] J.A. Bamberger and M.S. Greenwood. Non-invasive characterization of fluid foodstuffs based on ultrasonic measurements. *Food Research International*, 37:621–625, 2004.

[12] J. A. Bamberger and M. S. Greenwood. Absorption and velocity dispersion due to crystallization and melting of emulsion droplets. *Ultrasonics*, 31:145–148, 2004.

[13] M. Whitaker, R.G. Baker, J. Westrup, P. A. Goulding, D.R. Rudd, R.M. Belchamer, and M. P. Collins. Application of acoustic emission to the monitoring and end point determination of a high shear granulation process. *International Journal of Pharmaceutics*, 205:79–91, 2000.

[14] H. Tsujimoto and T. Yokoyama. Monitoring particle fluidization in fluidized bed granulator with an acoustic emission sensor. *Powder technology*, 113:88–96, 2000.

[15] D.J. McClement, M.J.M. Povey, M. Jury, and E. Betsanis. Ultrasonic characterisation of food emulsions. *Ultrasonics*, 28:266–272, 1990.

[16] V. Stolojanu and A. Prakash. Characterisation of slurry systems by ultrasonic techniques. *Chemical Engineering Journal*, 84:215–222, 2001.

[17] A. Nordon, R. J. H. Waddell, L. J. Bellamy, A. Gachagan, D. McNab, D. Littlejohn, and G. Hayward. Monitoring of a heterogeneous reaction by acoustic emission. *Analysis*, 129:463–467, 2004.

[18] T.J. Holroyd. Acoustic emission from an industrial application viewpoint. *J. Acoustic Emiss.*, 7:193–199, 1989.

[19] J.G Bourchard and P.A. Szyszko. Non invasive measurement of process states using acoustic emission techiques coupled with advanced signal processing. *Transactions of the Institution of Chemical Engineers*, 72:20–25, 1994.

[20] R. E. Challis, M. J. Povey, M. L. Mather, and A. K. Holmes. Ultrasound techiques for characterising colloidal dispersions. *Rep. Prog. Phys.*, 68:1541–1647, 2005.

[21] W. Schroer, J. Kser, and F. Kuhnen. Lightscattering in turbid fluids: The single-scattering intensity. *Journal of Molecular Liquids*, 134(1-3):40–48, 2007.

[22] B. A. Yegin and A. Lamprecht. Lipid nanocapsule size analysis by hydrodynamic chromatography and photon correlation spectroscopy. *International Journal of Pharmaceutics*, 320(1-2):165–170, 2006.

[23] K. Petersson, D. Ilver, C. Johansson, and A. Krozer. Brownian motion of aggregating nanoparticles studied by photon correlation spectroscopy and measurements of dynamic magnetic properties. *Analytica Chimica Acta*, 573-574:138–146, 2006.

[24] F. Scheffold. Particle sizing with diffusing wave spectroscopy. *Journal of Dispersion Science and Technology*, 23(5):591 – 599, 2002.

[25] C. D. Patz, A. Blieke, R. Ristow, and H. Dietrich. Application of ft-mir spectrometry in wine analysis. *Analytica Chimica Acta*, 513(1):81–89, 2004.

[26] J. Luypaert, M.H. Zhang, and D.L. Massart. Feasibility study for the use of near infrared spectroscopy in the qualitative and quantitative analysis of green tea camellia sinensis (l.). *Analytica Chimica Acta*, 478(2):303–312, 2003.

[27] S. B. Abeb, X. Z. Wang, R. Li, K. J. Roberts, and X. Lai. The information content in nir spectral data for slurries of organic crystals. *Powder Technology*, 443(1):12–31, 2007.

[28] D. J. Buttle and C. B. Scruby. Characterization of particle impact by quantitative acoustic emission. *Material Physics and Metallurgy*, 137:69–90, 1989.

[29] J.Hidaka, H.Ito A.Simosaka, and S.Miwa. Instantaneous measurement of particle size and flow rate by the parameters of impact sound between particles and a circular plate. *Kona*, 10:175–183, 1992.

[30] R. Hou, A. Hunt, and R. A. Williams. Acoustic monitoring of pipeline flows: particulate slurries. *Powder Technol*, 106:30–36, 1999.

[31] J. R. W. Boyd and J. Varley. The uses of passive measurement of acoustic emissions from chemical engineering processes. *Chemical Engineering Science*, 56:1749–1767, 2001.

[32] M. Leach, F. Rubin, and G.A. Williams. Particle size determination from acoustics emissions. *Powder Technology*, 16:153–158, 1978.

[33] J. Hidaka, A. Shimosaka, and S. Miwa. The effects of particle properties on the parameters of impact sound between two particles. *Kona*, 7:4–14, 1989.

[34] R. Herrmann, W. Schwieger, O. Scharf, C. Stenzel, H. Toufar, M. Schmachtl, B. Ziberi, and W. Grill. In situ diagnostics of zeolite crystallization by ultrasonic monitoring. *Microporous and Mesoporous Materials*, 80:1–9, 2005.

[35] Tily, P.j. Porada, S. Scruby, and C.B. Lidington. Monitoring of mixing processes using acoustic emission, fluid mixing. volume 108 of *Symposium series*, pages 75–94, 1987.

[36] T. L. Friesen, G. H. Brusewitz, and R. L. Lowery. An acoustic method of measuring moisture content in grain. *Journal of Agricultural Engineering Research*, 39:49–56, 1998.

[37] D.J. McClement. Ultrasonic measurements in particle size analysis. *Encyclopedia of Analytica Chemistry*, 2002.

[38] P. Troccaz, R. Woodcock, and F. Laville. Acoustic radiation due to the inelastic impact of a sphere on a rectangular plate. *J. Acoust. Soc.*, 108(5):2197–2202, 2000.

[39] D. Takahashi. Frequency analysis of sound radiation from an impactexcited plate. *J. Acoust. Soc. Am.*, 19(5):2708–2713, 1992.

[40] P. D. Thorne and P. R. Foden. Generation of underwater sound by colliding spheres. *Journal of the Acoustical Society of America*, 84:2144–2152, 1988.

[41] P.D. Thorne. Laboratory and marine measurements on the acoustic detection of sediment transport. *J. Acoust. Soc. Am.*, 80:899–910, 1986.

[42] P. D. Thorne. The measurement of acoustic noise generated by moving artificial sediments. *Journal of the Acoustical Society of America*, 78:1013–1023, 1995.

[43] G. Carson and A. J. Mulholland. Particle sizing using hertz-zener impact theory and acoustic emission spectra. Technical report, Strathclyde University, 2006.

[44] D.J. McClement. Particle sizing of food emulsions using ultrasonic spectrometry: principle, techniques and applications.

[45] U. Riebel and F. Loffler. The foundametal of particle size analysis by mean of ultrasonic spectrometry. *Part. Part. Syst. Charact.*, 6:135–143, 1989.

[46] D.J. McClement, M.J.M. Povey, and E. Dickinson. Absorption and velocity dispersion due to crystallization and melting of emulsion droplets. *Ultrasonics*, 31:433–437, 1993.

[47] M. J.W.Povey and T.J.Mason. *Ultrasound in Food Processing*. B.A.A. Professional, 1998.

[48] P.D.M. Spelt, M. Norato, A.S. Sangani, M.S. Greenwood, and L. Tavlarides. Attenuation of sound in concentrated suspensions: theory and experiments. *Journal of Fluid Mechanics*, 430:51–86, 2001.

[49] Farnborough Hampshire GU14 9RX UK PAA Ltd, Falcon House Fernhill Road.

[50] Siemens Head Office Macquarie University Research Park. Cnr Talavera and Herring Roads. North Ryde NSW. USA www.siemens.com.

[51] IL 60106 USA www.lesman.com Lesman, Chicagoland 135 Bernice Drive Bensenville.

[52] www.ultrasonic-scientific.com Sonas Technologies, 42 Ailesbury Grove Dundrum Dublin 16 IRELAND.

[53] Dispersion Technology Inc. 364 Adams Street Bedford Hills NY 10507 http://www.dispersion.com.

[54] http://www.malvern.co.uk Malvern Instruments Ltd. Enigma Business Park Grovewood Road Malvernc Worcestershire United Kingdom WR14 1XZ.

[55] High resolution ultrasonic spectroscopy for analysis of industrial emulsions and www.ultrasonic-scientific.com supensions.

[56] A. Nordon, Y. Carella, A. Gachagan, D. Littlejohn, and G. Hayward. Factors affecting broadband acoustic emission measurements of a heterogeneous reaction. *Analysis*, 131:323–330, 2006.

[57] J. R. Allegra and S. A. Hawley. Attenuation of sound in suspensions and emulsions: theory and experiments. *J. Acoust. Soc. Am.*, 51:1545–1564, 1972.

[58] A. B. Wood. *The Textbook of Sound*. G. Bell and Son, 1941.

[59] D.J. McClement. Principles of ultrasonic droplet size determination. *Langmuir*, 12:3454–3461, 1996.

[60] M.J.M. Povey, D.J. McClement, and E. Dickinson. Ultrasonics in food engineering: Part i. introduction and experimental methods. *J. Food Eng.*, 8:217–245, 1998.

[61] D.J. McClement, Y. Hemar, and Y. Herrmann. Influence of flocculation on the ultrasonic properties of emulsions: theory. *J. Phys*, 31:2950–2955, 1998.

[62] P. C. Waterman and R. Truell. Multiple scattering of waves. *J. Math, Phys.*, 2:512–537, 1961.

[63] J. C. Austin and R. E. Challis. The effects of flocculation on the propagation of ultrasound in dilute kaolin slurries. *Journal of Colloid and Interface Science*, 206 (1):146–157, 1998.

[64] J. S. Tebbutt and R. E. Challis. Ultrasonic wave propagation in colloidal suspensions and emulsions: a comparison of four models. *Ultrasonics*, 34 (2-5):363–368, 1996.

[65] M. J.W.Povey. *Ultrasonic techniques for fluid characterisation*. Academic Press, 1997.

[66] L. Schwartz and L. Plona. Ultrasonic propagation in close-packed disordered suspensions. *J. Appl. Phys.*, 55:3971–3977, 1984.

[67] Mathworks Inc. Natick Massachussetts.

[68] W.K. Sakamotoa, P. Marin-Franchb, and D.K. Das-Guptab. Characterization and application of pzt/pu and graphite doped pzt/pu composite. *Sensors and Actuators*, 100:165–174, 2002.

[69] T. Boczar and M. Lorenc. Determining the repeatability of acoustic emission generated by the hsu-nielsen calibrating source. *The Molecular and Quantum Acoustics Journal*, 25, 2004.

[70] Weidlinger Associates. Pzflex.

[71] http://www.britannica.com/.

[72] R. G. Sargent. Verification and validation of simulation models. *Proc of 1998a Winter Simulation Conf.*, pages 121–130, 1998.

[73] R. G. Sargent. Verifying and validation simulation models. *Proc of 1996a Winter Simulation Conf.*, pages 55–64, 1996.

[74] http://www.pacuk.co.uk/.

[75] G. Carson, A. J. Mulholland, A. Nordon, M. Tramontana, A. Gachagan, and G. Hayward. The dependency of the acoustic emission spectrum on multi-particle impact parameters. *JASA*, 43:1–15, 2007.

[76] W. Goldsmith. *Impact: the theory and the physical behaviour of colliding solids*. Edward Arnold, 1960.

[77] B. Leroy. Collision between two balls accompanied by deformation: A qualitative approach to hertz's theory. *J. Phys*, 53:346–349, 1985.

[78] A. Akay and M. Latcha. Sound radiation from an impact-excited clamped circular plate in an infinite baffle. *J. Acoustic Soc. Am.*, 74(2):640–648, 1993.

[79] C. Zener. Intrinsic inelasticity of large plates. *Phys. Rev.*, 59:669–673, 1941.

[80] I.M. Hutchings. Strain effect of microparticles impact. *J. Physics*, 10:179–184, 1977.

[81] www.wai.com.

[82] R. Popescu. Finite element assessment of the effects of seismic loading rate on soil liquefaction. *Canadian Geotechnical Journal*, 39(2):331–344, 2002.

[83] F. Moser, L. J. Jacobs, and J. Qu. Application of finite element methods to study transient wave propagation in elastic wave guides. *Proceedings of the 24th Annual Review of Progress in Quantitative Nondestructive Evaluation*, 17A:161–167, 1998.

[84] M. Aare and S. Kleiven. Evaluation of head response to ballistic helmet impacts using the finite element method. *International Journal of Impact Engineering*, 4-3:596–608, 2005.

[85] K.M.A. Jaleel, N.N. Kishore, and V. Sundararajan. Finite-element simulation of elastic wave propagation in orthotropic composite materials. *Material evaluations*, pages 830–838, 1993.

[86] R. Hill, S. A. Forsyth, and P. Macey. Finite element modelling of ultrasound, with reference to transducers and ae waves. *Ultrasonics*, 42-2:253–258, 2004.

[87] J. A. Hossack. *Modelling techniques for 1-3 Composite Transducers*. PhD thesis, Strathclyde University, 1990.

[88] www.cue.co.uk.

[89] E. K. Akdogan, M. Allahverdi, and A. Safari. Piezoelectric composites for sensor and actuator applications. *IEEE Transaction on Ultrasonics, Ferroelectics and frequency control*, 52(5):746–775, 2005.

[90] J. D. Achenbach. *Wave Propagation in Elastic Solids*. Elsevier, New York, 1984.

[91] Alba Ultrasound Ltd Glasgow http://www.alba ultrasound.co.uk.

[92] S. K. Edelman. *Understanding Ultrasound Physics, Third Edition*. E.S.P. Ultrasound, 2004.

[93] M. J. Crocker. *Handbook of Acoustics*. ISBN-10: 047125293X. Wiley-Interscience.

[94] H.W. Kwan and M. Leach. Characterization of cylindrical particles from their acoustic emission. *Ultrasonics*, 41:233–238, 1985.

[95] Oppenheim and Schafer. *Digital Signal Processing*. Prentice-Hall International, 1975.

[96] A. Gachagan and G. Hayward. Improving the bandwidth of 1-3 connectivity composite receivers using mode coupling. *Journal of the Acoustical Society of America*, 103:3344–3352, 1998.

[97] T.R. Gururaja, W.A. Schulze, L.E. Cross, and R.E. Newnham. Piezoelectric composite materials for ultrasonic transducer applications part 2, evaluation of ultrasonic medical applications. *IEEE Trans.Sonics Ultrason. SU-22*, 4:499513, 1985.

[98] T.R. Gururaja, W.A. Schulze, L.E. Cross, and R.E. Newnham. Piezoelectric composite materials for ultrasonic transducer applications part 1:resonant modes of vibration of pzt rod-polymer composites. *IEEE Trans.Sonics Ultrason. SU-22*, 4:481– 498, 1985.

[99] P. Reynolds. *Analysis and design of piezocomposite ultrasonic transducers using finite element techiques and surface displacement analysis.* PhD thesis, CUE Department of EEE, University of Strathclyde, 1998.

[100] D.D.N. Hall, D.J. Powell, and G. Hayward. Theorical and experimental performance appraisal of active multi-layered piezo-polymer transducer structure. *Ultrasonics Int. Conf. Proc*, pages 375–391, 1991.

[101] R.L. O'Leary, M. Kijowsky, G. Hayward, and T. McCunnie. 3-3 connectivity multilayered piezoelectric composites. *IEEE Ultrasonics Symposium*, pages 1686–1689, 2004.

[102] G. Hayward, A. Gachagan, R. Hamilton, D. A. Hutchins, and W. M. D. Wright. Ceramic epoxy composite transducers for non contacting ultrasonic applications. *SPIE*, 1733:42–56, 1992.

[103] J. M. Powers, M. B. Moffett, and J. C. McGrath. Broadband, acoustically transparent, nonresonant pvdf hydrophone. Patent number: 4789971, Dec 6, 1988.

[104] R. C. Preston, A. J. Livett, and K. Rajendran. Pvdf membrane hydrophone performance properties and their relevance to the measurement of the acoustic output of medical equipment. *J. Phys. E: Sci. Instrum.*, 16, 1983.

[105] W.A. Smith and B.A Auld. Modelling 1-3 composite piezoelectric : thickness mode oscillations. *IEEE Trans UFFC*, 38:40–47, 1990.

[106] J. A. Hossack and G. Hayward. Finite-element analysis of 1-3 composite transducers. *IEEE Transactions on Ultrasonics Ferroelectrics and Frequency Control*, 6:618–629, 1991.

[107] G. Hayward and J. Hossack. Unidimensional modelling of 1-3 composite transducers. *IEEE Trans UFFC*, 88, 1990.

[108] IEEE Standard on Piezoelectricity. Special issue of transactions sonics ultrasonics, 1984. (IEEE : New York 1987).

[109] T.R. Gururaja. Piezoelectric transducers for medical ultrasonic imaging. *Applications of Ferroelectrics*, 43:259–265, 1992.

[110] G. Hayward, D. Gillies, and T. S. Durrani. A multidimentiona linear system model of the piezoelectric transducer. *Ultrasonic Symposium*, pages 790–793, 1984.

[111] G. Hayward, D. Gillies, and T. S. Durrani. A systems model of the thickness mode piezoelectric transducer. *JASA*, 76(2):369–382, 1990.

[112] H.P. Savakus, K.A. Klicker, and R.E. Newnham. Pzt epoxy piezoelectric transducers : a simplified fabrication process. *Materials Research Bulletin*, 16:667–680, 1980.

[113] A. Cochran, P. Reynolds, and G. Hayward. Progress in stacked piezocomposite ultrasonic transducers for low frequency applications. *Ultrasonics*, 36:969–977, 1998.

[114] D.J. Powell, G. Hayward, and R.Y. Ting. Unidimensinal modelling of multi-layered piezoelectric transducer structures. *IEEE Trans. Ultrasonics. Ferroelec. and Freq. Control*, 45:667–677, 1998.

[115] Ferroperm and http://www.ferroperm.com Piezo-electric product literature Hejreskovvej Denmark.

[116] UK Loadpoint Ldt Cricklate Swindon Wilts.

[117] C.D.F Motchenbacher. *Low noise electronic design.* Wiley-Interscience, 1973.

[118] E. Maione, P. Tortoli, G. Lypacewicz, and A. Nowicki. Pspice modelling of ultrasound transducers: comparison of softwaremodels to experiment. *Ultrasonics, Ferroelectrics and Frequency Control, IEEE Transactions on*, 46, 1999.

[119] Y. Yanez, M.J. Garcia-Hernandez, J. Salazar, A. Turo, and J.A. Chavez. Design amplifiers with low output noise for high impedance piezoelectric transducers. *NDT International*, 38:491–496, 2005.

[120] One Techology Way P.O. 9160 Norwood MA 02062-9106 USA www.analog.com AD797 Application Notes, Analogue Devices.

[121] A. Turo, A. Salazar, J.A. Chavez, H.B. Kichou, and F.R. Gomez della Spinosa. Ultra low noise front end electronics for air coupled ultrasonic non destructive evaluation. *NDT and E Int*, 36(2):93–100, 2003.

[122] CA 95134 USA http://www.orcad.com Orcad 2655 Seely Avenue San Jose.

[123] M.S. Greenwood and S. Ahmed. Ultrasonic diffraction grating spectroscopy and the measurement of particle size. *Ultrasonics*, 44:13851393, 2006.

[124] J.W. Garner. Estimation of suspended solids concentration based on acoustical backscatter intensity: theoretical background. turbidity and other sediment surrogates workshop. *Turbidity and Other Sediment Surrogates Workshop*, 2002.

[125] F. Calliada, R. Campani, O. Bottinelli, A. Bozzini, and MG. Sommaruga. Ultrasound contrast agents: basic principles. *J. Radiol.*, 27:S157–60, 1998.

[126] P. J. A. Frinking et al. Ultrasound contrast imaging - patent., 2004. Patent number: 6726629.

[127] E. G. Schutt. Harmonic ultrasound imaging with microbubbles, 1994. Patent number: 5540909.

[128] J.M. Correas, O. Helenon, M. Cherkaoui, and J.F. Moreau. Ultrasound contrast agents: clinical applications. *Ultrasonics Symposium, IEEE*, 2:1773 – 1778, 1998.

[129] Nico de Jong, P. J. A. Frinking, A. Bouakaza, and Folkert J. Ten Cate. Detection procedures of ultrasound contrast agents. *Ultrasonics*, 38(1):87–92, 2000.

[130] K. Petersson, D. Ilver, C. Johansson, and A. Krozer. Parameter of non-linearity in fluids. *J. Acoust. Soc. Am.*, 32(6), 1960.

[131] H. Ootaki, Y. Murata, K. Minagawa, and K. Koyama. Basic study of particle characterization using the ultrasonic finite amplitude method. *Journal of Materials Science Letters*, 14(3):182–184, 1995.

[132] Z. Cheng-ya S. Tao X.F. Gong, F. Ruo. Ultrasonic investigation of the non-linearity parameter b/a in biological media. *J. Acoust. Soc. Am.*, 76:949–950, 1984.

[133] M.F. Hamilton and D.T. Blackstock. *Nonlinear Acoustics: Theory and Applications*. Academic Press, 1997.

[134] H. Fukukita. Ultrasound pulse reflection mode measurement of non-linearity parameter b/a and attenuation coefficient. *J. Acoustic Soc.*, 99(5):2275–2281, 1996.

[135] K. D. Wallace, C. W. Lloyd, M. R. Holland, and J. G. Miller. Finite amplitude measurements of the non-linear parameter b/a for liquid mixtures spanning a range relevant to tissue harmonic mode. *Ultrasound Med Biol.*, 33(4):620629, 2007.

[136] T. Christopher. Finite amplitude distortion-based inhomogeneous pulse echo ultrasonic imaging. *Trans. Ultrason. Few. Freq. Control IEEE*, 44:125–139, 1997.

[137] WK. Law, LA. Frizzell, and F. Dunn. Determination of the non-linearity parameter b/a of biological media. *Ultrasound Med Biol*, 11:307318, 1995.

[138] C.K. Yeh, K.W. Ferrara, and D.E. Kruse. High-resolution functional vascular assessment with ultrasound. *Medical Imaging*, 10:1263– 1275, 2004.

[139] Forsberg F, DA Merton, J.B. Liu, L. Needleman, and B.B. Goldberg. Clinical applications of ultrasound contrast agents. *Ultrasonics*, 36(1-5):695–701, 1998.

[140] L. Yiyao, M. Hirokazu, and M. Nakamura. Encapsulated ultrasound microbubbles: Therapeutic application in drug/gene delivery. *Journal of Controlled Release*, 114:89–99, 2006.

[141] C. Kollmann. New sonographic techniques for harmonic imagingunderlying physical principles. *European Journal of Radiology*, 2:33–41, 2007.

[142] P. J. A. Frinking, A. Bouakak, F. J. T. Cate J. Kirkhorn, and Nico De Jong. Ultrasound contrast imaging: current and new potential methods. *Ultrasound in Med. and Biol.*, 26(3):965–975, 2000.

[143] M. Tang and R. J. Eckersley. Non-linear propagation of ultrasound through microbubble contrast agents and implications for imaging. *Trans. Ultrason. Few. Freq. Control IEEE*, 53(12):2406–2415, 2006.

[144] N. de Jong, R. Cornet, , and C. T. LanC. Higher harmonics of vibrating gas-filled microspheres. *Ultrason.*, 32:455–459, 1994.

[145] J.M. Borsboom, C.T. Chin, A. Bouakaz, M. Versluis, and N. de Jong. Harmonic chirp imaging method for ultrasound contrast agent. *Trans. Ultrason. Few. Freq. Control IEEE*, 52(2):241–249, 2005.

[146] K. Commander and A. Prosperetti. Linear pressure waves in bubbly liquids: Comparison between theory and experiments. *J. Acoust. Soc. Am.*, 85:732–746, 1989.

[147] Y. Izuka. High signal to noise ratio ultrasonic testing system using chirp pulse compression. *Insight*, 4(40):282– 285, 1998.

[148] F. Nishiyama and H. Murakami. A blind march filter method for a wideband ground radar system. *Antennas, Radar, and Wave Propagation*, 245:133–142, 2004.

[149] T. H. Gana, D. A. Hutchins, D. R. Billsona, and F.C. Wong. Ultrasonic tomographic imaging of an encased highly-attenuating solid media. *Research in Nondestructive Evaluation*, 13(3):131–152, 2001.

[150] S. N. Ramadas. Ultrasound in process control. Master's thesis, University of Strathclyde, 2002.

[151] A. Gachagan, D. Speirs, and A. McNab. The design of a high power ultrasonic test cell using finite element modelling techniques. *Ultrasonics*, 41:283–288, 2003.

[152] http://www.panametrics ndt.com/.

[153] T. A. Litovitz and C. M. Davis. *Structural and shear relaxation in liquids, properties of gases, liquids and solutions*, volume II Part A. Academic Press, 1965.

[154] Suite 7 Sunnyvale CA 94089 http://www.ondacorp.com Onda Corporation, 592 Weddell Drive.

[155] S.W. Ament. Sound propagation in gross mixtures. *Journal of Acoustical Society of America*, 25:638–641, 1953.

[156] A.H. Harker et al. Velocity and attenuation of ultrasound in suspensions of particles in fluids. *J. Phys. D: Appl. Phys.*, 21:1576–1588, 1988.

[157] V.J. Pinfield, M.J. Povey, and E. Dickinson. The application of modified forms of the urick equation to the interpretation of ultrasound velocity in scattering systems. *Ultrasonics*, 33:243–251, 1995.

[158] G. Guidarelli, F. Craciun, C. Galassi, and E. Roncari. Ultrasonic characterization of solid-liquid suspensions. *Ultrasonics*, 36 (125):467, 1998.

[159] A.K. Hipp, G. Storti, and M. Morbidelli. On multiple-particle effects in the acoustic characterization of colloidal dispersions. *Journal of Physics D: Applied Physics,*, 32 (5):568–576(9), 1999.

[160] S. S. Kutateladze, V. I. Popov, and E. M. Khabakhpasheva. Hydrodynamics of fluids of variable viscosity. *Journal Journal of Applied Mechanics and Technical Physics*, 7(1):27–31, 1966.

[161] J. Stor-Pellinen, E. Haeggstrom, and M. Luukkala. Measurement of the effect of high-power ultrasound on wetting of paper. *Ultrasonics*, 38 (10):953–959(7), 2000.

[162] A. Savitzky and M.J.E Golay. Smoothing and differentiation of data by simplified least squares procedures. *Analytical Chemistry*, 36(8):16271639, 1964.

[163] C. Ruffing and R. King. The analysis of hyperspectral data using savitzky-golay filtering-theoretical basis. *Geoscience and Remote Sensing Symposium*, 2:756–758, 1999.

[164] J. C. Austin and R. E. Challis. Ultrasonic propagation through aqueous kaolin suspensions during degassing. *Ultrasonics*, 37:299302, 1999.

[165] K.K. Shung and M. Zipparo. Ultrasonic transducers and arrays. *Engineering in Medicine and Biology, IEEE*, pages 20–30, 1996.

[166] H. Ohigashi et.al. Analysis of frequency response characteristics of polymer ultrasonic transducers. *Japanese Journal of Applied Physics*, 27(3):354–360, 1998.

[167] Nasa: M. W. Hooker Lockheed Martin Engineering and Sciences Co. Properties of pzt-based piezoelectric ceramics between 150-250 celsius degrees, 1988.